

Involvement of BRCT Family Proteins in DNA Damage Response

by

Luxin Sun

A thesis submitted in partial fulfillment of the requirements for the degree of

Doctor of Philosophy

Department of Biochemistry  
University of Alberta

© Luxin Sun, 2017

## **Abstract**

The BRCT domain family is a group of proteins that is primarily involved in the regulation of DNA replication, cell cycle checkpoint activation, DNA damage repair, and many other DNA damage responses (DDR). Mutations in BRCT proteins often result in genomic instability, one of the leading sources of many human diseases including cancers. My thesis focuses on two important BRCT family proteins: Breast cancer associated proteins 1 (BRCA1) and Topoisomerase II  $\beta$  Binding Protein 1 (TopBP1).

BRCA1 is a well-known tumor suppressor protein that acts mainly in the homologous recombination (HR) pathway which repairs the DNA double-strand breaks (DSB) in cells. Mutations in BRCA1 have been found to associate with elevated risk of hereditary breast and ovarian cancers in humans. However, over 95% of sporadic breast and ovarian cancer patients carry wild-type BRCA1, making them less susceptible to DNA damaging cancer therapy. Since interaction between BRCA1 BRCTs and many phosphorylated protein partners are critical for the function of BRCA1 in DDR, including the proper activation of HR, inhibitors of BRCA1 BRCTs have great potential as chemotherapeutic agents. Unfortunately, the development of these inhibitors has been very challenging. While the shallow protein interface of BRCA1 BRCTs makes it difficult to stabilize any small molecule inhibitors, the strong dependency on the phosphate-binding pocket of BRCA1 makes the preservation of active phosphate on peptide inhibitors a major technical barrier. Here, I have successfully verified the first nonphosphopeptide inhibitor of BRCA1 BRCTs and solved the

crystal structure of this inhibitor in complex with BRCA1 BRCTs. My study reveals new structural features that can be included to guide the development of BRCA1 BRCTs inhibitors. It also provides the structural basis that supports the possibility of phosphorylation-independent interaction between DNA PKcs and BRCA1 BRCTs.

TopBP1, on the other hand, is an important scaffold protein that mediates many protein-protein interactions (PPIs) involved in DNA replication stress signaling, cell cycle checkpoint activation, and DNA damage response via its ATR activation domain (AAD) and nine BRCT domains. In particular, the BRCT5 from the internal tandem repeats (BRCT4/5) of TopBP1 has been found to play critical roles in the recruitment of TopBP1 to the sites of DNA damage and replication stress. Several DNA damage-associated proteins have been suggested to interact with the TopBP1 BRCT5 domain in a phosphorylation-dependent manner. My study has been focusing on the interactions between TopBP1 BRCT4/5 and two of these proteins, the mediator of DNA damage checkpoint protein 1 (MDC1) and the Bloom syndrome, Rec Q helicase like protein (BLM). Consistent with the existing structural model of TopBP1 BRCT4/5 in complex with MDC1 SDT repeat peptide, my mutagenesis study of TopBP1 BRCT5 has validated that TopBP1 engages MDC1 mainly through electrostatic interactions. The interaction with MDC1 is largely induced by TopBP1 dimerization. On the contrary, my structural and functional study of TopBP1/ BLM interaction shows that TopBP1 BRCT5 engages BLM through a higher affinity, monomer-based interaction. The orientation

of BLM peptide on the peptide interface of TopBP1 BRCT5 is opposite to the one observed in MDC1 peptide. I have proved that the interaction between BLM and TopBP1 is highly dependent on phosphorylation of Ser304 of BLM, not pSer338. Additional hydrophobic interactions are crucial for stabilizing the TopBP1/BLM complex while electrostatic interactions only play a supportive role. Since a similar interaction has also been observed between Rad4<sup>TopBP1</sup> BRCT1/2 and Crb2<sup>53BP1</sup> in *S. Pombe*, I propose the interaction between TopBP1 BRCT5 and 53BP1 likely adopted this mechanism as well.

Together, my studies of BRCA1 and TopBP1 further demonstrate the structural diversity of BRCT domain architecture. The structural insights revealed by my research can be used as a guideline for not only the modeling of other PPIs but also the development of synthetic compounds with therapeutic potential for DNA damaging cancer therapy.

## Preface

Some of the researches from this thesis are conducted as a part of an international research collaborations.

The research project described in Chapter 2 is in collaboration with Dr. Matt Hartman's group (Virginia Commonwealth University). Dr. White, E. from Harman's group carried out the BRCA1 inhibitor peptide screening to identify the non-phosphorylated peptide inhibitor: peptide 8.6 and peptide 8.6 Nat. Dr. White also performed the alanine scanning of the peptide using ITC. I solved the crystal structure of peptide 8.6 in complex with BRCA1 BRCTs and carried out the mutagenesis study of BRCA1 BRCTs with peptide 8.6 *in vitro* using FP assay.

The research project described in Chapter 3 is in collaboration with Dr. Junjie Chen's group (University of Texas, MD Anderson Cancer Center). Dr. Leung, C., an alumnus from my group, has solved the apo structure of TopBP1 BRCT4/5 and the complex structure of TopBP1 BRCT4/5 with MDC1 SDT repeat peptide. I carried out the functional study of TopBP1 BRCT4/5 interaction with MDC1 peptide *in vitro* using FP assay. Dr. Gong, Z. from Dr. Chen's group carried out the foci formation assay to examine the effect of mutations on the recruitment of TopBP1 to DNA damage sites in the cells.

The research project described in Chapter 4 is in collaboration with Dr. Wojciech Niedzwiedz's group (Virginia Commonwealth University). I solved the X-ray crystal structure of mouse TopBP1 BRCT4/5 in complex with BLM peptide. I carried out all the *in vitro* interaction study between TopBP1 4/5 and BLM peptide using FP assay. Dr. Niedzwiedz's group provided the BLM peptide compounds used in my study, and Blackford, A.N. reviewed the final manuscript of the paper.

The research project described in Appendix A is in collaboration with Dr. Yaffe, M.B.'s group (Massachusetts Institute of Technology). I performed the GST pull-down assays to identify the functional domains involved in the interaction between Brd4 and

TopBP1. After I proved that Brd4 ET domain interacts with TopBP1 BRCT6 domain, I used size exclusion chromatography and BS3 cross-linking assay to test the stability of the Brd4 ET-TopBP1 BRCT6 complex. I designed the S35 methionine pull-down experiment and provided the purified TopBP1 BRCT proteins (BRCT0/1/2, BRCT4/5, BRCT6 and BRCT7/8) for Dr. Lam, F. from Dr. Yaffe's group to use. Dr. Lam, F. also carried out immuno-precipitation and foci formation assay to study the function of TopBP1 BRCT6 interaction with Brd4 ET domain in the cell.

## **Acknowledgements**

I would like to thank my supervisor, Dr. Mark Glover, for being a great mentor. My committee members, Dr. Andrew MacMillan and Joanne Lemieux, for being very supportive during my graduate study. Special thanks to my internal examiner, Dr. Bart Haze, for reviewing my thesis. My external examiner, Dr. John Pascal (University of Montreal), for joining my thesis defense in Edmonton.

I want to thank the past and present members of the Glover lab. Especially Dr. Stephen Campbell for guiding me through my first year and getting me interested in the BRCT family proteins. Dr. Charles Leung for initiating the TopBP1-MDC1 project in my lab and giving me many resources I can use towards my research. Thanks to our X-ray technician, Sheraz Khan, for helping me with pre-screening of my crystals on our instrument before preparing all the synchrotron shipments to other facilities. Everyone from the Glover lab has been very generous in providing his/her help and expertise for me over the years. Thanks to them, I enjoy my time at work almost as much as my free time at home.

Last but not the least, I want to thank my finance, Wen Wu, who warms my heart and keeps my spirits up in the long cold winter of Edmonton. My parents, Keqin Sun and Yulin Sun, for their unconditional love. I would not be able to make it this far without their support.

# Table of Contents

## Chapter 1 Introduction

1.1 DNA damage and repair: the Ying and Yang of life	
1.1.1 Mapping the blueprint of life: a historical overview of early DNA researches.....	2
1.1.2 DNA damage and response.....	2
1.1.3 Cell cycle regulation.....	7
1.1.4 DNA damage repair.....	9
1.2 Genomic instability and cancer	
1.2.1 Genomic instability and diseases.....	13
1.2.2 Cancer.....	15
1.2.3 DNA damaging cancer therapy: a double edged sword.....	17
1.3 BRCT family proteins	
1.3.1 BRCT domain.....	22
1.3.2 BRCA1.....	25
1.3.3 TopBP1.....	28
1.4 Thesis overview.....	32

1.5	Reference.....	34
<b>Chapter 2 Development of BRCA1 BRCT inhibitor for cancer therapy</b>		
2.1	Introduction.....	48
2.2	Results	
2.2.1	Peptide 8.6 inhibits BRCA1 BRCT interaction with other phosphorylated protein partners.....	52
2.2.2	The crystal structure of nonphosphopeptide inhibitor in complex with BRCA1 BRCT.....	52
2.2.3	The E-x-x-F motif can partially mimic pS-x-x-F in BRCA1 BRCT recognition.....	54
2.2.4	Additional interactions that support peptide 8.6 recognition by BRCA1 BRCT.....	58
2.2.5	Structure-guided mutagenesis study reveal additional interphase for inhibitor design.....	58
2.2.6	Peptide 8.6 interferes with DNA damage response.....	64
2.3	Discussion.....	64
2.4	Material and Methods.....	68

2.5	Reference.....	72
<b>Chapter 3</b>	<b>Insights into MDC1 recognition by TopBP1 in DNA replication checkpoint control</b>	
3.1	Introduction.....	77
3.2	Results	
3.2.1	TopBP1 BRCT5 interacts with MDC1 in a dimerization-induced manner.....	82
3.2.2	TopBP1 BRCT5 prefers phosphorylated MDC1 SDT repeats.....	85
3.2.3	+2 Val/Asp in SDT repeats aids MDC1 recognition by TopBP1.....	85
3.2.4	Functional study of TopBP1 BRCT5 binding interface by mutagenesis.....	86
3.2.5	TopBP1 BRCT4/5 interacts with DNA.....	88
3.3	Discussion.....	94
3.4	Material and Methods.....	99
3.5	Reference.....	101
<b>Chapter 4</b>	<b>Structural Insight into BLM Recognition by TopBP1</b>	

4.1	Introduction.....	105
4.2	Results	
4.2.1	TopBP1 BRCT5 interacts with BLM mainly through pSer304 and not pSer338.....	106
4.2.2	The crystal structure of TopBP1 BRCT4/5 bound to phosphorylated BLM.....	108
4.2.3	Modeling of TopBP1-BLM binding interaction.....	111
4.2.4	Comparison of BLM and MDC1 recognition by TopBP1 .....	116
4.3	Discussion.....	121
4.4	Material and Methods.....	124
4.5	Reference.....	130
 <b>Chapter 5 General Discussion</b>		
5.1	Overall Summary.....	134
5.2	Structural diversity of BRCT tandem repeats .....	134
5.3	Novel aspects of BRCT mediated protein interactions.....	138
5.4	Therapeutic potential in BRCT family proteins.....	142
5.5	Reference.....	148
 <b>Bibliography List.....</b>		 152

**Appendix A Interaction between TopBP1 and Brd4 regulates DNA damage induced replication stress response**

A.1	Introduction.....	175
A.2	Results	
A.2.1	Brd4 interacts with TopBP1 BRCT6 through its ET domain.....	176
A.2.2	Disruptions of TopBP1/Brd4 interaction induces replication stress and DNA damage.....	181
A.2.3	Protein complex of TopBP1 BRCT6/Brd4 ET domain is unstable <i>in vitro</i> .....	183
A.3	Discussion.....	188
A.4	Material and Methods.....	189
A.5	Reference.....	193

**Appendix B: Structure analogs of TopBP1 BRCT4/5 in *Saccharomyces cerevisiae***

B.1	Introduction.....	197
B.2	Results	

B.2.1 Engineering of bacteria based expression constructs of Dpb11	
BRCTs.....	201
B.2.2 Rtt107 BRCT3/4 is the structural analog of TopBP1	
BRCT4/5.....	205
B.2.3 Constructs design of Rtt107 BRCT3/4 for bacteria based	
expression.....	210
B.2.4 Purification of GST-Rtt107 BRCT3/4 produced by <i>E. coli</i>	
cells.....	214
B.2.5 Purification of His-Rtt107 BRCT3/4 produced by <i>E. coli</i>	
cells.....	216
B.3 Discussion.....	218
B.4 Material and Methods.....	221
B.5 Reference.....	225

## List of Tables

Chapter 1, Table 1.....	10
Chapter 1, Table 2.....	14
Chapter 1, Table 3.....	16
Chapter 2, Table 1.....	56
Chapter 2, Table 2.....	61
Chapter 2, Table 3.....	63
Chapter 3, Table 1.....	84
Chapter 3, Table 2.....	92
Chapter 4, Table 1.....	113
Chapter 4, Table 2.....	117
Chapter 4, Table 3.....	125
Appendix B, Table 1.....	207
Appendix B, Table 2.....	208
Appendix B, Table 3.....	212
Appendix B, Table 4.....	213
Appendix B, Table 5.....	222

## List of Figures

Chapter 1, Figure 1.....	3
Chapter 1, Figure 2.....	5
Chapter 1, Figure 3.....	6
Chapter 1, Figure 4.....	8
Chapter 1, Figure 5.....	12
Chapter 1, Figure 6.....	19
Chapter 1, Figure 7.....	21
Chapter 1, Figure 8.....	23
Chapter 1, Figure 9.....	26
Chapter 1, Figure 10.....	27
Chapter 1, Figure 11.....	29
Chapter 1, Figure 12.....	31
Chapter 2, Figure 1.....	50
Chapter 2, Figure 2.....	51
Chapter 2, Figure 3.....	53
Chapter 2, Figure 4.....	55
Chapter 2, Figure 5.....	57
Chapter 2, Figure 6.....	59
Chapter 2, Figure 7.....	60

Chapter 2, Figure 8.....	65
Chapter 2, Figure 9.....	67
Chapter 2, Figure 10.....	69
Chapter 3, Figure 1.....	78
Chapter 3, Figure 2.....	79
Chapter 3, Figure 3.....	81
Chapter 3, Figure 4.....	83
Chapter 3, Figure 5.....	87
Chapter 3, Figure 6.....	89
Chapter 3, Figure 7.....	91
Chapter 3, Figure 8.....	93
Chapter 3, Figure 9.....	97
Chapter 4, Figure 1.....	107
Chapter 4, Figure 2.....	109
Chapter 4, Figure 3.....	110
Chapter 4, Figure 4.....	112
Chapter 4, Figure 5.....	114
Chapter 4, Figure 6.....	115
Chapter 4, Figure 7.....	119

Chapter 4, Figure 8.....	120
Chapter 4, Figure 9.....	123
Chapter 4, Figure 10.....	126
Chapter 5, Figure 1.....	136
Chapter 5, Figure 2.....	137
Chapter 5, Figure 3.....	139
Chapter 5, Figure 4.....	145
Chapter 5, Figure 5.....	146
Appendix A, Figure 1.....	177
Appendix A, Figure 2.....	178
Appendix A, Figure 3.....	179
Appendix A, Figure 4.....	180
Appendix A, Figure 5.....	182
Appendix A, Figure 6.....	184
Appendix A, Figure 7.....	186
Appendix A, Figure 8.....	187
Appendix B, Figure 1.....	198
Appendix B, Figure 2.....	202

Appendix B, Figure 3.....	203
Appendix B, Figure 4.....	204
Appendix B, Figure 5.....	206
Appendix B, Figure 6.....	209
Appendix B, Figure 7.....	211
Appendix B, Figure 8.....	215
Appendix B, Figure 9.....	217
Appendix B, Figure 10.....	219



HPV	Human papillomavirus HPV
HU	Hydroxyurea
IR	Ionizing radiation
IP	Immuno-precipitation
IPTG	Isopropyl $\beta$ -D-1-thiogalactopyranoside
$K_D$	Dissociation constant
LB	Luria-Bertani
MBP	Maltose binding protein
MDC1	Mediator of DNA damage checkpoint protein 1
MGMT	Methyl guanine methyl transferase
MR	Mismatch repair
MRN	Mre11-Rad50-Nbs1
NBS	Nijmegen breakage syndrome
NER	Nucleotide excision repair
NHEJ	Non-Homologous End Joining
NLS	Nucleus localization signals
NSCLC	Nonsmall cell lung cancer
PALB2	Partner and localizer of BRCA2
PAR	Poly ADP ribose
PARP	Poly ADP-ribose polymerase
PARPi	Poly ADP-ribose polymerase inhibitor
PPIs	Protein-protein interactions
P-TEFb	Positive transcription elongation factor b
RING	Really interesting new gene
RNA Pol II	RNA polymerase II
RPA	Replication Protein A
Rtt107	Regulator of Ty1 transposition protein 107
SAM	S-adenosylmethionine
SCEs	Sister chromatid exchanges
SDT	Ser-Asp-Thr
<i>S. pombe</i>	Schizosaccharomyces pombe
<i>S. cerevisiae</i>	Saccharomyces cerevisiae
SSB	Single strand break
Timeless: Tipin	Timeless-interacting protein
TNRs	Trinucleotide Repeats
Top3A	Topoisomerase IIIA
TopBP1	Topoisomerase II $\beta$ Binding Protein 1
TRX	His-thioredoxin
UV	Ultraviolet light
XFL	XRCC4 like factor
XP	xeroderma pigmentosa
XRCC1	X-ray repair cross-complementing protein 1
XRCC4	X-ray cross complementing protein 4

## **Chapter 1**

### **Introduction**

## **1.1 DNA damage and repair: the Ying and Yang of life**

### **1.1.1 Mapping the blueprint of life: a historical overview of early DNA research**

Deoxyribonucleic acid (DNA) was first discovered as a microscopic substance, isolated from the pus of discarded surgical bandages, by a physician named Friedrich Miescher in 1869 (Dahm, 2008) (Figure1-1). Then Phoebus Levene soon deciphered the chemical composition of DNA in 1919 (Levene, 1917, 1918, 1920; Levene and La Forge, 1912). However, the structure and function of DNA remained unclear. It became apparent by the early 1940s that mutagenic agents (such as ionizing and UV radiation) could damage hereditary material in cells. In 1944, Oswald Avery and his colleagues first demonstrated that DNA carries the hereditary material of the cell using the Avery-Macleod-McCarty experiment (Avery et al., 1944). Unfortunately, this theory was not well accepted by the scientific community, because most researchers believed protein was the hereditary material at that time. A breakthrough occurred in 1953 when James Watson and Francis Crick presented their double helix model of DNA structure (Watson and Crick, 1953). Shortly, Francis Crick proposed an “adaptor theory” that foretold the relationship between DNA, RNA, and protein. These soon lead to the discovery of replication mechanism and genetic codes (Crick et al., 1961), which finally confirmed that DNA is the blueprint of life.

As more is known about DNA, many DNA repair mechanisms surfaced. From the discovery of enzymatic photoactivation (EPR) in bacteria (Williams, 1957) to the validation of excision repair (ER) in both bacteria and mammalian cells (Lindahl, 1974; Rasmussen and Painter, 1964), it was becoming more clear that various kinds of DNA damaging and repair mechanisms occur naturally in cells. Achieving a balanced dynamic between DNA damage and repair is essential for cell survival. Henceforth, researchers have focused on deciphering these complicated mechanisms for decades.

### **1.1.2 DNA damage and response**

DNA damage is a naturally occurring event that causes alteration of the chemical structure of DNA. These DNA damages exist in various forms and can be caused by both

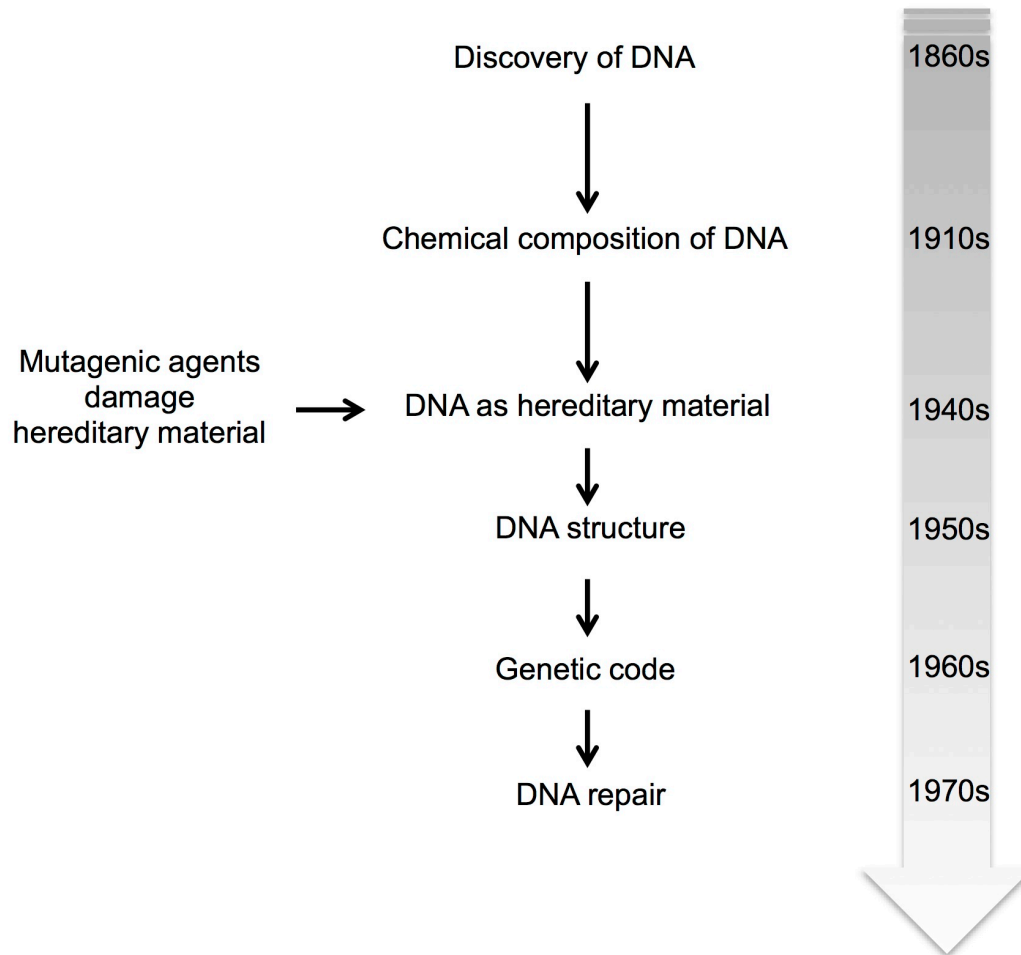


**Figure 1-1. Milestone events in the early history DNA research.**

This figure has only summarized major breakthroughs in DNA research field before 1980s.

endogenous cellular processes and exogenous sources (Figure 1-2). Spontaneous hydrolysis and oxidation are the two primary sources of endogenous DNA damage. They both occur up to  $10^4$  times per day per cell (De Bont and van Larebeke, 2004). Oxidation caused by active oxygen species mainly results in the formation of 8-hydroxyl-guanine (8oxoG) from guanine. This 8oxoG pairs with adenine instead of cytosine to generate a transversion mutation after replication (Chen et al., 1991; Kasai et al., 1984; Shibutani et al., 1991). Hydrolysis, on the other hand, comes in many forms. Depurination is the most typical hydrolysis reaction. It occurs through cleaving the  $\beta$ -N-glycosidic bond in DNA, which produces an apurinic (AP) site in DNA that alters its structure further (Lindahl and Andersson, 1972). Deamination is another form of hydrolysis, which mainly causes a base transition of cytosine to uracil in DNA (Lindahl, 1993). Besides, mismatches generated by DNA replication errors and base alkylations are also found on a daily basis. One of the examples is the methylation caused by S-adenosylmethionine (SAM). All these endogenous DNA lesions, which add up to  $10^5$  per cell per day in humans (Hoeijmakers, 2009), are in milder forms and can be handled by existing DNA repair mechanisms in cells.

On the other hand, exogenous DNA damages pose a bigger threat to genome stability. These include pyrimidine dimerization caused by exposure to ultraviolet light (UV) from sunlight, and single-strand break (SSB)/ double-strand break (DSB) caused by ionizing radiation (IR) from cosmic rays or natural decay of radionuclides, such as uranium, from our living environment. These also contain a huge variety of DNA adducts that are caused by exposure to various industrial chemicals in modern human life (Hoeijmakers, 2009; Swenberg et al., 2011).

If left unrepaired, DNA damage can activate cell death pathways, and result in apoptosis or senescence in cells (Choi et al., 2015; Hoeijmakers, 2009). Luckily, the cell has a complex DNA damage response machinery that allows it to quickly sense different DNA lesions, signal proper cellular responses, activate cell cycle checkpoint, and actively repair these DNA damages (Nowsheen and Yang, 2012) (Figure 1-3). However, DNA damage sometimes causes DNA replication or repair errors in rapidly dividing cells, thus resulting in DNA mutations. While many DNA mutations that alter functional proteins in cells are highly

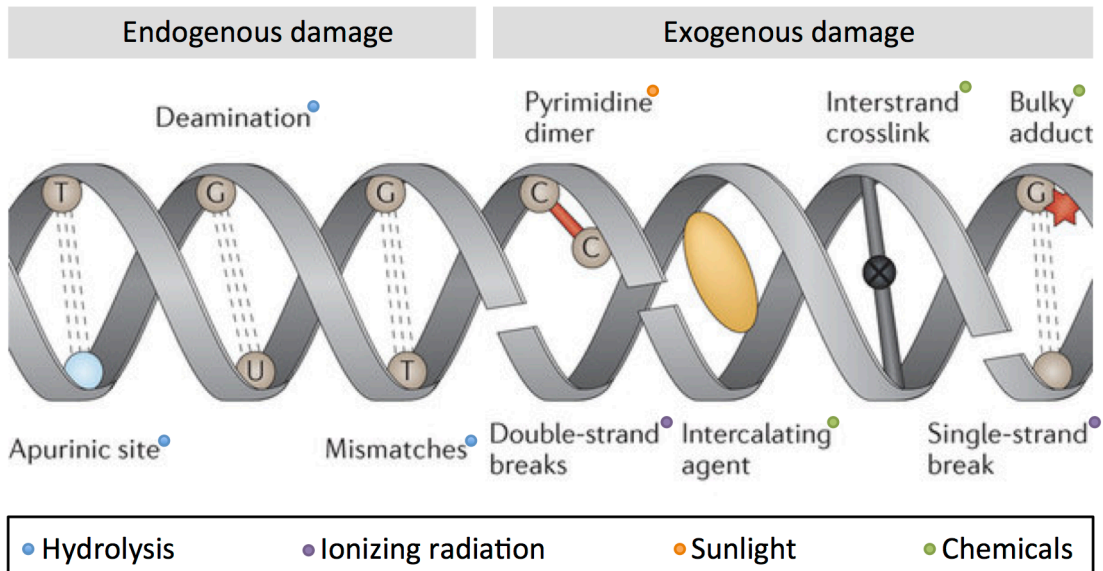


**Figure 1-2. Overview of different DNA damages in cell.**

Three forms of endogenous DNA damage and six forms of exogenous DNA damages are included here. Each type of DNA damage is color-coded based on its sources. Chemical compounds that can cause DNA damage includes platinum-based compound such as cisplatin, which leads to bulky adducts or inter-strand crosslinks; intercalating agents such as actinomycin-D; and DNA alkylating agents such as methyl methanesulphonate (MMS). This figure is adapted from (Helleday et al., 2014).

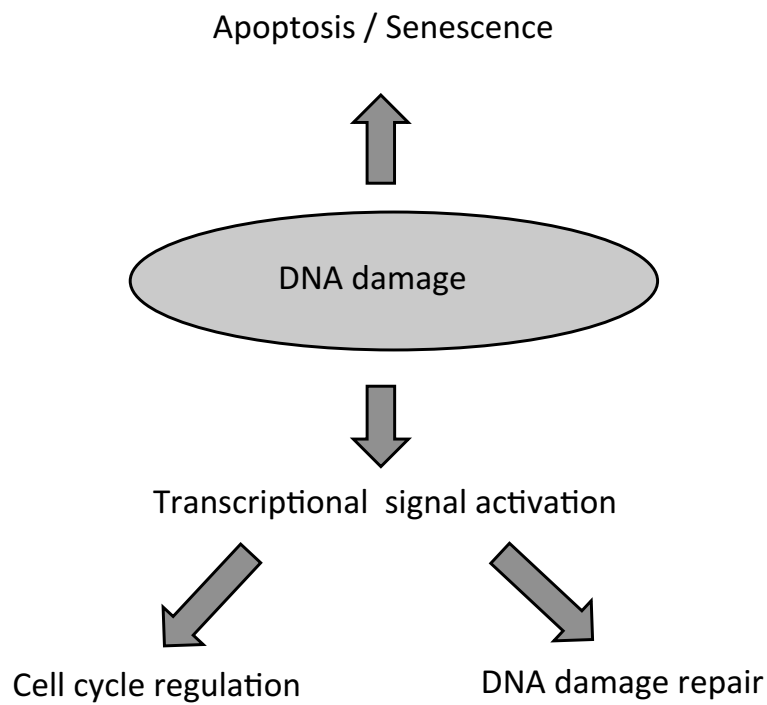


**Figure 1-3. Overview of DNA damage response.**

The oval shape represents the cell with damaged DNA, and the arrows point to different DDR events triggered by DNA damage signals in the cell.

associated with human diseases (Castilla et al., 1994), some mutations may also generate unique phenotypes with advantages such as resistance to HIV virus (Sullivan et al., 2001).

### **1.1.3 Cell cycle regulation**

To give the cells sufficient time to repair before division, DNA damage activates cell cycle checkpoints to pause the cells at G1/S or G2/M boundaries and intra-S phase. While many signal cascades are involved in the coordination of checkpoint and DNA repair processes in cells, the two major pathways are ATM-Chk2 and ATR-Chk1 pathways (Figure 1-4).

The ATM-Chk2 pathway is often activated at DNA damage induced DSB sites. After sensing the DNA damage signal, the inactive ATM in homodimer form dissociates into active monomer form with the help of intermolecular autophosphorylation (Bakkenist and Kastan, 2003). Acetylation of ATM by TIP60 acetyl-transferase further activates kinase activity of ATM (Lavin and Kozlov, 2007). After Mre11-Rad50-Nbs1 (MRN) protein complex assembles on DSB sites, the C-terminus of Nbs1 recruits ATM monomer through direct interaction (Falck et al., 2005; Lavin, 2008), and fully activates ATM at DSB sites to phosphorylate various local substrates (Fernandez-Capetillo et al., 2004; Lavin, 2008). One important local substrate of ATM is checkpoint kinase 2 (Chk2). After initial activation by ATM, Chk2 further activates itself by autophosphorylation (Oliver et al., 2006). Once fully activated, Chk2 can dissociate from DSB sites, travel through the nucleus, and pass the DNA damage signal downstream via phosphorylation of other substrates outside of the nucleus (Bartek and Lukas, 2003). For example, ATM can indirectly activate G1 checkpoint through phosphorylation of Chk2, since Chk2 can phosphorylate tumor suppressor protein p53 and stability regulator of p53 (MDMX) (Chehab et al., 2000). However, ATM can also phosphorylate other substrates that are not solely localized at DSB sites including p53. Phosphorylation of p53, MDM2, and MDMX by ATM directly triggers downstream G1 checkpoint activation (Chen et al., 2005; Lavin and Kozlov, 2007).

Replication errors or UV induced DNA damages often block the normal replication

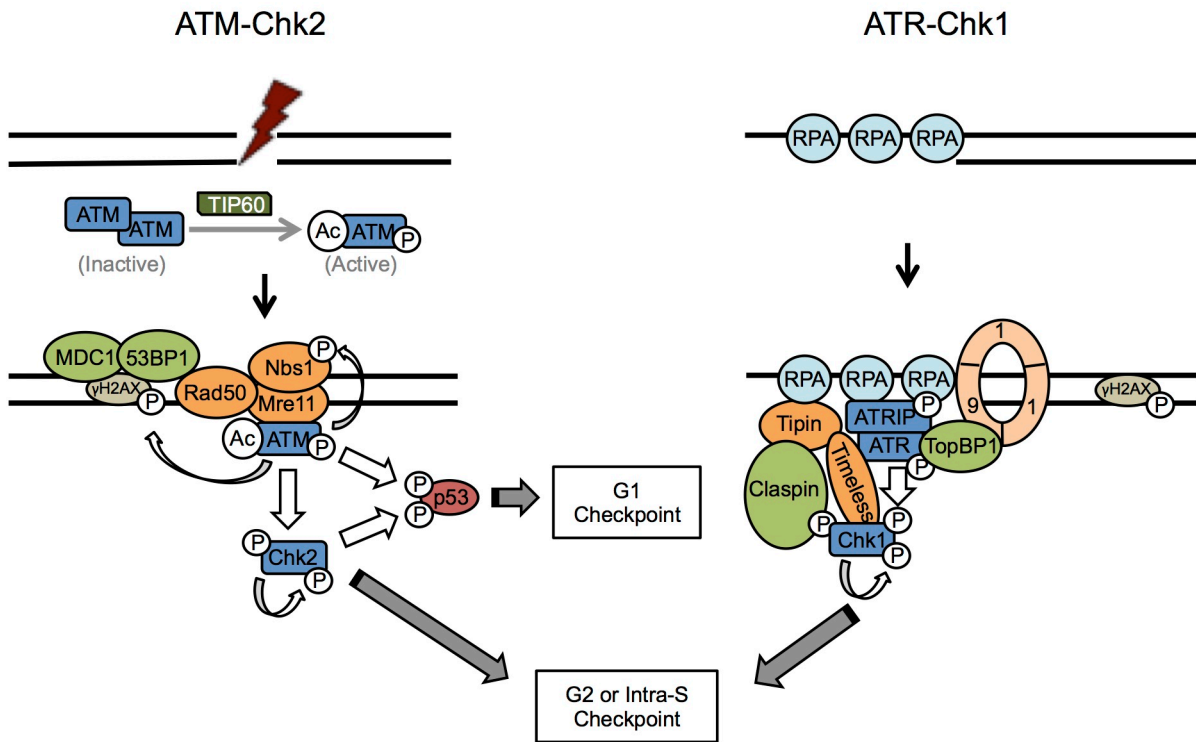


**Figure 1-4. Cell cycle checkpoint activation by ATM-Chk2 and ATR-Chk1 pathways.** The ATM-Chk2 pathway is active on DNA damage induced DSB site. The ATR-Chk1 pathway is active on RPA loaded ssDNA segment at replication arrest site. Many phosphorylation events occur within these two pathways, but only a few important events are shown in this figure. White arrows are pointing toward specific phosphorylation targets of individual kinases. This figure is adapted from (Smith et al., 2010).

process. The ATR-Chk1 pathway is then activated at the replication arrest site (Abraham, 2001). The uncoupled helicase and polymerase activity at this site can generate a single strand DNA (ssDNA) region that is quickly loaded by Replication Protein A (RPA) (Byun et al., 2005). The ATR: ATR Interacting Protein (ATRIP) complex is then recruited to RPA loaded ssDNA via interaction between ATRIP and RPA. Meanwhile, two critical mediator proteins that function in the ATR-Chk1 signal cascade, Topoisomerase II  $\beta$  Binding Protein 1 (TopBP1) and Claspin are also recruited. TopBP1 is brought to stalled replication forks with the help of Rad9-Hus1-Rad1 (9-1-1) complex (Delacroix et al., 2007; Greer et al., 2003). TopBP1 is a key regulator of DNA replication, checkpoint activation and damage response (Garcia et al., 2005; Wardlaw et al., 2014). While detailed functions of TopBP1 will be discussed later in this chapter (section 1.3.3), its effects on ATR-Chk1 signal cascade will be briefly summarized here. Through direct interaction with ATR, TopBP1 can activate ATR with its ATR activation domain (AAD), then additional contact between C terminal BRCT7/8 of TopBP1 and autophosphorylated ATR further stimulates ATR kinase activity (Liu et al., 2011). Claspin is recruited to the stalled replication fork by the Timeless-interacting protein (Timeless: Tipin) complex. While Timeless interacts with both ATR and Chk1, Tipin interacts with RPA and Claspin (Kemp et al., 2010). After phosphorylation by ATM, Claspin can recruit Chk1 to ssRPA loaded DNA (Jeong et al., 2003; Kumagai and Dunphy, 2003), where it is further stabilized by Timeless. As a result, it allows ATR to phosphorylate Chk1 directly (Kumagai et al., 2004). Similar to Chk2, after further activation through autophosphorylation (Kumagai et al., 2004), fully activated Chk1 is released from Claspin to act on downstream substrates that are from both nucleus and cytoplasm (Bartek and Lukas, 2003).

#### **1.1.4 DNA damage repair**

Many repair mechanisms exist in the cell to defeat different types of DNA damage (Table 1-1). The DNA replication errors are the targets of mismatch repair (MR) (Kolodner, 2016). While the small chemical alternations such as 7MeG can be fixed by direct reversal using methylguanine methyltransferase (MGMT) (Yarosh et al., 1984), bigger alterations

**Table 1-1. Summary of DNA Damage Repair Mechanisms**

Damage		Repair
DNA replication errors		Mismatch repair (MR)
Oxidations	8oxoG	Base excision repair (BER)
Chemical alterations	7MeG	Methyl guanine methyl transferase (MGMT)
	Bulk DNA adducts	Nucleotide excision repair (NER)
	Pyrimidine dimer	
Single strand breaks (SSB)		Base excision repair (BER)
Double strand breaks (DSB)		Non-homologous end joining (NHEJ) or Homologous recombination (HR)

such as bulky DNA adducts or pyrimidine dimers are corrected by nucleotide excision repair (NER) (Scharer, 2013). Other small lesions from 8oxoG to SSBs can all be resolved by base excision repair (BER) (Lu et al., 2001; Wallace, 2014).

Two pathways can be used to repair the more complex DSBs lesions: Non-Homologous End Joining (NHEJ) and Homologous Recombination (HR) (Le Guen et al., 2015) (Figure 1-5). NHEJ occurs throughout the cell cycle and repairs most DSBs in mammalian cells. It can directly ligate DNA ends in an unconventional manner without the presence of template DNA. At induced DSBs, NHEJ starts with the recruitment of the Ku70/80 heterodimer to the double-strand DNA (dsDNA) ends. This Ku: DNA end complex then acts as a scaffold that recruits other NHEJ proteins (Lieber, 2010). The DNA dependent protein kinase catalytic subunit (DNA PKcs) complexes with Artemis on dsDNA ends and phosphorylates Artemis to activate its endonuclease activity (Goodarzi et al., 2006; Ma et al., 2002). DNA PKcs also phosphorylates other NHEJ proteins, including Ku70/80, DNA Ligase VI, X-ray cross complementing protein 4 (XRCC4), and XRCC4 like factor (XFL). But all these phosphorylation are proved to be unnecessary for proper NHEJ *in vivo* (Wang et al., 2004; Yu et al., 2008; Yu et al., 2003). After the DNA Pkcs: Artemis complex trims off damaged DNA overhangs, further processing of DNA ends may be done by other factors such as polymerase  $\mu$  and  $\lambda$  (Ma et al., 2004). Finally, autophosphorylation of DNA PKcs relieves the DNA Pkcs: Artemis complex, allowing the XRCC4: Ligase VI: XFL complex to complete the ligation of DNA ends (Blackford and Jackson, 2017; Gu et al., 2007). The leftover Ku70/80 will likely get degraded from DNA after ubiquitination (Feng and Chen, 2012).

On the contrary, HR only occurs in late S phase to G2 phase of the cell cycle (Krejci et al., 2012). Recruitment of breast cancer associated proteins 1 and 2 (BRCA1 and BRCA2) is critical for the activation of HR. After rapid recruitment of the Mre11-Rad50-Nbs1 complex to the DSB site, the MRN complex recruits CtBP-interacting Protein (CtIP) and initiates 5' to 3' resection of DNA through the nuclease activity of Mre11 (Williams et al., 2007). The CtIP can then recruit BRCA1 directly after phosphorylation activation by ATM (Yun and Hiom, 2009). However, the ubiquitination pathway can also promote recruitment of BRCA1 (Huen et al., 2010). Through interaction with Nbs1 and phosphorylated  $\gamma$ H2A

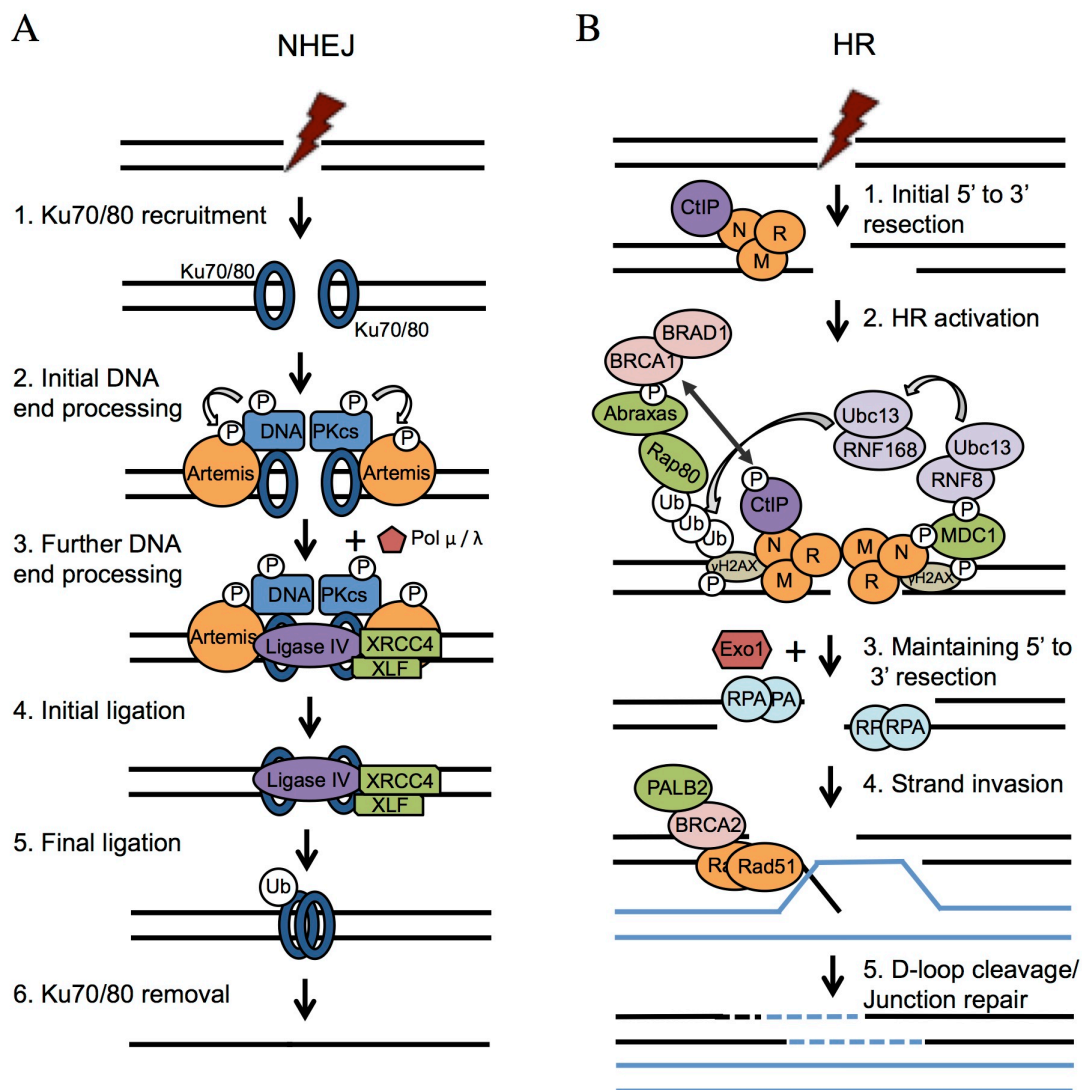


**Figure 1-5. Overview of the two major DNA DSB repair mechanisms.**

(A) NHEJ pathway. This pathway is mainly activated by the recruitment of Ku70/80 and kinase activity of DNA PKcs. Important phosphorylation events are highlighted by white arrows. (B) HR pathway. This pathway is mainly activated by the recruitment of MRN complex to initiate 5' to 3' DNA resection. While phosphorylation by ATM activates most proteins in this pathway, MDC1 phosphorylation by CK2 also plays important role in the activation of ubiquitination signal cascade. The interaction between BRCA1 and CtIP is highlighted by double-arrrowed line, and the sequential activation of ubiquitination pathways are highlighted by grey arrows. Panel A is adapted from figure 3 of existing paper (Blackford and Jackson, 2017).

/H2AX, the mediator of DNA damage checkpoint protein 1 (MDC1) is recruited to DSB. Then MDC1 is phosphorylated by Casein Kinase 2 (CK2) to recruit RNF8. While RNF8/Ubc13 activates ubiquitination signal cascade by building K63 linked ubiquitin on H2A/H2AX, RNF168/ Ubc13 amplifies this ubiquitin chain. This polyubiquitin chain recruits Rap80, which interact with Abraxas from the BRCA1-A complex (Li et al., 2017), and finally, brings BRCA1 to the DSB site. After further DNA resection with the 5' to 3' endonuclease Exo1, loading of RPA onto ssDNA can temporarily maintain the DNA resection on the DSB site (Wold, 1997). Depending on the stage of cell cycle, cells can choose to either activate the checkpoint with the help of ATR or proceed into HR directly. Further activation of HR requires the recruitment of BRCA2 to DSB site by BRCA1 via the partner and localizer of BRCA2 (PALB2) (Anantha et al., 2017). BRCA2 then recruits Rad51 to activate strand invasion and form a D-loop on the DNA (Esashi et al., 2005; Galkin et al., 2005). This D-loop can either be cleaved directly (West, 2003) or form a Holliday junction that can be repaired through resolution (Ciccia et al., 2008; Fekairi et al., 2009) or dissolution (Bizard and Hickson, 2014).

## **1.2 Genomic instability and cancer**

### **1.2.1 Genomic instability and diseases**

Genome instability refers to alternations to the genome of cell lineage that ranges from mutations in nucleic acid sequence to chromosomal rearrangements (Aguilera and Gomez-Gonzalez, 2008). Since preservation of genome integrity is critical for cell homeostasis, genome instability can lead to many pathological disorders in human (Table 1-2).

The human nervous system is highly susceptible to oxidative stress because neurons generally exhibit high mitochondrial respiration, and produce many reactive oxygen species that can cause DNA damage (Weissman et al., 2007). Unrepaired DNA lesions in neurons can cause many aging-related neurodegenerative disorders, such as Alzheimer's and Parkinson's diseases (Kulkarni and Wilson, 2008). Moreover, alteration to DNA Trinucleotide Repeats (TNRs) can result in neurological and muscular diseases, including

**Table 1-2. DDR Defects and Genomic Instability Diseases**

Syndrome/Disease	Phenotype	Gene Mutation
Parkinson's disease	Tremor, posture rigidity and postural instability, degeneration of dopaminergic neurons in substantia nigra area	Mutations in $\alpha$ -Synuclein and Parkin variants
Alzheimer's disease	Progressive neuro-degeneration leading to dementia, memory loss and cognitive decline	Increased oxidative stress and damage
Hungtinton's disease	Progressive chorea and dementia, severe neuronal loss in the striatum and cerebral cortex	CAG repeat expansion in <i>huntingtin (HD)</i>
Friedreich's ataxias	Limb ataxia, cerebellar dysarthria, sensory loss, skeletal deformities	GAA repeat expansion in <i>frataxin (FXN)</i>
spinocerebellar ataxias	Similar to Huntington's disease, progressive neuron loss	CAG repeat expansion in various genes
ataxia telangiectasia (AT)	Telangiectases, cerebellar ataxia, immunodeficiency, predisposition to malignancy	ATM
AT-like disorder	Mild A-T like features, possibly cancer predisposed	Mre11
Nijmegen breakage syndrome (NBS)	Microcephaly, growth retardation, mental retardation, immunodeficiency, cancer predisposition	Nbs1
NBS-like disorder	NBS-like phenotype	Rad50
Bloom's syndrome	Microcephaly, growth retardation, mental retardation, immunodeficiency, predisposition to all cancers	BLM
Werner's syndrome	Premature ageing, cancer predisposition	WRN

\* Adapted from (Jakson and Bartek, 2006)

myotonic dystrophy, fragile X syndrome, Kennedy's disease, Huntington's disease, Friedreich's ataxia and spinocerebellar ataxia (Castel et al., 2010). However, mutations in DDR proteins can also result in many other diseases. For instance, the ataxia telangiectasia (AT) patients with mutated ATM, and the AT-like disorder patients with mutated Mre11 have not only cerebellar ataxia but also experience many immune defects. Similar immunodeficiency is found in the Nijmegen breakage syndrome (NBS) the ataxia telangiectasia (AT) patients with mutated ATM, and the AT-like disorder patients with mutated Mre11 have not only cerebellar ataxia but also experience many immune defects. Similar immunodeficiency is found in the Nijmegen breakage syndrome (NBS) patients with Nbs1 mutation, and the NBS-like patients with Rad50 mutation (Maciejczyk et al., 2017). In addition, they also suffer growth retardation or premature aging, another common symptom that can be found in other genomic instability diseases, especially DNA helicase deficiency syndromes, such as Bloom's syndrome and Werner's syndrome (de Renty and Ellis, 2017). Nevertheless, the most common feature, shared between most genomic instability diseases, is the predisposition to cancer.

### **1.2.2 Cancer**

Cancer is not a single disease, but a group of related disorders characterized by abnormal cells that divide without control and invade neighboring tissues. Indeed, exogenous DNA-damaging agents, such as tobacco smoke (Phillips and Venitt, 2012), may overload the DNA repair pathways, and result in cancers, especially lung (Warren and Cummings, 2013) and colon cancer (Cancer Genome Atlas, 2012). However, inherited mutations in many DDR proteins that impair proper DNA repair are often directly associated with increased risk of many different types of cancer in humans (Table1-3). For example, mutations in MutL and Mut S homologs that impair MR (Truninger et al., 2005), and mutations in MutY homolog that impair BER can both lead to colorectal cancer as well (Cleary et al., 2009). BRCA1/BRCA2 mutations that result in HR defect are also well-known examples (Nagaraju and Scully, 2007), as they are the leading causes of familial breast and ovarian cancer in women (King et al., 2003). While mutations in some HR/NHEJ related proteins, such as

**Table 1-3. Inherited DDR Protein Mutations Associate with Increased Cancer Risks**

Mutation Gene	Effectuated DDR Pathway	Cancer type
MSH2, MSH6, MSL1	MR	Colon cancer
MUTYH	BER	Colon cancer
XPA, XPB, XPC, XPD, XPE, XPF, XPG	NER	Skin cancer
BRCA1/BRCA2	HR	Breast or ovarian cancer
Mre11	HR or NHEJ	Breast cancer
Nbs1	NHEJ	Lymphoid cancer
ATM	HR or NHEJ	Leukemia, lymphomas, breast cancer
ATR	Likely HR	Acute myelogenous leukemia (AML)
BLM	HR	Leukemia, lymphomas, carcinoma in lung, colon, skin, etc
WRN	HR, NHEJ or BER	Sarcoma, colorectal, skin, thyroid and pancreatic cancer
RECQ	Likely HR	Skin cancer, osteosarcoma
FANC	HR or TLS	Leukemia, liver tumor

ATM or Mre11, might also alter the risk of breast cancer, they are often associated with increased risk of other lymphoid cancers (Bartkova et al., 2008; Rothblum-Oviatt et al., 2016). Mutations in other HR-related proteins, including ATR and Fanconi's Anemia (FANC) proteins, are also highly associated with leukemia. Skin cancer is another common disease related to DDR defect. Mutations in xeroderma pigmentosa (XP) proteins that impair NER (Lambert and Lambert, 2015), or mutations in DNA helicases, such as BLM, WRN and RecQ, that impair HR can all result in elevated risk of skin cancer (Arora et al., 2014; Chun et al., 2011; Monnat, 2010).

### **1.2.3 DNA damaging cancer therapy: a double-edged sword**

Although exogenous DNA damage and DDR deficiencies can both result in cancers, further stimulation by DNA damaging agents can easily activate apoptotic signal cascades in cancer cells and trigger cell death in cancer cells, but not in normal cells. Therefore, in addition to surgery, immunotherapy, cytotoxic chemotherapy, targeted therapy and hormonal therapy, DNA damaging therapies are often engaged in cancer treatments. The DNA damaging treatments can be employed in two forms: radiotherapy and chemotherapy (Figure 1-6).

Ionizing radiation (IR) that generates various strand breaks in DNA is often used in radiotherapy of cancer patients. It can be utilized both to cure cancer directly, and as a palliative treatment to reduce symptoms caused by cancer. About 50% of all cancer patients will receive radiotherapy during their treatment (Delaney et al., 2005). Limited by their differences in sensitivity to radiation, not all cancer can be cured directly with radiotherapy. Examples of early cancers that can be cured by IR alone included prostate carcinomas, cervical carcinomas, non-small cell lung carcinomas and head and neck carcinomas. Other cancers such as breast carcinomas, bladder carcinomas and locally advanced cervix, lung or head and neck carcinomas are also curable under radiation, but only in combination with other treatment modalities (Baskar et al., 2012). When used in conjunction with surgery, radiation can be used to either shrink the tumor before surgery or to destroy remaining microscopic tumor cells after surgery. However, since IR damages both cancer cells and the

normal cells, increased DNA lesions in the normal cells may give rise to other diseases in cancer patients. For instance, radiotherapy for breast and lung cancer often result in exposure of heart to some radiation, thus elevated the risk of heart disease in the patient (Ming et al., 2016; Taylor and Kirby, 2015).

Similar to radiotherapy, chemotherapy can also be used either with curative intent or as a palliative treatment to reduce cancer symptoms and prolong life. Traditional chemotherapy often uses cytotoxic agents to interfere with cell mitosis. Since the cancer cell exhibits uncontrolled rapid cell division, they are typically more susceptible to these agents than the normal cell. However, normal cells from bone marrow, hair follicles or digestive tracts that divide rapidly are often sensitive to anti-mitotic drugs as well. Hence, common side effects of traditional chemotherapy included myelosuppression, mucositis, and alopecia (Barreto et al., 2014; Shin et al., 2015; Toucheffeu et al., 2014). To encounter this lack of specificity, three other chemotherapies are developed: hormonal therapy and targeted therapy that both aim to inhibit abnormal cell growth and DNA damaging chemotherapy that target to induce DNA lesions and promote cell death (Figure 1-6).

DNA damaging chemotherapeutic agents varies from the alkylating agents such as cyclophosphamide that promote DNA alkylation (Puyo et al., 2014), to platinum-based compounds that cross-link with DNA, and anthracyclines that induce DNA strand breaks (Jaffe, 2014). Although these compounds may also cause DNA damage in normal cells, they are more lethal to cancer cells. Because cancer cells often carry mutations in DDR proteins that inhibit their proper function, these defective DDR proteins can impair their downstream DNA repair signal cascades. In fact, proper selection of chemotherapeutic agents based on known DDR protein defects in the patient allows clinicians to target tumor cells selectively by inducing specific DNA lesions that only tumor cells are unable to repair. This more personalized DNA damaging chemotherapy can improve the treatment efficiency significantly. Moreover, when used in combination with other treatments such as radiation or cytotoxic chemotherapy, it may also help to lower the dose level of other treatments and reduced unwanted side effect. For example, mutations in breast cancer associated genes BRCA1 and BRCA2 are highly associated with not only breast and ovarian cancer but also other types of cancer. Meanwhile, BRCA1 and BRCA2 proteins both play important roles in

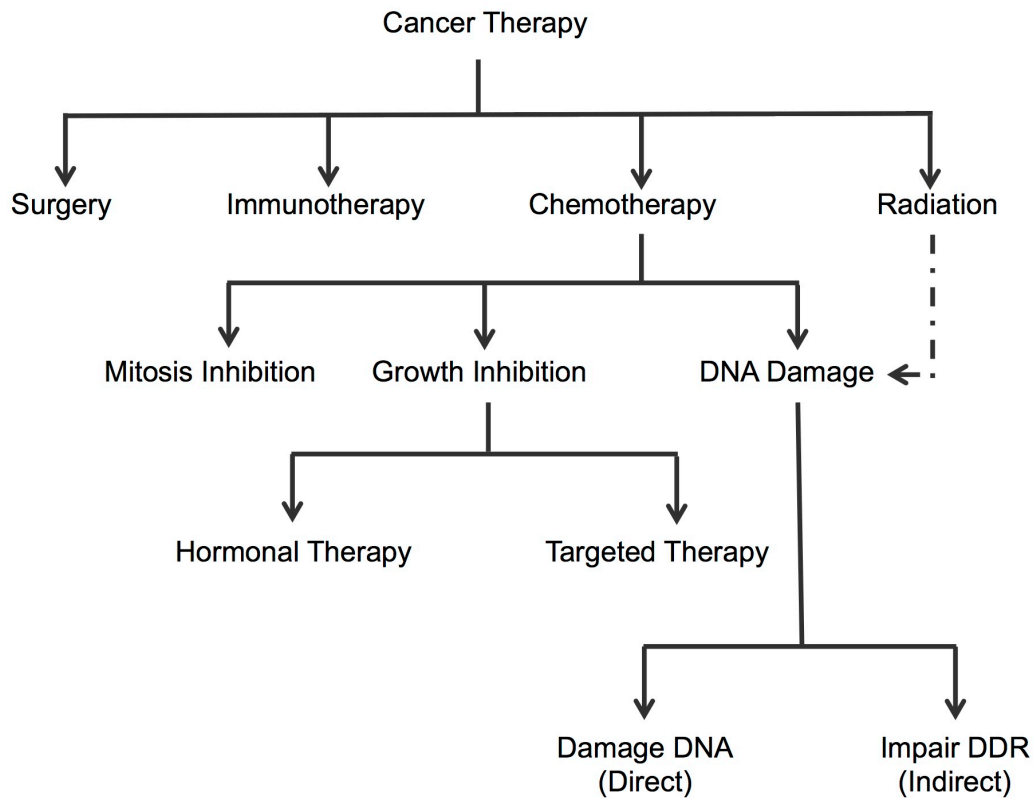


**Figure 1-6. Outline of modern cancer therapies.**

The modern cancer therapies are categorized into four major types based on their different treatment methods. Surgery normally involves removal of tumors and surrounding tissues directly. Immunotherapy utilizes existing immune systems of cancer patients to target tumor cells, and this treatment is mainly antibody based. Chemotherapy uses various chemical compounds as drugs to suppress cancer cell aggression or kill cancer cells. Radiation aims to induce tumor death by ionizing radiation. This is also a type of DNA damaging therapy because IR aims to trigger programmed cell death by damaging cellular DNAs. Although both targeting inhibition of tumor cell growth, hormonal therapy aims to inhibit growth-related hormones while targeted therapy aims to inhibit other players that affect tumor growth, such as tyrosine kinase receptor-associated proteins.

HR, a DNA repair pathway that is mainly responsible for accurate removal of double-strand damages such as DSBs and inter-strand cross-links. Therefore, patients with BRCA1/BRCA2 defects often respond better to chemotherapy containing anthracyclines such as Doxorubicin that induces strand-breaks (Fourquet et al., 2009), or platinum-based compound such as cisplatin that causes inter-strand cross-links (Narod, 2010).

Aside from chemicals agents that directly damage DNA in cells, compounds that aim to induce DDR defect through inhibition of other DDR proteins also has great therapeutic potential in cancer treatments. These compounds include not only the inhibitors of various DNA damage repair mechanisms but also the inhibitors of DNA replication and cell cycle checkpoint activation. While most of them are still developed under the experimental stage, some are already in preclinical or clinical trials. These included novel ATR inhibitors, NU6027 and VE-821 (Peasland et al., 2011; Prevo et al., 2012), and the Chk1 inhibitor SCH90077 (Garrett and Collins, 2011). Synthetic lethality, a term developed by geneticists to describe the situation where the individual defect of two genes has little effect on the cell, but the combined defects of two genes together trigger cell death, became a popular concept in the field of cancer biology (Garber, 2002). When tumor cells carry certain DDR protein defect that impairs one of the DNA repair pathways, the cell will likely rely more on the remaining DNA repair pathways for survival. Therefore, compounds that target inhibition of the remaining DNA repair may also be useful drugs for selective killing of these tumor cells. The most successful example of synthetic lethality approach in DNA damaging cancer treatment is the use of poly ADP-ribose polymerase inhibitors (PARPis) against tumors with BRCA1 or BRCA2 deficiency (Figure 1-7) (Bryant et al., 2005; Farmer et al., 2005).

PARP1 and PARP2 are both important proteins activated by DNA damage in cells. They play critical roles in the activation of SSB repair, especially BER. As members of the PARP family of proteins, they are both enzymes that catalyze the synthesis of (poly ADP-ribose) PAR chain on target proteins. PARP inhibitors were initially developed as part of a combinational therapy to sensitize cancer cell to radiation or other chemotherapy that directly induce DNA damages (Purnell and Whish, 1980). The first PARPi used in human clinical trials, rucaparib (Rubraca, Clouis), also works as a sensitizer in combination with a DNA alkylating agent, temozolomide, to treat patients with advanced metastatic melanoma

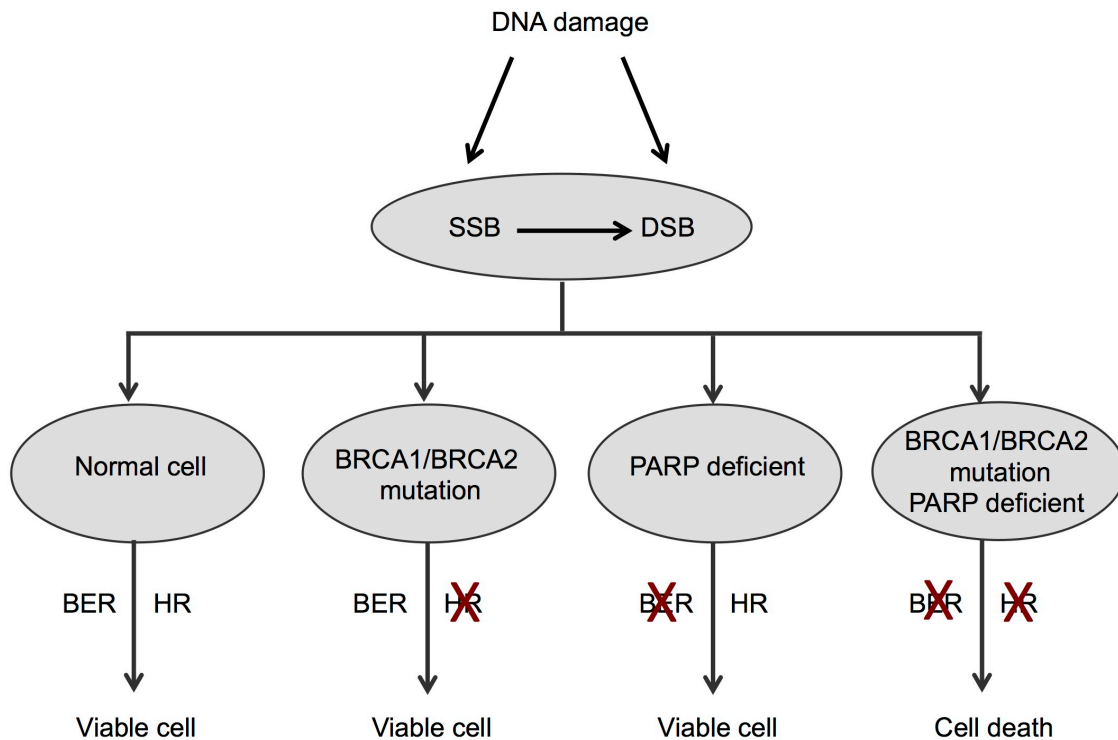


**Figure 1-7. Synthetic lethality with PARP inhibitor.**

DNA damage that naturally occurs in cells or induced by DNA damaging cancer therapy can lead to both SSBs and DSBs in DNA. In normal cells, BER and HR can repair all existing DNA strand breaks collaboratively to preserve viable cells. Even exposure to low doses of DNA damaging treatment may be tolerated by these cells. In tumor cells with BRCA1/BRCA2 mutations that result in HR deficiency, cells rely more on BER that can still resolve all SSBs. Therefore, tumor cells with a limited amount of DSB may be less healthy, but they are still viable. In tumor cells without BRCA1/BRCA2 mutations, although PARP inhibitor can impair BER, the unrepaired SSBs can be transformed to DSBs that are then repaired by HR. Therefore, these tumor cells are less susceptible to PARP inhibitor treatment. In cancer cells with BRCA1/BRCA2 mutations that cause HR deficiency, PARP inhibitors can impair BER too. Together, they result in the efficient killing of cancer cells. Figure adapted from (Comen and Robson, 2010).

(Plummer et al., 2008). However, Olaparib (Lynparza, AstraZeneca) is the first PARPi that has gained the U.S. Food and Drug Administration (FDA) approval as a treatment for patients with advanced ovarian cancer (Kim et al., 2015). This is because Olaparib offers effective treatment for breast and ovarian cancer patients with HR-deficient BRCA mutations using the synthetic lethality mechanism (Bryant et al., 2005; Farmer et al., 2005). Since PARP1 plays a critical role in activation of BER, inhibition of PARP1 leads to over-accumulation of SSBs, which can be converted to DSBs in replicating cells. As these DSBs cannot be adequately repaired either due to the HR defects in BRCA1/2 mutant cells, the application of PARPi itself can selectively kill these BRCA1/BRCA2 deficient cancer cell via synthetic lethality. Benefiting from this selectivity, Olaparib offers similar treatment efficacy in comparison with other conventional chemotherapies, but with much lighter side effects (Fong et al., 2009). Currently, researchers are further exploring the clinical potential of Olaparib in treating other cancers, such as colorectal or prostate cancers (Morra et al., 2017; Xu et al., 2015). Meanwhile, other PARPi drugs also shows great therapeutic potential in cancer treatment. Both niraparib (Zejula, TESARO) and rucaparib have gained FDA approval in cancer treatments, while talazoparib (Pfizer) is currently under stage III clinical trial (Lord and Ashworth, 2017).

### **1.3 BRCT family proteins**

#### **1.3.1 BRCT family proteins**

Initially identified in breast cancer associated protein BRCA1, the BRCA1 C terminal (BRCT) domain was soon found to characterize a family of proteins that is named BRCT family proteins (Koonin et al., 1996). Although the sequence conservation between BRCT family proteins is fairly low, most of these proteins are involved in the DDR signal cascades (Bork et al., 1997) (Figure 1-8). Therefore, deciphering the structural and functional features of these proteins can be beneficial for many genome instability diseases including cancer. The first crystal structure of BRCT domain solved was the N-terminal BRCT domain of X-ray repair cross-complementing protein 1 (XRCC1) (Zhang et al., 1998). This structure features four  $\beta$ -strands in the center with one  $\alpha$ -helix on one side and two  $\alpha$ -helices on the

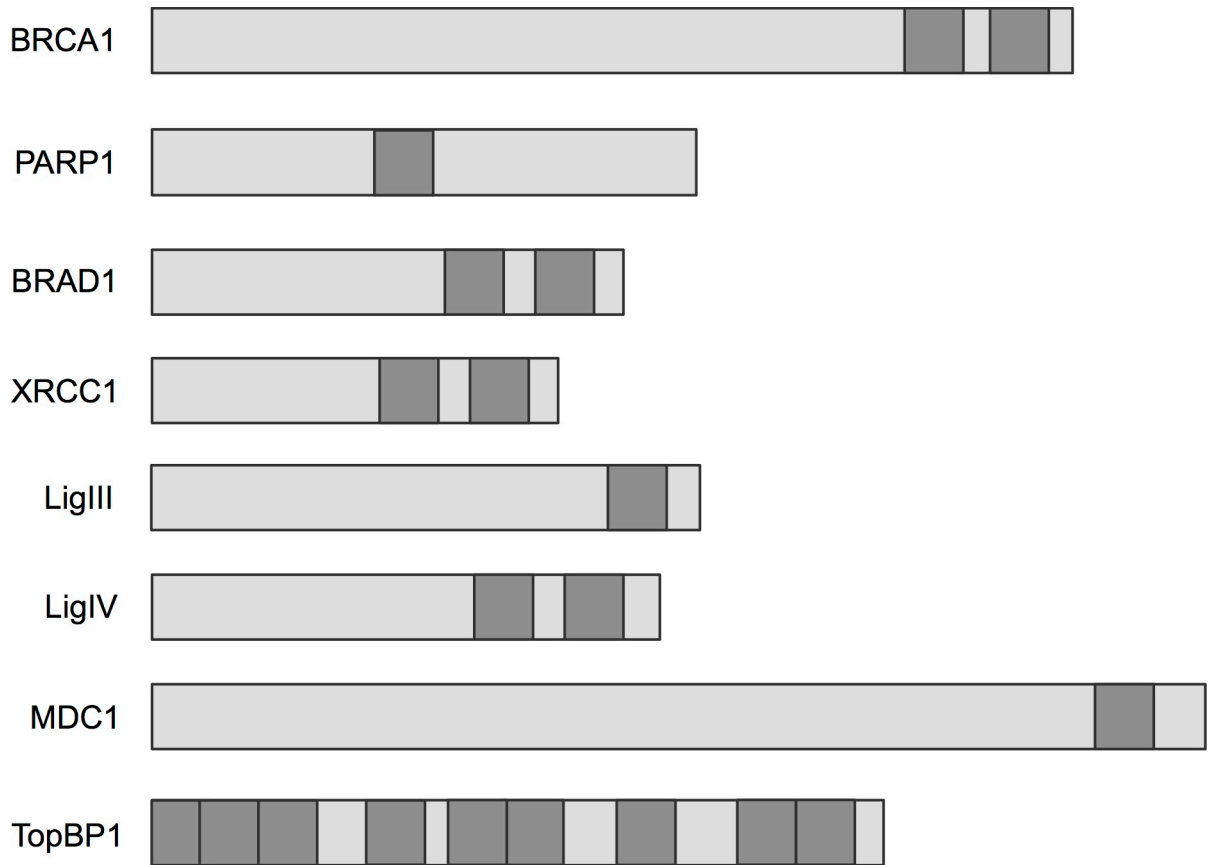


**Figure 1-8. Examples of BRCT family proteins.**

The length of each light grey bar reflects the known protein sequences length of each protein. Grey boxes indicate the BRCT domains.

opposite side. Although BRCT domains of other proteins adopt these general structural features of XRCC1 BRCT, their functional architecture varies. In general, there are two types of BRCT architectures: Single BRCT and tandem BRCTs. Single BRCT domain means there is only one BRCT, such as in PARP1 or DNA ligase III proteins. But it also refers to multiple distinct singular BRCTs isolated by other functional domains, like the BRCT3 and BRCT6 of TopBP1. Tandem BRCTs refers to multiple BRCT domains that function together as a whole. A classical example of tandem BRCTs is BRCA1 BRCTs, which will be discussed in detail in the next section (Section 1.3.2). Interestingly, the BRCT-BRCT domain packing of BRCA1, which consists of hydrophobic residues from the  $\alpha_2$  helix of the N-terminal BRCT, and  $\alpha_1'$  and  $\alpha_3'$  helices of the C-terminal BRCT, is conserved in several other BRCT family proteins (Williams et al., 2001). These include MDC1, BRCA1-associated RING domain protein 1 (BARD1) and TopBP1 BRCT7/8 (Birrane et al., 2007; Lee et al., 2005; Rappas et al., 2011). Another common feature of all these tandem BRCT structures is that they all contain a phosphate-binding pocket that can be used to interact with many phosphorylated protein partners. On the contrary, a single BRCT domain often lacks the ability to engage phosphorylated protein partner. For instance, the phosphate-binding pocket that is well conserved between tandem BRCTs is absent in both TopBP1 BRCT6 and Ligase III BRCT (Leung et al., 2010; Tomkinson and Sallmyr, 2013). Instead, single BRCTs are found to interact with many other partners, including DNA and PAR chains. It has been shown that replication factor C (RFC) p140 and NAD<sup>+</sup> ligase can both interact with DNA (Feng et al., 2004; Kobayashi et al., 2006), while XRCC1 BRCT1 and TopBP1 BRCT6 have both been implied to interact with PAR (Pleschke et al., 2000). Tandem BRCTs, such as BRCA1 BRCTs and TopBP1 BRCTs, have been suggested to interact with DNA as well (Acevedo et al., 2016; Choi et al., 2009; Simons et al., 2006). Moreover, BRCT family proteins may also interact with each other via their BRCT. For example, the interaction between single BRCT domain of ligase III and the BRCT2 of XRCC1 allows them to function together in base excision repair (Tomkinson and Sallmyr, 2013). These various interactions of BRCT domains perhaps explain why many BRCT family proteins act as scaffold proteins and play complicated roles in multiple DDR signal cascades.

### 1.3.2 BRCA1

BRCA1 is a well-known tumor suppressor protein that is mainly involved in the HR pathway. Patients with familial breast or ovarian cancer often carry mutations in BRCA1 (Castilla et al., 1994; Futreal et al., 1994; Miki et al., 1994). In addition to the tandem BRCT domains, it also contains an N-terminal RING domain, a coiled-coil (CC) domain and a region enriched in nucleus localization signals (NLS) (Figure 1-9A). As mentioned in the last section (1.3.1), the BRCT domain of BRCA1 can interact with many phosphorylated protein partners. While the interaction of tandem BRCTs with Abraxas and CtIP both assist in the recruitment of BRCA1 to DNA damage site (Wu et al., 2016; Yun and Hiom, 2009), the BRCA1 BRCTs interaction with BRCA1 associated C-terminal helicase/Fanconi Anemia J group proteins (BACH1/FANCI) also play important role in proper activation of DDR (Cantor et al., 2001). The RING domain of BRCA1 can interact with a similar RING domain of BARD1 (Wu et al., 1996), and forms a complex that has substantial ubiquitin ligase activity (Densham et al., 2016). Recently, this BRCA1/BARD1 complex was also found to enhance recombinase activity of Rad51 via direct interactions, thus promoting the DNA invasion in HR (Zhao et al., 2017). The CC domain of BRCA1 can also assist in HR activation. It interacts with PALB2, which bridges the recruitment of BRCA2 to DNA damage sites (Sy et al., 2009). Since inhibitors that target any of these three functional domains of BRCA1 can result in HR deficiency, they have great potential as chemotherapeutic agents. Not only can these BRCA1 inhibitors improve the sensitivity of tumor cell to general DNA DSB inducing chemo-reagents such as Cisplatin and Doxorubicin, but they can also be used in combination with PARP inhibitors to directly kill tumor cells through synthetic lethality (Figure 1-10) (Anantha et al., 2017).

The tandem BRCTs domain has been the primary target for BRCA1 inhibitor drug design for years (Anisimov et al., 2011; Joseph et al., 2010; Lokesh et al., 2007; Lokesh et al., 2006; Pessetto et al., 2012; Yuan et al., 2011) The tandem BRCTs domain of BRCA1 has distinct structural features that allow it to specifically target a pS-X-X-F motif of the phosphorylated peptide (Figure 1-9B). The N terminal BRCT has a phosphate-binding pocket formed by Gly1656, Ser1655, Thr1700 and Lys1702. While the main chain NH of Gly1656

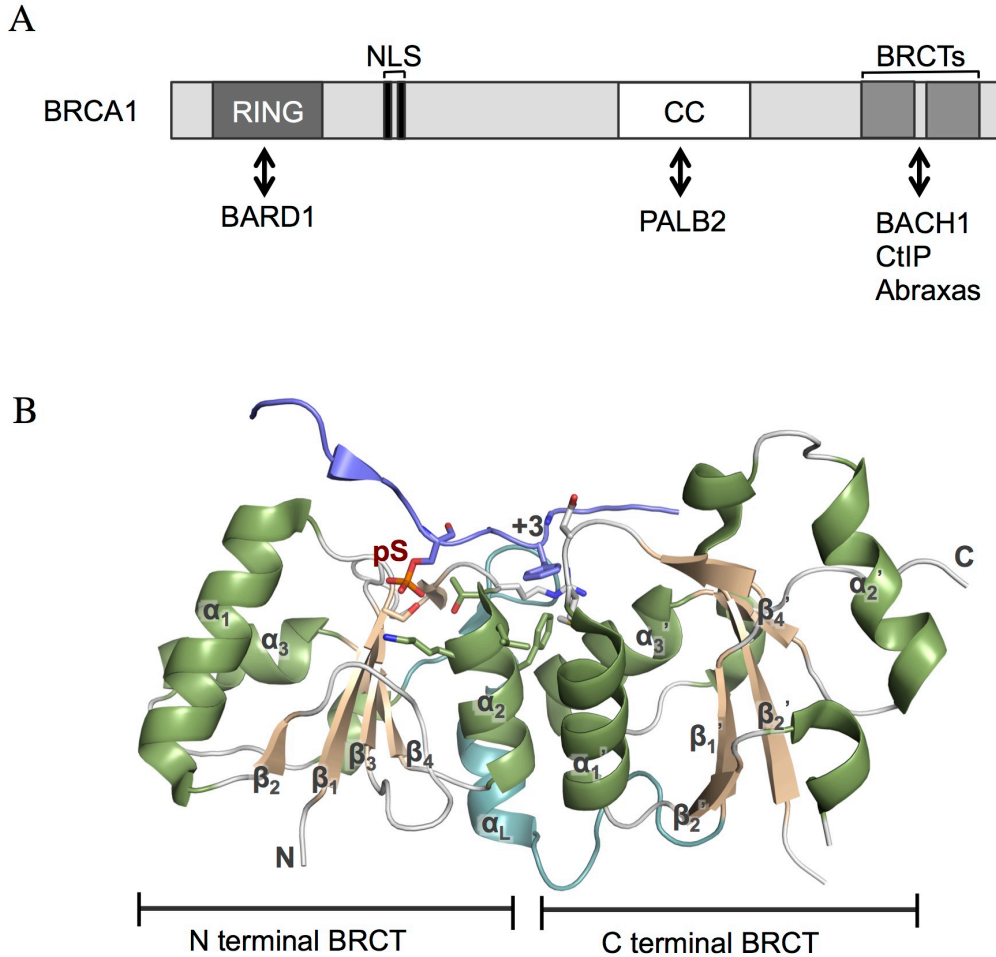


**Figure 1-9. BRCA1 BRCT is a good target for HR inhibitor.**

(A) Outline of functional domains in BRCA1 and their protein interaction partners. (B) Structural overview of BRCA1 BRCT interaction with phosphorylated protein partners. The figure is made using Pymol with known X-ray structure of BRCA1 BRCT in complex with pS-x-x-F motif containing peptide (PDB ID: 1T2V). Helices are colored green, beta sheets are colored orange, and the linker region between two BRCTs is colored light blue. The phosphorylated peptide is colored dark blue. Important residues from pSer and +3 Phe binding pockets are all highlighted in stick representation.

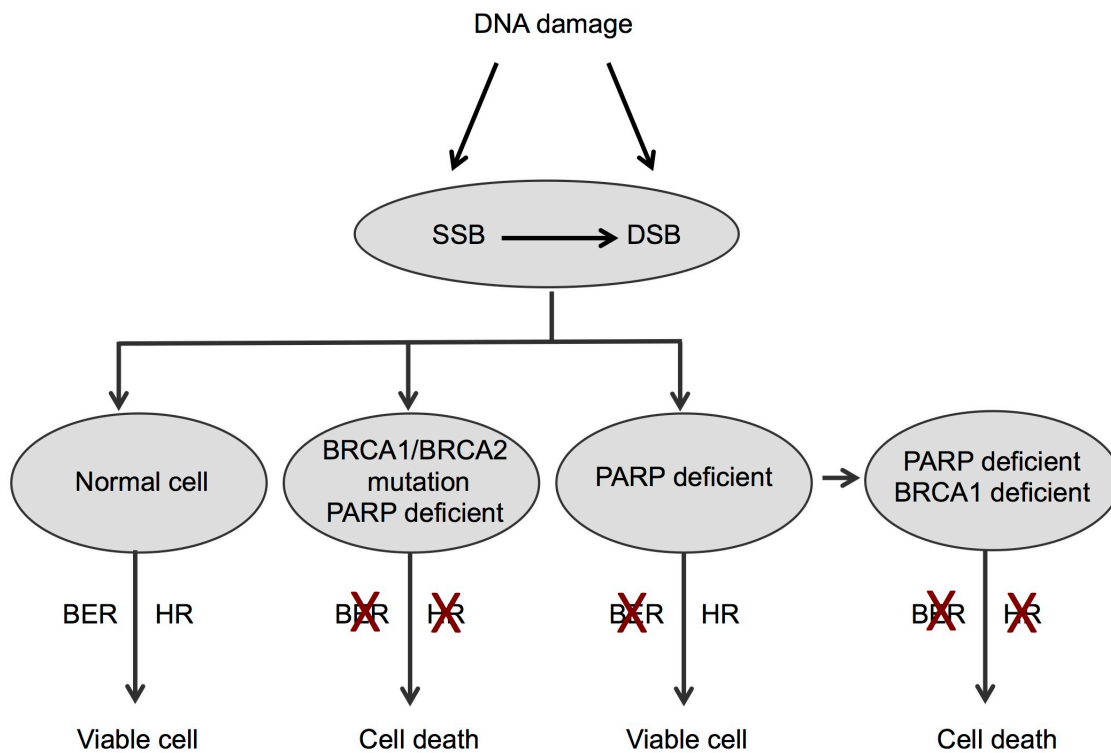


**Figure 1-10. Synthetic lethality with BRCA1 inhibitor.**

As mentioned in Figure 1-6, application of PARP inhibitor can selectively kill tumor cell with BRCA1/BRCA2 mutations via synthetic lethality without harming the normal cell. However, PARP inhibitor is not efficient in killing tumor cells without BRCA1/BRCA2 mutations, because the HR pathway remains active in repair DSBs. BRCA1 inhibitor aims to benefit cancer patients without BRCA1/BRCA1 mutations by blocking their HR pathway manually, thus creating the synthetic lethality in cells.

and the hydroxyl group of Ser1655 both donate a hydrogen bond to the phosphate head group of pSer, the Thr1700 hydrogen bond with the hydroxyl group of pSer to secure the interaction. Besides, the salt bridge of the phosphate group with Lys 1702, assisted by Val 1654 and Asn1678, also further improve the binding affinity of this interaction. The hydrophobic +3 binding pocket is located on the interface between the two BRCT repeats. Hydrophobic residues, Leu1701, Phe1704, Met 1775 and Leu1839, decorate the base of this pocket. However, the sides of this pocket consist of many charged residues, including Arg1699, Asn1774 and Arg1835. It is worth noting that the main chain carbonyl of Arg1699 can form a hydrogen bond with the main chain NH of the +3 residue from the phosphopeptide to adjust the +3 residue position in the pocket. The two important protein-binding pockets on BRCA1 BRCT are both very selective, making them suitable targets for inhibitor design. However, both pockets are relatively shallow, making it difficult to stabilize any small molecule inhibitor solely in either pocket.

### **1.3.3 TopBP1**

TopBP1 is a key protein interaction hub that regulates DNA replication, checkpoint activation and damage response (Garcia et al., 2005; Wardlaw et al., 2014). TopBP1 protein interactions are mediated by its nine BRCT repeats, as well as its AAD that is particularly critical for its role in DNA replication stress signaling which initiates with ATR activation (Figure 1-11). Although dozens of PPIs involving the TopBP1 BRCT domains have been reported in the literature, how many of these distinct domains collaborate with different protein partners remain unclear. It has been shown that the three N terminal BRCTs (BRCT0/1/2) of TopBP1 can interact with the phosphorylated Rad9 tail of the Rad9-Hus1-Rad1 (9-1-1) complex to assist ATR-mediated activation of Chk1 in mammalian cells (Delacroix et al., 2007; Greer et al., 2003). The C terminal BRCT7/8 next to the ADD can bind to phosphorylated ATR and enables TopBP1 to engage ATR-ATRIP and stimulate ATR kinase activity (Liu et al., 2011). This BRCT7/8 also interacts with BACH1/ FANCI. This subsequently extends single-stranded DNA regions and enhances RPA loading at stalled replication forks (Gong et al., 2010). The BRCT5 of internal tandem repeats (BRCT4/5) has



long been known to be critical for TopBP1 recruitment to sites of DNA damage and replication stress (Yamane et al., 2002) and several DNA damage-associated proteins have been suggested to interact with this domain in a phosphorylation-dependent manner. The first potential partner identified for BRCT5 was p53-binding protein 1 (53BP1), whose interaction was proposed to mediate recruitment of TopBP1 to sites of DNA DSBs during the G1 phase (Cescutti et al., 2010; Yamane et al., 2002). Other proteins that may interact with BRCT5 including DNA double-strand break mediator, MDC1 (Leung et al., 2013; Wang et al., 2011), and Bloom syndrome, RecQ helicase-like protein, BLM (Wang et al., 2013). The neighboring single repeat, BRCT6, has also been reported to interact with PARP1, transcription factor E2F1 and ePHD protein SPBP (Liu et al., 2003; Sjøttem et al., 2007; Wollmann et al., 2007). However, the structure of BRCT6 reveals a degenerate phosphate-binding pocket. (Leung et al., 2010) Structural alignment of the phosphate-binding pocket of BRCA1 with TopBP1 BRCT6 shows only one (Ser1655) of the three key residues (Ser1655, Gly1656, and Lys1702), that hydrogen-bonding with the pSer of phosphopeptide, in BRCA1 is conserved in TopBP1 BRCT6 (Ser913). Instead, side chains of Lys914 point directly into the place in the pocket where normally hosts the phosphate head group of pSer/pThr, leaving no space for phosphopeptide to bind. In addition, the replacement of positively charged Lys with negatively charged Glu957 in the pocket further repels the negatively charged phosphate group (Figure 1-12).

TopBP1 is found to be associated with various types of cancers, which make it a promising target for developing cancer therapy. For years, overexpression of TopBP1 has been linked with progression of hereditary breast cancer (Forma et al., 2012). A recent study reveals that TopBP1 participates in HR through regulating Rad51 phosphorylation and chromatin loading (Moudry et al., 2016). Therefore, mutations in TopBP1 may also impair HR and improved PARP inhibitor sensitivity in cancer patients. Meanwhile, TopBP1 was also found to affect chemosensitivity of non-small cell and lung cancer (NSCLC) by upregulating the p53 signal in cells (Lv et al., 2016). Further study has shown that Calcein acetoxymethyl ester (calcein-AM) can enhance the antitumor effect of doxorubicin in NSCLC by regulating the TopBP1/p53 signal cascade(Lv et al., 2017).

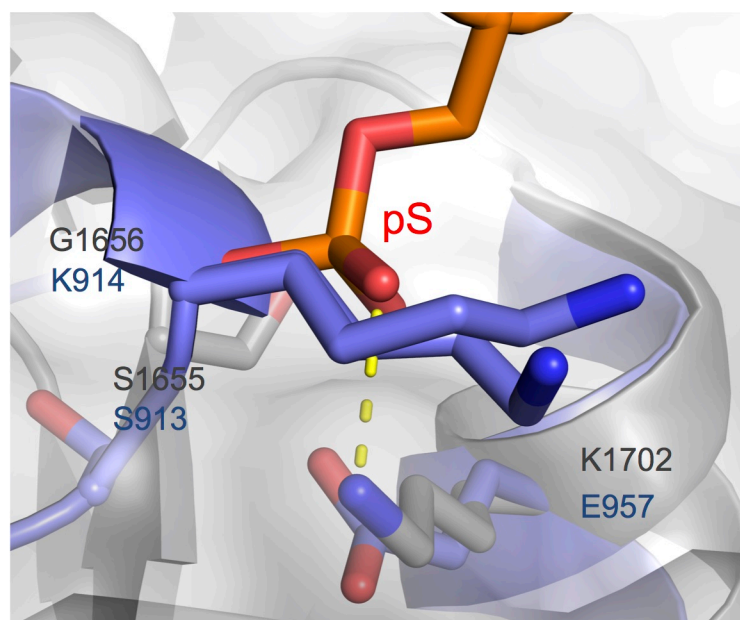


**Figure 1-12. Structural comparison of phosphate binding pocket in TopBP1 BRCT6 and BRCA1 tandem BRCTs.**

Structural alignment of the pSer binding pocket of BRCA1 (PDB ID: 1T2V, colored in grey) with TopBP1 BRCT6 (PDB ID: 3JV, colored in blue). The BACH1 phospho-peptide is shown in orange. Hydrogen bonding is designated as yellow dotted lines. Hydrogen bonding residues in BRCA1 (below) aligned with TopBP1 (above) are displayed.

## 1.4 Thesis overview

This thesis aims to investigate two major BRCT family proteins, TopBP1 and BRCA1, to understand how they function in DDR through PPI and explore the therapeutic potential of them in treating genomic instability diseases.

**BRCA1 Inhibitor Development (Chapter 2).** For years, BRCA1 BRCT has been considered as a potential target of synthetic lethality inhibitor drug development for cancer therapy. However, generation of a viable cellular inhibitor of BRCA1 BRCT has been very challenging. Here, we present the first non-phosphorylated peptidomimetic inhibitor of BRCA1 BRCT that is developed through an mRNA displaying library screen. Our X-ray structure of BRCA1 BRCT/inhibitor complex provided useful insight and new features that can guide the development of better small molecule inhibitors.

**TopBP1/MDC1 (Chapter 3).** MDC1 recognition by TopBP1 BRCT4/5 plays an important role in the regulation of DNA replication checkpoint. Based on the known structure of TopBP1 BRCT4/5 in complex with MDC1, we carried out a series of biochemical analyses of this interaction to further understand this mechanism. Our study reveals a unique electrostatic interaction between TopBP1 BRCT5 and the SDT repeats of MDC1. We hypothesized that TopBP1 BRCT5 use the same positively charged surface to recognize other highly negatively charged molecules such DNAs to assist TopBP1 recruitment at DNA damage site.

**TopBP1/BLM (Chapter 4).** The interaction between BLM and TopBP1 BRCT4/5 has been shown to help the maintenance of genome stability in cells. However, conflicting results suggested both pSer304 and pSer338 of BLM could be the primary target of recognition by TopBP1, and the precise mechanism of this interaction remains unclear. We proved it is pSer304, not pSer338 of BLM that is essential for this interaction, and solved the X-ray structure of TopBP1 BRCT4/5 in complex with BLM. With further mutagenesis and biochemical studies *in vivo* on this interaction, we reveal a new model of interaction between TopBP1/BLM that is distinct from the TopBP1/MDC1 model. We propose that TopBP1 BRCT5 may interact with 53BP1 like BLM.

**General Discussion (Chapter 5).** The final chapter will summarize the results described in this thesis, and discuss the future directions in many aspects to tie these findings together towards a better understanding of how TopBP1 and BRCA1 regulate different PPI in DDR. New PPI mechanisms revealed in this thesis also have therapeutic potential in treating genomic instability diseases. Structural insights from our study are not only useful for the prediction of targeting region of known BRCT domains on their protein partners but also provide a guideline for the development of new inhibitors of BRCT family proteins. Together, this thesis further illustrates the structural and functional diversity of BRCT domains in DDR proteins.

**TopBP1/BRD4 (Appendix A).** Unlike other tandem BRCT repeat from TopBP1 that is mainly involved in phosphorylation-dependent PPI, the structure of BRCT6 indicated it has no phosphate binding pocket. However, BRCT6 has been reported to interact with various DNA damage response proteins including PARP1, E2F1, and SPBP. A recent study from our collaborator, Dr. Lam (MIT), identified an interaction between TopBP1 and BRD4. We carried out a structure guided *in vitro* interaction screening between known BRD4 and TopBP1 BRCT domains. Our study reveals that the ET domain of BRD4 can interact with the BRCT6 domain of TopBP1.

**Dpb11/Rtt107 (Appendix B).** Dpb11 and Rtt107 are both important BRCT family proteins that mediate the replication stress response in *S. cerevisiae*. However, the structures of tandem BRCTs from both proteins remain unsolved. We carried out series of sequence alignments with secondary structure predictions of Dpb11 and Rtt107 BRCTs with human TopBP1 and the *S. pombe* TopBP1 homolog Rad4. Our study has revealed that both Dpb11 BRCT1/2 and Rtt107 BRCT3/4 are potential structure analogs of TopBP1 BRC4/5. Also, Dpb11 BRCT3/4 appears to be a structural analog of Rad4 BRCT3/4. Guided by our prediction, we designed several *E. coli* based protein expression constructs of Dpb11 BRCT1/2, BRCT3/4, and Rtt107 BRCT3/4. Once successfully expressed and purified, these proteins may be useful for further functional or structural study of these tandem BRCT repeats.

## 1.5 Reference

1. Abraham, R.T. (2001). Cell cycle checkpoint signaling through the ATM and ATR kinases. *Genes Dev* 15, 2177-2196.
2. Acevedo, J., Yan, S., and Michael, W.M. (2016). Direct Binding to Replication Protein A (RPA)-coated Single-stranded DNA Allows Recruitment of the ATR Activator TopBP1 to Sites of DNA Damage. *J Biol Chem* 291, 13124-13131.
3. Aguilera, A., and Gomez-Gonzalez, B. (2008). Genome instability: a mechanistic view of its causes and consequences. *Nat Rev Genet* 9, 204-217.
4. Anantha, R.W., Simhadri, S., Foo, T.K., Miao, S., Liu, J., Shen, Z., Ganesan, S., and Xia, B. (2017). Functional and mutational landscapes of BRCA1 for homology-directed repair and therapy resistance. *Elife* 6.
5. Anisimov, V.M., Ziemys, A., Kizhake, S., Yuan, Z., Natarajan, A., and Cavasotto, C.N. (2011). Computational and experimental studies of the interaction between phosphopeptides and the C-terminal domain of BRCA1. *J Comput Aided Mol Des* 25, 1071-1084.
6. Arora, H., Chacon, A.H., Choudhary, S., McLeod, M.P., Meshkov, L., Nouri, K., and Izakovic, J. (2014). Bloom syndrome. *Int J Dermatol* 53, 798-802.
7. Avery, O.T., Macleod, C.M., and McCarty, M. (1944). Studies on the Chemical Nature of the Substance Inducing Transformation of Pneumococcal Types : Induction of Transformation by a Desoxyribonucleic Acid Fraction Isolated from Pneumococcus Type Iii. *J Exp Med* 79, 137-158.
8. Bakkenist, C.J., and Kastan, M.B. (2003). DNA damage activates ATM through intermolecular autophosphorylation and dimer dissociation. *Nature* 421, 499-506.
9. Barreto, J.N., McCullough, K.B., Ice, L.L., and Smith, J.A. (2014). Antineoplastic agents and the associated myelosuppressive effects: a review. *J Pharm Pract* 27, 440-446.
10. Bartek, J., and Lukas, J. (2003). Chk1 and Chk2 kinases in checkpoint control and cancer. *Cancer Cell* 3, 421-429.
11. Bartkova, J., Tommiska, J., Oplustilova, L., Aaltonen, K., Tamminen, A., Heikkinen, T., Mistrik, M., Aittomaki, K., Blomqvist, C., Heikkila, P., *et al.* (2008). Aberrations of the MRE11-RAD50-NBS1 DNA damage sensor complex in human breast cancer: MRE11 as a candidate familial cancer-predisposing gene. *Mol Oncol* 2, 296-316.
12. Baskar, R., Lee, K.A., Yeo, R., and Yeoh, K.W. (2012). Cancer and radiation therapy: current advances and future directions. *Int J Med Sci* 9, 193-199.

13. Birrane, G., Varma, A.K., Soni, A., and Ladias, J.A. (2007). Crystal structure of the BARD1 BRCT domains. *Biochemistry* *46*, 7706-7712.
14. Bizard, A.H., and Hickson, I.D. (2014). The dissolution of double Holliday junctions. *Cold Spring Harb Perspect Biol* *6*, a016477.
15. Blackford, A.N., and Jackson, S.P. (2017). ATM, ATR, and DNA-PK: The Trinity at the Heart of the DNA Damage Response. *Mol Cell* *66*, 801-817.
16. Bork, P., Hofmann, K., Bucher, P., Neuwald, A.F., Altschul, S.F., and Koonin, E.V. (1997). A superfamily of conserved domains in DNA damage-responsive cell cycle checkpoint proteins. *Faseb J* *11*, 68-76.
17. Bryant, H.E., Schultz, N., Thomas, H.D., Parker, K.M., Flower, D., Lopez, E., Kyle, S., Meuth, M., Curtin, N.J., and Helleday, T. (2005). Specific killing of BRCA2-deficient tumours with inhibitors of poly(ADP-ribose) polymerase. *Nature* *434*, 913-917.
18. Byun, T.S., Pacek, M., Yee, M.C., Walter, J.C., and Cimprich, K.A. (2005). Functional uncoupling of MCM helicase and DNA polymerase activities activates the ATR-dependent checkpoint. *Genes Dev* *19*, 1040-1052.
19. Cancer Genome Atlas, N. (2012). Comprehensive molecular characterization of human colon and rectal cancer. *Nature* *487*, 330-337.
20. Cantor, S.B., Bell, D.W., Ganesan, S., Kass, E.M., Drapkin, R., Grossman, S., Wahrer, D.C., Sgroi, D.C., Lane, W.S., Haber, D.A., *et al.* (2001). BACH1, a novel helicase-like protein, interacts directly with BRCA1 and contributes to its DNA repair function. *Cell* *105*, 149-160.
21. Castel, A.L., Cleary, J.D., and Pearson, C.E. (2010). Repeat instability as the basis for human diseases and as a potential target for therapy. *Nat Rev Mol Cell Bio* *11*, 165-170.
22. Castilla, L.H., Couch, F.J., Erdos, M.R., Hoskins, K.F., Calzone, K., Garber, J.E., Boyd, J., Lubin, M.B., Deshano, M.L., Brody, L.C., *et al.* (1994). Mutations in the BRCA1 gene in families with early-onset breast and ovarian cancer. *Nat Genet* *8*, 387-391.
23. Cescutti, R., Negrini, S., Kohzaki, M., and Halazonetis, T.D. (2010). TopBP1 functions with 53BP1 in the G1 DNA damage checkpoint. *EMBO J* *29*, 3723-3732.
24. Chehab, N.H., Malikzay, A., Appel, M., and Halazonetis, T.D. (2000). Chk2/hCds1 functions as a DNA damage checkpoint in G(1) by stabilizing p53. *Genes Dev* *14*, 278-288.
25. Chen, L., Gilkes, D.M., Pan, Y., Lane, W.S., and Chen, J. (2005). ATM and Chk2-dependent phosphorylation of MDMX contribute to p53 activation after DNA damage. *EMBO J* *24*, 3411-3422.

26. Chen, Y.H., Matsumoto, Y., Shibutani, S., and Bogenhagen, D.F. (1991). Acetylaminofluorene and aminofluorene adducts inhibit in vitro transcription of a *Xenopus* 5S RNA gene only when located on the coding strand. *Proc Natl Acad Sci U S A* 88, 9583-9587.
27. Choi, J.H., Kim, S.Y., Kim, S.K., Kemp, M.G., and Sancar, A. (2015). An Integrated Approach for Analysis of the DNA Damage Response in Mammalian Cells: NUCLEOTIDE EXCISION REPAIR, DNA DAMAGE CHECKPOINT, AND APOPTOSIS. *J Biol Chem* 290, 28812-28821.
28. Choi, J.H., Lindsey-Boltz, L.A., and Sancar, A. (2009). Cooperative activation of the ATR checkpoint kinase by TopBP1 and damaged DNA. *Nucleic Acids Res* 37, 1501-1509.
29. Chun, S.G., Shaeffer, D.S., and Bryant-Greenwood, P.K. (2011). The Werner's Syndrome RecQ helicase/exonuclease at the nexus of cancer and aging. *Hawaii Med J* 70, 52-55.
30. Ciccica, A., McDonald, N., and West, S.C. (2008). Structural and functional relationships of the XPF/MUS81 family of proteins. *Annu Rev Biochem* 77, 259-287.
31. Cleary, S.P., Cotterchio, M., Jenkins, M.A., Kim, H., Bristow, R., Green, R., Haile, R., Hopper, J.L., LeMarchand, L., Lindor, N., *et al.* (2009). Germline MutY human homologue mutations and colorectal cancer: a multisite case-control study. *Gastroenterology* 136, 1251-1260.
32. Comen, E.A., and Robson, M. (2010). Poly(ADP-ribose) polymerase inhibitors in triple-negative breast cancer. *Cancer J* 16, 48-52.
33. Crick, F.H., Brenner, S., Watstobi.Rj, and Barnett, L. (1961). General Nature of Genetic Code for Proteins. *Nature* 192, 1227-&.
34. Dahm, R. (2008). Discovering DNA: Friedrich Miescher and the early years of nucleic acid research. *Hum Genet* 122, 565-581.
35. De Bont, R., and van Larebeke, N. (2004). Endogenous DNA damage in humans: a review of quantitative data. *Mutagenesis* 19, 169-185.
36. de Renty, C., and Ellis, N.A. (2017). Bloom's syndrome: Why not premature aging?: A comparison of the BLM and WRN helicases. *Ageing Res Rev* 33, 36-51.
37. Delacroix, S., Wagner, J.M., Kobayashi, M., Yamamoto, K., and Karnitz, L.M. (2007). The Rad9-Hus1-Rad1 (9-1-1) clamp activates checkpoint signaling via TopBP1. *Genes Dev* 21, 1472-1477.

38. Delaney, G., Jacob, S., Featherstone, C., and Barton, M. (2005). The role of radiotherapy in cancer treatment: estimating optimal utilization from a review of evidence-based clinical guidelines. *Cancer* *104*, 1129-1137.
39. Densham, R.M., Garvin, A.J., Stone, H.R., Strachan, J., Baldock, R.A., Daza-Martin, M., Fletcher, A., Blair-Reid, S., Beesley, J., Johal, B., *et al.* (2016). Human BRCA1-BARD1 ubiquitin ligase activity counteracts chromatin barriers to DNA resection. *Nat Struct Mol Biol* *23*, 647-655.
40. Esashi, F., Christ, N., Gannon, J., Liu, Y., Hunt, T., Jasin, M., and West, S.C. (2005). CDK-dependent phosphorylation of BRCA2 as a regulatory mechanism for recombinational repair. *Nature* *434*, 598-604.
41. Falck, J., Coates, J., and Jackson, S.P. (2005). Conserved modes of recruitment of ATM, ATR and DNA-PKcs to sites of DNA damage. *Nature* *434*, 605-611.
42. Farmer, H., McCabe, N., Lord, C.J., Tutt, A.N., Johnson, D.A., Richardson, T.B., Santarosa, M., Dillon, K.J., Hickson, I., Knights, C., *et al.* (2005). Targeting the DNA repair defect in BRCA mutant cells as a therapeutic strategy. *Nature* *434*, 917-921.
43. Fekairi, S., Scaglione, S., Chahwan, C., Taylor, E.R., Tissier, A., Coulon, S., Dong, M.Q., Ruse, C., Yates, J.R., 3rd, Russell, P., *et al.* (2009). Human SLX4 is a Holliday junction resolvase subunit that binds multiple DNA repair/recombination endonucleases. *Cell* *138*, 78-89.
44. Feng, H., Parker, J.M., Lu, J., and Cao, W. (2004). Effects of deletion and site-directed mutations on ligation steps of NAD<sup>+</sup>-dependent DNA ligase: a biochemical analysis of BRCA1 C-terminal domain. *Biochemistry* *43*, 12648-12659.
45. Feng, L., and Chen, J. (2012). The E3 ligase RNF8 regulates KU80 removal and NHEJ repair. *Nat Struct Mol Biol* *19*, 201-206.
46. Fernandez-Capetillo, O., Lee, A., Nussenzweig, M., and Nussenzweig, A. (2004). H2AX: the histone guardian of the genome. *DNA Repair (Amst)* *3*, 959-967.
47. Fong, P.C., Boss, D.S., Yap, T.A., Tutt, A., Wu, P., Mergui-Roelvink, M., Mortimer, P., Swaisland, H., Lau, A., O'Connor, M.J., *et al.* (2009). Inhibition of poly(ADP-ribose) polymerase in tumors from BRCA mutation carriers. *N Engl J Med* *361*, 123-134.
48. Forma, E., Krzeslak, A., Bernaciak, M., Romanowicz-Makowska, H., and Brys, M. (2012). Expression of TopBP1 in hereditary breast cancer. *Mol Biol Rep* *39*, 7795-7804.
49. Fourquet, A., Stoppa-Lyonnet, D., Kirova, Y.M., Sigal-Zafrani, B., Asselain, B., Institut Curie Breast Cancer Study, G., and Institut Curie Breast Ovary Cancer Risk Study, G. (2009). Familial breast cancer: clinical response to induction chemotherapy or radiotherapy related to BRCA1/2 mutations status. *Am J Clin Oncol* *32*, 127-131.

50. Futreal, P.A., Liu, Q., Shattuck-Eidens, D., Cochran, C., Harshman, K., Tavtigian, S., Bennett, L.M., Haugen-Strano, A., Swensen, J., Miki, Y., *et al.* (1994). BRCA1 mutations in primary breast and ovarian carcinomas. *Science* *266*, 120-122.
51. Galkin, V.E., Esashi, F., Yu, X., Yang, S., West, S.C., and Egelman, E.H. (2005). BRCA2 BRC motifs bind RAD51-DNA filaments. *Proc Natl Acad Sci U S A* *102*, 8537-8542.
52. Garber, K. (2002). Synthetic lethality: killing cancer with cancer. *J Natl Cancer Inst* *94*, 1666-1668.
53. Garcia, V., Furuya, K., and Carr, A.M. (2005). Identification and functional analysis of TopBP1 and its homologs. *DNA Repair* *4*, 1227-1239.
54. Garrett, M.D., and Collins, I. (2011). Anticancer therapy with checkpoint inhibitors: what, where and when? *Trends Pharmacol Sci* *32*, 308-316.
55. Gong, Z., Kim, J.E., Leung, C.C., Glover, J.N., and Chen, J. (2010). BACH1/FANCI acts with TopBP1 and participates early in DNA replication checkpoint control. *Mol Cell* *37*, 438-446.
56. Goodarzi, A.A., Yu, Y., Riballo, E., Douglas, P., Walker, S.A., Ye, R., Harer, C., Marchetti, C., Morrice, N., Jeggo, P.A., *et al.* (2006). DNA-PK autophosphorylation facilitates Artemis endonuclease activity. *EMBO J* *25*, 3880-3889.
57. Greer, D.A., Besley, B.D., Kennedy, K.B., and Davey, S. (2003). hRad9 rapidly binds DNA containing double-strand breaks and is required for damage-dependent topoisomerase II beta binding protein 1 focus formation. *Cancer Res* *63*, 4829-4835.
58. Gu, J., Lu, H., Tsai, A.G., Schwarz, K., and Lieber, M.R. (2007). Single-stranded DNA ligation and XLF-stimulated incompatible DNA end ligation by the XRCC4-DNA ligase IV complex: influence of terminal DNA sequence. *Nucleic Acids Res* *35*, 5755-5762.
59. Helleday, T., Eshtad, S., and Nik-Zainal, S. (2014). Mechanisms underlying mutational signatures in human cancers. *Nat Rev Genet* *15*, 585-598.
60. Hoeijmakers, J.H. (2009). DNA damage, aging, and cancer. *N Engl J Med* *361*, 1475-1485.
61. Huen, M.S., Sy, S.M., and Chen, J. (2010). BRCA1 and its toolbox for the maintenance of genome integrity. *Nat Rev Mol Cell Biol* *11*, 138-148.
62. Jaffe, N. (2014). Historical perspective on the introduction and use of chemotherapy for the treatment of osteosarcoma. *Adv Exp Med Biol* *804*, 1-30.

63. Jeong, S.Y., Kumagai, A., Lee, J., and Dunphy, W.G. (2003). Phosphorylated claspin interacts with a phosphate-binding site in the kinase domain of Chk1 during ATR-mediated activation. *J Biol Chem* 278, 46782-46788.
64. Joseph, P.R., Yuan, Z., Kumar, E.A., Lokesh, G.L., Kizhake, S., Rajarathnam, K., and Natarajan, A. (2010). Structural characterization of BRCT-tetrapeptide binding interactions. *Biochem Biophys Res Commun* 393, 207-210.
65. Kasai, H., Hayami, H., Yamaizumi, Z., Saito, H., and Nishimura, S. (1984). Detection and identification of mutagens and carcinogens as their adducts with guanosine derivatives. *Nucleic Acids Res* 12, 2127-2136.
66. Kemp, M.G., Akan, Z., Yilmaz, S., Grillo, M., Smith-Roe, S.L., Kang, T.H., Cordeiro-Stone, M., Kaufmann, W.K., Abraham, R.T., Sancar, A., *et al.* (2010). Tipin-replication protein A interaction mediates Chk1 phosphorylation by ATR in response to genotoxic stress. *J Biol Chem* 285, 16562-16571.
67. Kim, G., Ison, G., McKee, A.E., Zhang, H., Tang, S., Gwise, T., Sridhara, R., Lee, E., Tzou, A., Philip, R., *et al.* (2015). FDA Approval Summary: Olaparib Monotherapy in Patients with Deleterious Germline BRCA-Mutated Advanced Ovarian Cancer Treated with Three or More Lines of Chemotherapy. *Clin Cancer Res* 21, 4257-4261.
68. King, M.C., Marks, J.H., Mandell, J.B., and New York Breast Cancer Study, G. (2003). Breast and ovarian cancer risks due to inherited mutations in BRCA1 and BRCA2. *Science* 302, 643-646.
69. Kobayashi, M., Figaroa, F., Meeuwenoord, N., Jansen, L.E., and Siegal, G. (2006). Characterization of the DNA binding and structural properties of the BRCT region of human replication factor C p140 subunit. *J Biol Chem* 281, 4308-4317.
70. Kolodner, R.D. (2016). A personal historical view of DNA mismatch repair with an emphasis on eukaryotic DNA mismatch repair. *DNA Repair (Amst)* 38, 3-13.
71. Koonin, E.V., Altschul, S.F., and Bork, P. (1996). BRCA1 protein products ... Functional motifs. *Nat Genet* 13, 266-268.
72. Krejci, L., Altmannova, V., Spirek, M., and Zhao, X. (2012). Homologous recombination and its regulation. *Nucleic Acids Res* 40, 5795-5818.
73. Kulkarni, A., and Wilson, D.M., 3rd (2008). The involvement of DNA-damage and -repair defects in neurological dysfunction. *Am J Hum Genet* 82, 539-566.
74. Kumagai, A., and Dunphy, W.G. (2003). Repeated phosphopeptide motifs in Claspin mediate the regulated binding of Chk1. *Nat Cell Biol* 5, 161-165.
75. Kumagai, A., Kim, S.M., and Dunphy, W.G. (2004). Claspin and the activated form of ATR-ATRIP collaborate in the activation of Chk1. *J Biol Chem* 279, 49599-49608.

76. Lambert, W.C., and Lambert, M.W. (2015). Development of effective skin cancer treatment and prevention in xeroderma pigmentosum. *Photochem Photobiol* *91*, 475-483.
77. Lavin, M.F. (2008). Ataxia-telangiectasia: from a rare disorder to a paradigm for cell signalling and cancer. *Nat Rev Mol Cell Biol* *9*, 759-769.
78. Lavin, M.F., and Kozlov, S. (2007). ATM activation and DNA damage response. *Cell Cycle* *6*, 931-942.
79. Le Guen, T., Ragu, S., Guirouilh-Barbat, J., and Lopez, B.S. (2015). Role of the double-strand break repair pathway in the maintenance of genomic stability. *Mol Cell Oncol* *2*, e968020.
80. Lee, M.S., Edwards, R.A., Thede, G.L., and Glover, J.N. (2005). Structure of the BRCT repeat domain of MDC1 and its specificity for the free COOH-terminal end of the gamma-H2AX histone tail. *J Biol Chem* *280*, 32053-32056.
81. Leung, C.C., Kellogg, E., Kuhnert, A., Hanel, F., Baker, D., and Glover, J.N. (2010). Insights from the crystal structure of the sixth BRCT domain of topoisomerase IIbeta binding protein 1. *Protein Sci* *19*, 162-167.
82. Leung, C.C., Sun, L., Gong, Z., Burkat, M., Edwards, R., Assmus, M., Chen, J., and Glover, J.N. (2013). Structural insights into recognition of MDC1 by TopBP1 in DNA replication checkpoint control. *Structure* *21*, 1450-1459.
83. Levene, P.A. (1917). The structure of yeast nucleic acid. *Journal of Biological Chemistry* *31*, 591-598.
84. Levene, P.A. (1918). The structure of yeast nucleic acid II. Uridinephosphoric acid. *Journal of Biological Chemistry* *33*, 229-U221.
85. Levene, P.A. (1920). The structure of yeast nucleic acid. V. Ammonia hydrolysis. *Journal of Biological Chemistry* *41*, 19-23.
86. Levene, P.A., and La Forge, F.B. (1912). The yeast nucleic acid. V. The structure of pyrimidin-nucleoside. *Ber Dtsch Chem Ges* *45*, 608-620.
87. Li, Y., Luo, K., Yin, Y., Wu, C., Deng, M., Li, L., Chen, Y., Nowsheen, S., Lou, Z., and Yuan, J. (2017). USP13 regulates the RAP80-BRCA1 complex dependent DNA damage response. *Nat Commun* *8*, 15752.
88. Lieber, M.R. (2010). The mechanism of double-strand DNA break repair by the nonhomologous DNA end-joining pathway. *Annu Rev Biochem* *79*, 181-211.
89. Lindahl, T. (1974). N-Glycosidase from Escherichia-Coli That Releases Free Uracil from DNA Containing Deaminated Cytosine Residues. *P Natl Acad Sci USA* *71*, 3649-3653.

90. Lindahl, T. (1993). Instability and decay of the primary structure of DNA. *Nature* *362*, 709-715.
91. Lindahl, T., and Andersson, A. (1972). Rate of chain breakage at apurinic sites in double-stranded deoxyribonucleic acid. *Biochemistry* *11*, 3618-3623.
92. Liu, K., Lin, F.T., Ruppert, J.M., and Lin, W.C. (2003). Regulation of E2F1 by BRCT domain-containing protein TopBP1. *Mol Cell Biol* *23*, 3287-3304.
93. Liu, S., Shiotani, B., Lahiri, M., Marechal, A., Tse, A., Leung, C.C., Glover, J.N., Yang, X.H., and Zou, L. (2011). ATR autophosphorylation as a molecular switch for checkpoint activation. *Mol Cell* *43*, 192-202.
94. Lokesh, G.L., Muralidhara, B.K., Negi, S.S., and Natarajan, A. (2007). Thermodynamics of phosphopeptide tethering to BRCT: the structural minima for inhibitor design. *J Am Chem Soc* *129*, 10658-10659.
95. Lokesh, G.L., Rachamalla, A., Kumar, G.D., and Natarajan, A. (2006). High-throughput fluorescence polarization assay to identify small molecule inhibitors of BRCT domains of breast cancer gene 1. *Anal Biochem* *352*, 135-141.
96. Lord, C.J., and Ashworth, A. (2017). PARP inhibitors: Synthetic lethality in the clinic. *Science* *355*, 1152-1158.
97. Lu, A.L., Li, X., Gu, Y., Wright, P.M., and Chang, D.Y. (2001). Repair of oxidative DNA damage: mechanisms and functions. *Cell Biochem Biophys* *35*, 141-170.
98. Lv, Y., Huo, Y., Yu, X., Liu, R., Zhang, S., Zheng, X., and Zhang, X. (2016). TopBP1 contributes to the chemoresistance in non-small cell lung cancer through upregulation of p53. *Drug Des Devel Ther* *10*, 3053-3064.
99. Lv, Y., Liu, R., Xie, S., Zheng, X., Mao, J., Cai, Y., and Chen, W. (2017). Calcein-acetoxymethyl ester enhances the antitumor effects of doxorubicin in nonsmall cell lung cancer by regulating the TopBP1/p53RR pathway. *Anticancer Drugs*.
100. Ma, Y., Lu, H., Tippin, B., Goodman, M.F., Shimazaki, N., Koiwai, O., Hsieh, C.L., Schwarz, K., and Lieber, M.R. (2004). A biochemically defined system for mammalian nonhomologous DNA end joining. *Mol Cell* *16*, 701-713.
101. Ma, Y., Pannicke, U., Schwarz, K., and Lieber, M.R. (2002). Hairpin opening and overhang processing by an Artemis/DNA-dependent protein kinase complex in nonhomologous end joining and V(D)J recombination. *Cell* *108*, 781-794.
102. Maciejczyk, M., Mikoluc, B., Pietrucha, B., Heropolitanska-Pliszka, E., Pac, M., Motkowski, R., and Car, H. (2017). Oxidative stress, mitochondrial abnormalities and antioxidant defense in Ataxia-telangiectasia, Bloom syndrome and Nijmegen breakage syndrome. *Redox Biol* *11*, 375-383.

103. Miki, Y., Swensen, J., Shattuck-Eidens, D., Futreal, P.A., Harshman, K., Tavtigian, S., Liu, Q., Cochran, C., Bennett, L.M., Ding, W., *et al.* (1994). A strong candidate for the breast and ovarian cancer susceptibility gene BRCA1. *Science* 266, 66-71.
104. Ming, X., Feng, Y., Yang, C., Wang, W., Wang, P., and Deng, J. (2016). Radiation-induced heart disease in lung cancer radiotherapy: A dosimetric update. *Medicine (Baltimore)* 95, e5051.
105. Monnat, R.J., Jr. (2010). Human RECQ helicases: roles in DNA metabolism, mutagenesis and cancer biology. *Semin Cancer Biol* 20, 329-339.
106. Morra, F., Merolla, F., Napolitano, V., Ilardi, G., Miro, C., Paladino, S., Staibano, S., Cerrato, A., and Celetti, A. (2017). The combined effect of USP7 inhibitors and PARP inhibitors in hormone-sensitive and castration-resistant prostate cancer cells. *Oncotarget* 8, 31815-31829.
107. Moudry, P., Watanabe, K., Wolanin, K.M., Bartkova, J., Wassing, I.E., Watanabe, S., Strauss, R., Troelsgaard Pedersen, R., Oestergaard, V.H., Lisby, M., *et al.* (2016). TOPBP1 regulates RAD51 phosphorylation and chromatin loading and determines PARP inhibitor sensitivity. *J Cell Biol* 212, 281-288.
108. Nagaraju, G., and Scully, R. (2007). Minding the gap: the underground functions of BRCA1 and BRCA2 at stalled replication forks. *DNA Repair (Amst)* 6, 1018-1031.
109. Narod, S.A. (2010). Compliance with tamoxifen in women with breast cancer and a BRCA1 or BRCA2 mutation. *J Clin Oncol* 28, e698-699; author reply e700.
110. Nowsheen, S., and Yang, E.S. (2012). The intersection between DNA damage response and cell death pathways. *Exp Oncol* 34, 243-254.
111. Oliver, A.W., Paul, A., Boxall, K.J., Barrie, S.E., Aherne, G.W., Garrett, M.D., Mittnacht, S., and Pearl, L.H. (2006). Trans-activation of the DNA-damage signalling protein kinase Chk2 by T-loop exchange. *EMBO J* 25, 3179-3190.
112. Peasland, A., Wang, L.Z., Rowling, E., Kyle, S., Chen, T., Hopkins, A., Cliby, W.A., Sarkaria, J., Beale, G., Edmondson, R.J., *et al.* (2011). Identification and evaluation of a potent novel ATR inhibitor, NU6027, in breast and ovarian cancer cell lines. *Br J Cancer* 105, 372-381.
113. Pessetto, Z.Y., Yan, Y., Bessho, T., and Natarajan, A. (2012). Inhibition of BRCT(BRCA1)-phosphoprotein interaction enhances the cytotoxic effect of olaparib in breast cancer cells: a proof of concept study for synthetic lethal therapeutic option. *Breast Cancer Res Treat* 134, 511-517.
114. Phillips, D.H., and Venitt, S. (2012). DNA and protein adducts in human tissues resulting from exposure to tobacco smoke. *Int J Cancer* 131, 2733-2753.

115. Pleschke, J.M., Kleczkowska, H.E., Strohm, M., and Althaus, F.R. (2000). Poly(ADP-ribose) binds to specific domains in DNA damage checkpoint proteins. *J Biol Chem* 275, 40974-40980.
116. Plummer, R., Jones, C., Middleton, M., Wilson, R., Evans, J., Olsen, A., Curtin, N., Boddy, A., McHugh, P., Newell, D., *et al.* (2008). Phase I study of the poly(ADP-ribose) polymerase inhibitor, AG014699, in combination with temozolomide in patients with advanced solid tumors. *Clin Cancer Res* 14, 7917-7923.
117. Prevo, R., Fokas, E., Reaper, P.M., Charlton, P.A., Pollard, J.R., McKenna, W.G., Muschel, R.J., and Brunner, T.B. (2012). The novel ATR inhibitor VE-821 increases sensitivity of pancreatic cancer cells to radiation and chemotherapy. *Cancer Biol Ther* 13, 1072-1081.
118. Purnell, M.R., and Whish, W.J. (1980). Novel inhibitors of poly(ADP-ribose) synthetase. *Biochem J* 185, 775-777.
119. Puyo, S., Montaudon, D., and Pourquier, P. (2014). From old alkylating agents to new minor groove binders. *Crit Rev Oncol Hematol* 89, 43-61.
120. Rappas, M., Oliver, A.W., and Pearl, L.H. (2011). Structure and function of the Rad9-binding region of the DNA-damage checkpoint adaptor TopBP1. *Nucleic Acids Res* 39, 313-324.
121. Rasmussen, R.E., and Painter, R.B. (1964). Evidence for Repair of Ultra-Violet Damaged Deoxyribonucleic Acid in Cultured Mammalian Cells. *Nature* 203, 1360-&.
122. Rothblum-Oviatt, C., Wright, J., Lefton-Greif, M.A., McGrath-Morrow, S.A., Crawford, T.O., and Lederman, H.M. (2016). Ataxia telangiectasia: a review. *Orphanet J Rare Dis* 11, 159.
123. Scharer, O.D. (2013). Nucleotide excision repair in eukaryotes. *Cold Spring Harb Perspect Biol* 5, a012609.
124. Shibutani, S., Takeshita, M., and Grollman, A.P. (1991). Insertion of specific bases during DNA synthesis past the oxidation-damaged base 8-oxodG. *Nature* 349, 431-434.
125. Shin, H., Jo, S.J., Kim, D.H., Kwon, O., and Myung, S.K. (2015). Efficacy of interventions for prevention of chemotherapy-induced alopecia: a systematic review and meta-analysis. *Int J Cancer* 136, E442-454.
126. Simons, A.M., Horwitz, A.A., Starita, L.M., Griffin, K., Williams, R.S., Glover, J.N., and Parvin, J.D. (2006). BRCA1 DNA-binding activity is stimulated by BARD1. *Cancer Res* 66, 2012-2018.

127. Sjøttem, E., Rekdal, C., Svineng, G., Johnsen, S.S., Klenow, H., Uglehus, R.D., and Johansen, T. (2007). The ePHD protein SPBP interacts with TopBP1 and together they co-operate to stimulate Ets1-mediated transcription. *Nucleic Acids Res* 35, 6648-6662.
128. Smith, J., Tho, L.M., Xu, N., and Gillespie, D.A. (2010). The ATM-Chk2 and ATR-Chk1 pathways in DNA damage signaling and cancer. *Adv Cancer Res* 108, 73-112.
129. Sullivan, A.D., Wigginton, J., and Kirschner, D. (2001). The coreceptor mutation CCR5Delta32 influences the dynamics of HIV epidemics and is selected for by HIV. *Proc Natl Acad Sci U S A* 98, 10214-10219.
130. Swenberg, J.A., Lu, K., Moeller, B.C., Gao, L., Upton, P.B., Nakamura, J., and Starr, T.B. (2011). Endogenous versus exogenous DNA adducts: their role in carcinogenesis, epidemiology, and risk assessment. *Toxicol Sci* 120 Suppl 1, S130-145.
131. Sy, S.M., Huen, M.S., and Chen, J. (2009). PALB2 is an integral component of the BRCA complex required for homologous recombination repair. *Proc Natl Acad Sci U S A* 106, 7155-7160.
132. Taylor, C.W., and Kirby, A.M. (2015). Cardiac Side-effects From Breast Cancer Radiotherapy. *Clin Oncol (R Coll Radiol)* 27, 621-629.
133. Tomkinson, A.E., and Sallmyr, A. (2013). Structure and function of the DNA ligases encoded by the mammalian LIG3 gene. *Gene* 531, 150-157.
134. Touchefeu, Y., Montassier, E., Nieman, K., Gastinne, T., Potel, G., Bruley des Varannes, S., Le Vacon, F., and de La Cochetiere, M.F. (2014). Systematic review: the role of the gut microbiota in chemotherapy- or radiation-induced gastrointestinal mucositis - current evidence and potential clinical applications. *Aliment Pharmacol Ther* 40, 409-421.
135. Truninger, K., Menigatti, M., Luz, J., Russell, A., Haider, R., Gebbers, J.O., Bannwart, F., Yurtsever, H., Neuweiler, J., Riehle, H.M., *et al.* (2005). Immunohistochemical analysis reveals high frequency of PMS2 defects in colorectal cancer. *Gastroenterology* 128, 1160-1171.
136. Wallace, S.S. (2014). Base excision repair: a critical player in many games. *DNA Repair (Amst)* 19, 14-26.
137. Wang, J., Chen, J., and Gong, Z. (2013). TopBP1 controls BLM protein level to maintain genome stability. *Mol Cell* 52, 667-678.
138. Wang, J., Gong, Z., and Chen, J. (2011). MDC1 collaborates with TopBP1 in DNA replication checkpoint control. *J Cell Biol* 193, 267-273.

139. Wang, Y.G., Nnakwe, C., Lane, W.S., Modesti, M., and Frank, K.M. (2004). Phosphorylation and regulation of DNA ligase IV stability by DNA-dependent protein kinase. *J Biol Chem* 279, 37282-37290.
140. Wardlaw, C.P., Carr, A.M., and Oliver, A.W. (2014). TopBP1: A BRCT-scaffold protein functioning in multiple cellular pathways. *DNA Repair* 22, 165-174.
141. Warren, G.W., and Cummings, K.M. (2013). Tobacco and lung cancer: risks, trends, and outcomes in patients with cancer. *Am Soc Clin Oncol Educ Book*, 359-364.
142. Watson, J.D., and Crick, F.H.C. (1953). The Structure of DNA. *Cold Spring Harb Sym* 18, 123-131.
143. Weissman, L., de Souza-Pinto, N.C., Stevensner, T., and Bohr, V.A. (2007). DNA repair, mitochondria, and neurodegeneration. *Neuroscience* 145, 1318-1329.
144. West, S.C. (2003). Molecular views of recombination proteins and their control. *Nat Rev Mol Cell Biol* 4, 435-445.
145. Williams, R.J. (1957). The Chemical Basis of Heredity - Mcelroy, Wd, Glass, B. *Eugen Quart* 4, 171-171.
146. Williams, R.S., Green, R., and Glover, J.N. (2001). Crystal structure of the BRCT repeat region from the breast cancer-associated protein BRCA1. *Nat Struct Biol* 8, 838-842.
147. Williams, R.S., Williams, J.S., and Tainer, J.A. (2007). Mre11-Rad50-Nbs1 is a keystone complex connecting DNA repair machinery, double-strand break signaling, and the chromatin template. *Biochem Cell Biol* 85, 509-520.
148. Wold, M.S. (1997). Replication protein A: a heterotrimeric, single-stranded DNA-binding protein required for eukaryotic DNA metabolism. *Annu Rev Biochem* 66, 61-92.
149. Wollmann, Y., Schmidt, U., Wieland, G.D., Zipfel, P.F., Saluz, H.P., and Hanel, F. (2007). The DNA topoisomerase IIbeta binding protein 1 (TopBP1) interacts with poly (ADP-ribose) polymerase (PARP-1). *J Cell Biochem* 102, 171-182.
150. Wu, L.C., Wang, Z.W., Tsan, J.T., Spillman, M.A., Phung, A., Xu, X.L., Yang, M.C., Hwang, L.Y., Bowcock, A.M., and Baer, R. (1996). Identification of a RING protein that can interact in vivo with the BRCA1 gene product. *Nat Genet* 14, 430-440.
151. Wu, Q., Paul, A., Su, D., Mehmood, S., Foo, T.K., Ochi, T., Bunting, E.L., Xia, B., Robinson, C.V., Wang, B., *et al.* (2016). Structure of BRCA1-BRCT/Abraxas Complex Reveals Phosphorylation-Dependent BRCT Dimerization at DNA Damage Sites. *Mol Cell* 61, 434-448.
152. Xu, K., Chen, Z., Cui, Y., Qin, C., He, Y., and Song, X. (2015). Combined olaparib and oxaliplatin inhibits tumor proliferation and induces G2/M arrest and gamma-H2AX foci formation in colorectal cancer. *Onco Targets Ther* 8, 3047-3054.

153. Yamane, K., Wu, X., and Chen, J. (2002). A DNA damage-regulated BRCT-containing protein, TopBP1, is required for cell survival. *Mol. Cell. Biol.* 22, 555-566.
154. Yarosh, D.B., Rice, M., Day, R.S., 3rd, Foote, R.S., and Mitra, S. (1984). O6-Methylguanine-DNA methyltransferase in human cells. *Mutat Res* 131, 27-36.
155. Yu, Y., Mahaney, B.L., Yano, K., Ye, R., Fang, S., Douglas, P., Chen, D.J., and Lees-Miller, S.P. (2008). DNA-PK and ATM phosphorylation sites in XLF/Cernunnos are not required for repair of DNA double strand breaks. *DNA Repair (Amst)* 7, 1680-1692.
156. Yu, Y., Wang, W., Ding, Q., Ye, R., Chen, D., Merkle, D., Schriemer, D., Meek, K., and Lees-Miller, S.P. (2003). DNA-PK phosphorylation sites in XRCC4 are not required for survival after radiation or for V(D)J recombination. *DNA Repair (Amst)* 2, 1239-1252.
157. Yuan, Z., Kumar, E.A., Campbell, S.J., Palermo, N.Y., Kizhake, S., Mark Glover, J.N., and Natarajan, A. (2011). Exploiting the P-1 pocket of BRCT domains toward a structure guided inhibitor design. *ACS Med Chem Lett* 2, 764-767.
158. Yun, M.H., and Hiom, K. (2009). CtIP-BRCA1 modulates the choice of DNA double-strand-break repair pathway throughout the cell cycle. *Nature* 459, 460-463.
159. Zhang, X., Morera, S., Bates, P.A., Whitehead, P.C., Coffey, A.I., Hainbucher, K., Nash, R.A., Sternberg, M.J., Lindahl, T., and Freemont, P.S. (1998). Structure of an XRCC1 BRCT domain: a new protein-protein interaction module. *EMBO J* 17, 6404-6411.
160. Zhao, W., Steinfeld, J.B., Liang, F., Chen, X., Maranon, D.G., Jian Ma, C., Kwon, Y., Rao, T., Wang, W., Sheng, C., *et al.* (2017). BRCA1-BARD1 promotes RAD51-mediated homologous DNA pairing. *Nature* 550, 360-365.

## Chapter 2

### Development of BRCA1 inhibitors for cancer therapy

**A version of this chapter has been published in:**

White, E., **Sun, L.**, Ma Z., Beckta, J., Danzig, B., Hacker, D., Huie, Melissa., William, D., Edwards, R., Valerie, K., Glover, J.N.M., Hartman, M. A peptide library approach to uncover phosphomimetic inhibitors of BRCA1 C-terminal domain. *ACS Chemical Biology*, 10(5): 1198-208. (2015)

## 2.1 Introduction

Many current cancer treatments employ chemotherapy or ionizing radiation to induce DNA damage in cells, thus triggering cell cycle arrest or cell death. However, the efficacies of general DNA damaging cancer treatments are largely limited by the lack of specificity to target cancer cells, and the long-term treatment resistance caused by feedback activation of DNA damage repair in cancer cells. Therefore, development of inhibitory compounds that target DDR proteins can improve the specificity of many existing DNA damaging cancer therapies (Murai, 2017; O'Connor, 2015; Samadder et al., 2016).

BRCA1 is an important tumor suppressor protein, and mutations in the BRCA1 gene can result in increased risk of hereditary breast and the female ovarian cancer in human (Castilla et al., 1994; Miki et al., 1994; Petrucelli et al., 1993). Whereas BRCA1 plays important roles in response to DSB and drives HR (Huen et al., 2010; Mermershtain and Glover, 2013), it has been shown that breast or ovarian cancer patients with HR-deficient BRCA1 mutations (such as M1775R/K) are highly sensitive to PARP inhibitors treatment that mainly targets to suppress SSB repair in cells (De Lorenzo et al., 2013). However, over 95% of sporadic breast and ovarian cancer patients carry WT BRCA1 (Johnson et al., 2013). Several studies have indicated that mutations on BRCA1 BRCTs that abolish phosphoprotein-binding activity of BRCA1 are also highly associated with HR deficiency (Lee et al., 2010). Therefore, development of inhibitory compounds that target BRCA1 BRCT may produce a functional mimic of HR-deficient BRCA1 mutant, and suppress DSB repair in tumor cell under DNA damaging cancer therapy.

Development of inhibitory drug compounds that target BRCA1 BRCTs remains challenging. Attempts using either virtual or high-throughput screening failed to yield any promising small molecule compound. Although several peptidomimetic compounds with ideal specificity toward BRCA1 BRCTs are known (Pessetto et al., 2012; Yuan et al., 2011), these are all phosphopeptides that has poor cellular permeability due to the presence of their

polar phosphate head group. In addition, hydrolysis of the phosphate group by phosphatases in cells makes it difficult to preserve the phosphate group on the phosphopeptide until it reaches the targeting BRCA1 proteins. Recently, our collaborator, Dr. Matt Hartman (Department of Chemistry, Virginia Commonwealth University), has incorporated unnatural amino acids into an mRNA displayed peptide library using a reconstituted *Escherichia coli* (*E. coli*) ribosomal translation system they called PURE (Ma and Hartman, 2012) and screened  $1.3 \times 10^{13}$  mRNA-peptides against human BRCA1 BRCTs (Figure 2-1). Among all the non-phosphorylated peptides from their library, they found peptide 8.6 (MCTIDFaDEYRFaRKT-NH<sub>2</sub>, Fa: 4-FluoroPhenylalanine) has the highest affinity towards BRCA1 BRCTs. After replacing the 4-FluoroPhenylalanine (FPhe) in peptide 8.6 with phenylalanine in the peptide 8.6 Nat (MCTIDFDEYRFRKT-NH<sub>2</sub>), the interaction with BRCA1 BRCTs is further enhanced (Figure 2-2). Using a competitive fluorescence polarization assay, we have validated that peptide 8.6 competes with BACH1/FANCJ peptide in the interaction with tandem BRCT domains of BRCA1 *in vitro*. We also have successfully co-crystallized a shorter analog of peptide inhibitor 8.6 3-14 (which lacks the N-terminal Met-Cys) in complex with human BRCA1 BRCTs and solved its structure to 3.05 Å. Our structure together with our mutagenesis analysis *in vitro* implies the E-X-X-F<sup>4-fluoro</sup> motif from inhibitor peptide 8.6 can partially mimic the pS-X-X-F motif of BACH1/FANCJ in interaction with BRCA1 BRCTs. Moreover, we discovered a small hydrophobic groove in BRCA1 BRCTs between  $\beta 1$  and  $\alpha 1$ , which forms van der Waals interactions with N-terminal hydrophobic residues (-2 Phe and -4 Ile) of the peptide. While *in vivo* study results from our collaborator provided promising drug potential of peptide inhibitor 8.6 Nat, we believe the structure insight revealed by our study could guide further refinement of this non-phosphopeptide inhibitor. Also, our study may provide new strategies for the small molecule inhibitor development of BRCA1 BRCTs using virtual screening techniques.

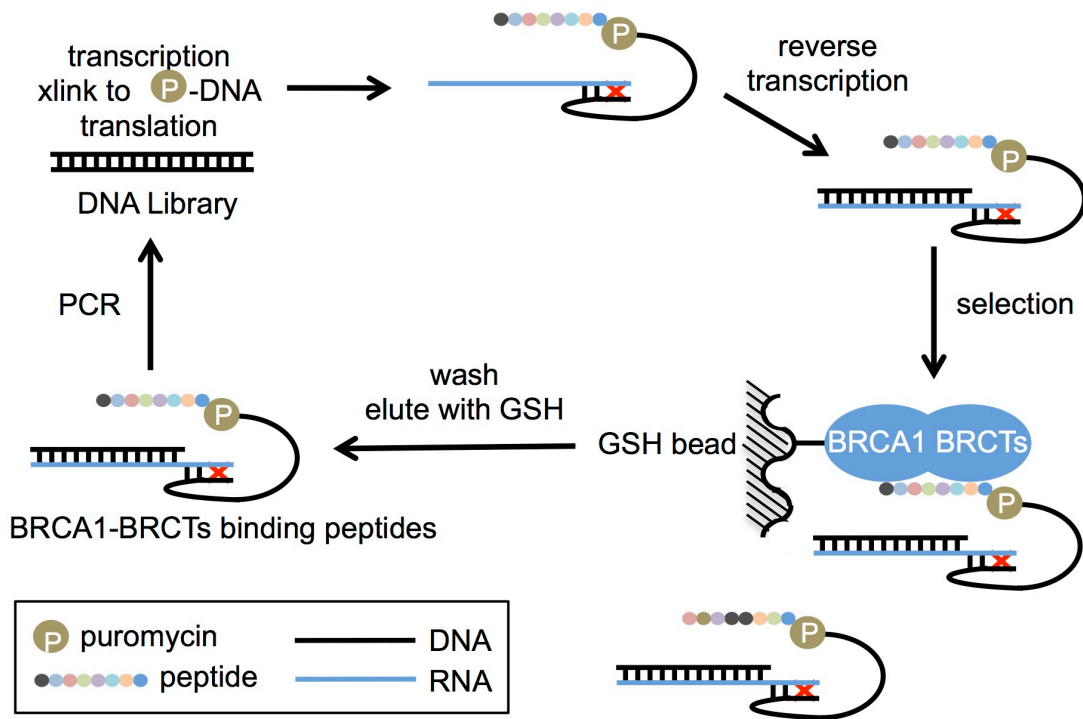
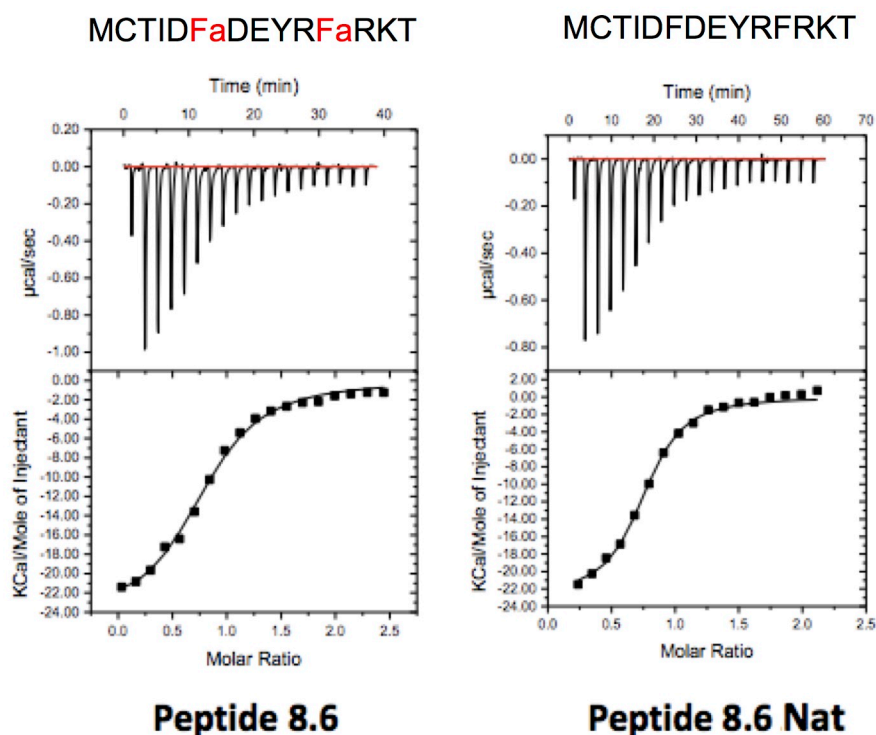


**Figure 2-1. *In vitro* screening for BRCA1 BRCTs inhibitors.**

Starting with a single-stranded cDNA library encodes a 12 amino acid random region with an N-terminal cysteine, an mRNA library is prepared by *in vitro* transcription. This mRNA is then photo-crosslinked to a puromycin-containing linker. *In vitro* translation then leads to a linear peptide which is purified on Oligo(dT)-Cellulose. During this process, the unnatural amino acids are incorporated into the peptide library along with 14 canonical amino acids. After mRNA-peptide fusion formation, peptides with a second cysteine are cyclized with dibromoxylene on the oligo(dT) column. Purified mRNA-peptide fusions then undergo reverse transcription before being selected for binding to GST-BRCA1 BRCTs fusion immobilized on magnetic resin. Unbound peptides are washed away, and bound peptides are eluted, PCR amplified, and carried through another round of selection.



Peptide	N (Sites)	K ( $M^{-1}$ )	$\Delta H$ (kcal/mol)	$\Delta G$ (kcal/mol)	$T\Delta S$ (cal/mol/deg)	$1/K$ ( $\mu M$ )
8.6	$0.80 \pm 0.01$	$2.7 \cdot 10^5 \pm 3 \cdot 10^4$	$-24.6 \pm 0.6$	$-7.40 \pm 0.06$	$-17.3 \pm 0.6$	$3.69 \pm 0.11$
8.6 Nat	$0.73 \pm 0.01$	$9.9 \cdot 10^5 \pm 1 \cdot 10^4$	$-22.7 \pm 0.5$	$-8.17 \pm 0.01$	$-14.6 \pm 0.6$	$1.01 \pm 0.01$

**Figure 2-2. BRCA1 BRCTs interaction with peptide 8.6 characterized by isothermal titration calorimetry.**

Titration were conducted with the indicated peptides into TR-BRCA1 BRCTs fusion protein (BRCA1 BRCTs with N- terminal thioredoxin fusion) in a buffer containing 300 mM NaCl, 2.7 mM KCl, and 10 mM phosphate, pH 7.4. All measurements were conducted at 25 °C with TR-BRCA1 BRCTs concentrations of 30-33  $\mu M$ , and peptide concentrations of 426  $\mu M$  and 323  $\mu M$  for peptides 8.6 and 8.6 Nat, respectively. This experiment was done by Dr. Hartman's group. The sequences of each peptide are displayed on their ITC results. Fa: 4-FluoroPhenylalanine.

## 2.2 Results

### 2.2.1 Peptide 8.6 inhibits BRCA1 BRCTs interaction with other phosphorylated protein partners

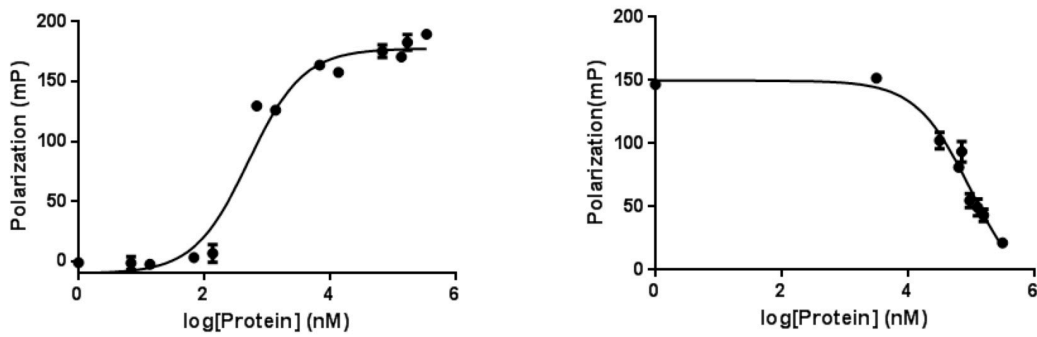
It is well known that BRCA1 BRCTs can interact with many protein partners including BACH1/FANCI (Clapperton et al., 2004), Abraxas (Wu et al., 2016) and CtIP (Varma et al., 2005) in a phosphorylation-dependent manner. Using the fluorescence polarization assay, we first measured the interaction between BACH1/FANCI peptide and BRCA1 BRCTs and obtained a binding affinity of  $K_d \approx 0.28 \mu\text{M}$  (Figure 2-3A left). Interested in whether peptide 8.6 can block BRCA1 BRCTs interaction with BACH1/FANCI peptide *in vitro*, we carried out a competition assay by treating BRCA1 BRCTs with increasing concentration of peptide 8.6. We observed a clear decrease in polarization, indicating peptide 8.6 has inhibited BRCA1 BRCTs interaction with the BACH1/FANCI peptide. The inhibition curve has an  $IC_{50} \approx 98.3 \mu\text{M}$ , which is equivalent to  $K_i \approx 11 \mu\text{M}$  (Figure 2-3A right).

Our collaborator also examined the effectiveness of peptide 8.6 Nat in inhibiting BRCA1 BRCTs interaction with CtIP using immunoprecipitation assay with crude cell lysate. As shown by the western result, we observed an apparent inhibition of CtIP interactions with peptide 8.6 Nat treatment of  $> 5 \mu\text{M}$  and almost complete inhibition around  $50 \mu\text{M}$  (Figure 2-3B). Together, we concluded that peptide 8.6 is indeed an inhibitory compound that blocks PPI of BRCA1 BRCTs.

### 2.2.2 The crystal structure of nonphosphopeptide inhibitor in complex with BRCA1 BRCT

To define the mechanism by which peptide 8.6 binds the BRCA1 BRCTs, we

A



B

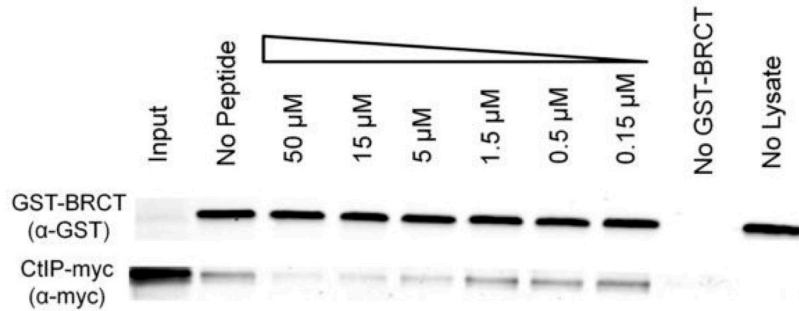


**Figure 2-3. Peptide 8.6 blocks BRCA1 BRCTs PPIs.**

(A) FP competition assay of peptide 8.6 against BACH/FANCJ peptide (both FITC labeled) on BRCA1 BRCTs. (B) Pull-down Western blot showing the effect of increasing concentrations of the peptide 8.6 Nat on the capture of phospho-CtIP from cell lysates with BRCA1 BRCTs beads. Only a portion of CtIP is phosphorylated; hence, the contrast in intensity between input and bound. Panel B of this figure is result from Dr. Hartman's group.

successfully solved the crystal structure of peptide 8.6 3-14 (which lacks the N-terminal Met-Cys and is more soluble) bound to human BRCA1 BRCTs. Distinct from the BRCA1 BRCTs apo structure (PDB ID: 1JNX) which belong to the  $P6_22$  space group, our crystals belong to the tetragonal space group  $P4_1$  and contain only one protein/peptide complex in the asymmetric unit. After initial molecular replacement against BRCA1 BRCTs apo structure, we observed apparent density for the peptide on the phosphopeptide binding interface. We were able to model in the entire peptide sequence and refine the whole structure at 3.05 Å resolution (Figure 2-4 and Table 2-1).

### **2.2.3 The E-x-x-F motif can partially mimic pS-x-x-F in BRCA1 BRCT recognition**

An alignment of our structure with the structure of BACH1/FANCI peptide bound to BRCA1 BRCTs reveals that the Glu-X-X-4FPhe (E-X-X-F) motif of peptide 8.6 tracks closely along the pSer-X-X-Phe (pS-X-X-F) motif and the structures of the BRCA1 BRCT domains are essentially identical (RMSD 0.4 Å for all C $\alpha$  atoms) (Figure 2-5A). The 4FPhe residue at the +3 position of peptide 8.6 overlays closely upon the phenylalanine of the natural peptide (Figure 2-5B), while the phosphomimetic glutamate is positioned to provide two of the three hydrogen bond/salt bridge interactions within the phosphate binding pocket (Figure 2-5C). The two available oxygen atoms of the glutamate side chain form hydrogen bonds with the Ser1655 side chain hydroxyl and the Gly1656 main chain amide. However, this binding mode sacrifices the salt bridge to Lys1702. Instead, a long-range (~4.5 Å) electrostatic interaction between Lys1702 e-amino group and the glutamate may partially stabilize binding. The selected peptide also contains a Lys at +5, which makes salt bridging interactions with Glu1836 and Asp1840, an interaction that is also observed in the BRCA1 BRCTs-BACH1/FANCI peptide complex (Figure 2-5E).

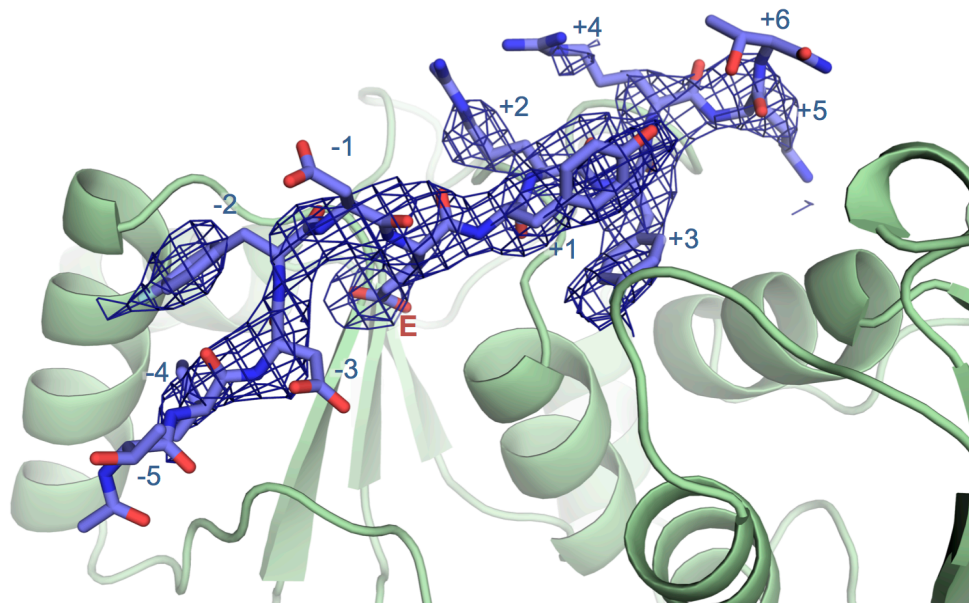


**Figure 2-4. Representative bias-reduced electron density of BRCA1 BRCT bound to peptide 8.6 3-14.**

The structural view shown is directed into the peptide-BRCT interface with the peptide and associated electron density (contoured at 2.0 sigma level) colored blue, and the BRCA1 BRCT colored green. The electron density map was calculated using the “prime-and-switch” method using the final refined structure to calculate the initial phases used in the bias reduction procedure.

---

**Table 2-1. Data Collection, Phasing and Refinement Statistics**

BRCA1 BRCTs- peptide 8.6 Complex	
Space group	P 41
Unit cell dimensions (Å)	
a	37.811
b	37.811
c	175.933
Resolution range (Å) <sup>a</sup>	37.8-3.05 (3.16-3.05)
No. of observed reflections	20159
Completeness (%)	100
Overall I/sigma (I)	11.08 (2.65)
R <sub>sym</sub> <sup>b</sup>	13.5 (63.9)
R <sub>free</sub> / R <sub>work</sub> (%) <sup>c</sup>	23.75/21.05
Number of atoms	1791
Average B factor	60.9
Ramachandran Plot (%)	
Most favoured	95
R.M.S. Deviation	
Bonds (Å)	0.004
Angles (°)	1.060

---

<sup>a</sup>Values in parentheses are from the highest resolution shell.  
<sup>b</sup> $R_{sym} = \sum |I - \langle I \rangle| / \sum I$   
<sup>c</sup> $R = \sum ||F_o| - |F_c|| / \sum |F_o|$

---

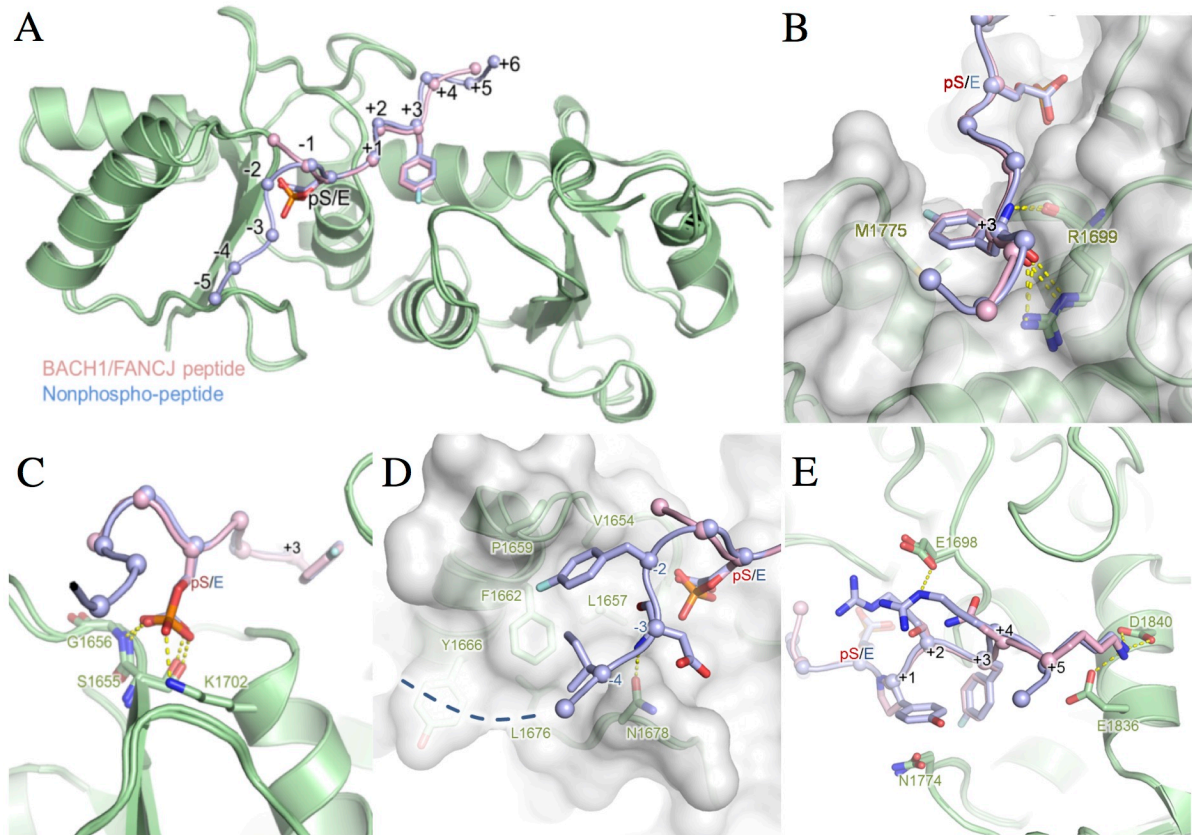


**Figure 2-5. Crystal structure of BRCA1 BRCT bound to peptide 8.6.**

(A) The overall structure of the BRCA1 BRCT-peptide complex (peptide in blue and the BRCT domain in green) superimposed on the structure of BRCA1 BRCT-BACH1 peptide complex (PDB ID: 1T15; BACH1 peptide in pink). (B) Comparison of interactions in the BRCA1 BRCT phosphate binding pocket between peptide 8.6 Glu and the BACH1 pSer with hydrogen bonds highlighted in yellow. (C) Recognition of the peptide +3 residue. (D) Interactions between N-terminal BRCT and residues -2 to -4 of peptide 8.6. Additional residues N-terminal to the -5 position are indicated by the blue dashed line. (E) The interaction between the C-terminal BRCT and peptide +1 to +5 residues.

#### **2.2.4 Additional interactions that support peptide 8.6 recognition by BRCA1 BRCT**

The substitution of the phospho-serine for a glutamate is expected to dramatically reduce peptide binding affinity (Lokesh et al., 2007). To compensate for this loss in binding energy, peptide 8.6 makes several additional contacts to the BRCTs. Residues N-terminal to the glutamate (residues -2 to -5) occupy a hydrophobic groove in the BRCTs domain between  $\beta 1$  and  $\alpha 1$ . In particular, the -2 4FPhe and the -4 Ile residues pack in this cleft, providing van der Waals contacts (Figure 2-5D). Although the peptide utilized in crystallization terminates at -5, the actual peptide 8.6 extended to -7 with the additional -6 Met and -7 Cys residues that could interact with this groove. In addition, residues at the +1, +2 and +4 positions also contact the BRCTs in ways that are predicted to enhance binding (Figure 2-5E). The selected Tyr at +1 stacks against Asn1774 and also packs at against the Phe at +3. The +1 position is either a proline or a tyrosine in all structures determined to date that have a pS-x-x-F motif in peptides. Arginine residues are selected at the +2 and +4 positions, which are oriented towards Glu 1698, providing electrostatic contacts that are absent in any of the complexes determined with pS-X-X-F containing peptides. A summary of the crystal structure contacts is shown in Figure 2-6A.

#### **2.2.5 Structure-guided mutagenesis study reveal additional interface for inhibitor design**

To further characterize the difference between peptide 8.6 and the native pSer peptide from BACH1 in interaction with the BRCA1 BRCTs, we generated several BRCA1 BRCT mutants and examined their affinity with both peptides using a fluorescence polarization (FP) assay (Figure 2-6B, 2-7A and Table 2-2). As expected, mutations within the conserved pS-X-X-F recognition groove (M1775R, S1655A, K1702M) completely abolished recognition of the pSer peptide. In contrast, only M1775R mutant completely abrogated

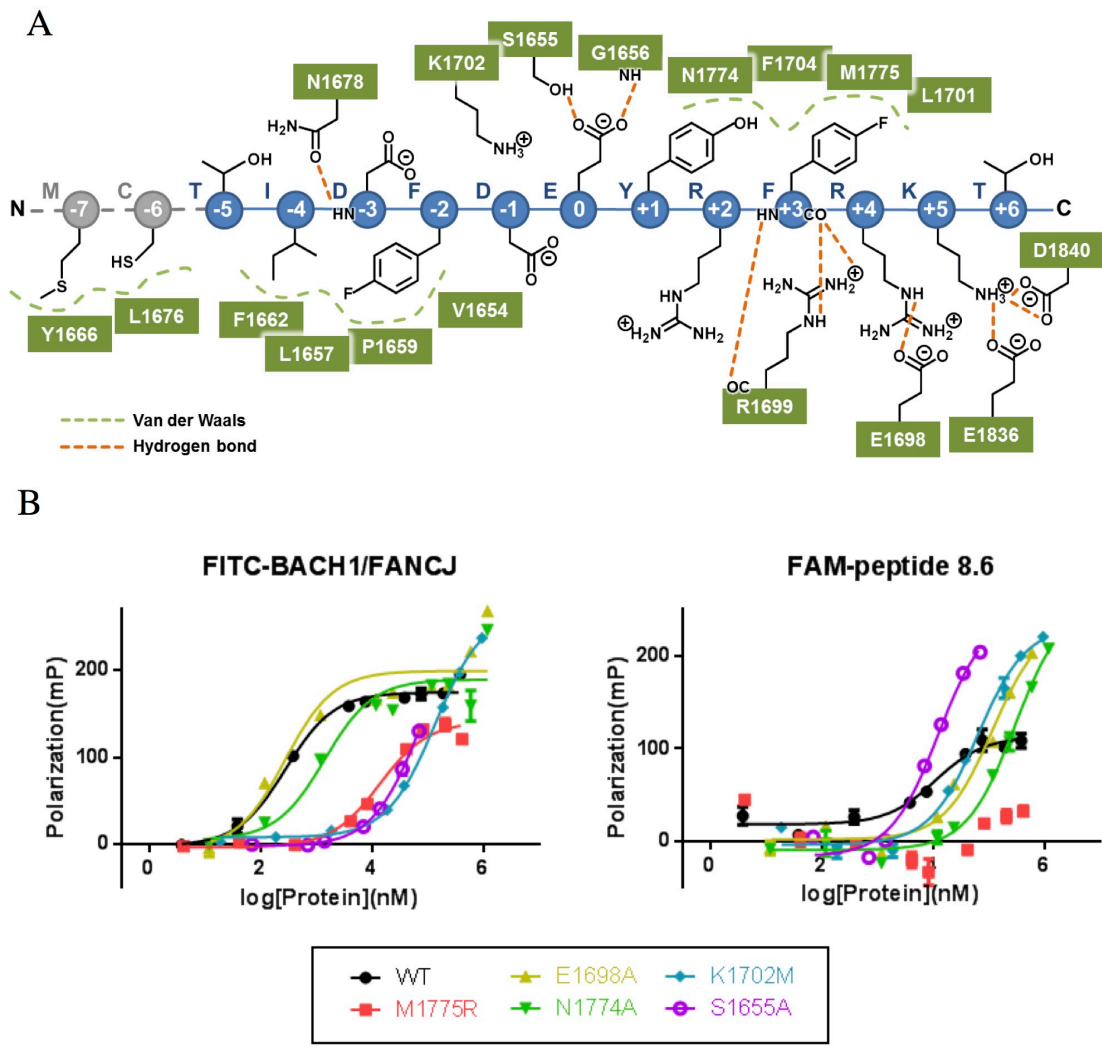


**Figure 2-6. Crystal structure of BRCA1 BRCT bound to peptide 8.6.**

(A) Summary of the crystal structure contacts of peptide 8.6 with the BRCA1 BRCT domain. Residues absent in crystal structure are shown in grey. (B) Binding curves of the pSer-containing BACH1 peptide or Fam-8.6 to various protein mutants.

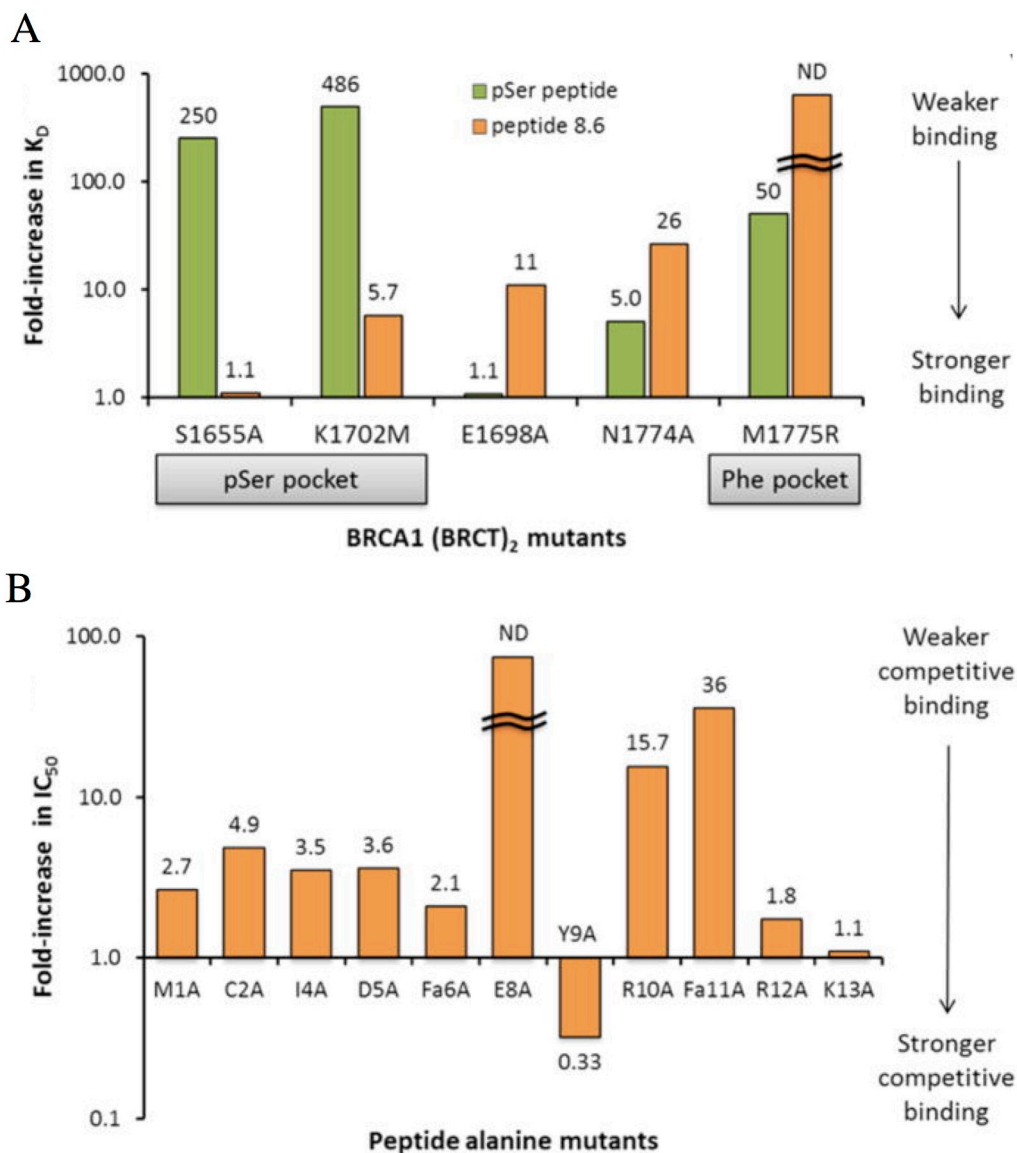


**Figure 2-7. Analysis of binding with protein and peptide mutants by fluorescence polarization.**

(A) Comparison of binding affinities of peptides (FITC-BACH1 or FAM-8.6) with a series of GST-BRCA1 BRCTs mutants. The fold-increases in  $K_D$  values were normalized against the  $K_D$  of the WT GST-BRCA1 BRCTs. (B) Changes in competitive binding observed with alanine mutants of peptide 8.6. The values reported were derived by dividing the  $IC_{50}$  of the mutant peptide with the  $IC_{50}$  of WT peptide 8.6 under identical conditions. ND = no binding or competitive binding detected. Fa refers to 4-fluorophenylalanine. These results are from Dr. Hartman's group.

**Table 2-2. Summary of Fluorescence Polarization Study Results**

<b>Protein</b>	<b>BRCA1-peptide <math>K_D</math> (<math>\mu</math>M)</b>	
	<b>FITC-BACH1 peptide</b>	<b>Fam-peptide 8.6</b>
WT	$0.28 \pm 0.04$	$11 \pm 3$
M1775R	$14 \pm 2$	ND <sup>b</sup>
E1698A	$0.3 \pm 0.1$	$120 \pm 20$
N1774A	$1.4 \pm 0.5$	$290 \pm 40$
K1702M	$136 \pm 9$	$63 \pm 9$
S1655A	$70 \pm 10$	$12 \pm 2$

<sup>a</sup> GST-BRCA1 BRCTs

<sup>b</sup> ND = no binding or competitive binding detected.

binding of peptide 8.6. The K1702M mutant only reduced peptide 8.6 binding by ~6-fold, and the S1655A mutant demonstrated binding that is indistinguishable from wild type. This suggests that the Phe recognition pocket at the interface between the two BRCT repeats is critical for peptide 8.6 binding, and that the integrity of the pSer binding pocket, formed by Ser1655 and Lys1702, is less important. The finding that the K1702M mutation significantly impacts peptide 8.6 binding but the S1655A mutation does not is consistent with the idea that the positive charge of Lys1702 acts to stabilize the negative charge of the glutamate. The fact that the S1655A mutation does not impact binding could be explained if the glutamate residue can rotate to hydrogen bond with the main chain NH of Gly1656 and Lys1702. The novel contacts involving Glu1698 and Asn1744 were also tested. The results reveal significant 11- and 26-fold reductions in binding affinity for E1698A and N1774A, respectively to peptide 8.6, but no significant change in affinity to the wild type pSer peptide.

To validate our mutagenesis result, our collaborator performed an alanine scan to further understand how each residue contributes to the affinity of the peptide (Figure 2-7B and Table 2-3). The N-terminal residues that we tested all affect competitive binding; including those that sit in the hydrophobic groove (I4, and F<sub>a</sub>6) and the N-terminal Met and Cys, which were not present in the crystallized peptide. Based on the crystal structure, it was not surprising that the Glu-Tyr-Arg-4FPhe portion of the peptide contained the residues most essential for binding. Substituting either the Glu (E8) or the 4FPhe (F<sub>a</sub>11) residues resulted in the largest reductions in competitive binding. The Arg (R10) alanine mutant also showed a large (16-fold) reduction in affinity which validates the importance of the interaction with E1698 in the crystal structure. We were surprised to find that the Tyr to alanine mutant (Y9A) competed more effectively for binding than the wild-type 8.6, which suggests that either the interaction between the Tyr side chain and N1774 is unimportant, or that the loss in that interaction is compensated for by a reduction in the entropic cost of binding. Finally, the C-terminal Arg (R12) and Lys (K13), although they both form salt bridges in the crystal structure, were not required for competitive binding.

**Table 2-3. Summary of Alanine Scan Result of Peptide 8.6**

Peptide	Sequence <sup>a, b</sup>	IC <sub>50</sub> (μM) <sup>c</sup>
WT	Ac -MCTIDFDEYRFRKT -NH <sub>2</sub>	2.0 ± 0.2
M1A	Ac -ACTIDFDEYRFRKT -NH <sub>2</sub>	5.3 ± 0.3
C2A	Ac -MATIDFDEYRFRKT -NH <sub>2</sub>	10 ± 1
I4A	Ac -MCTADFDEYRFRKT -NH <sub>2</sub>	7 ± 1
D5A	Ac -MCTIAFDEYRFRKT -NH <sub>2</sub>	7 ± 3
F6A	Ac -MCTIDADEYRFRKT -NH <sub>2</sub>	4.2 ± 0.9
E8A	Ac -MCTIDFDAYRFRKT -NH <sub>2</sub>	ND <sup>d</sup>
Y9A	Ac -MCTIDFDEARFRKT -NH <sub>2</sub>	0.8 ± 0.1
R10A	Ac -MCTIDFDEYAFRKT -NH <sub>2</sub>	31 ± 5
R12A	Ac -MCTIDFDEYRFAKT -NH <sub>2</sub>	3.5 ± 0.5
K13A	Ac -MCTIDFDEYRFRAT -NH <sub>2</sub>	2.2 ± 0.7

<sup>a</sup> Unnatural amino acids are highlighted by bold text.

<sup>b</sup> Position equivalent to pSPTF motif in peptide 8.6 were highlighted by grey background.

<sup>c</sup> IC<sub>50</sub> values are based on a competition FP assay with 20 nM of peptide FAM-β-A-pSPTF and 2.7 μM of thioredoxin-BRCA1 BRCTs fusion and variable concentrations of each peptide. IC<sub>50</sub> values were calculated by fitting with a four parameter logistic equation.

<sup>d</sup> ND = no binding or competitive binding detected.

### 2.2.6 Peptide 8.6 interferes with DNA damage response

Although we have shown that peptide 8.6 can actively inhibit BRCA1 BRCT interaction with a protein partner involved in HR, it was unclear whether this could inhibit HR in cells subjected to with DNA damage. To further examine the effect of peptide 8.6 in cells, T98 human glioblastoma cells transduced with EGFP or EGFP tagged peptide 8.6 Nat were examined by our collaborator. They first evaluated DSB level in cells by analyzing  $\gamma$ -H2AX foci. Cells treated with DOX to initiate induction of EGFP-8.6 Nat production showed a significantly (2.3-fold) higher background of  $\gamma$ -H2AX foci than untreated cells, suggesting that the induction of EGFP-8.6 Nat correlates with increased DNA damage (Figure 2-8A). Upon irradiation, the level of  $\gamma$ -H2AX foci also increased in the presence of EGFP-8.6 Nat as compared to cells lacking DOX induction (6.8-fold vs 4.3-fold). Neither of these effects are observed in cells expressing EGFP alone, although the comparative data with these cells is somewhat obscured by a higher basal level of foci. They then analyzed the Rad51 foci that mark HR level in these cells and observed a similar trend. Rad51 foci are increased in EGFP-8.6 Nat cells after induction with DOX both in the presence and absence of IR. This enhancement is not observed in T98 cells expressing EGFP alone (Figure 2-8B). This suggests that the inhibition of DNA repair caused by peptide 8.6 is likely due to aberrant homologous recombination.

## 2.3 Discussion

In summary, we have validated the first non-phosphorylated peptide inhibitor (peptide 8.6) of BRCA1 BRCTs *in vitro*, and in cells results from our collaborator further proved this peptide could block PPIs of the BRCA1 BRCTs and disrupt DNA repair by HR. We successfully solved the crystal structure of BRCA1 BRCTs-peptide 8.6 complex. Comparison of our structure with the BRCA1 BRCTs-BACH/FANCI peptide complex shows the Glu-X-X-4FPhe motif of inhibitor peptide 8.6 mimics the pSer-X-X-Phe motif

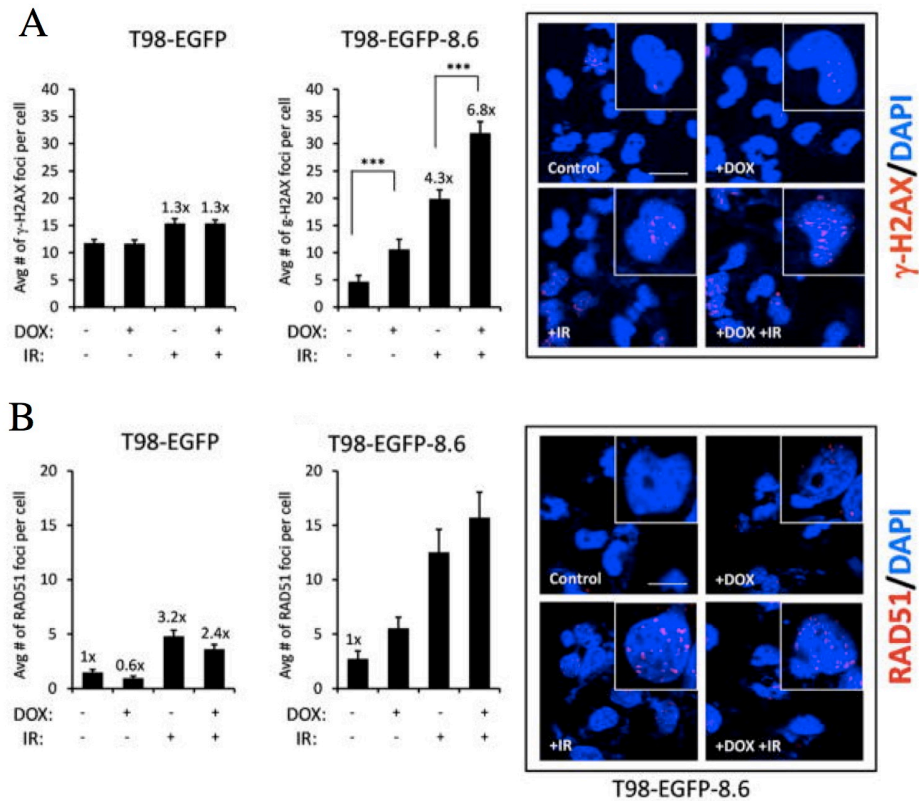


**Figure 2-8. Peptide 8.6 interferes with the DNA damage response.**

T98 cells transduced with either a TRIPZ-EGFP (T98-EGFP) or TRIPZ-EGFP-8.6 Nat (T98-EGFP-8.6) construct were treated with or without DOX for 7 days. DOX-treated T98-EGFP-8.6 cells had significantly ( $p < 0.05$ ) higher (A)  $\gamma$ -H2AX and (B) Rad51 foci than untreated cells, an effect that was more pronounced after 5 Gy radiation. Cells were fixed 3 h after irradiation. Right panel: foci appearing in TRIPZ-EGFP-8.6 Nat cells as quantified in the bar diagram. Blue staining (DAPI) indicates nuclei, red staining indicates (A)  $\gamma$ -H2AX or (B) RAD51. Single cell inset shows digital magnification of representative 63 $\times$  field. Scale bar is equal to 33.5  $\mu$ m. Results in this figure are from Dr. Hartman's lab.

from conventional phosphorylated peptide while interacting with BRCA1 BRCTs. However, as previously indicated by other researchers (Lokesh et al., 2007), the E-X-X-F motif itself does not have enough binding affinity towards BRCA1 BRCTs. Results from our structural guided mutagenesis study of BRCA1 BRCTs-peptide 8.6 interaction reveals many new features that are absent in the BRCA1 BRCTs-BACH/FANCI peptide complex. We identified a new hydrophobic groove in the BRCTs domain between  $\beta_1$  and  $\alpha_1$  occupied by N-terminal hydrophobic residues from peptide 8.6, and some additional electrostatic interactions between arginine at +2 and +4 positions of peptide 8.6 and Glu1698 from BRCA1 BRCTs.

It has been shown that BRCTs from several other DDR proteins also bind phosphorylated peptide targets (Rodriguez et al., 2003; Rodriguez and Songyang, 2008). Our structure models of peptide 8.6 docking into phosphopeptide binding pocket of other BRCTs indicates the core E-X-X-F interactions remain conserved for MDC1 BRCTs (Figure 2-9A) and TopBP1 BRCT7/8 (Figure 2-9B). Interested in the specificity of peptide 8.6, our collaborator also examined peptide 8.6 interactions with other BRCTs, which function as peptide-binding modules. They found no significant interaction between peptide 8.6 and other BRCTs, suggesting peptide 8.6 has very high specificity against BRCA1 BRCTs (Figure 2-9C). Alignments of our structure models show the new electrostatic or hydrophobic interactions between peptide 8.6 and BRCA1 BRCT are no longer conserved with other BRCTs (Figure 2-9B). Since previous virtual screening of BRCA1 BRCT inhibitors mainly focused on docking towards the phosphate binding pocket and the +3 hydrophobic groove that interact with the core pS-x-x-F motif, we believe the new structural features, such as the additional hydrophobic groove between  $\beta_1$  and  $\alpha_1$ , revealed by our study, could be used to guide the development of new small molecule inhibitors.

Although better known for its interactions with phosphoproteins, BRCA1 BRCT is also found to interact with several proteins in a phosphorylation independent manner

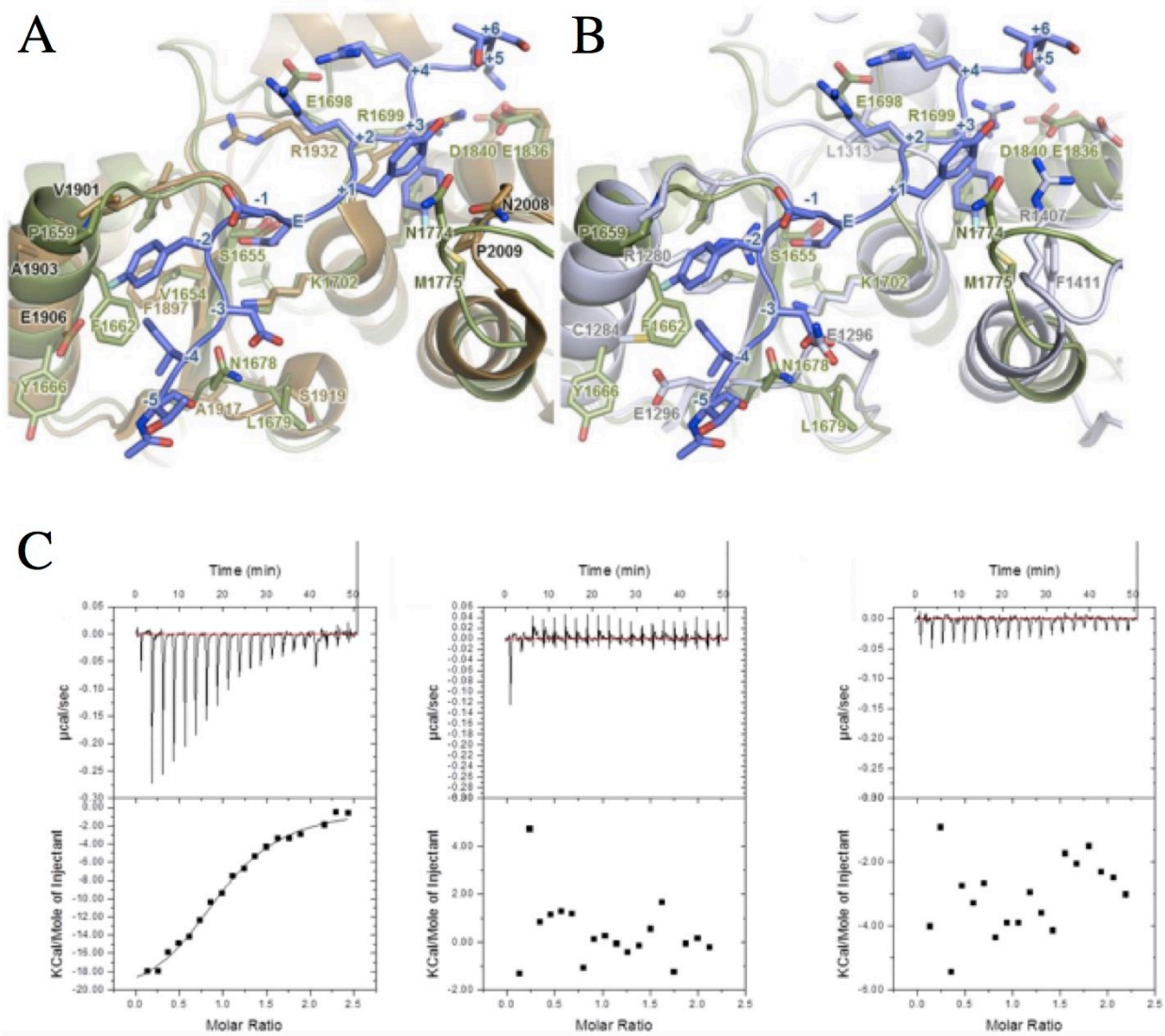


**Figure 2-9. Peptide 8.6 binds specifically to the BRCA1 BRCT and not to other related BRCT proteins.**

(A) Alignment of the BRCA1 BRCT – peptide 8.6 complex (green and blue, respectively) with the MDC1 BRCT domain (brown, PDB code 2AD0). Key residues at the BRCT-peptide interface are shown as sticks and labeled. (B) Alignment of the BRCA1-peptide 8.6 complex with TopBP1 BRCT7/8 (grey, PDB code 3AL3). (C) Isothermal titration calorimetric measurements reveal an interaction with BRCA1 BRCTs (left), but not MDC1 BRCTs (middle) or TopBP1 7/8 BRCTs (right). Results in panel C are from Dr. Hartman’s lab.

(Woods et al., 2012). A recent study from Dr. David Chen's lab suggested that the DNA-dependent protein kinase catalytic subunit (DNA PKcs) interacts with BRCA1 BRCT in a phosphorylation independent manner. However, they were only able to narrow down the BRCA1 BRCT target on DNA PKcs between residues 1500-2182 (Davis et al., 2014). Interestingly, this region contains four E-X-X-F motifs (Figure 2-10). It will be interesting to examine these motifs to see whether they are involved in BRCA1 BRCTs recognition.

Finally, our study also showed that the new phosphomimetic peptides screening method developed by our collaborator is useful in identifying potential peptide targets of specific BRCT domains. Future application of this technology to BRCT domains from other BRCT family proteins as well as other phosphoserine-mediated PPIs can not only help us to develop useful phosphomimetic peptide tools but may also unravel a new mechanism of interaction between DDR proteins.

## **2.4 Material and Methods**

### ***Cloning, expression and purification***

Human BRCA1-BRCTs (1646-1859) was expressed as an untagged recombinant protein in *E. coli* strain BL21 (DE3) then purified as previously described (Williams et al., 2001). Human BRCA1-BRCTs (1646-1859) was re-cloned into pGEX6P-1 vector, and used to make the mutants: S1655A, E1698A, K1702M, N1774A using QuickChange Lightning site-directed mutagenesis kit (Stratagene) (Braman et al., 1996; Kunkel, 1985; Nelson and McClelland, 1992; Sugimoto et al., 1989; Taylor et al., 1985; Vandeyar et al., 1988). GST tagged recombinant proteins were expressed in *E. coli* strain BL21 (DE3) and purified as previously described (Campbell et al., 2010).

### ***Crystallization***

The BRCA1 BRCT protein was concentrated to 10 mg/mL in storage buffer (400 mM NaCl,

		-7-6-5-4-3-2-1		+1+2+3+4+5+6	
Peptide 8.6			MCTIDFDE	YRFRKT	
DNA PKcs	1508		QLASGLLE	LAFAFG	1522
	1768		MEQQHVME	EELFQSS	1782
	1951		VICCVFNE	LKIFYQG	1965
	2147		AKLVINRE	EEVFRPY	2161

**Figure 2-10. Potential DNA PKcs targets of BRCA1 BRCTs.**

The non-phosphopeptide BRCA1 BRCT inhibitor is used as a template and its alignment with all 14 amino acid length sequences from DNA PKcs (1500-2182) that contain E-X-X-F motifs (Glu in blue, Phe in green) is shown here.

10 mM Tris-HCl, pH 7.5) then incubated with –MC peptide 8.6 at 1:3 protein to peptide ratio for 2 hours at 4°C. Crystals were grown using sitting drop method by mixing 0.8 µL of protein/peptide mixture with 1.0 µL of crystallization buffer (0.1 M sodium cacodylate, 0.1 M magnesium acetate, 24% PEG 6000, pH 6.5) and harvested after 24 hours. Suitable crystals were cryo-protected by immersion in crystallization buffer supplemented with 20% glycerol (v/v) prior to freeze in liquid nitrogen.

#### ***Data collection and structure refinement.***

Data were collected at beamline 08B1-1 (Canadian Light Source), and the intensity data were processed with HKL2000 (Otwinowski and Minor, 1997). The crystals are in cylinder shape. Crystals belonged to the tetragonal space group  $P 41$  ( $a = b = 37.8 \text{ \AA}$ ,  $c = 176.0 \text{ \AA}$ ,  $\alpha = \beta = \gamma = 90.0^\circ$ ) with a single protein/peptide complex in the asymmetric unit. The complex structure was solved with Phaser (McCoy, 2007) using the BRCA1 BRCTs crystal structure (PDB ID:1JNX) (Williams et al., 2001) as a search model. The inhibitor peptide was then built in manually in Coot (Emsley and Cowtan, 2004) based on the additional electron density around the conserved pSer-X-X-Phe motif recognition site. The BRCT domain from the higher resolution structure of the BRCA1 BRCTs/ATRIP peptide complex (PDB ID: 4IGK) (Liu and Ldias, 2013) was superimposed on the current model and used as the basis for further refinement. Loop regions 1792-1807 and 1816-1819 were modeled based on their conformation in 1JNX. Due to a lack of density, residues Glu1817 and Asp1818 were left out of the final model. Statistics of data collection, processing, and refinement are provided in Table 2-1.

#### ***Fluorescence polarization (FP) assay***

The affinity of the BRCA1-BRCTs proteins for either the N-terminally fluorescein labeled version of 8.6 (FAM-8.6: FAM- $\beta$ -Ala-MCTIDFDEYRFRKT-NH<sub>2</sub>) as well as a pSer-x-x-Phe peptide derived from BACH1 (FITC-SRSTpSPTFNK-NH<sub>2</sub>) were both determined through a direct FP binding assay. Labeled peptide (10 nM of FAM-8.6 or FITC-BACH1) were mixed

with freshly concentrated WT or mutant BRCTs (20 nM-300  $\mu$ M). In the first competition assay I performed between peptide 8.6 and FITC labeled BACH1, peptide 8.6 (MCTIDFDEYRFRKT-NH<sub>2</sub>) was incubated at various concentrations with a mixture of BRCA1 BRCTs (2.5  $\mu$ M) and 10nM FITC-BACH1 peptide. In the second set of competition assays done by Dr. Hartman's group, each alanine mutant of peptide 8.6 was incubated at various concentrations with a mixture of BRCA1 BRCTs (2.5  $\mu$ M) and the peptide FAM- $\beta$ -Ala-pSPTF-NH<sub>2</sub> (20 nM). All measurements were performed using an Envision multi-label plate reader on a 384-well OptiPlate (Perkin Elmer). FP was measured using an excitation wavelength of 485 nm and an emission wavelength of 538 nm after 15 minutes incubation at room temperature. The FP titration data was analyzed, and the dissociation constant ( $K_D$ ) was calculated using GraphPad Prism software.

## 2.5 Reference

1. Braman, J., Papworth, C., and Greener, A. (1996). Site-directed mutagenesis using double-stranded plasmid DNA templates. *Methods Mol Biol* 57, 31-44.
2. Campbell, S.J., Edwards, R.A., and Glover, J.N. (2010). Comparison of the structures and peptide binding specificities of the BRCT domains of MDC1 and BRCA1. *Structure* 18, 167-176.
3. Castilla, L.H., Couch, F.J., Erdos, M.R., Hoskins, K.F., Calzone, K., Garber, J.E., Boyd, J., Lubin, M.B., Deshano, M.L., Brody, L.C., *et al.* (1994). Mutations in the BRCA1 gene in families with early-onset breast and ovarian cancer. *Nat Genet* 8, 387-391.
4. Clapperton, J.A., Manke, I.A., Lowery, D.M., Ho, T., Haire, L.F., Yaffe, M.B., and Smerdon, S.J. (2004). Structure and mechanism of BRCA1 BRCT domain recognition of phosphorylated BACH1 with implications for cancer. *Nat Struct Mol Biol* 11, 512-518.
5. Davis, A.J., Chi, L., So, S., Lee, K.J., Mori, E., Fattah, K., Yang, J., and Chen, D.J. (2014). BRCA1 modulates the autophosphorylation status of DNA-PKcs in S phase of the cell cycle. *Nucleic Acids Res* 42, 11487-11501.
6. De Lorenzo, S.B., Patel, A.G., Hurley, R.M., and Kaufmann, S.H. (2013). The Elephant and the Blind Men: Making Sense of PARP Inhibitors in Homologous Recombination Deficient Tumor Cells. *Front Oncol* 3, 228.
7. Emsley, P., and Cowtan, K. (2004). Coot: model-building tools for molecular graphics. *Acta Crystallogr D Biol Crystallogr* 60, 2126-2132.
8. Huen, M.S., Sy, S.M., and Chen, J. (2010). BRCA1 and its toolbox for the maintenance of genome integrity. *Nat Rev Mol Cell Biol* 11, 138-148.
9. Johnson, N., Johnson, S.F., Yao, W., Li, Y.C., Choi, Y.E., Bernhardt, A.J., Wang, Y., Capelletti, M., Sarosiek, K.A., Moreau, L.A., *et al.* (2013). Stabilization of mutant BRCA1 protein confers PARP inhibitor and platinum resistance. *Proc Natl Acad Sci U S A* 110, 17041-17046.
10. Kunkel, T.A. (1985). Rapid and efficient site-specific mutagenesis without phenotypic selection. *Proc Natl Acad Sci U S A* 82, 488-492.

11. Lee, M.S., Green, R., Marsillac, S.M., Coquelle, N., Williams, R.S., Yeung, T., Foo, D., Hau, D.D., Hui, B., Monteiro, A.N., *et al.* (2010). Comprehensive analysis of missense variations in the BRCT domain of BRCA1 by structural and functional assays. *Cancer Res* 70, 4880-4890.
12. Liu, X., and Ladas, J.A. (2013). Structural basis for the BRCA1 BRCT interaction with the proteins ATRIP and BAAT1. *Biochemistry* 52, 7618-7627.
13. Lokesh, G.L., Muralidhara, B.K., Negi, S.S., and Natarajan, A. (2007). Thermodynamics of phosphopeptide tethering to BRCT: the structural minima for inhibitor design. *J Am Chem Soc* 129, 10658-10659.
14. Ma, Z., and Hartman, M.C. (2012). In vitro selection of unnatural cyclic peptide libraries via mRNA display. *Methods Mol Biol* 805, 367-390.
15. McCoy, A.J. (2007). Solving structures of protein complexes by molecular replacement with Phaser. *Acta Crystallogr D Biol Crystallogr* 63, 32-41.
16. Mermershtain, I., and Glover, J.N. (2013). Structural mechanisms underlying signaling in the cellular response to DNA double strand breaks. *Mutat Res* 750, 15-22.
17. Miki, Y., Swensen, J., Shattuck-Eidens, D., Futreal, P.A., Harshman, K., Tavtigian, S., Liu, Q., Cochran, C., Bennett, L.M., Ding, W., *et al.* (1994). A strong candidate for the breast and ovarian cancer susceptibility gene BRCA1. *Science* 266, 66-71.
18. Murai, J. (2017). Targeting DNA repair and replication stress in the treatment of ovarian cancer. *Int J Clin Oncol*.
19. Nelson, M., and McClelland, M. (1992). *Methods Enzymol* 216, 24.
20. O'Connor, M.J. (2015). Targeting the DNA Damage Response in Cancer. *Mol Cell* 60, 547-560.
21. Otwinowski, Z., and Minor, W. (1997). Processing of X-ray diffraction data collected in oscillation mode. *Methods Enzymol* 276, 307-326.
22. Pessetto, Z.Y., Yan, Y., Bessho, T., and Natarajan, A. (2012). Inhibition of BRCT(BRCA1)-phosphoprotein interaction enhances the cytotoxic effect of olaparib in breast cancer cells: a proof of concept study for synthetic lethal therapeutic option. *Breast Cancer Res Treat* 134, 511-517.

23. Petrucelli, N., Daly, M.B., and Pal, T. (1993). BRCA1- and BRCA2-Associated Hereditary Breast and Ovarian Cancer. In *GeneReviews(R)*, R.A. Pagon, M.P. Adam, H.H. Ardinger, S.E. Wallace, A. Amemiya, L.J.H. Bean, T.D. Bird, N. Ledbetter, H.C. Mefford, R.J.H. Smith, and K. Stephens, eds. (Seattle (WA)).
24. Rodriguez, M., Yu, X., Chen, J., and Songyang, Z. (2003). Phosphopeptide binding specificities of BRCA1 COOH-terminal (BRCT) domains. *J Biol Chem* *278*, 52914-52918.
25. Rodriguez, M.C., and Songyang, Z. (2008). BRCT domains: phosphopeptide binding and signaling modules. *Front Biosci* *13*, 5905-5915.
26. Samadder, P., Aithal, R., Belan, O., and Krejci, L. (2016). Cancer TARGETases: DSB repair as a pharmacological target. *Pharmacol Ther* *161*, 111-131.
27. Sugimoto, M., Esaki, N., Tanaka, H., and Soda, K. (1989). A simple and efficient method for the oligonucleotide-directed mutagenesis using plasmid DNA template and phosphorothioate-modified nucleotide. *Anal Biochem* *179*, 309-311.
28. Taylor, J.W., Ott, J., and Eckstein, F. (1985). The rapid generation of oligonucleotide-directed mutations at high frequency using phosphorothioate-modified DNA. *Nucleic Acids Res* *13*, 8765-8785.
29. Vandeyar, M.A., Weiner, M.P., Hutton, C.J., and Batt, C.A. (1988). A simple and rapid method for the selection of oligodeoxynucleotide-directed mutants. *Gene* *65*, 129-133.
30. Varma, A.K., Brown, R.S., Birrane, G., and Ladas, J.A. (2005). Structural basis for cell cycle checkpoint control by the BRCA1-CtIP complex. *Biochemistry* *44*, 10941-10946.
31. Williams, R.S., Green, R., and Glover, J.N. (2001). Crystal structure of the BRCT repeat region from the breast cancer-associated protein BRCA1. *Nat Struct Biol* *8*, 838-842.
32. Woods, N.T., Mesquita, R.D., Sweet, M., Carvalho, M.A., Li, X., Liu, Y., Nguyen, H., Thomas, C.E., Iversen, E.S., Jr., Marsillac, S., *et al.* (2012). Charting the landscape of tandem BRCT domain-mediated protein interactions. *Sci Signal* *5*, rs6.
33. Wu, Q., Paul, A., Su, D., Mehmood, S., Foo, T.K., Ochi, T., Bunting, E.L., Xia, B., Robinson, C.V., Wang, B., *et al.* (2016). Structure of BRCA1-BRCT/Abraxas Complex Reveals Phosphorylation-Dependent BRCT Dimerization at DNA Damage Sites. *Mol Cell* *61*, 434-448.

34. Yuan, Z., Kumar, E.A., Campbell, S.J., Palermo, N.Y., Kizhake, S., Mark Glover, J.N., and Natarajan, A. (2011). Exploiting the P-1 pocket of BRCT domains toward a structure guided inhibitor design. *ACS Med Chem Lett* 2, 764-767.

## **Chapter 3**

### **Insights into MDC1 recognition by TopBP1 in DNA replication checkpoint control**

**A version of this chapter is published in:**

Leung, C.C., **Sun, L.**, Gong, Z., Burkat, M., Edwards, R., Assmus, M., Chen, J., and Glover, J.N. (2013). Structural insights into recognition of MDC1 by TopBP1 in DNA replication checkpoint control. *Structure* 21, 1450-1459.

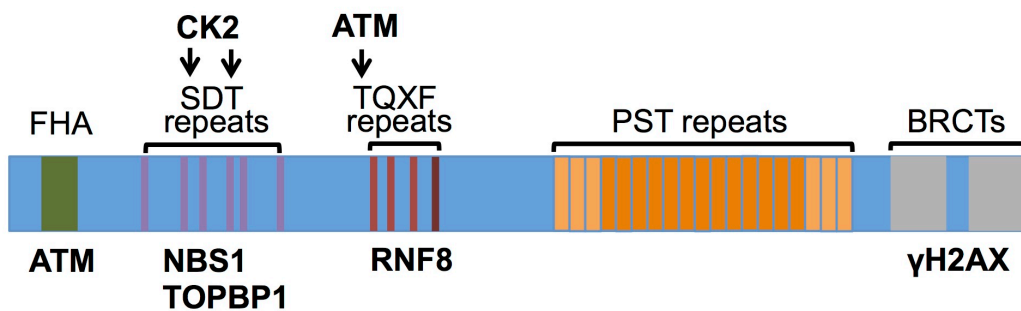
### 3.1 Introduction

Mediator of DNA damage checkpoint protein 1 (MDC1) is an important scaffold protein that plays multiple roles in DNA damage response (DDR) (Coster and Goldberg, 2010). It contains two major domains that can facilitate numerous interactions with other DDR proteins (Figure 3-1A). At the DSB site where the Mre11-Rad50-Nbs1 (MRN) complex binds first, ATM is then recruited by interaction with the C terminal motif of Nbs1 to actively phosphorylate histone H2AX (Falck et al., 2005). The C-terminal BRCTs of MDC1 can then recognize the pSXXF/Y-COOH tail of already phosphorylated H2AX ( $\gamma$ H2AX), while the N-terminal forkhead-associated (FHA) domain of MDC1 forms an additional interaction with pSer1981 of ATM. This recruitment and retention of ATM by MDC1 at a DSB site allows phosphorylation of more neighboring H2AX and creates a positive feedback loop that further amplifies the DNA damage signal.

Meanwhile, MDC1 also contains several sets of repetitive motifs that can mediate more interactions with DDR proteins. Phosphorylation of threonine in TQXF repeats by ATM allows MDC1 to interact with the FHA domain of RNF8 to activate a downstream ubiquitination signal cascade (Huen et al., 2007; Kolas et al., 2007; Mailand et al., 2007). Furthermore, phosphorylation of the SDT repeats of MDC1 by CK2 has also been shown to initiate interaction with Nbs1 to assist prolonging retention of MRN complex at DSB site (Figure 3-1B) (Chapman and Jackson, 2008; Melander et al., 2008; Spycher et al., 2008; Wu et al., 2008).

Recently, the study of our collaborator, Dr. Junjie Chen (University of Texas MD Anderson Cancer Center), suggested that the SDT repeats of MDC1 could also facilitate interaction with the BRCT5 domain of TopBP1 during replication checkpoint control (Wang et al., 2011). Previously, Dr. Charles Chung Yun Leung from our lab solved the X-ray crystallography structure of human TopBP1 BRCT4/5 (Figure 3-2A). This structure reveals unconventional tandem BRCTs which hosts a phosphate binding pocket (Ser654, Lys661,

A



B

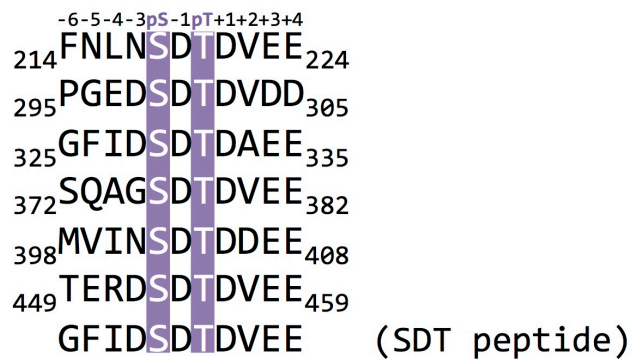
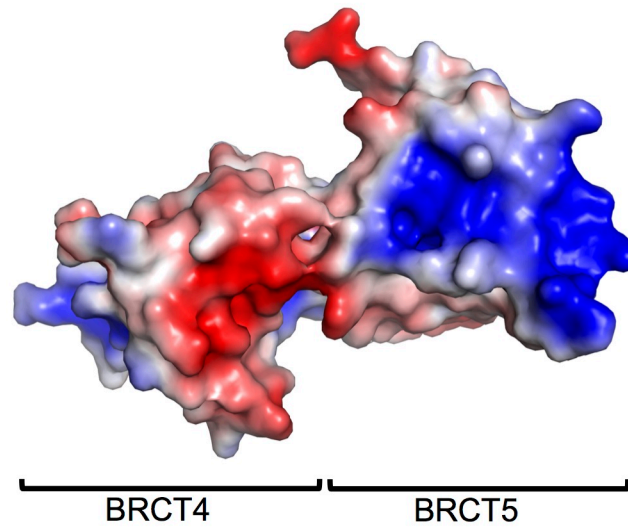


**Figure 3-1. MDC1 contains six SDT repeats.**

(A) Overview of functional domains of MDC1 (B) Sequence alignment of six SDT repeats from MDC1. The phosphorylated Ser and Thr residues are highlighted in purple. The sequence of MDC1 SDT peptide used in our study is also included.

A



B

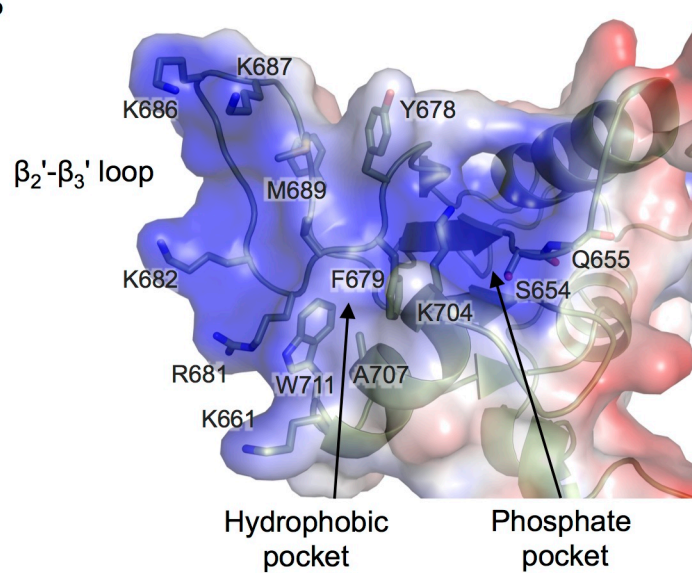


**Figure 3-2. The X-ray crystal structure of TopBP1 BRCT4/5.**

(A) The overall structure of TopBP1 BRCT4/5 with surface charges displayed. Blue indicates basic surface, red indicates acidic surface, and grey indicates non-polar surface. (B) Predicted protein interface on Topbp1 BRCT5.

and Lys704) together with a shallow hydrophobic pocket (A701, Trp711 and Phe679) on its C terminal BRCT5. In addition, a rigid  $\beta_2'$ - $\beta_3'$  loop enriched in Arg/Lys residues extends the positively charged surface on BRCT5, and provides an ideal platform for interaction with any negatively charged protein partners (Figure 3-2B). Interested in the molecular basis of TopBP1/MDC1 interaction, he then co-crystallized TopBP1 BRCT4/5 in complex with a peptide that was constructed based on the consensus sequence of MDC1 SDT repeats (Figure 3-1B). In this complex structure, a single MDC1 SDT peptide is sandwiched between two TopBP1 BRCT4/5 protomers, and MDC1 makes contact exclusively with the predicted binding surface on the BRCT5 domain of TopBP1 (Figure 3-3A). Surprisingly, only the pThr from the MDC1 SDT repeat fits in the predicted phosphate-binding pocket on BRCT5 of protomer A (Figure 3-3B). The MDC1 peptide interacts more extensively with BRCT5 of protomer B, and it places a -3 Asp in the phosphate-binding pocket of protomer B instead of pSer. The extended positively charged  $\beta_2'$ - $\beta_3'$  loop further secures the conserved C terminal acidic residues of the SDT repeat from MDC1 on the BRCT5 interface through multiple electrostatic interactions. The +2 Val that sits in a small hydrophobic pocket may also add more specificity to the interaction (Figure 3-3C).

To validate the structural model of the MDC1/TopBP1 complex and gain more insight in the interaction between TopBP1 BRCT4/5 and MDC1, we further examined this interaction *in vitro* using the FP assay. Our data indicates MDC1 interacts with TopBP1 BRCT5 in a dimerization-induced manner. Phosphorylation of serine and threonine residues in the SDT repeats appears to be equally important for the recognition of MDC1 by TopBP1. Detailed mutagenesis of the TopBP1 BRCT5 interface with MDC1 shows this interaction is highly dependent on electrostatics. Preliminary interaction study between TopBP1 and DNA suggests that TopBP1 BRCT5 can also interact with DNA using its positively charge  $\beta_2'$ - $\beta_3'$  loop. Therefore, we hypothesize that the interaction between DNA and TopBP1 BRCT5 may adopt the similar low specificity, electrostatics-based mechanism observed in MDC1 recognition. We speculate that TopBP1 BRCT5 interactions with DNA and MDC1 can both

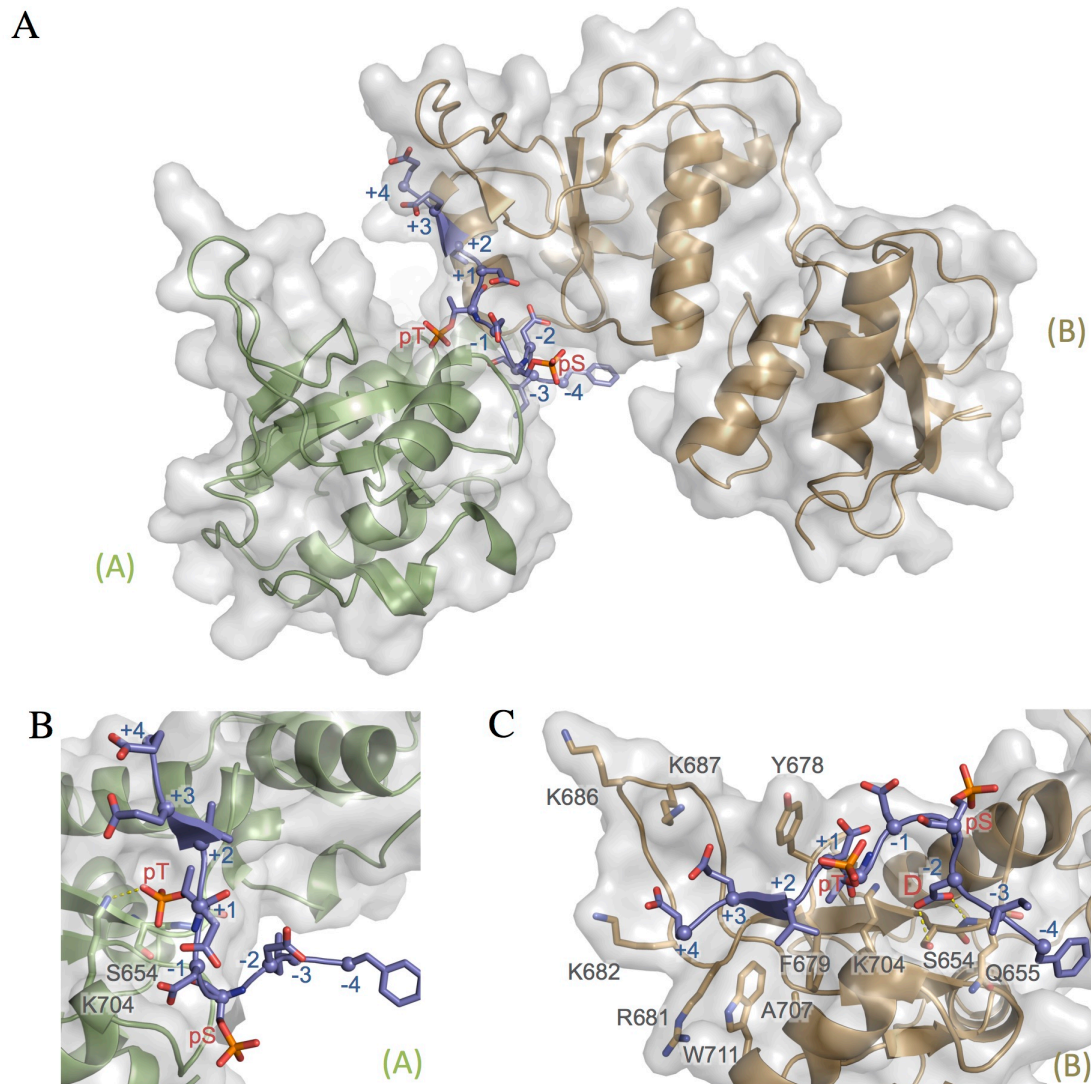


**Figure 3-3. The X-ray crystal structure of TopBP1 BRCT4/5 in complex with MDC1 SDT repeat peptide.**

(A) Overview of MDC1 peptide binding induced TopBP1 BRCT4/5 dimer. The MDC1 peptide in stick-view is colored blue. The TopBP1 BRCT4/5 protomers A (green) and B (yellow) are shown in both cartoon-view and surface representation (grey). (B) MDC1 peptide interaction with protomer A. (C) MDC1 peptide interaction with protomer B.

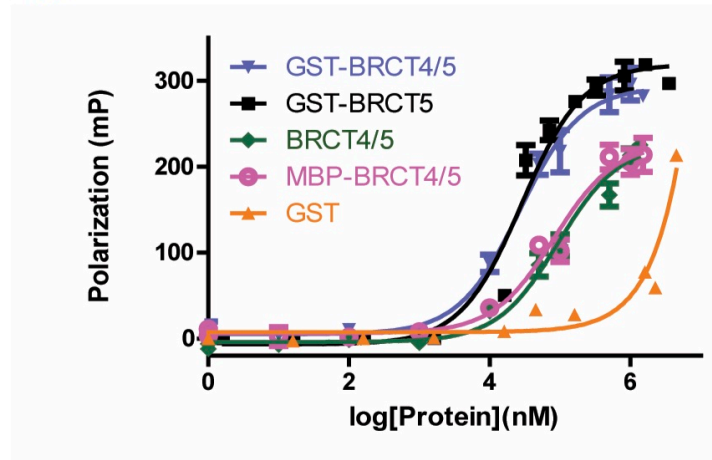
assist in the recruitment of TopBP1 to DNA damage sites during replication checkpoint control.

## **3.2 Results**

### **3.2.1 TopBP1 BRCT5 interacts with MDC1 in a dimerization-induced manner**

Unlike conventional tandem BRCT repeats that function together to form a phospho-peptide binding surface (Glover et al., 2004), our structure suggested that TopBP1 BRCT5 interacts with MDC1 SDT repeat peptide on its own. Interested in the potential role of TopBP1 BRCT4, we compared the interactions of MDC1 with GST-BRCT4/5 and GST-BRCT5 using FP spectroscopy (Figure 3-4A). The GST-BRCT4/5 interacts with similar affinity as GST-BRCT5 ( $K_D = 27 \pm 4 \mu\text{M}$  for GST-BRCT4/5,  $K_D = 28 \pm 4 \mu\text{M}$  for GST-BRCT5), indicating the presence of BRCT4 is irrelevant to MDC1 recognition (Table 3-1). It appears that interaction between MDC1 peptide and TopBP1 BRCT5 may induce the formation of a homodimer of BRCT5 in the complex structure of TopBP1/MDC1. However, previous attempts of Dr. Leung failed to obtain the MDC1 peptide bound TopBP1 BRCT5 dimer using methods including size exclusion chromatography, chemical cross-linking and EMSA. Interestingly, we observed a tighter interaction between GST-BRCT4/5 and MDC1 in comparison with the interaction between untagged BRCT4/5 with MDC1 peptide ( $K_D = 97 \pm 15 \mu\text{M}$ ) during FP study. Control measurement of interaction between GST and MDC1 peptide indicates no interaction, indicating that the GST tag itself does not bind MDC1. Since the GST tag is known to improve dimerization of tagged protein (Vinckier et al., 2011), we hypothesized that this GST induced dimerization could improve the BRCT5 affinity for MDC1. Examination of the interaction of MDC1 with MBP-BRCT4/5 gives a similar affinity ( $K_D = 82 \pm 16 \mu\text{M}$ ) compared to untagged BRCT5. This suggests the enhanced affinity we observed in GST tagged BRCT5 cannot be achieved by just any other N-terminal tags.

A



B

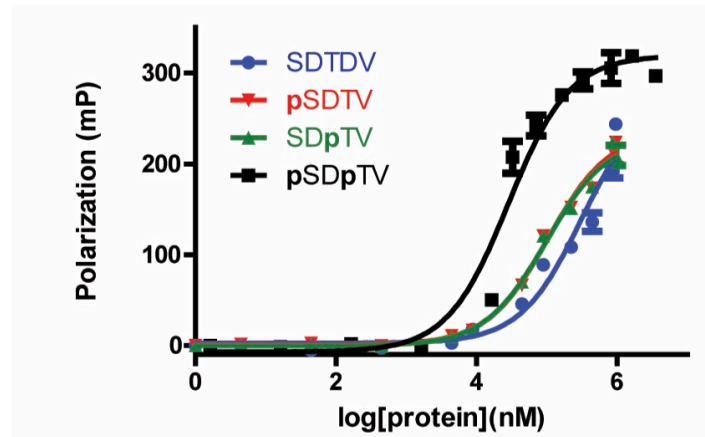


**Figure 3-4. TopBP1 BRCT5 interaction with phosphorylated MDC1 SDT peptide.**

(A) FP result of MDC1 SDT peptide interaction with TopBP1 protein BRCT domain variants. Diphosphorylated FITC labeled MDC1 SDT peptide is used in this study. (B) FP result of TopBP1 BRCT5 interaction with MDC1 SDT peptide variants. GST tagged TopBP1 BRCT5 protein is used in this study.

**Table 3-1. Summary of Fluorescence Polarization Study Results of Protein-peptide Interactions**

<b>Protein</b>	<b>Peptide Sequence<sup>a</sup></b>	<b>K<sub>D</sub> (μM)</b>
GST-BRCT4/5	FITC-GFID <b>pSDp</b> TDVEEE-NH2	27 ± 4
MBP-BRCT4/5	FITC-GFID <b>pSDp</b> TDVEEE-NH2	82 ± 16
BRCT4/5	FITC-GFID <b>pSDp</b> TDVEEE-NH2	94 ± 15
GST	FITC-GFID <b>pSDp</b> TDVEEE-NH2	ND <sup>b</sup>
GST-BRCT5	FITC-GFID <b>S</b> DTVEEE-NH2	310 ± 70
	FITC-GFID <b>pS</b> DTVEEE-NH2	105 ± 9
	FITC-GFID <b>S</b> D <b>p</b> TDVEEE-NH2	98 ± 9
	FITC-GFID <b>pSDp</b> TDVEEE-NH2	28 ± 4
	FITC-GFID <b>pSDp</b> TDDEEE-NH2	24 ± 3
<b>GST-BRCT5 Mutants</b>		
S654A	FITC-GFID <b>pSDp</b> TDVEEE-NH2	32 ± 3
R681E/K682E	FITC-GFID <b>pSDp</b> TDVEEE-NH2	280 ± 60
K704A	FITC-GFID <b>pSDp</b> TDVEEE-NH2	210 ± 50
A707D	FITC-GFID <b>pSDp</b> TDVEEE-NH2	120 ± 10
A707K	FITC-GFID <b>pSDp</b> TDVEEE-NH2	12.0 ± 0.9

<sup>a</sup>Residues from the central motif of SDT repeat peptide are highlighted in Bold.

<sup>b</sup>ND = no binding or competitive binding detected.

Therefore, we concluded that TopBP1 BRCT5 may interact with MDC1 peptide in a dimerization induced manner. After two GST tags dimerized in solution, this brings the two TopBP1 BRCT4/5 attached to these tags in close proximity, making it easier for them to bind a single MDC1 SDT peptide as a homodimer.

### **3.2.2 TopBP1 BRCT5 prefers phosphorylated MDC1 SDT repeats**

Based on our complex structure of TopBP1 BRCT4/5-MDC1 peptide, only the pThr from MDC1 SDT repeat binds loosely to the phosphate-binding pocket of protomer A, making one direct hydrogen bond with K704. The -3 Asp is found in the phosphate-binding pocket of protomer B, leaving the -2 pSer outside which only makes a potential long-range electrostatic interaction with the  $\epsilon$  amino nitrogen of Lys661 from protomer A and a water-bridged hydrogen bond with the main chain of Arg700 from protomer B (Figure 3-3B, C). Interested in the importance of pThr and pSer from SDT in MDC1 recognition by TopBP1 BRCT5, we tested the interaction between BRCT5 and variants of SDT repeat peptides using FP (Figure 3-4B). The diphosphorylated peptide binds BRCT5 with ~11 fold higher affinity than the non-phosphorylated peptide ( $K_D = 310 \pm 70 \mu\text{M}$ ), indicating the importance of phosphorylation on SDT repeat. To our surprise, both mono-phosphorylated peptides bind BRCT5 with ~3.5 fold reduction in affinity ( $K_D = 98 \pm 9 \mu\text{M}$  for SDpT,  $K_D = 105 \pm 9 \mu\text{M}$  for pSDT), suggesting pThr and pSer are equally important. However, the overall dependency of phosphorylation on SDT repeat of MDC1 in its interaction with TopBP1 appears to be less significant compared to conventional phosphorylation-dependent recognition by BRCT repeats. For example, the BRCT7/8 of TopBP1 interacts with BACH1 with ~100 fold reduced affinity after BACH1 became dephosphorylated (Gong et al., 2010).

### **3.2.3 +2 Val/Asp in SDT repeats aids MDC1 recognition by TopBP1**

Aside from the phosphate-binding pocket, many tandem BRCTs also have sequence preference in residues upstream of pSer/pThr (Glover et al., 2004). For instance, the BRCTs of BRCA1 and PTIP both contain a hydrophobic groove that specifically interacts with the +3 hydrophobic side chain from their target proteins (Clapperton et al., 2004; Glover et al., 2004; Manke et al., 2003). In TopBP1 BRCT5, we also identified a shallow hydrophobic pocket formed by A701, Trp711 and Phe679 that engages the +2 Val of the MDC1 peptide (Figure 3-3C). Since this +2 Val is partially conserved in SDT repeats, curious about the importance of this hydrophobic interaction with TopBP1, we generated a +2 Asp mutant of the MDC1 peptide (FITC-GFIDpSDpTDEE). To our surprise, this peptide mutant binds TopBP1 BRCT5 with similar affinity as the original di-phosphopeptide ( $K_D = 24 \pm 4 \mu\text{M}$  for pSDpTD), indicating +2 Val is not part of the consensus sequence required for MDC1 recognition by TopBP1 (Figure 3-5A). This shallow hydrophobic pocket sits in the center of the positively charged surface on BRCT5. We hypothesize that the loss of Van der Waals interaction with +2 Val may be compensated by the gain of electrostatic interaction with +2 Asp. To validate our speculation, we generate two TopBP1 mutants (A707D, A707K) of the key hydrophobic residue Ala707 from the hydrophobic pocket. As expected, mutation to positively charged Lysine does not affect MDC1 peptide recognition, but MDC1 interaction with negatively charged mutant much weaker (Figure 3-5B). Therefore, we concluded the shallow hydrophobic pocket of TopBP1 BRCT5 interacts with SDT repeats of MDC1 less specifically. TopBP1 BRCT5 equally prefers +2 Val and +2 Asp in SDT repeats.

### **3.2.4 Functional study of TopBP1 BRCT5 binding interface by mutagenesis**

Overall, our structure suggested the interaction between TopBP1 and MDC1 seems to be mainly charge-based. We found a large positively charged surface extended from the phosphate-binding pocket to the  $\beta 2'$ - $\beta 3'$  loop on the BRCT5 of protomer B, which is engaging with the conserved C terminal residues (EE/DD) from SDT repeats that are highly

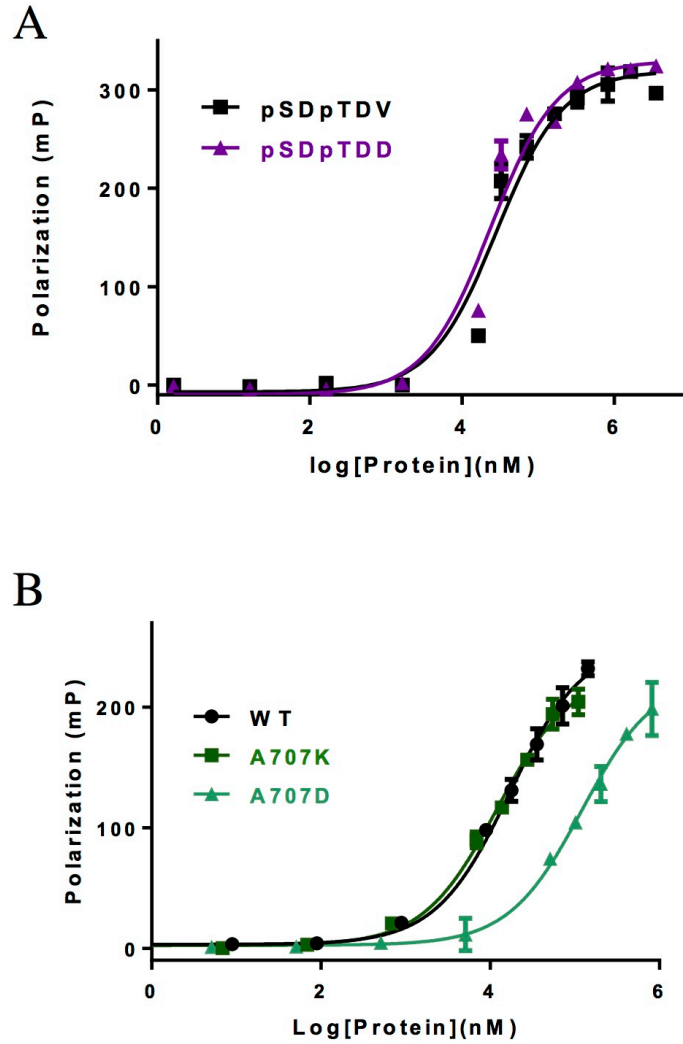


**Figure 3-5. +2 Val/Asp in SDT repeats aids MDC1 recognition by TopBP1.**

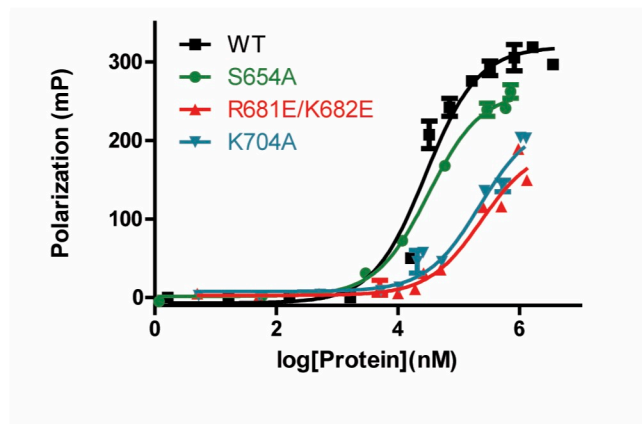
(A) Comparison of TopBP1 interaction with +2 Val or +2 Asp containing MDC1 SDT peptide by FP. (B) Mutagenesis study of A707 from TopBP1 BRCT5 by FP

positively charged. Furthermore, the -3 Asp in the phosphate-binding pocket could form hydrogen bonds with the main chain of Glu655 and side chain of Ser654, and establish additional water bridged interaction with the side chain of Lys704 and the main chain of -1 Asp (Figure 3-3C). We introduced several mutations on the BRCT5 interface to validate their importance *in vitro* using FP study. Mutations in the phosphate-binding pocket (K704A) and  $\beta 2'$ - $\beta 3'$  loop (R681E/K682E) of BRCT5 both largely reduced its interaction with MDC1 ( $K_D = 210 \pm 50 \mu\text{M}$  for K704A,  $K_D = 280 \pm 60 \mu\text{M}$  for R681E/K682E). However, the S654A mutant binds MDC1 with almost the same affinity as the wild type (WT) ( $K_D = 32 \pm 3 \mu\text{M}$ ) (Figure 3-6A).

It has been shown previously by Dr. Chen's lab that BRCT5 of TopBP1 can facilitate its localization to DNA damage site at stalled replication forks (Wang et al., 2011). Interested in the functional relevance of these BRCT5 mutants, Dr. Chen's lab examined their abilities to form hydroxyurea (HU)-induced foci in the cell. In this study, the HU-induced DNA damage sites in cells were indicated by the locations of  $\gamma\text{H2AX}$  foci. Since MDC1 co-localized with  $\gamma\text{H2AX}$ , the co-localization of WT TopBP1 foci with  $\gamma\text{H2AX}$  foci in cells this data also supports a role of MDC1 in the recruitment of TopBP1 to DNA damage sites in cells. In agreement with our FP result, K704A and R681E/682E mutation both abolish the foci formation, while the S654A mutation only slightly lowers the fluorescence intensity of foci in cells (Figure 3-6B). These suggested that the mutations in K704A and R681E/682E of TopBP1 BRCT5 could both disrupt TopBP1 interaction with MDC1 and inhibit its recruitment to DNA damage site. Together, our results implied that phosphorylation dependent recognition and electrostatic interaction are equally important for the interaction between TopBP1 BRCT4/5 and MDC1 SDT repeats.

### **3.2.5 TopBP1 BRCT4/5 interacts with ssDNA**

A



B

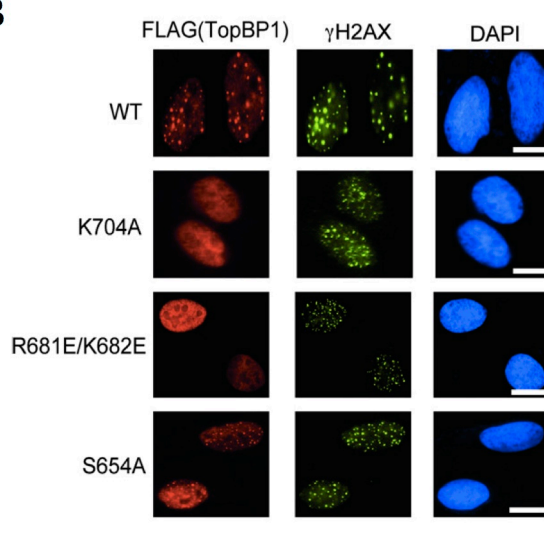


**Figure 3-6. Mutagenesis study of the TopBP1 BRCT5 binding interface.**

(A) FP binding studies of MDC1 FITC-labeled diposphopeptide with GST-fusion proteins of wild-type BRCT5 and various missense variants. (B) Replication stress-induced focus formation of wild-type and TopBP1 mutants. U2OS cells transfected with plasmids encoding SFB-tagged WT or mutants of TopBP1 were exposed to 2 mM HU for 3 hr. Cells were fixed and immunostained with anti-FLAG and anti- $\gamma$ -H2AX antibodies. Bar: 10  $\mu$ m. Panel B shows results from Dr. Chen's lab.

Several studies implied that BRCT domains might interact with DNA (Yamane et al., 2000; Yamane and Tsuruo, 1999), and TopBP1 BRCT5 contains a large positively charged surface that likely attracts a highly negatively charged molecule such as DNA. A recent study from Dr. W. Matthew Michael's lab (Department of Biological Science, University of South California) revealed that BRCT4 and BRCT5 both seem to possess the ability to bind ssDNA (Acevedo et al., 2016). Interested in the molecular basis of the interaction between TopBP1 4/5 and ssDNA, we first examined the interaction between TopBP1 BRCT5 and 16NT ssDNAs *in vitro* using FP study. Since previous studies of other BRCT family proteins indicated that BRCT domains might prefer binding of DNAs with 5' phosphate group (Feng et al., 2004; Kobayashi et al., 2006), we have examined DNAs with or without phosphate on 3' end. Both ssDNAs bind TopBP1 BRCT5 well, but DNA with 3' phosphate binds slightly tighter ( $K_D = 16 \pm 2 \mu\text{M}$  for 3' P end,  $K_D = 22 \pm 3 \mu\text{M}$  for 3' OH end) (Figure 3-7A, Table 3-2). However, both affinities are comparable to MDC1 SDT peptide interaction, suggesting DNA could be a binding partner of BRCT5 as well.

We then further examined the interaction between BRCT5 and 3' P end ssDNA constructs of different length. The 20NT ssDNA binds BRCT5 much better than the 5NT ssDNA ( $K_D = 15 \pm 3 \mu\text{M}$  for 20NT,  $K_D = 260 \pm 30 \mu\text{M}$  for 5NT), but its affinity is similar to 16NT ssDNA. It appears that longer ssDNA has a higher affinity towards TopBP1. To test whether the interaction with DNA occurs through the positively charged surface of BRCT5, we examined the R681E/K682E mutation from  $\beta_2$ '- $\beta_3$ ' of BRCT5. The DNA binding affinity for 20NT ssDNA is reduced by  $\sim 4$  fold ( $K_D = 70 \pm 13 \mu\text{M}$ ), indicating the positive charges from this loop is important for this interaction (Figure 3-7B).

Interested in the potential role of BRCT4, we also measured the interaction between BRCT4/5 and ssDNA. Similar affinities were observed for BRCT4/5 and BRCT5, indicating that BRCT4 has no significant contribution to the interaction with ssDNAs (Figure 3-7C). To further validate this interaction we observed in FP study, we examined the interaction between ssDNA and TopBP1 BRCT4/5 using EMSA. An apparent shift of BRCT5 bound

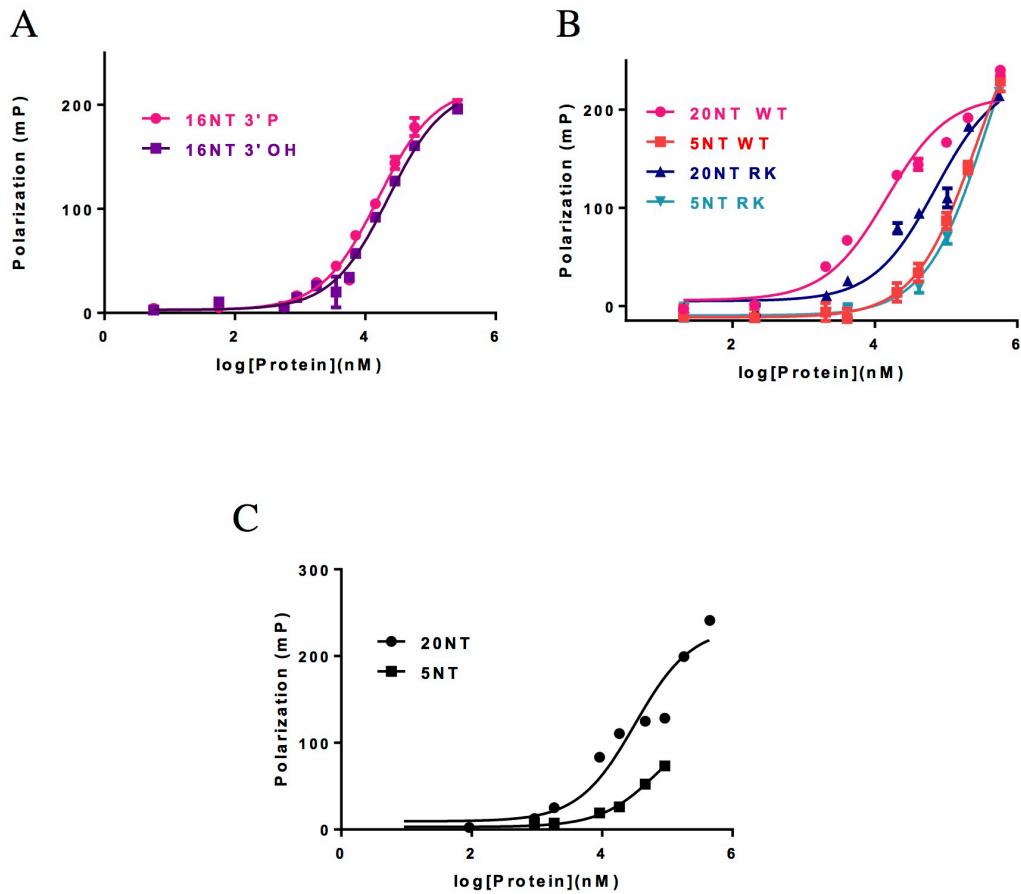


**Figure 3-7. FP results of TopBP1 BRCT4/5 interaction with ssDNA variants.**

(A) TopBP1 BRCT5 interaction with 16NT ssDNA containing 3'OH end or 3'P end. (B) Comparison study of WT and RK mutant of TopBP1 BRCT5 interaction with 20NT or 5NT ssDNA. ssDNAs used in this study are all 3'P end. (C) TopBP1 BRCT4/5 interaction with 20NT or 5NT ssDNA. ssDNAs used in this study all have 3'P end and 5' Fam label.

**Table 3-2. Summary of Fluorescence Polarization Study Results of Protein-DNA Interactions**

Protein	DNA	DNA Sequence <sup>a</sup>	K <sub>D</sub> (μM)
GST-BRCT5 (WT)	16NT 3'OH	FAM-TAGCACCTACCGATTG-OH	22 ± 3
	16NT 3'P	FAM-TAGCACCTACCGATTG-P	16 ± 2
	20NT 3'P	FAM-TAGCACCTACCGATTGTATG-P	15 ± 3
	5NT 3'P	FAM-TAGCA-P	260 ± 30
GST-BRCT5 (RK mutant)	20NT 3'P	FAM-TAGCACCTACCGATTGTATG-P	70 ± 13
	5NT 3'P	FAM-TAGCA-P	380 ± 40
BRCT4/5	20 3'P	FAM-TAGCACCTACCGATTGTATG-P	32 ± 7
	5NT 3'P	FAM-TAGCA-P	70 ± 16

<sup>a</sup>All the ssDNAs are 5' FAM labeled with 3'OH or 3' P end

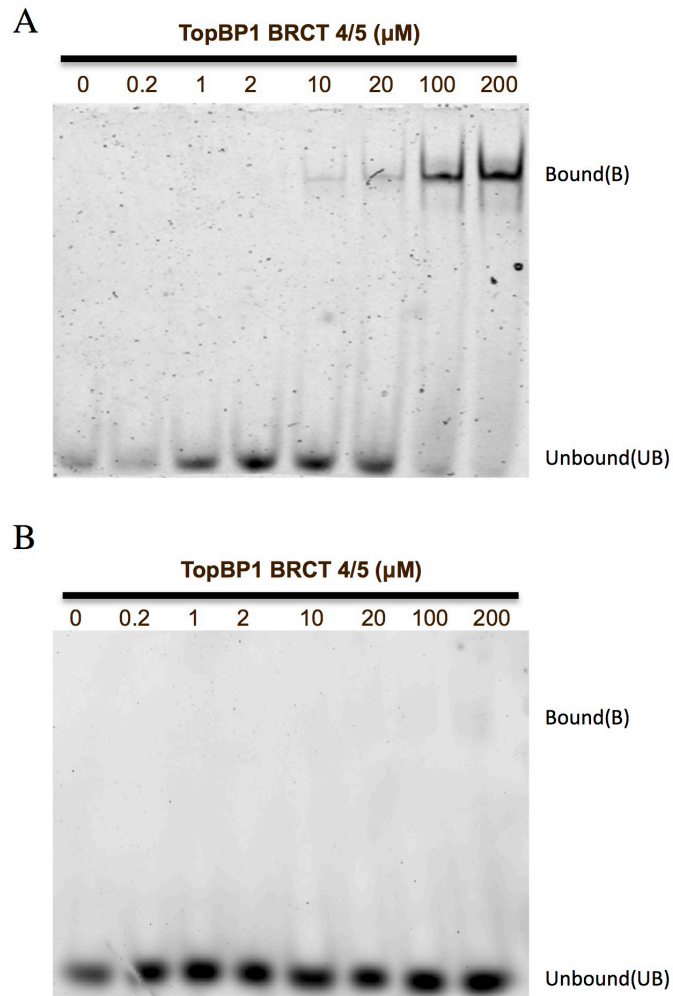


**Figure 3-8. EMSA result of TopBP1 BRCT4/5 interaction with ssDNAs.**

The interaction between 20nM of Fam labeled ssDNAs (3'P end) and increasing concentration of TopBP1 BRCT4/5 are analyzed by gel electrophoresis. (A) TopBP1 BRCT4/5 interaction with 20NT ssDNA. (B) TopBP1 BRCT4/5 interaction with 5NT ssDNA. ssDNAs used in this study all have 3'P end and 5' Fam label.

DNA was found with the 20NT ssDNA but not the 5NT ssDNA, indicating the length of ssDNA affects its interaction with TopBP1 (Figure 3-8).

Together, we conclude that TopBP1 BRCT5 can interact with ssDNA using the same positively charged surface involved in MDC1 recognition. Our preliminary data suggested that TopBP1 BRCT5 preferably binds a ssDNA with 3' phosphate end and a minimum length of 16NT.

### **3.3 Discussion**

TopBP1 is a multi-functional protein that plays important roles in DNA replication checkpoint control, and its internal BRCT5 domain is mainly involved in the recruitment of TopBP1 at DSB site and stalled replication fork. We have shown here that the recognition of conserved SDT repeats of MDC1 by TopBP1 BRCT5 can assist TopBP1 recruitment, and further amplify the ATR activation signal cascade. Our detailed functional study of MDC1 interaction with TopBP1 BRCT4/5 not only validates the structural model Dr. Leung obtained from the X-ray crystallography structure of TopBP1 BRCT4/5 in complex with MDC1 SDT repeat peptide, but also reveals many interesting aspects of this interaction.

Perhaps the most interesting observation we have is the apparent MDC1 SDT peptide-induced dimerization of TopBP1 BRCT4/5. Although previous studies failed to obtain a stable peptide-induced dimer in solution, we have demonstrated that a GST tag, but not an MBP tag, promotes TopBP1 BRCT4/5 interaction with MDC1 peptide, consistent with the hypothesis that the dimerization of GST stabilizes the binding of two TopBP1 BRCT4/5 protomers to MDC1 (Vinckier et al., 2011). Since we didn't observe any contact between BRCT4/5 protomers in the TopBP1/MDC1peptide complex structure, we hypothesize that the oligomerization of BRCT5 on MDC1 SDT repeats could be induced by interaction of other regions of TopBP1. For instance, the TopBP1 BRCT7/8-mediated

recognition of an internal pSer1159-containing motif in TopBP1 has been suggested to assist TopBP1 oligomerization (Liu et al., 2006). However, further experiments would be needed to address its relevance to TopBP1/MDC1 interaction. For example, it would be interesting to create a fusion protein of TopBP1 BRCT4/5 and BRCT7/8, and then examine how it interact with MDC1 SDT peptide.

Unlike other canonical tandem BRCT repeats, TopBP1 BRCT4/5 binds MDC1 SDT repeats solely through its C-terminal BRCT5 domain with a unique electrostatic based mechanism. In addition to the conserved phosphate binding pocket formed by Ser654, Lys661, and Lys704, an arginine and lysine residue enriched  $\beta_2'$ - $\beta_3'$  loop further extended the positively charged surface on BRCT5 to enhance its interaction with the negatively charged MDC1 SDT repeats. Although our FP result indicated both pSer and pThr of SDT repeat are important for MDC1 recognition, removal of both phosphate groups only resulted in ~11 fold reduced affinity for the interaction with TopBP1 BRCT5, suggesting the interaction between MDC1 and TopBP1 is less phosphorylation dependent. Mutation of conserved Ser654 in the phosphate binding pocket also has no significant impact on phosphopeptide binding or TopBP1 foci formation, which further implies the specificity in this pocket is relatively poor. This can be explained by the lack of strong and direct interaction between either pSer or pThr of MDC1 with phosphate binding pocket of TopBP1 BRCT5. Our structural model shows only the pThr from core SDT motif interacts directly with the phosphate binding pocket of BRCT5, while the rest of the interactions are mainly provided by the semi-conserved acidic residues in SDT repeats. Not only can the C-terminal acidic residues (EE/DD from +3 and +4 position) engage with the basic  $\beta_2'$ - $\beta_3'$  loop, but also the well-conserved -3 Asp is found to partially mimic the role of the phosphate group in hydrogen bonding with residues from phosphate binding pocket of BRCT5. Although the BRCT5 also possessed a small hydrophobic pocket that can interact with the +2 Val slightly upstream of pThr, this interaction appears to be less exclusive. Empowered by the overall

positive charges on BRCT5, this hydrophobic interaction could be easily replaced by electrostatic interactions with +2 Asp.

Overall, the interaction between TopBP1 BRCT4/5 and MDC1 SDT peptide is mainly electrostatic and has lower specificity in comparison to other tandem BRCT based interactions. Since there are six different regions of SDT repeats from MDC1, it is possible that TopBP1 BRCT5 adopted this lower specificity interaction mechanism to target multiple SDT repeats. Further investigation is needed to understand how many of the six SDT repeat regions from MDC1 are involved in the interaction with TopBP1 BRCT5. Besides, the interaction between MDC1 SDT repeats and TopBP1 BRCT4/5 is not exclusive. While TopBP1 BRCT5 has been suggested in the interaction with other protein such as 53BP1 (Cescutti et al., 2010), MDC1 SDT repeats are well known for their recognition by Nbs1 FHA-BRCT-BRCT domains as well (Chapman and Jackson, 2008; Melander et al., 2008; Spycher et al., 2008; Wu et al., 2008). Although no one has solved the structure of Nbs1 in complex with MDC1 SDT repeat, the apo structure of *S. pombe* Nbs1 FHA-BRCT-BRCT and the complex structure of it with Ctp1 (CtIP in human) peptide bound are both solved (Williams et al., 2009). It has been suggested that MDC1 interact with Nbs1 using two of its SDT repeats, one engaging the FHA domain in a pThr dependent manner, while the other engaging with the BRCT-BRCT likely using both pThr and pSer (Figure 3-9A). Interestingly, similar to the SDT repeat of MDC1, Ctp1 contains a conserved SXT motif and has an acidic residue enriched region immediately downstream of pThr (Figure 3-9B). The SXT motif interacts with phosphate binding pocket of Nbs1 FHA domain using its pThr only, and the acidic residues from Ctp1 bind multiple lysine residues from FHA domain of Nbs1 to further secure the interaction (Figure 3-9C). This implies that electrostatic interaction is also important in MDC1 interaction with Nbs1, and the acidic residues immediately downstream of SDT motif are an essential part of the consensus sequence in MDC1 as well. We

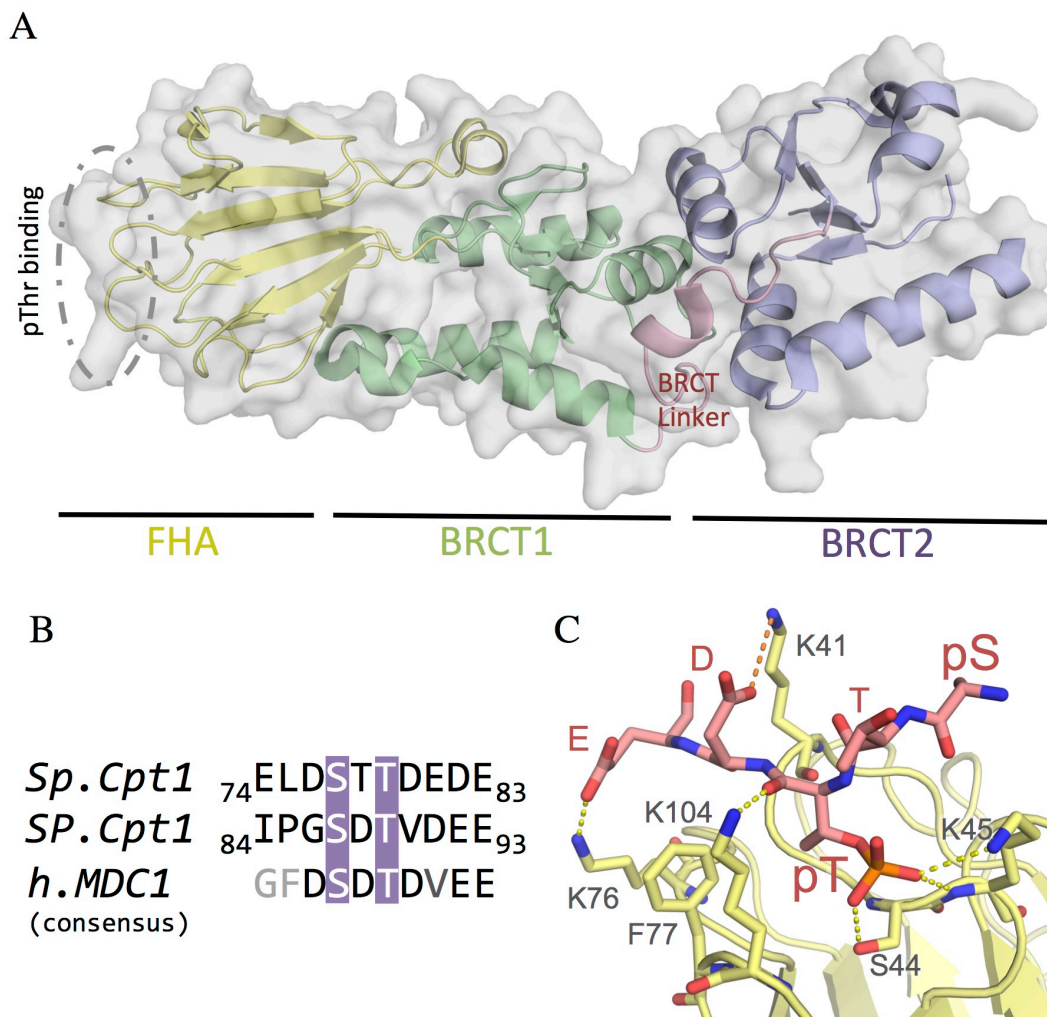


**Figure 3-9. MDC1 SDT repeats interaction with other BRCTs.**

(A) The X-ray crystal structure of Nbs1 FHA-BRCT-BRCT domains. The region from the FHA domain that can interact with pThr containing protein sequence is circled by the dashed line. (B) Sequence alignment of SDT repeats from Cpt1 and MDC1. Phosphorylated serine and threonine are highlighted in purple blocks, and residues that are not well conserved in MDC1 consensus sequence are indicated in grey. (C) Structural overview of the interaction between Nbs1 FHA domain and Cpt1. Peptide from residue 74-83 of Cpt1 is used.

hypothesize similar electrostatic dependency would also exist in the interaction between Nbs1 BRCT-BRCT and MDC1 SDT repeat. The overall interaction between MDC1 and Nbs1 proteins is likely monomer based, but the FHA-BRCT-BRCT domains of Nbs1 may interact with two MDC1 SDT peptides. It would be interesting to measure the binding affinity between the MDC1 SDT peptide and FHA-BRCT-BRCT domains of Nbs1 and solve the complex structure of MDC1 SDT peptide-Nbs1-BRCT-BRCT domains if possible. In addition, further investigation on which two SDT motifs from the MDC1 are involved in the interaction with Nbs1 would also provide more insights on the specificity of this interaction.

It has been implied in other studies that recruitment of TopBP1 to a replication checkpoint may also occur through direct interaction with DNA (Acevedo et al., 2016). Our preliminary data suggested that TopBP1 BRCT4/5 can interact with ssDNA solely using its BRCT5, and the positively charged loop on BRCT5 appears to be essential for this interaction. So far, we have identified a preference of 3' P end with a minor length of 16NT in the targeting ssDNA sequence of TopBP1 BRCT5. Previously, Dr. Leung has shown that TopBP1 BRCT5 can also interact with dsDNA in a charge-depend manner (Leung, 2011). Moreover, his EMSA result suggested BRCT5 binds dsDNA with higher affinity compared to ssDNA. Since we haven't tested TopBP1 BRCT5 interaction with dsDNA, further experiments would be required to address this question. Nevertheless, it is clear that TopBP1 BRCT5 interacts with DNA using the same electrostatic based mechanism adopted in MDC1 SDT repeat recognition.

In conclusion, this study validated a unique electrostatic based interaction model of TopBP1 BRCT5. We have shown that TopBP1 BRCT5 can interact with the SDT repeats of MDC1 using this model, and this interaction likely assists TopBP1 recruitment to the replication fork. We also obtained preliminary data that indicated TopBP1 BRCT5 might interact with ssDNA using the same mechanism, and we hypothesized that this interaction could also assist in TopBP1 recruitment during replication checkpoint control.

### 3.4 Material and Methods

#### *Cloning, expression, and purification*

Human TopBP1 BRCT5 (641-746) and BRCT4/5 (549-746) were cloned into pGEX-6P-1 (GE Healthcare). Mutants (S654A, K704A, R681A/K682A) of human TopBP1 BRCT5 were created from a WT template described above using QuickChange Lightning site-directed mutagenesis kit (Stratagene) (Braman et al., 1996; Kunkel, 1985; Nelson and McClelland, 1992; Sugimoto et al., 1989; Taylor et al., 1985; Vandeyar et al., 1988). All the GST fusion proteins were expressed in *Escherichia coli* BL21-Gold cells and purified using glutathione affinity chromatography with glutathione sepharose 4B beads (GE Healthcare) and eluted with elution buffer (20 mM Tris-HCl pH 7.5, 150 mM NaCl, 20mM reduced glutathione and 0.1%  $\beta$ ME). GST-fusion protein of BRCT5 was purified by Superdex 200 16/60 column in storage buffer (10 mM Tris-HCl pH 8.0, 150 mM NaCl, 1 mM DTT). GST-fusion protein of TopBP1 BRCT4/5 was cleaved with PreScission protease overnight at 4 °C. BRCT4/5 was purified by anion exchange chromatography (buffer A: 50 mM HEPES pH 7.0, 0.1%  $\beta$ ME; buffer B: 50 mM HEPES pH 7.0, 1 M NaCl, 0.1%  $\beta$ ME). Residual GST was removed by incubation with glutathione sepharose 4B beads (GE Healthcare) prior to a final purification step on a Superdex 75 26/60 column in storage buffer (10 mM Tris-HCl pH 7.5, 150 mM NaCl, 1 mM DTT).

#### *Fluorescence polarization (FP) assay*

FP measurements were carried out using an Envision multi-label plate reader (Perkin Elmer) on a 384-well OptiPlate (Perkin Elmer). All the MDC1 peptide variants (FITC-GFIDpSDpTDVEEEE-NH<sub>2</sub>, FITC-GFIDSDpTDVEEEE-NH<sub>2</sub>, FITC-GFIDpSDTDVEEEE-NH<sub>2</sub>, FITC-GFIDSDDTDVEEEE-NH<sub>2</sub>, FITC-GFIDpSDpTDDEEEE-NH<sub>2</sub>) were synthesized and purified by Biomatik. All ssDNAs ( 5' FAM-TAGCACCTACCGATTGTA TG-3' P, 5' FAM-TAGCACCTACCG ATTG-3' P, 5' FAM-TAGCA-3' P ) were synthesized by Integrated DNA Technology. FP assays were performed by mixing 10 nM FITC-labelled phospho-peptide or Fam-labelled DNA with

freshly concentrated TopBP1 proteins in FP assay buffer (10 mM Tris-HCl pH 7.5, 150 mM NaCl, 1 mM DTT, 0.05 % Tween-20) and incubated for 15 min at room temperature. FP measurements were taken at an excitation wavelength of 485 nm and an emission wavelength of 538 nm. Curve fitting and  $K_D$  calculations were obtained using PRISM software (GraphPad Prism).  $K_D$  values summarized in Table 2 are the average of at least three individual measurements. For binding curves that haven't reach saturation due to the limitation of protein stability, the  $K_D$  value generated based on existing data point is only an estimate of real affinity.

#### ***Electrophoretic mobility shift assay (EMSA)***

The reaction was prepared by mixing 4  $\mu$ L of H<sub>2</sub>O, 10  $\mu$ L of EMSA buffer (50 mM Tris-HCl pH 7.5, 150 mM KCl, 1mM MgSO<sub>4</sub>, 1 mM DTT, 10% glycerol), 2  $\mu$ L of poly dIdC, 2  $\mu$ L of 0.5  $\mu$ M Fam-labeled DNA with 2  $\mu$ L of increasing concentration of TopBP1 BRCT4/5 (0-250 nM) and equilibrated for 20 minutes at room temperature. Samples were analyzed by gel electrophoresis on a 6% native gel in Tris-Borate-EDTA (TBE) buffer (45 mM Tris-Borate pH 8.3, 1 mM EDTA). The gel was pre-run at 80 mV for 10 minutes, then ran for 50 minutes at 100 mV with 20  $\mu$ L sample loaded per lane at 4 °C. Finally, the gel was visualized by a Typhoon Imager (GE healthcare).

### 3.5 Reference

1. Acevedo, J., Yan, S., and Michael, W.M. (2016). Direct Binding to Replication Protein A (RPA)-coated Single-stranded DNA Allows Recruitment of the ATR Activator TopBP1 to Sites of DNA Damage. *J Biol Chem* 291, 13124-13131.
2. Braman, J., Papworth, C., and Greener, A. (1996). Site-directed mutagenesis using double-stranded plasmid DNA templates. *Methods Mol Biol* 57, 31-44.
3. Cescutti, R., Negrini, S., Kohzaki, M., and Halazonetis, T.D. (2010). TopBP1 functions with 53BP1 in the G1 DNA damage checkpoint. *EMBO J* 29, 3723-3732.
4. Chapman, J.R., and Jackson, S.P. (2008). Phospho-dependent interactions between NBS1 and MDC1 mediate chromatin retention of the MRN complex at sites of DNA damage. *EMBO Rep* 9, 795-801.
5. Clapperton, J.A., Manke, I.A., Lowery, D.M., Ho, T., Haire, L.F., Yaffe, M.B., and Smerdon, S.J. (2004). Structure and mechanism of BRCA1 BRCT domain recognition of phosphorylated BACH1 with implications for cancer. *Nat Struct Mol Biol* 11, 512-518.
6. Coster, G., and Goldberg, M. (2010). The cellular response to DNA damage: a focus on MDC1 and its interacting proteins. *Nucleus* 1, 166-178.
7. Falck, J., Coates, J., and Jackson, S.P. (2005). Conserved modes of recruitment of ATM, ATR and DNA-PKcs to sites of DNA damage. *Nature* 434, 605-611.
8. Feng, H., Parker, J.M., Lu, J., and Cao, W. (2004). Effects of deletion and site-directed mutations on ligation steps of NAD<sup>+</sup>-dependent DNA ligase: a biochemical analysis of BRCA1 C-terminal domain. *Biochemistry* 43, 12648-12659.
9. Glover, J.N., Williams, R.S., and Lee, M.S. (2004). Interactions between BRCT repeats and phosphoproteins: tangled up in two. *Trends Biochem Sci* 29, 579-585.
10. Gong, Z., Kim, J.E., Leung, C.C., Glover, J.N., and Chen, J. (2010). BACH1/FANCI acts with TopBP1 and participates early in DNA replication checkpoint control. *Mol Cell* 37, 438-446.
11. Huen, M.S., Grant, R., Manke, I., Minn, K., Yu, X., Yaffe, M.B., and Chen, J. (2007). RNF8 transduces the DNA-damage signal via histone ubiquitylation and checkpoint protein assembly. *Cell* 131, 901-914.
12. Kobayashi, M., Figaroa, F., Meeuwenoord, N., Jansen, L.E., and Siegal, G. (2006). Characterization of the DNA binding and structural properties of the BRCT region of human replication factor C p140 subunit. *J Biol Chem* 281, 4308-4317.

13. Kolas, N.K., Chapman, J.R., Nakada, S., Ylanko, J., Chahwan, R., Sweeney, F.D., Panier, S., Mendez, M., Wildenhain, J., Thomson, T.M., *et al.* (2007). Orchestration of the DNA-damage response by the RNF8 ubiquitin ligase. *Science* *318*, 1637-1640.
14. Kunkel, T.A. (1985). Rapid and efficient site-specific mutagenesis without phenotypic selection. *Proc Natl Acad Sci U S A* *82*, 488-492.
15. Mailand, N., Bekker-Jensen, S., Faustrup, H., Melander, F., Bartek, J., Lukas, C., and Lukas, J. (2007). RNF8 ubiquitylates histones at DNA double-strand breaks and promotes assembly of repair proteins. *Cell* *131*, 887-900.
16. Manke, I.A., Lowery, D.M., Nguyen, A., and Yaffe, M.B. (2003). BRCT repeats as phosphopeptide-binding modules involved in protein targeting. *Science* *302*, 636-639.
17. Melander, F., Bekker-Jensen, S., Falck, J., Bartek, J., Mailand, N., and Lukas, J. (2008). Phosphorylation of SDT repeats in the MDC1 N terminus triggers retention of NBS1 at the DNA damage-modified chromatin. *J Cell Biol* *181*, 213-226.
18. Nelson, M., and McClelland, M. (1992). *Methods Enzymol* *216*, 24.
19. Spycher, C., Miller, E.S., Townsend, K., Pavic, L., Morrice, N.A., Janscak, P., Stewart, G.S., and Stucki, M. (2008). Constitutive phosphorylation of MDC1 physically links the MRE11-RAD50-NBS1 complex to damaged chromatin. *J Cell Biol* *181*, 227-240.
20. Sugimoto, M., Esaki, N., Tanaka, H., and Soda, K. (1989). A simple and efficient method for the oligonucleotide-directed mutagenesis using plasmid DNA template and phosphorothioate-modified nucleotide. *Anal Biochem* *179*, 309-311.
21. Taylor, J.W., Ott, J., and Eckstein, F. (1985). The rapid generation of oligonucleotide-directed mutations at high frequency using phosphorothioate-modified DNA. *Nucleic Acids Res* *13*, 8765-8785.
22. Vandeyar, M.A., Weiner, M.P., Hutton, C.J., and Batt, C.A. (1988). A simple and rapid method for the selection of oligodeoxynucleotide-directed mutants. *Gene* *65*, 129-133.
23. Vinckier, N.K., Chworos, A., and Parsons, S.M. (2011). Improved isolation of proteins tagged with glutathione S-transferase. *Protein Expr Purif* *75*, 161-164.
24. Wang, J., Gong, Z., and Chen, J. (2011). MDC1 collaborates with TopBP1 in DNA replication checkpoint control. *J Cell Biol* *193*, 267-273.
25. Williams, R.S., Dodson, G.E., Limbo, O., Yamada, Y., Williams, J.S., Guenther, G., Classen, S., Glover, J.N., Iwasaki, H., Russell, P., *et al.* (2009). Nbs1 flexibly tethers Ctp1 and Mre11-Rad50 to coordinate DNA double-strand break processing and repair. *Cell* *139*, 87-99.

26. Wu, L., Luo, K., Lou, Z., and Chen, J. (2008). MDC1 regulates intra-S-phase checkpoint by targeting NBS1 to DNA double-strand breaks. *Proc Natl Acad Sci U S A* *105*, 11200-11205.
27. Yamane, K., Katayama, E., and Tsuruo, T. (2000). The BRCT regions of tumor suppressor BRCA1 and of XRCC1 show DNA end binding activity with a multimerizing feature. *Biochem Biophys Res Commun* *279*, 678-684.
28. Yamane, K., and Tsuruo, T. (1999). Conserved BRCT regions of TopBP1 and of the tumor suppressor BRCA1 bind strand breaks and termini of DNA. *Oncogene* *18*, 5194-5203.

**Chapter 4**  
**Structural Insight into BLM Recognition by TopBP1**

**A version of this chapter is published in:**

**Sun, L.**, Huang, Y., Edwards, R. A., Yang, S., Blackford, A. N., Niedzwiedz, W. and Glover, J. N. M. (2017) Structural Insight into BLM Recognition by TopBP1. *Structure* 25, 1582-1588

## 4.1 Introduction

RecQ helicases are an important family of proteins that are well conserved from bacteria to human. In human, there are five RecQ helicases that all play important roles in maintenance of genome stability (Croteau et al., 2014). Bloom syndrome, RecQ helicase-like protein (BLM) is one of these helicases, and mutations in BLM cause Bloom syndrome, a disease characterized by growth retardation, immunodeficiency, genomic instability, and cancer predisposition (German, 1993). Like other ATP dependent RecQ helicases, BLM mainly functions as a 3' → 5' helicase, and Bloom syndrome related mutations typically result in deletion of this helicase activity (Karow et al., 1997). However, BLM also acts as an important part in the “dissolvasome” which also consist of Rim1, Rim2, and Topoisomerase IIIA (Top3A). Together, this complex can dissolve double holiday junction at the late stage of HR and prevent meiotic crossover outcomes (Bizard and Hickson, 2014).

Recently, two reports have shown that BLM may also interact with TopBP1 BRCT5 in a phosphorylation and cell-cycle dependent manner (Blackford et al., 2015; Wang et al., 2013). Disruption of BLM-TopBP1 interaction in cells leads to elevated sister chromatid exchanges (SCEs) and chromosomal aberrations, features that are commonly found in Bloom syndrome patients (Blackford et al., 2015; Chaganti et al., 1974; German et al., 1965; Wang et al., 2013). While some evidence suggests that TopBP1 interacts with BLM pSer338 to stabilize BLM during S phase (Wang et al., 2013), other evidence has suggested that pSer304 of BLM is more crucial for this interaction, and that TopBP1 has no effect on BLM stability

(Blackford et al., 2015). Here we use fluorescence polarization (FP) spectroscopy to demonstrate that TopBP1 BRCT5 specifically binds phosphopeptides corresponding to the pSer304 region of BLM but not the pSer338 region. The X-ray crystal structure of mammalian TopBP1 BRCT4/5 in complex with a BLM peptide reveals specific recognition of pSer304 by the phosphate binding pocket of BRCT5 and recognition of the residues N-terminal to pSer304 by a hydrophobic groove and positively charged loop in BRCT5. The same surface is used by BRCT5 to bind a phosphorylated SDT repeat in the DNA damage checkpoint mediator, MDC1, but the orientation of BLM binding is reversed compared to MDC1. We suggest that TopBP1 BRCT5 can engage alternative protein partners to regulate DNA replication checkpoints.

## **4.2 Results**

### **4.2.1 TopBP1 BRCT5 interacts with BLM mainly through pSer304 and not pSer338**

To assess the likelihood that either Ser304 or Ser338 could serve as targets for TopBP1 BRCT5, we probed the conservation of sequences in this region in a number of vertebrate organisms (Figure 4-1A). Both Ser304 and Ser338 belong to the BLM N-terminal domain (1-636) that is largely unstructured and poorly conserved. The alignment shows striking conservation of residues N-terminal to the phosphorylation site of Ser304, with acidic residues conserved at the -7 and -5 positions, and a hydrophobic F(V/I)PP motif conserved from -4 to -1 (Figure 4-1A). In contrast, there is much poorer sequence conservation around Ser338. To directly investigate TopBP1 BRCT5 interactions with peptide targets *in vitro*, we synthesized FITC labeled BLM peptides corresponding to both sites (297-DTDFVPPpSPEEII-309, 331-KEDVLSTpSKDL-341) and tested their ability to

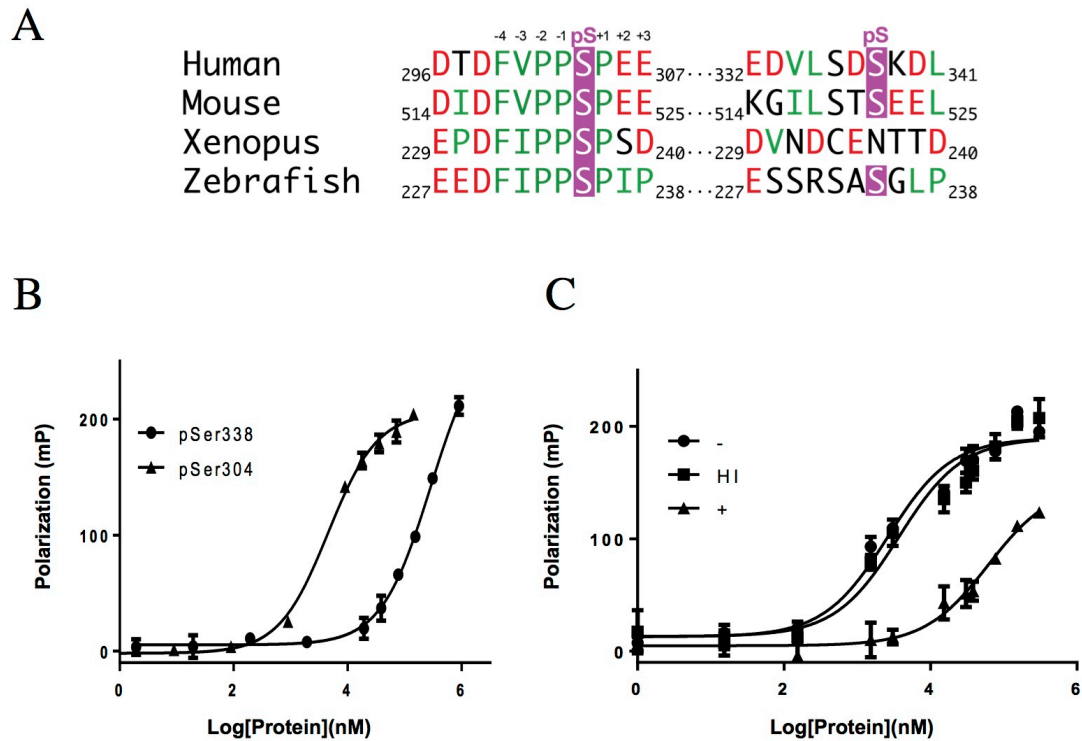


**Figure 4-1. BLM interacts with TopBP1 via pSer304, not pSer338.**

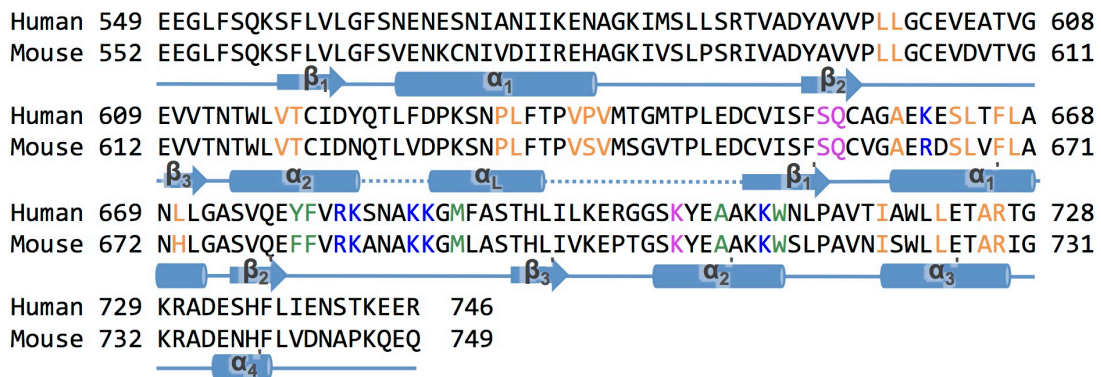
(A) Sequence alignment of BLM orthologs around pSer304 and pSer338. The pSer residues are colored in purple, hydrophobic residues are colored in green, and positively charged residues are colored in red. (B) TopBP1 BRCT4/5 binds more tightly to BLM pSer304 than BLM pSer338. TopBP1 BRCT4/5 protein was titrated against BLM phosphopeptides corresponding to either the pSer304 or pSer338 regions and binding was monitored by fluorescence polarization spectroscopy. (C) TopBP1 BRCT4/5 binds BLM pSer304 in phosphorylation-dependent manner. BLM pSer304 peptide was dephosphorylated by treatment with Lambda phosphatase (+) and its interaction with GST-hTopBP1 BRCT5 protein was measured by FP. BLM pSer304 peptide treated without Lambda phosphatase (-) or with heat-inactivated phosphatase (HI) were also included as controls.

interact with TopBP1 BRCT5 using FP study. TopBP1 interacts tightly with pSer304 BLM peptide ( $K_D = 3.9 \pm 0.3 \mu\text{M}$ ), but weakly with the pSer338 BLM peptide ( $K_D \geq 300 \mu\text{M}$ ) (Figure 4-1B). Then interested in whether the interaction between TopBP1 BRCT5 and pSer304 BLM peptide is phosphorylation dependent, we dephosphorylated the pSer304 BLM peptide using  $\lambda$  phosphatase treatment and examined its interaction with TopBP1 BRCT5 *in vitro* by FP. The  $\lambda$  phosphatase treated peptide binds TopBP1 BRCT5 much more weakly ( $K_D \geq 60 \mu\text{M}$ ) in comparison with the untreated pSer304 BLM peptides (Figure 4-1C). In addition, control peptides treated under same condition without phosphatase ( $K_D = 2.6 \pm 0.4 \mu\text{M}$ ) or with heat inactivated phosphatase both bind BRCT5 at similar affinity compared to untreated BLM pSer304 peptide ( $K_D = 3.7 \pm 0.8 \mu\text{M}$ ), indicating the treatment itself did not affect peptide affinity to TopBP1 BRCT5. Together, we can conclude that the phosphorylation of Ser304 is essential for its interaction with TopBP1 BRCT5.

#### **4.2.2 The crystal structure of TopBP1 BRCT4/5 bound to phosphorylated BLM**

To gain molecular insight into the interactions involved in pSer304-dependent BLM recognition by TopBP1, we crystallized and determined the structure of TopBP1 BRCT4/5 bound to a pSer304-containing BLM peptide. Crystallization trials using human TopBP1 BRCT4/5 were unsuccessful, but we were able to crystallize and determine the structure of the murine TopBP1 BRCT4/5-BLM complex at 2.6 Å resolution. The murine TopBP1 BRCT4/5 and murine BLM Ser304 regions are highly conserved with the human counterparts and interact with similar affinity (Figure 4-2). The murine complex crystallizes in  $P2_1$  space group with 8 copies of TopBP1 BRCT4/5 per asymmetric unit. There exists a translational non-crystallographic symmetry between protomers ACBE and HDGF, with BLM bound to only half of these protomers (Figure 4-3A). Comparisons of the unbound (EFGH) and bound (ABCD) structures of BRCT4/5 suggest that the TopBP1 structure is largely unchanged upon peptide binding (averaged root-mean-square deviation [rmsd]

A



B

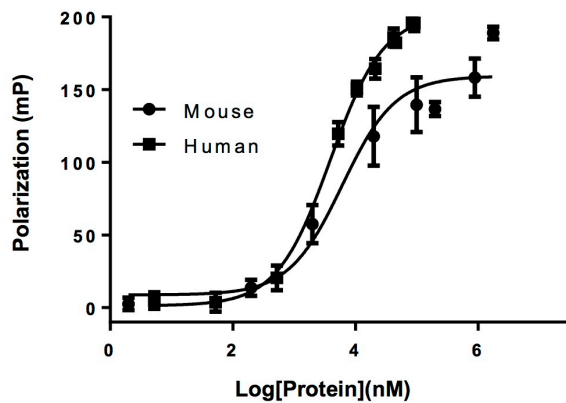


**Figure 4-2. Comparison of human versus mouse TopBP1 BLM interactions.**

(A) Sequence alignment of mouse versus human proteins with secondary structure by PROMALS3D. Residues forming the BRCT-BRCT interface are colored orange, residues from the peptide binding surface are colored blue (charged loop), purple (phosphate binding pocket), and green (hydrophobic groove). (B) Comparison of BLM interactions with the mouse and human TopBP1 BRCT4/5 by FP assay.

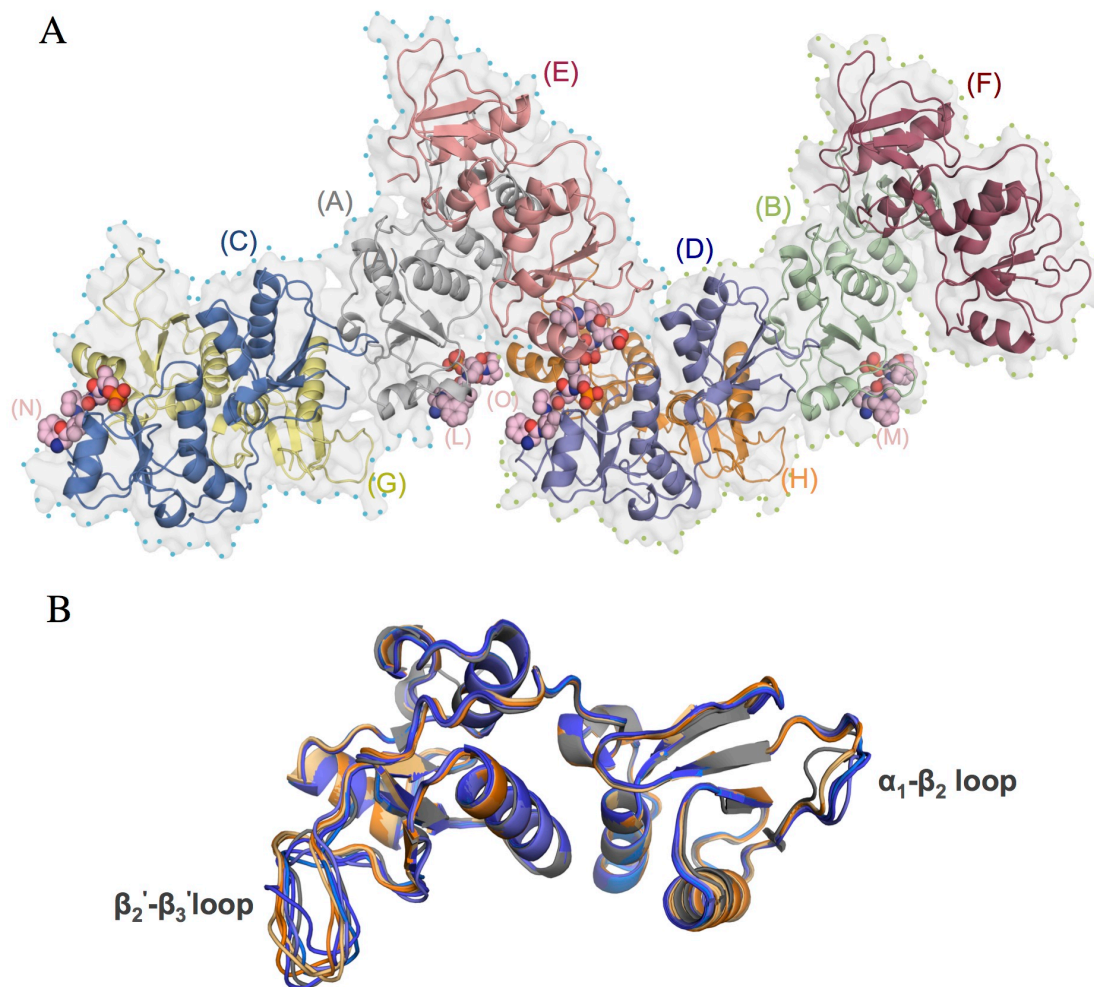


**Figure 4-3. X-ray crystallography structure of TopBP1 BRCT4/5 with BLM.**

(A) Overview of the crystallographic asymmetric unit. All BLM peptide chains (L, M, N, and O) are in space filling representation (pink). The two groups of protomers that are related by translational symmetry are highlighted with dotted lines. (B) Overlay of all protomers on the structure of human TopBP1 BRCT4/5 (3UEN) in light grey. Peptide bound protomers are in orange hues, apo protomers are in blue hues.

$C\alpha = 0.147 \text{ \AA}^2$  within each set, and  $C_\alpha = 0.469 \text{ \AA}^2$  between the peptide-bound and unbound sets). The structural differences are largely limited to the  $\alpha_1$ - $\beta_2$  and  $\beta_2'$ - $\beta_3'$  loops (Figure 4-3B). The  $\beta_2'$ - $\beta_3'$  loop directly contacts the BLM peptide, which restrains the loop conformation compared to the TopBP1 protomers with no bound peptide. The differences in the BRCT4  $\alpha_1$ - $\beta_2$  loops are likely caused by differences in crystal packing. The overall structure of murine TopBP1 BRCT4/5 adopts a head-to-head packing that is identical to human TopBP1 BRCT4/5, and nearly all residues involved in the BRCT-BRCT interface are conserved (Figure 4-2A). As suggested functionally in previous BLM-TopBP1 interaction studies (Blackford et al., 2015; Wang et al., 2013), our structure shows that TopBP1 interacts with BLM exclusively through its BRCT5 domain (Figure 4-3A) and indeed FP measurements indicate that BRCT5 and BRCT4/5 bind the BLM peptide with nearly identical affinities (Figure 4-4A).

### 4.2.3 Modeling of TopBP1-BLM binding interaction

The electron density enabled us to model the core of the BLM phosphopeptide sequence  $^{300}\text{Phe-Val-Pro-Pro-pSer-Pro}^{305}$  for each of the peptide-bound TopBP1 BRCT4/5 complexes (Table 4-1, Figure 4-5A). All peptide protomers adopt similar interactions with the TopBP1 BRCT5 except peptide O that interacts with two protomers (D and E) due to crystal packing (RMSD of  $C_\alpha = 0.084 \text{ \AA}^2$  between L, M, N, and  $C_\alpha = 0.201 \text{ \AA}^2$  with O) (Figure 4-6). The phosphate group of BLM pSer304 is bound in the phosphate-binding pocket of TopBP1 BRCT5 through a set of hydrogen-bonding interactions with side chains of Lys707, Ser657 and main chain NH of Gln658 that are conserved in other BRCT-phosphopeptide structures (Leung and Glover, 2011) (Figure 4-5B). The BLM peptide adopts a typical left-handed type II polyproline (PPII) helical structure. The phosphate group of BLM pSer304 is bound in the phosphate-binding pocket of TopBP1 BRCT5 through a set of hydrogen-bonding interactions with side chains of Lys707, Ser657 and main chain NH of Q658 that are conserved in other BRCT-phosphopeptide structures (Leung and Glover, 2011)

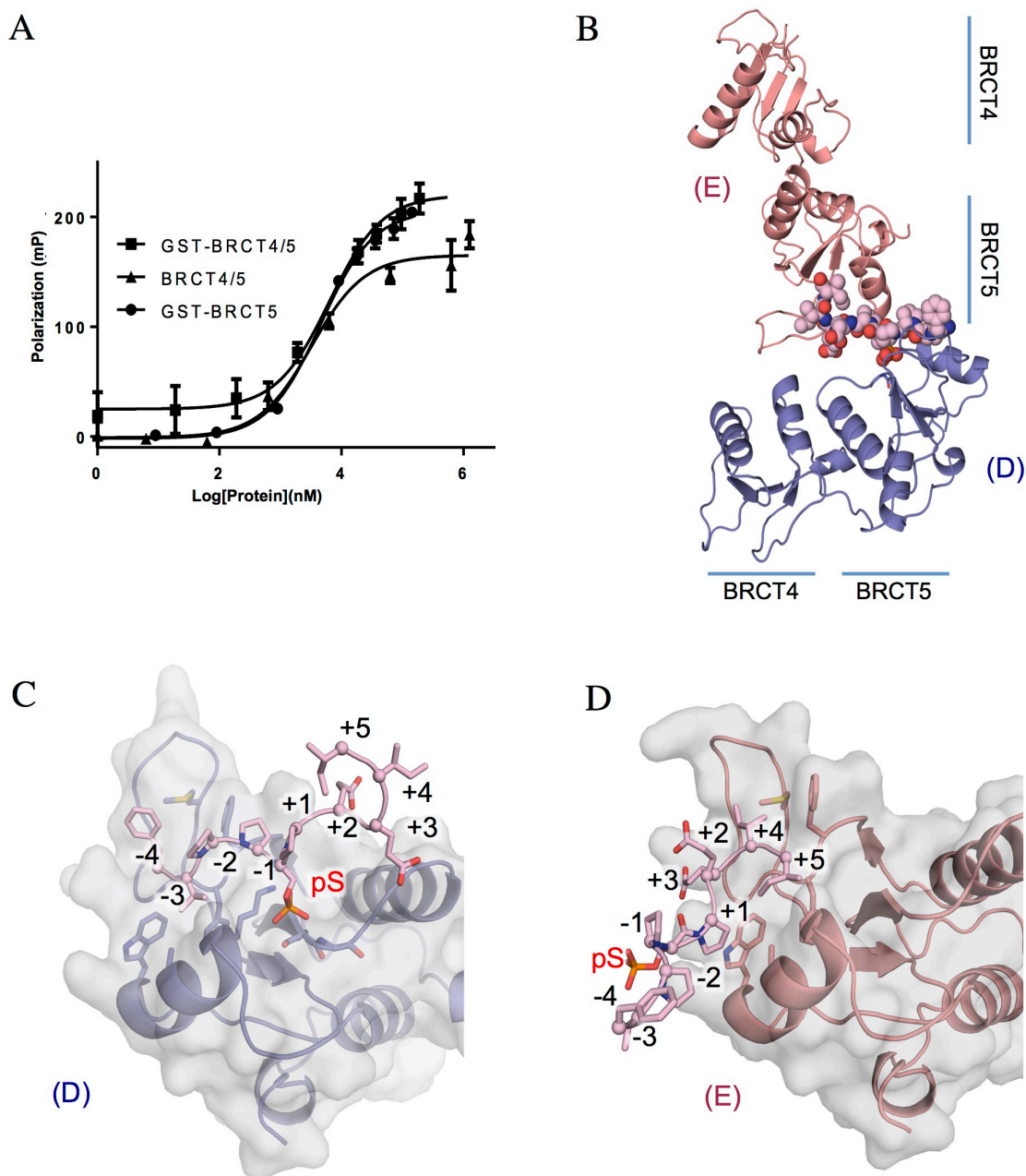


**Figure 4-4. Crystal packing induced dimer of TopBP1 BRCT4/5 with BLM.**

(A) FP study of TopBP1 BRCT5 interaction with BLM. (B) Overview of protomer E (salmon) and D (slate) dimmerized through peptide O (pink). (C) Conserved interaction of BLM with protomer D. (D) Packing enforced interaction of BLM with protomer E.

**Table 4-1. Data Collection, Phasing and Refinement Statistics**

TopBP1 BRCT4/5- BLM Complex

Space group	P 21
Unit cell dimensions	
a, b, c (Å)	98.16, 96.82, 127.05
$\alpha, \beta, \gamma$ (°)	90, 94.25, 90
Resolution range (Å) <sup>a</sup>	47.87-2.60 (2.63-2.60)
No. of unique reflections	71934
Completeness (%)	98.8
Overall I/sigma (I)	11.08 (2.65)
$R_{meas}$ <sup>b</sup>	0.136 (0.920)
CC <sub>1/2</sub>	0.970 (0.896)
$R_{free}/R_{work}$ (%) <sup>c</sup>	25.61/21.93
Number of atoms	11899
Wilson B factor (Å <sup>2</sup> )	54.87
Ramachandran Plot (%)	
Most favoured	96.7
Outlier	0.5
Clashscore	4.17
R.M.S. Deviation	
Bonds (Å)	0.003
Angles (°)	0.546

<sup>a</sup>Values in parentheses are from the highest resolution shell.

<sup>b</sup>
$$R_{meas} = \frac{\sum_{hkl} \sum_{i=1}^n |I_i(hkl) - \bar{I}(hkl)|}{\sum_{hkl} \sum_{i=1}^n I_i(hkl)}$$

<sup>c</sup>
$$R_{work/free} = \frac{\sum_{hkl} |F_{obs}(hkl) - F_{calc}(hkl)|}{\sum_{hkl} F_{obs}(hkl)}$$

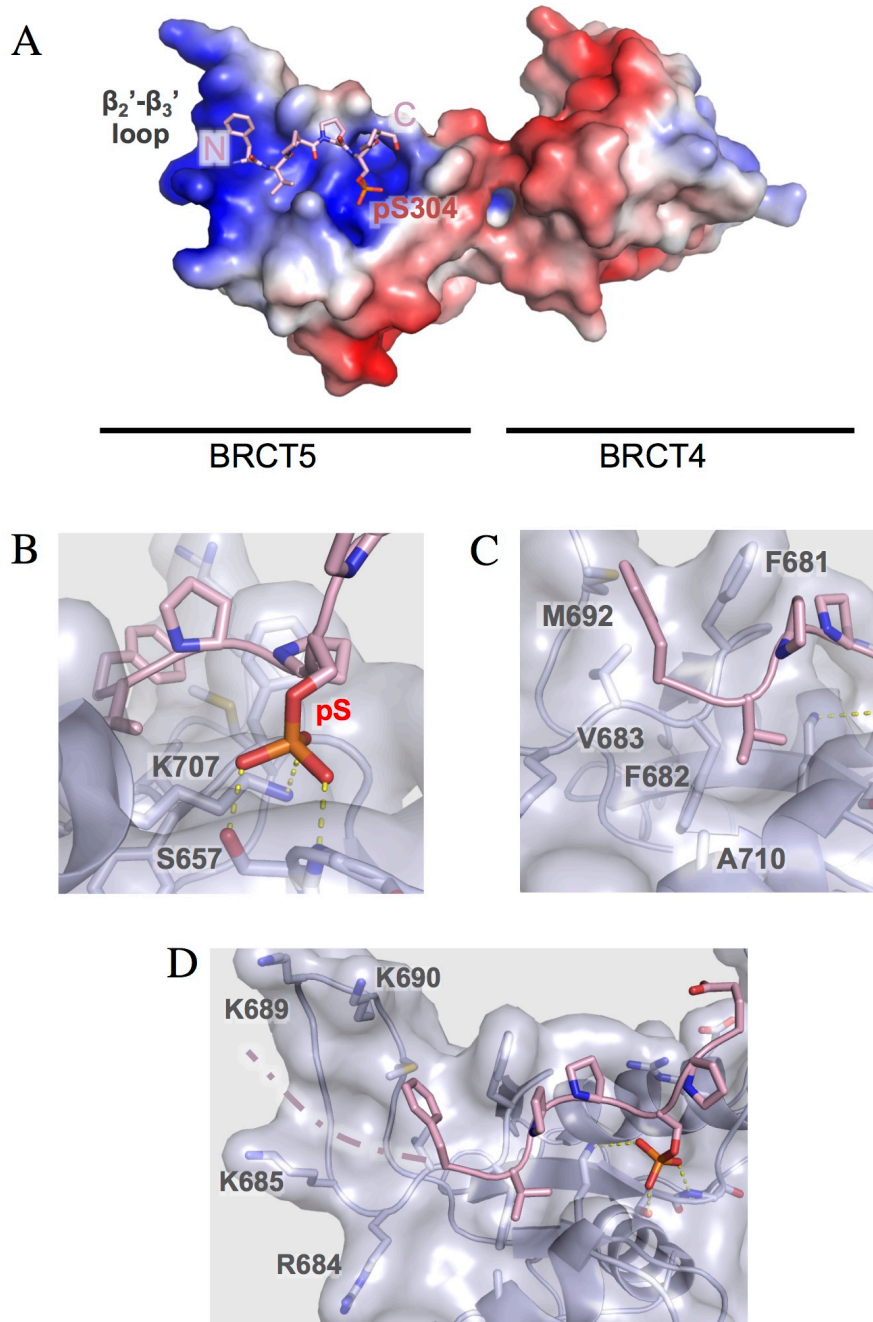


**Figure 4-5. Detailed structure model of BLM interaction with TopBP1 via pSer304.**  
 (A) Structural overview of TopBP1 BRCT4/5 in complex with pSer304 BLM peptide. An electrostatic charge surface is displayed for TopBP1 BRCT4/5 while the modeled BLM phosphopeptide is shown in pink sticks. The structural insight of phosphate binding pocket (B), hydrophobic groove (C), and negatively charged loop (D) is also included.

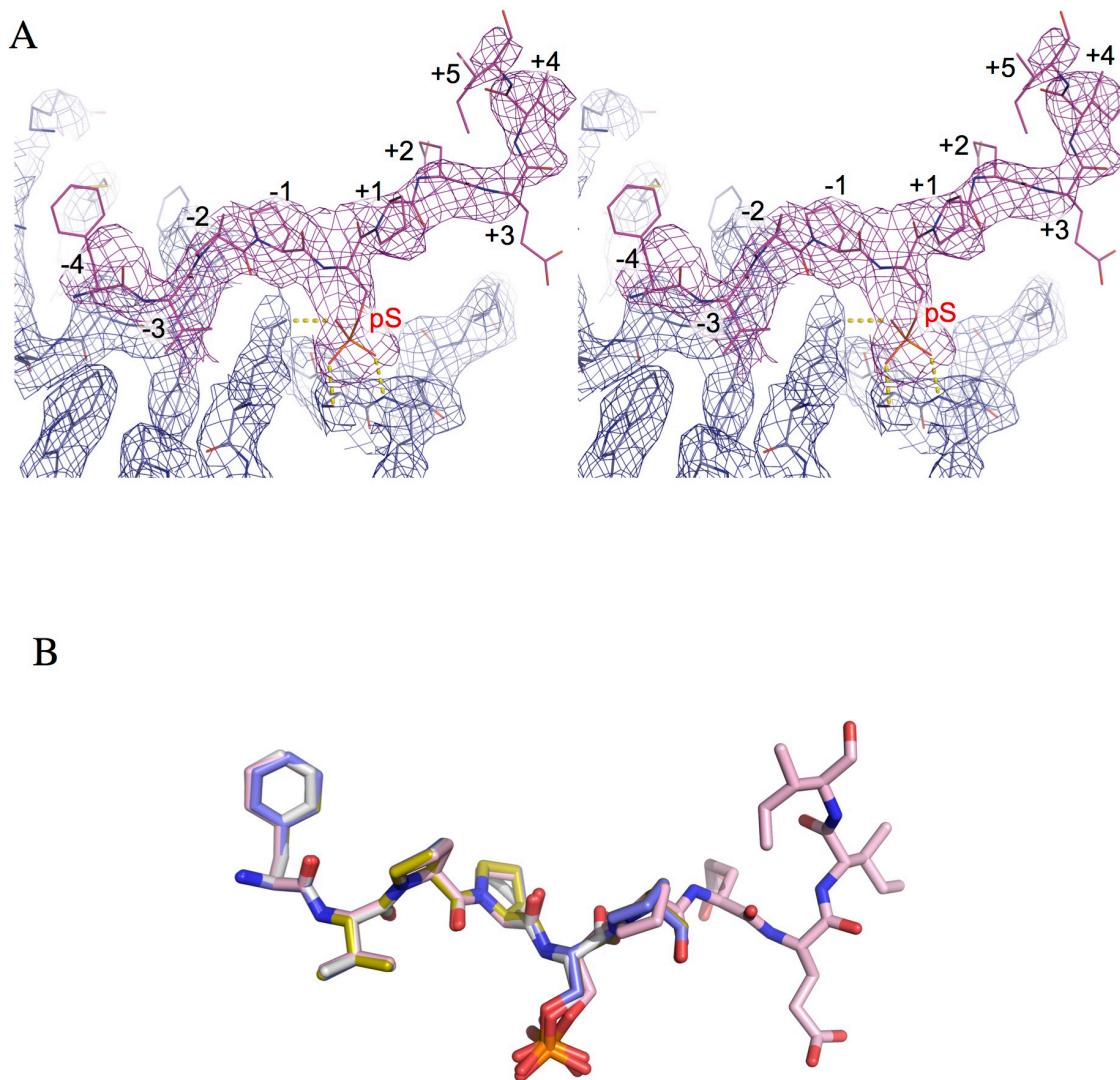


**Figure 4-6. Detail structures of pSer304 containing BLM peptides.**

(A) Representative bias-reduced density map of TopBP1 BRCT4/5 bound to BLM peptide. The stereo-view is directed into the peptide-BRCT interface between protomer D and peptide O. Density maps of the peptide (pink) and the BRCT4/5 (blue) are both contoured at 1.0 sigma level. The electron density map was calculated using the interact-build omit method. (B) The structural overlay of all BLM peptide protomers. Protomers M (blue), L (mustard), N (grey) and O (pink).

(Figure 4-5C). The conserved FVPP motif N-terminal to Ser304 contours through a hydrophobic groove on the surface of BRCT5 that leads to the  $\beta_2'$ - $\beta_3'$  loop. The tandem prolines at positions -1 and -2 pack against Phe681, the valine at -3 is buried within a hydrophobic pocket formed by residues Phe682, Ala710, and Trp714, and the phenylalanine at -4 packs against Met692 at the center of the  $\beta_2'$ - $\beta_3'$  loop (Figure 4-5C). Although we were unable to model the conserved Asp-Thr-Asp motif N-terminal to the core sequence due to lack of electron density, this acidic motif could potentially interact with basic residues including Arg684, Lys685, Lys689 and Lys690 from the  $\beta_2'$ - $\beta_3'$  loop, which, together with the phosphate binding pocket, render the peptide-binding surface highly electropositive (Figure 4-5D). C-terminal to pSer304, the peptide tracks away from BRCT5 and in 3 of the 4 complexes, there is no density observable for the semi-conserved Glu-Glu-Ile-Ile motif. In one of the complexes, however, this motif is visible and packs against another BRCT5 in the asymmetric unit (Figures 4-4B, C, D). We conclude that the primary TopBP1 binding determinant within the BLM target peptide is the core <sup>300</sup>Phe-Val-Pro-Pro-pSer<sup>304</sup> region, while the acidic N-terminal motif (<sup>297</sup>Asp-Thr-Asp<sup>299</sup>) may play a secondary role to enhance this interaction.

#### 4.2.4 Comparison of BLM and MDC1 recognition by TopBP1

MDC1 has also been identified as a potential binding partner of TopBP1 BRCT4/5 and the structure of a consensus MDC1 SDT repeat region (GFIPSDpTDVEEE) bound to TopBP1 BRCT4/5 was solved by X-ray crystallography (Leung et al., 2013). MDC1 interacts with TopBP1 in a manner not observed in other BRCT-peptide structures, with one MDC1 peptide sandwiched between two BRCT4/5 domains. There is no direct interface between the two BRCT4/5 protomers, and most of the MDC1 interaction involves just one of the protomers. Evidence that a TopBP1 dimer binds MDC1 more tightly than a monomer in solution comes from FP binding studies that show the untagged monomeric TopBP1 BRCT4/5 binds MDC1 significantly weaker than dimeric GST-BRCT4/5 or GST-BRCT5

**Table 4-2. Summary of Fluorescence Polarization Study Results**

Protein		TopBP1-peptide $K_D$ ( $\mu$ M)		
TopBP1		MDC1	BLM	
GST-hBRCT5	WT	$15 \pm 1$	$285 \pm 10$	pSer338
			$3.9 \pm 0.3$	pSer304
	S654A	$48 \pm 6$	$33 \pm 3$	
	K704A	$59 \pm 6$	$42 \pm 3$	
	R681E/K682E	$170 \pm 10$	$45 \pm 2$	
	K686E/K687E	$130 \pm 20$	$36 \pm 3$	
	A707K	$12.0 \pm 0.9$	$70 \pm 20$	
	A707D	$120 \pm 10$	$320 \pm 40$	
	M689A	$15 \pm 1$	$53 \pm 4$	
Y678A	$21 \pm 2$	$18 \pm 2$		
hBRCT4/5		$100 \pm 10$	$3.2 \pm 0.8$	
GST-hBRCT4/5		$30 \pm 4$	$6 \pm 1$	
mBRCT4/5		$170 \pm 20$	$6 \pm 2$	

(Leung et al., 2013) (Table 4-2). In contrast, both the untagged and GST-tagged forms interact with BLM with similar dissociation constants in the 3-6  $\mu\text{M}$  range that is significantly higher than MDC1 (Figure 4-4A, Table 4-2). This suggests that TopBP1 BRCT4/5 interacts with BLM as a monomer and with much higher affinity than MDC1.

In order to understand how TopBP1 BRCT4/5 interacts with two different partners, we first compared these interactions by superimposition of the structures of the TopBP1-BLM and TopBP1-MDC1 complexes (Figure 4-7A). The TopBP1 BRCT4/5 structures are quite similar between the two complexes (RMSD of  $C_{\alpha}$  = 0.497). The same BRCT5 groove is used to engage the two extended phosphopeptide partners. However, the orientations of the two peptides relative to the BRCT5 binding surface are reversed. To further probe the interactions of the two peptides with TopBP1, we compared the impact on peptide binding of a panel of human TopBP1 BRCT5 mutations using the FP assay (Figure 4-7B). Mutation of either Ser654 or Lys704 in the phosphate-binding pocket (equivalent of S657A and K707A in mouse) causes an 8 to 11 fold reduction in BLM binding affinity, consistent with the role of these residues in hydrogen-bonding with the pSer304 (Figure 4-8). These same mutations only result in a 3 to 4 fold reduction of affinity in MDC1 for TopBP1. The reduced importance of this pocket for MDC1 binding is consistent with the structure. In the TopBP1 protomer that makes the most extensive contacts with MDC1, the phosphate-binding pocket does not bind a phosphate and instead binds the -3 Asp of MDC1. The -3 Asp only partially mimics a pSer, preserving hydrogen-bonding interactions with Ser657 and the main chain NH of Gln658. In the other TopBP1 protomer, the MDC1 pThr is partially docked into the phosphate-binding pocket. Two different pairs of charge reversal mutations within the basic  $\beta_2'$ - $\beta_3'$  loop (R681E/K682E and K686E/K687E, equivalent of R684E/K685E or K689E/K690E in mouse) reduced TopBP1 affinity ~9- to 12-fold suggesting charged interactions involving this loop are important to stabilize either complex. In the MDC1 complex, the acidic residues at +3 and +4 are in proximity to the  $\beta_2'$ - $\beta_3'$  loop, while in the BLM complex, we propose it is the DTD motif at positions -5 to -7 that contacts

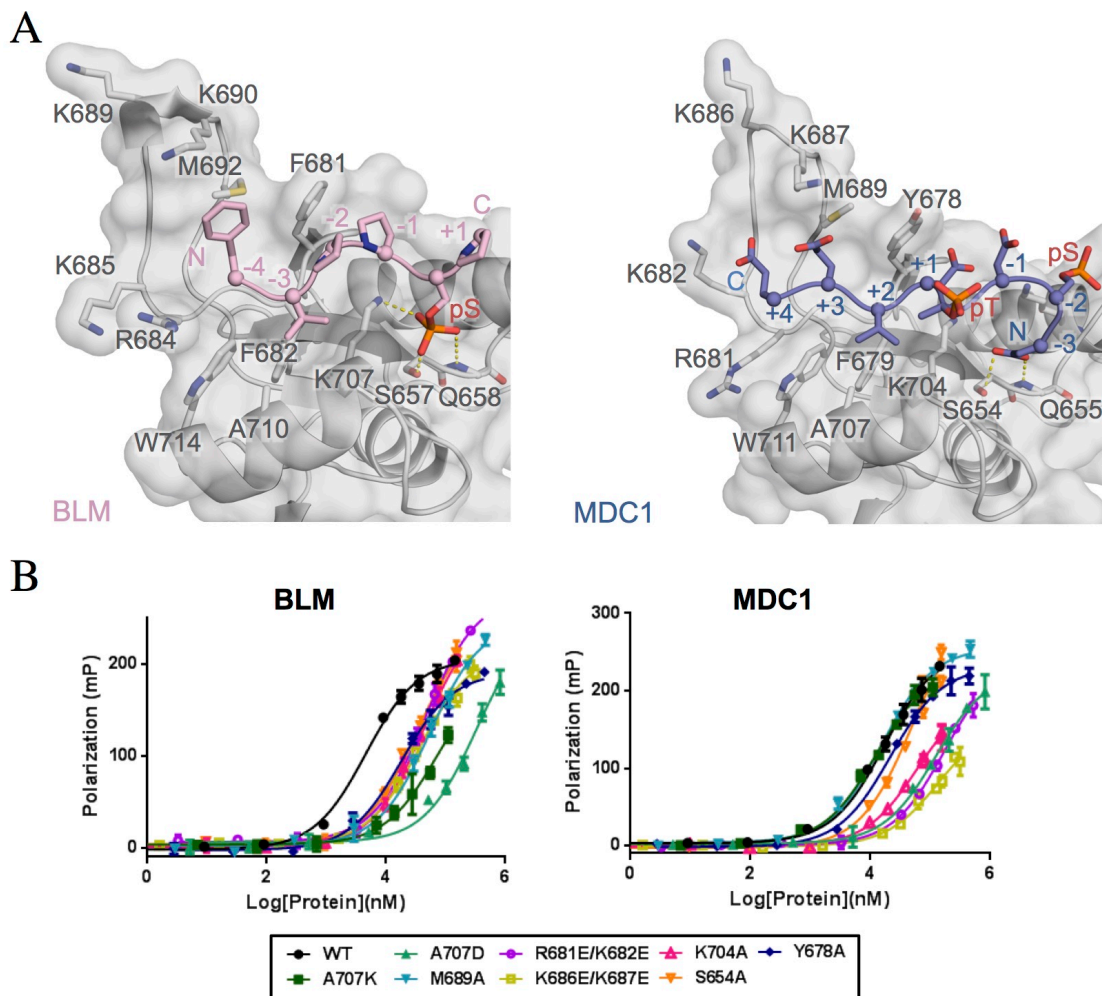


**Figure 4-7. Comparison of TopBP1 recognition of BLM and MDC1.**

(A) Structural comparison of TopBP1-BLM and TopBP1-MDC1 complexes. TopBP1-BLM complex (left) and TopBP1-MDC1 (right) are aligned by their BRCT5 main-chain C<sub>α</sub> positions. Both of the TopBP1 BRCT structures are displayed with a semi-transparent surface over a grey cartoon, while the BLM peptide is displayed as a pink cartoon and the MDC1 peptide is displayed as a blue cartoon. Key interacting residues are displayed as sticks and hydrogen bonds are indicated by yellow dash-lines. Residue numbering of mTopBP1 (left) and hTopBP1 (right) is differed by 3. (B) Comparison of the binding affinities of BLM and MDC1 phosphopeptides for a panel of human TopBP1 BRCT5 variants using FP. WT TopBP1 BRCT5 and a panel of eight missense variants were titrated against either BLM phosphopeptide (left) or the MDC1 phosphopeptide (right) and their binding affinities were assessed by FP.

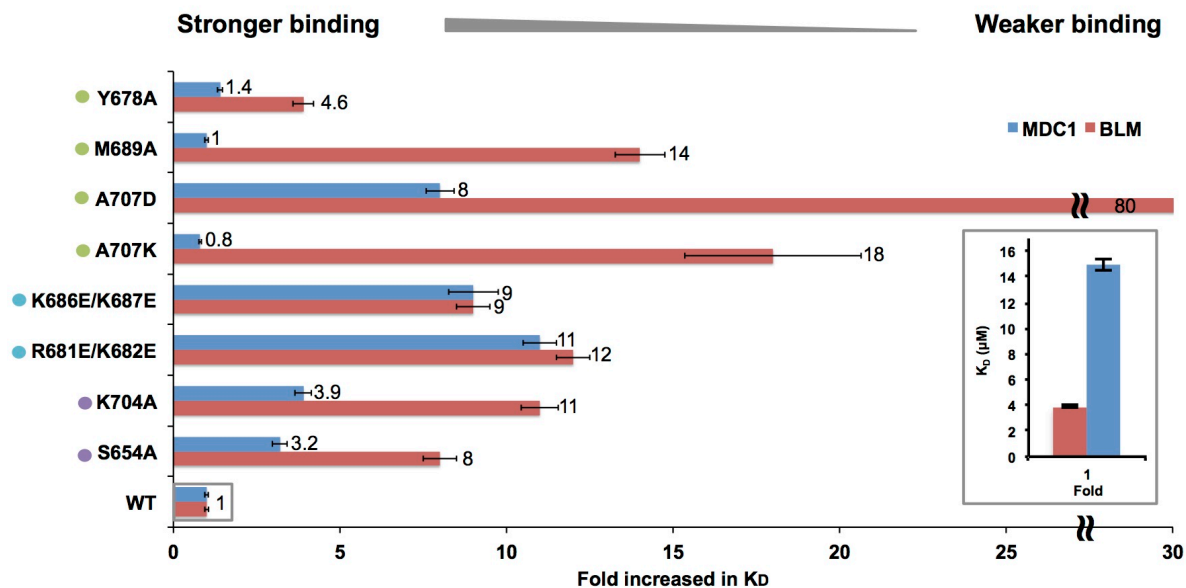


**Figure 4-8. Summary of effects of human TopBP1 BRCT5 missense mutations on the binding of either MDC1 or BLM.**

The fold increase in  $K_D$  is plotted for each BRCT5 variant normalized against the binding affinity for the WT. Results for BRCT5-MDC1 interactions are shown in blue, while the results for BRCT5-BLM interactions are shown in pink. Mutations from the different parts of BRCT5 are colored differently (Green for hydrophobic groove, blue for negatively charged loop, purple for phosphate binding pocket). The inset shows the relative difference in  $K_D$  between WT BRCT5-MDC1 and WT BRCT5-BLM.

this loop. Both MDC1 and BLM present a valine (position -3 in BLM, position +2 in MDC1) that docks into the TopBP1 hydrophobic pocket (Figure 4-7A). The floor of this pocket consists of a conserved alanine (Ala707 in human, Ala710 in mouse). Mutation of this alanine shows strikingly different effects on binding of the two peptides. Replacement of the alanine with either a positive (A707K) or negative (A707D) charge dramatically reduces BLM binding, but only the A707D reduces MDC1 peptide binding. This result suggests that the hydrophobic nature of this pocket is critical for the BLM interaction, but is much less important for the MDC1 interaction. Additional hydrophobic contacts observed in the BLM complex that are not found in the MDC1 complex (Figure 4-7A). The BLM proline at -2 docks against TopBP1 Phe681 and the BLM phenylalanine at -4 packs into a shallow hydrophobic depression in the surface of the  $\beta_2'$ - $\beta_3'$  loop formed by Met692, Val683, and Phe681. Mutations of residues that constitute these surfaces in the human protein (M689A or Y678A) have no appreciable impact on the MDC1 binding. However, these mutations result in significant reductions in BLM binding (Figure 4-7B, 4-8).

Taken together, these data indicate that BLM binds TopBP1 BRCT5 in a way that utilizes the electrostatic complementarity between the peptide and BRCT5, as well as hydrophobic contacts that impart additional specificity and binding affinity. In contrast, the MDC1-TopBP1 complex appears to be largely electrostatically driven and of much lower affinity than the BLM complex.

### **4.3 Discussion**

TopBP1 is distinguished by the range of protein partners that interact with its diverse BRCT domains. TopBP1 BRCT5 has been particularly interesting as it has been proposed to bind multiple phosphoprotein targets: BLM, MDC1, and 53BP1 (although the relevant phosphorylated residue in the latter has not yet been identified). Our work shows that the recognition of BLM is highly specific for the region surrounding pSer304 and likely does not involve pSer338, which was also proposed as a possible binding target (Wang et al., 2013).

While MDC1 recognition involves the same surface on BRCT5, the MDC1 peptide binds in an opposite orientation to that observed for BLM, and is of lower affinity and specificity, relying primarily on electrostatic interactions between the highly negatively charged MDC1 phosphopeptide and the positively charged surface of BRCT5. Our results raise further doubts as to whether MDC1 is a physiological binding partner for BRCT5 of TopBP1 (Blackford et al., 2015; Choi and Yoo, 2016), although a similar electrostatic interaction may also explain reports of interactions between BRCT5 and single-stranded DNA, which have been suggested to play a role in the recognition of stalled DNA replication forks (Acevedo et al., 2016).

TopBP1 BRCT4/5 has not only been shown to interact with BLM and MDC1, but has also been implicated in binding the key DNA damage signaling factor, 53BP1, in a phosphorylation-dependent interaction (Cescutti et al., 2010; Yamane et al., 2002). Insight into this interaction has been provided by structural studies of the *S. pombe* orthologs of these proteins, Rad4<sup>TopBP1</sup> and Crb2<sup>53BP1</sup> (Qu et al., 2013). Rad4<sup>TopBP1</sup> contains a pair of BRCTs (BRCT1 and BRCT2) which can both bind either of two Crb2<sup>53BP1</sup> phosphopeptides containing a VXXpT motif in a manner that is similar to the binding of BLM by TopBP1 BRCT5, both in terms of the tracking of the peptide across the BRCT surface and docking of the -3 Val into the BRCT hydrophobic pocket (Figure 4-9A). The major difference between TopBP1 BRCT5 and either BRCT1 or BRCT2 of Rad4<sup>TopBP1</sup> is the lack of the positively charged  $\beta_2'$ - $\beta_3'$  loop in the Rad4<sup>TopBP1</sup> BRCTs (Figure 4-9A,B) and the Crb2 phosphopeptide binding partner does not contain the conserved negatively charged residues at positions -4 to -7 observed in BLM (Figure 4-9C).

To probe the possibility that similar interactions might be responsible for TopBP1-53BP1 interactions in the mammalian homologs, we scanned the known 53BP1 phosphorylation sites for potential TopBP1 binding sites that contain the VXXpS/T motif. While many 53BP1 pSer/pThr sites conform to the VXXpS/T motif, only a few contain

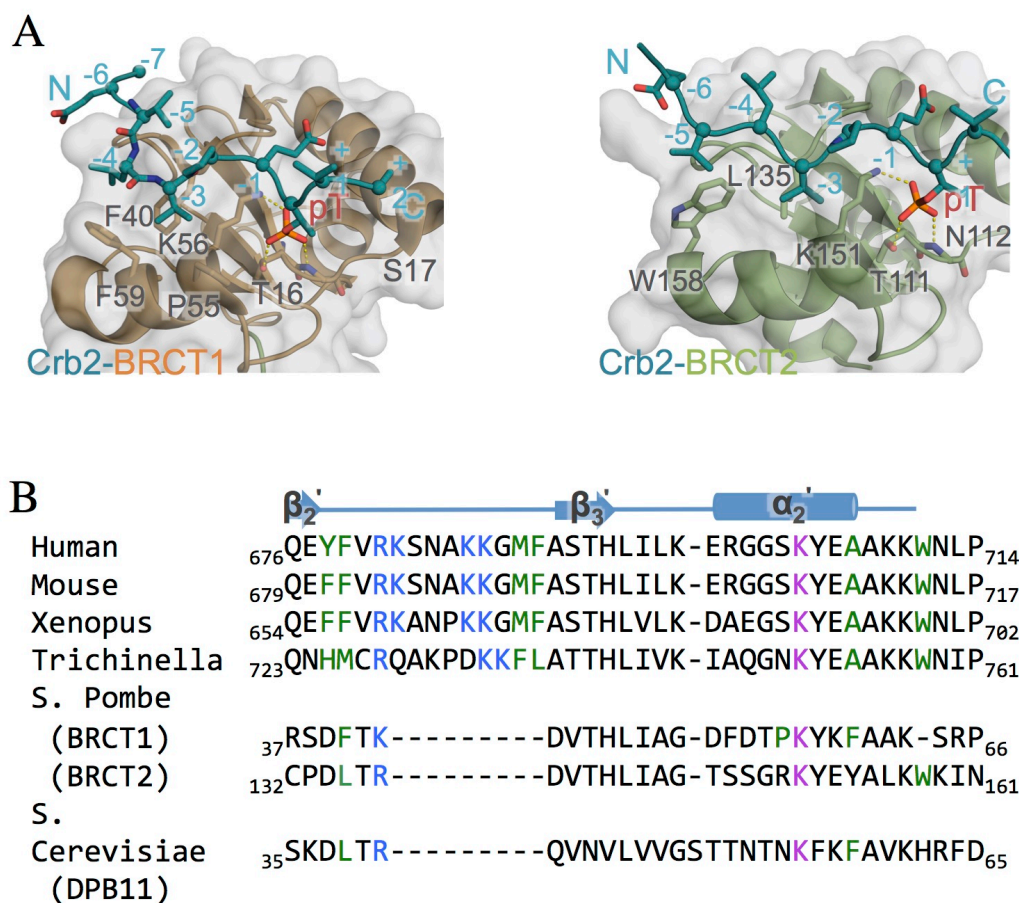


**Figure 4-9. TopBP1 BRCT5 may bind BLM and 53BP1 through similar mechanisms.**

(A) Structures of Rad4<sup>TopBP1</sup> BRCT repeats bound to Crb2<sup>53BP1</sup>. Rad4 BRCT1/Crb2 (left) and Rad4 BRCT2/Crb2 (right) structures (PDB code: 4BU0) are aligned with the TopBP1/BLM complex as in Figure 4-7. Both structures have surface and cartoon displayed for Rad4<sup>TopBP1</sup> (BRCT1 in orange, BRCT2 in green) and only cartoon displayed for Crb2<sup>53BP1</sup> (blue). Interacting residues are displayed as sticks. Hydrogen bonds are indicated by yellow dash-lines. (B) Sequence alignment of the peptide binding region TopBP1 BRCT5 homologs. Residues from the positively charged  $\beta_2'$ - $\beta_3'$  loop are colored blue, residues from phosphate binding pocket are colored purple, and residues lining hydrophobic groove are colored green.

additional acidic residues or potentially phosphorylated residues upper stream to the VXXpS/T motif that could provide electrostatic interactions with the  $\beta_2'$ - $\beta_3'$  loop (Table 4-3). However, the pSer366 and pSer379/pSer380 sites are closer hits because they the region around these site are also enriched with hydrophobic residues, such as Pro or Phe, that may form the poly-proline helix observed in BLM peptide (Figure 4-10A). Besides, residues around pSer336 and pSer379/pSer380 sites are both well conserved across species, which further support they are great candidates for the interaction with TopBP1 BRCT5 (Figure 4-10B). Further mutagenesis study of pSer336 and pSer379/pSer380 sites from 53BP1 *in vivo* is needed to validate which site is critical for 53BP1 interaction with TopBP1 in cells.

Agents that increase the replication stress load in cancer cells can be very effective chemotherapeutics. Cells in which the BLM-TopBP1 interaction is disrupted show increased replication stress, as evidenced by the increased DNA replication origin firing, chromosomal aberrations and SCEs (Blackford et al., 2015). Therefore, the structure of the BRCT domains of TopBP1 in complex with a BLM peptide lays the foundation for targeting of the BLM-TopBP1 interaction with small molecules as potential chemotherapeutic agents.

#### **4.4 Material and Methods**

##### ***Cloning, expression, and purification***

Expression cell lines for Human TopBP1 BRCT5 (641-746) and BRCT4/5 (549-746), and mutants (K704A, R681E/K682E, K686E/K687E) were made previously (Leung et al., 2013). Mouse TopBP1 BRCT4/5 (553-749) was cloned into pGEX-6P-1 (GE Healthcare). Mutants (Y678A, A707D, A707K, M689A) of human TopBP1 BRCT5 were created from the WT template using QuickChange Lighting site-directed mutagenesis kit (Stratagene) (Braman et al., 1996; Kunkel, 1985; Nelson and McClelland, 1992; Sugimoto et al., 1989; Taylor et al., 1985; Vandeyar et al., 1988). All recombinant TopBP1 protein domains were expressed

**Table 4-3. List of Potential Phosphorylation Sites on 53BP1 for TopBP1 Recognition**

LTP <sup>1</sup>	HTP <sup>2</sup>	P site	Sequeunce	Conservation
0	41	S366	SSDLVAPSPDAFR	high
0	13	S379	STPFIVPSSPTEQ	high
2	0	S380	TPFIVPSSPTEQE	high
0	3	S1290	CETEVSPSQTGGS	medium
0	1	T670	EVEEIPETPCESQ	low
0	4	S1025	GSTAVAESVASPQ	low

1. LTP:Phosphorylation site identified by low throughput biological study on 53BP1  
2. HTP:Phosphorylation site identified by high throughput screening methods

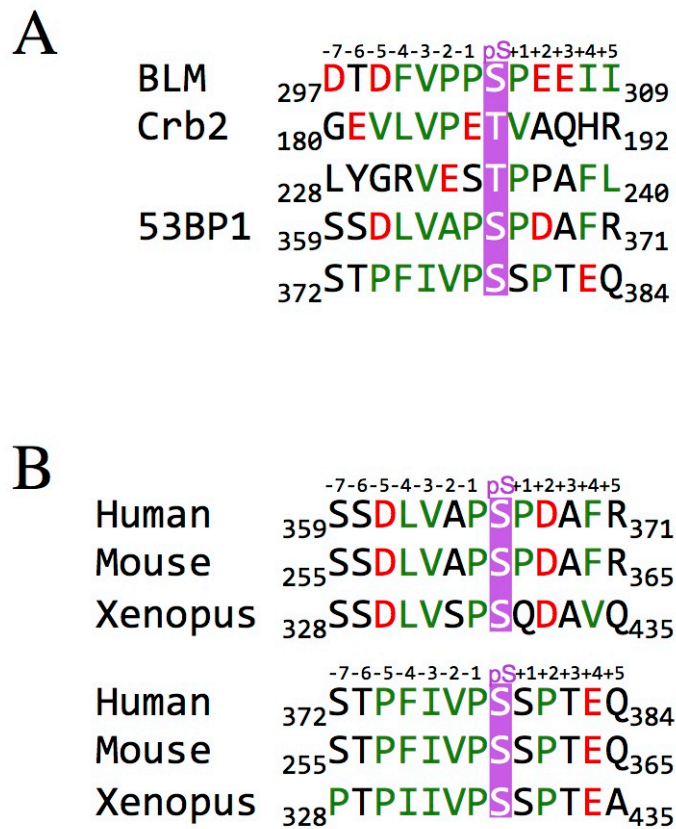


**Figure 4-10. Potential phosphorylation site of 53BP1 recognized by TopBP1.**  
 (A) Sequence alignment of BLM and 53BP1 phosphopeptide partners for TopBP1 BRCT5.  
 (B) Sequence alignment of potential TopBP1 BRCT5 binding regions in 53BP1.  
 Phosphorylated residues are colored purple, negatively charged residues are colored red and hydrophobic residues are colored green.

in *Escherichia coli* BL21-Gold cells with Luria-Bertani (LB) broth media containing 50 µg/mL kanamycin and 50 µg/mL ampicillin at 25°C. Recombinant protein expression was induced with 0.5 mM isopropyl-β-D-thiogalactopyranoside (IPTG) at a cell density (OD) of 0.5 – 0.8 and grown overnight (12 to 14 hours) at 22°C before harvest. All the GST fusion proteins were purified using glutathione affinity chromatography with glutathione sepharose 4B beads (GE Healthcare) and eluted in elution buffer (20 mM Tris-HCl pH 7.5, 150 mM NaCl, 20 mM reduced glutathione and 0.1% βME). GST-fusion protein of BRCT5 was purified by Superdex 200 16/60 column in storage buffer (10 mM Tris-HCl pH 8.0, 150 mM NaCl, 1 mM DTT). GST-fusion protein of TopBP1 BRCT4/5 was cleaved with PreScission protease overnight at 4 °C. BRCT4/5 was purified by anion exchange chromatography (buffer A: 50 mM HEPES pH 7.0, 0.1% βME; buffer B: 50 mM HEPES pH 7.0, 1M NaCl, 0.1% βME). Residual GST was removed by incubation with glutathione sepharose 4B beads (GE Healthcare) prior to a final purification step on a Superdex 75 26/60 column in storage buffer (10 mM Tris-HCl pH 7.5, 150 mM NaCl, 1 mM DTT).

### ***Crystallization***

Mouse TopBP1 BRCT4/5 concentrated to 10 mg/mL was incubated with 3-fold molar excess of BLM peptide (Ac-DTDFVPPpSPEEII-NH<sub>2</sub>, Genosphere Biotechnologies) for 2 hours on ice. Crystals of the complex were grown at room temperature using hanging drop vapor diffusion by mixing 1 µL of protein:peptide complex with 1 µL of reservoir solution (0.1 M sodium citrate pH 5.4 and 24% PEG 8000). Co-crystals were flash-cooled in reservoir solution supplemented with 20% glycerol.

### ***Data collection and structure determination***

Data for crystals of the BRCT4/5-pSer304 BLM peptide complex were collected at the CMCF 08ID-1 beamline (Canadian Light Source, Saskatoon). Intensity data were processed by DENZO, scaled and reduced using SCALEPACK (Adams et al., 2010) to the space group *P21* with unit cell dimensions:  $a = 98.62 \text{ \AA}$ ,  $b = 97.0 \text{ \AA}$ ,  $c = 127.3 \text{ \AA}$ ,  $\alpha = 90.0^\circ$ ,  $\beta = 94.3^\circ$ ,  $\gamma = 90.0^\circ$  (Otwinowski and Minor, 1997). The human TopBP1 BRCT4/5 structure

(PDB ID: 3UEN) was used in PHASER 25.6 to successfully find 8 copies in the asymmetric unit (McCoy et al., 2007). Model building was carried out in COOT and refined using TLS refinement (peptide bound molecule ABCD and unbound molecule EFGH are grouped separately) in PHENIX (Adams et al., 2010; Emsley and Cowtan, 2004). The BRCT4/5 molecules are related by translational symmetry (Supplementary Figure 2A). BRCT4/5 chain A and C lack the N-terminal 549–550 residues, C-terminal 742–746 residues, and  $\alpha_1$ - $\beta_2$  loop residues 584–588. Chain B and D lack the N-terminal 549–550 residues, C-terminal 743–746 residues, and  $\alpha_1$ - $\beta_2$  loop residues 584–589. The BRCT4/5 molecules were fully refined before building of the four peptides. Peptides were positioned by first docking in the key pSer304 residues using Ligandfit in Phenix, and the rest of peptide chain subsequently built manually in COOT (Koska et al., 2008). Peptide chains L and M lack the N-terminal 7 to 5 residues and C-terminal +1 to +5 residues, peptide N lacks the N-terminal 7 to 5 residues and C-terminal +1 to +5 residue, and peptide O only lacks the N-terminal 7 to 5 residues. The final model was refined in Phenix at 2.6 Å resolution to  $R_{\text{work}}$  and  $R_{\text{free}}$  of 0.256 and 0.219, respectively. The Ramachandran plot contained 96.7% of all residues in the favored region. All the 7 Ramachandran outliers come from the two flexible loop regions ( $\beta_2'$ - $\beta_3'$  loop and  $\alpha_1$ - $\beta_2$  loop) of TopBP1 BRCT4/5. Data collection and refinement statistics for the structures are listed in Table 1. Models were validated with MolProbity (Chen et al., 2010). Alignments with structure information were done by PROMAL3D. Bias reduced omit maps were generated by Phenix (Terwilliger et al., 2008). All structure figures were prepared with PyMOL (Version 1.8, [www.pymol.org](http://www.pymol.org)).

### ***Lambda protein phosphatase treatment***

Unphosphorylated Ser304 BLM peptide (FITC-DTDFVPPSPPEEII-NH<sub>2</sub>) was made by treating pSer304 BLM peptide (FITC-DTDFVPPpSPEEII-NH<sub>2</sub>) with lambda protein phosphatase (New England Biolabs) for 1 hour at 30 °C in reaction buffer (50 mM Tris-HCl, pH 7.5, 0.1 mM Na<sub>2</sub>EDTA, 5 mM DTT, and 0.01% Brij 35, 2 mM MnCl<sub>2</sub>) The inactive form of lambda protein phosphatase was made by 1 hour heat inactivation at 65 °C in the presence of 50 mM

EDTA. Then control peptides treated under same condition with either inactive phosphatase or in the absence of phosphatase were made.

### ***Fluorescence polarization assay***

FP measurements were carried out using an Envision multi-label plate reader (Perkin Elmer) using 384-well OptiPlates (Perkin Elmer). All pSer304 related BLM peptides (FITC-DTDFVPPpSPEEII-NH<sub>2</sub>, Ac-DTDFVPPpSPEEII-NH<sub>2</sub>, Ac-DTDFVPPpSPEEIIKK-NH<sub>2</sub>, Ac-DFVPPpSPEEII-NH<sub>2</sub>) were synthesized and purified by Genosphere Biotechnologies. The rest of peptides (FITC-KEDVLSTpSKDL-NH<sub>2</sub>, FITC-GFIDpSDpTDVEEE-NH<sub>2</sub>) were synthesized and purified by Biomatik. FP assays were performed by mixing 10 nM FITC-labelled phospho-peptide with freshly concentrated TopBP1 in FP assay buffer (10 mM Tris-HCl pH 7.5, 150 mM NaCl, 1 mM DTT, 0.05 % Tween-20) and incubated for 15 min at room temperature. FP measurements were carried out at an excitation wavelength of 485 nm and emission wavelength of 538 nm. Curve fitting and K<sub>D</sub> calculations were obtained using PRISM software (GraphPad Prism). K<sub>D</sub> values summarized in Table 1 are the average of at least three individual measurements.

## 4.5 Reference

1. Acevedo, J., Yan, S., and Michael, W.M. (2016). Direct Binding to Replication Protein A (RPA)-coated Single-stranded DNA Allows Recruitment of the ATR Activator TopBP1 to Sites of DNA Damage. *J Biol Chem* 291, 13124-13131.
2. Adams, P.D., Afonine, P.V., Bunkoczi, G., Chen, V.B., Davis, I.W., Echols, N., Headd, J.J., Hung, L.W., Kapral, G.J., Grosse-Kunstleve, R.W., *et al.* (2010). PHENIX: a comprehensive Python-based system for macromolecular structure solution. *Acta Crystallogr D Biol Crystallogr* 66, 213-221.
3. Bizard, A.H., and Hickson, I.D. (2014). The dissolution of double Holliday junctions. *Cold Spring Harb Perspect Biol* 6, a016477.
4. Blackford, A.N., Nieminuszczy, J., Schwab, R.A., Galanty, Y., Jackson, S.P., and Niedzwiedz, W. (2015). TopBP1 interacts with BLM to maintain genome stability but is dispensable for preventing BLM degradation. *Mol Cell* 57, 1133-1141.
5. Braman, J., Papworth, C., and Greener, A. (1996). Site-directed mutagenesis using double-stranded plasmid DNA templates. *Methods Mol Biol* 57, 31-44.
6. Cescutti, R., Negrini, S., Kohzaki, M., and Halazonetis, T.D. (2010). TopBP1 functions with 53BP1 in the G1 DNA damage checkpoint. *EMBO J* 29, 3723-3732.
7. Chaganti, R.S., Schonberg, S., and German, J. (1974). A manyfold increase in sister chromatid exchanges in Bloom's syndrome lymphocytes. *Proc Natl Acad Sci U S A* 71, 4508-4512.
8. Chen, V.B., Arendall, W.B., 3rd, Headd, J.J., Keedy, D.A., Immormino, R.M., Kapral, G.J., Murray, L.W., Richardson, J.S., and Richardson, D.C. (2010). MolProbity: all-atom structure validation for macromolecular crystallography. *Acta Crystallogr D Biol Crystallogr* 66, 12-21.
9. Choi, S.H., and Yoo, H.Y. (2016). Mdc1 modulates the interaction between TopBP1 and the MRN complex during DNA damage checkpoint responses. *Biochem Biophys Res Commun* 479, 5-11.
10. Croteau, D.L., Popuri, V., Opresko, P.L., and Bohr, V.A. (2014). Human RecQ helicases in DNA repair, recombination, and replication. *Annu Rev Biochem* 83, 519-552.

11. Emsley, P., and Cowtan, K. (2004). Coot: model-building tools for molecular graphics. *Acta Crystallogr D Biol Crystallogr* *60*, 2126-2132.
12. German, J. (1993). Bloom-Syndrome - a Mendelian Prototype of Somatic Mutational Disease. *Medicine* *72*, 393-406.
13. German, J., Archibald, R., and Bloom, D. (1965). Chromosomal Breakage in a Rare and Probably Genetically Determined Syndrome of Man. *Science* *148*, 506-507.
14. Karow, J.K., Chakraverty, R.K., and Hickson, I.D. (1997). The Bloom's syndrome gene product is a 3'-5' DNA helicase. *J Biol Chem* *272*, 30611-30614.
15. Koska, J., Spassov, V.Z., Maynard, A.J., Yan, L., Austin, N., Flook, P.K., and Venkatachalam, C.M. (2008). Fully automated molecular mechanics based induced fit protein-ligand docking method. *J Chem Inf Model* *48*, 1965-1973.
16. Kunkel, T.A. (1985). Rapid and efficient site-specific mutagenesis without phenotypic selection. *Proc Natl Acad Sci U S A* *82*, 488-492.
17. Leung, C.C., and Glover, J.N. (2011). BRCT domains: easy as one, two, three. *Cell Cycle* *10*, 2461-2470.
18. Leung, C.C., Sun, L., Gong, Z., Burkat, M., Edwards, R., Assmus, M., Chen, J., and Glover, J.N. (2013). Structural insights into recognition of MDC1 by TopBP1 in DNA replication checkpoint control. *Structure* *21*, 1450-1459.
19. McCoy, A.J., Grosse-Kunstleve, R.W., Adams, P.D., Winn, M.D., Storoni, L.C., and Read, R.J. (2007). Phaser crystallographic software. *J Appl Crystallogr* *40*, 658-674.
20. Nelson, M., and McClelland, M. (1992). *Methods Enzymol* *216*, 24.
21. Otwinowski, Z., and Minor, W. (1997). Processing of X-ray diffraction data collected in oscillation mode. *Methods Enzymol* *276*, 307-326.
22. Qu, M., Rappas, M., Wardlaw, C.P., Garcia, V., Ren, J.Y., Day, M., Carr, A.M., Oliver, A.W., Du, L.L., and Pearl, L.H. (2013). Phosphorylation-dependent assembly and coordination of the DNA damage checkpoint apparatus by Rad4(TopBP1). *Mol Cell* *51*, 723-736.

23. Sugimoto, M., Esaki, N., Tanaka, H., and Soda, K. (1989). A simple and efficient method for the oligonucleotide-directed mutagenesis using plasmid DNA template and phosphorothioate-modified nucleotide. *Anal Biochem* 179, 309-311.
24. Taylor, J.W., Ott, J., and Eckstein, F. (1985). The rapid generation of oligonucleotide-directed mutations at high frequency using phosphorothioate-modified DNA. *Nucleic Acids Res* 13, 8765-8785.
25. Terwilliger, T.C., Grosse-Kunstleve, R.W., Afonine, P.V., Moriarty, N.W., Adams, P.D., Read, R.J., Zwart, P.H., and Hung, L.W. (2008). Iterative-build OMIT maps: map improvement by iterative model building and refinement without model bias. *Acta Crystallogr D Biol Crystallogr* 64, 515-524.
26. Vandeyar, M.A., Weiner, M.P., Hutton, C.J., and Batt, C.A. (1988). A simple and rapid method for the selection of oligodeoxynucleotide-directed mutants. *Gene* 65, 129-133.
27. Wang, J., Chen, J., and Gong, Z. (2013). TopBP1 controls BLM protein level to maintain genome stability. *Mol Cell* 52, 667-678.
28. Yamane, K., Wu, X., and Chen, J. (2002). A DNA damage-regulated BRCT-containing protein, TopBP1, is required for cell survival. *Mol. Cell. Biol.* 22, 555-566.

## **Chapter 5**

### **General Discussion**

## **5.1 Overall Summary**

The BRCT domain family is an important group of proteins that are largely involved in cell cycle regulation, DNA damage response, and repair. Mutations in BRCT proteins often result in genomic instability and many diseases in humans including cancers. My thesis focuses on two important BRCT family proteins, BRCA1 and TopBP1. I have successfully verified the first nonphosphopeptide inhibitor of BRCA1 BRCTs and solved the crystal structure of this inhibitor in complex with BRCA1 BRCTs. My study reveals new structural insight that can guide the development of BRCA1 inhibitors and further support the possibility of phosphorylation-independent interaction of BRCA1 BRCTs (Chapter 1). Meanwhile, I have also studied the interactions between TopBP1 BRCT4/5 and two different protein partners, MDC1 (Chapter 2) and BLM (Chapter 3). Consistent with the existing structural model of TopBP1 BRCT4/5 in complex with MDC1 SDT repeat peptide, my mutagenesis study of TopBP1 BRCT5 validated that TopBP1 engages MDC1 mainly through electrostatic interactions. The interaction with MDC1 is largely induced by TopBP1 dimerization. However, my structural and functional study of TopBP1/BLM interaction reveals a different model of interaction. TopBP1 BRCT5 interacts with BLM in a monomer-based interaction that is highly dependent on phosphorylation of Ser304 of BLM. Additional hydrophobic interaction is crucial for stabilizing this complex while electrostatic interactions only play a supportive role. Together, my studies of BRCA1 and TopBP1 further illustrate the structural diversity of BRCT domain architecture and reveal new protein-protein interactions (PPIs) that have therapeutic potential for cancer therapy.

## **5.2 Structural diversity of BRCT tandem repeats**

Although both exist as tandem BRCT repeats, the overall domain architecture of BRCA1 BRCTs and TopBP1 BRCT4/5 differs significantly. Similar to other canonical

tandem BRCT repeats, the core beta sheets from BRCTs of BRCA1 are aligned in parallel with each other, as has been observed in MDC1 BRCTs and TopBP1 BRCT7/8 (Figure 5-1A) (Leung et al., 2011; Stucki et al., 2005). It is well known that BRCA1 BRCTs has a phosphate-binding pocket formed by Ser1655, Lys1702 and Gly1656 on its N-terminal BRCT, and a hydrophobic pocket containing Leu1701 and Met1775 on the interface between BRCTs (Figure 5-1A, 5-2A)(Williams et al., 2004). It is also no secret that a core pS-X-X-F motif is conserved between phosphopeptide partners of BRCA1 BRCTs (Liu and Ladas, 2013; Varma et al., 2005; Wu et al., 2016) (Figure 5-2C). Besides, Arg1699 from the BRCTs packing interface largely affects the positioning of the +3 residue from the peptide via interaction with the main chain at the +3 position. Likely due to this reason, BRCA1 BRCTs can only host peptide that has the N terminal to C terminal orientation. Comparing with internal peptide segments, it preferentially targets peptides with C terminal carboxylate at +3 position (Wu et al., 2015). Moreover, we recently discovered a second hydrophobic pocket, formed by Leu1657, Pro1659, Phe1662, and Leu1676, on BRCA1 BRCTs between the  $\beta_1$  and  $\alpha_1$ . This small hydrophobic groove further expands the peptide interface on the N-terminal BRCT of BRCA1 and facilitates interactions with the peptide that has N-terminal hydrophobic residues (White et al., 2015).

In contrast, the non-canonical BRCT4/5 of TopBP1 has its central beta sheets arranged in an antiparallel fashion, and binds peptide regardless of their orientation. The surface involved in interaction with partner proteins is found exclusively on the C-terminal BRCT5 (Figure 5-1B). This BRCT5 domain has a positively charged surface that runs from the phosphate binding pocket consists of Lys704, Ser654, and Gln655, to an extended arginine and lysine enriched  $\beta_2'$ - $\beta_3'$  loop (consist of Arg681, Lys682, Lys686, and Lys687). In addition, there is a hydrophobic groove consisting of Phe678, Phe679, Ala707, Trp711 and Met689 that sits in the middle of the positively charged surface, which adds more selectivity to this BRCT (Figure 5-2B) (Leung et al., 2013).

Interestingly, there is a third type of tandem BRCT repeat, in which both BRCT

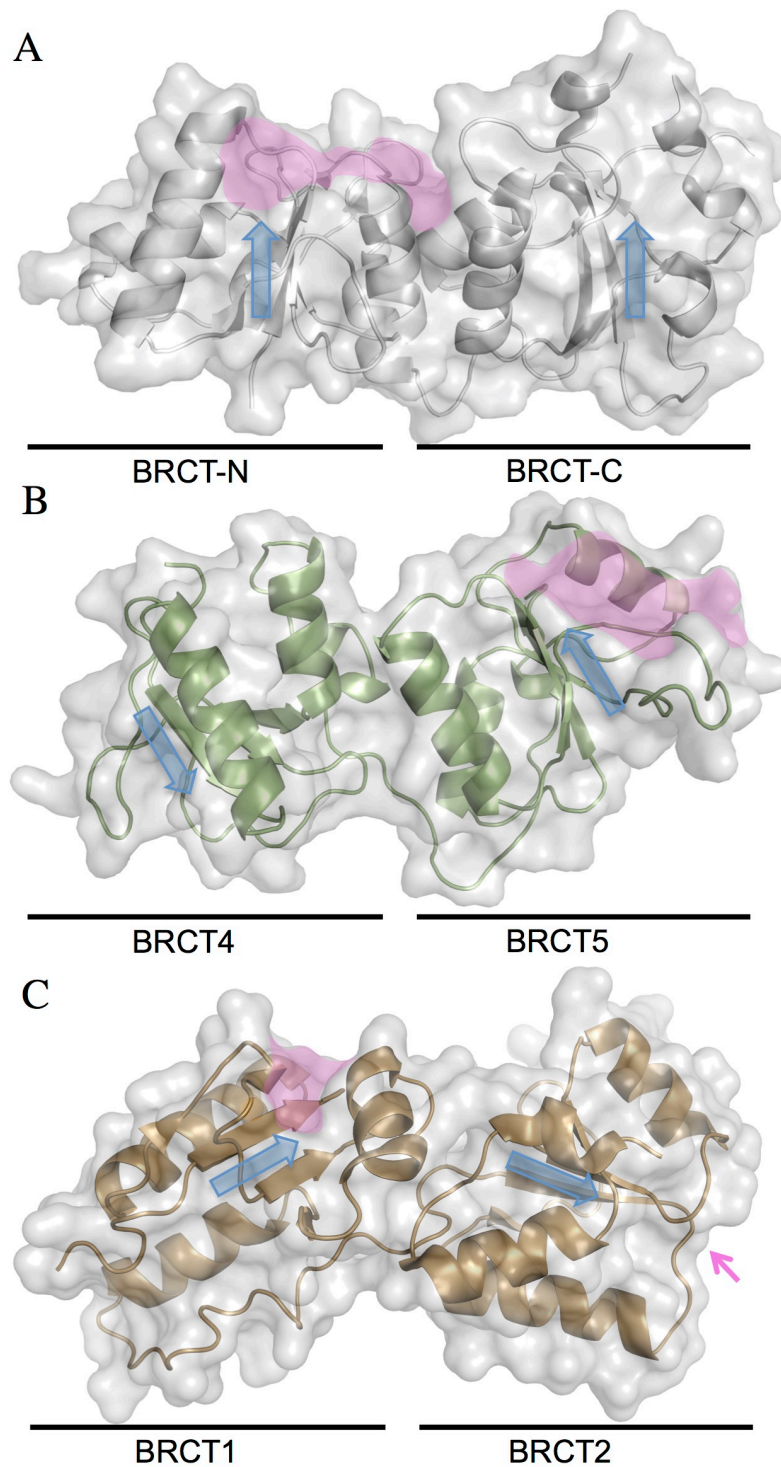


**Figure 5-1. Overview of tandem BRCT domains.**

X-ray structures of (A) BRCA1 BRCTs (PDB ID: 1JNX). (B) TopBP1 BRCT4/5 (PDB ID: 3UEN). (C) Rad4 BRCT1/2 (PDB ID: 4BU0). In each BRCT, blue arrows indicate the directions of core beta sheets. All the protein-binding surfaces are in pink except the one of Rad4 BRCT2 which is found on the back of the current view shown by a pink arrow.

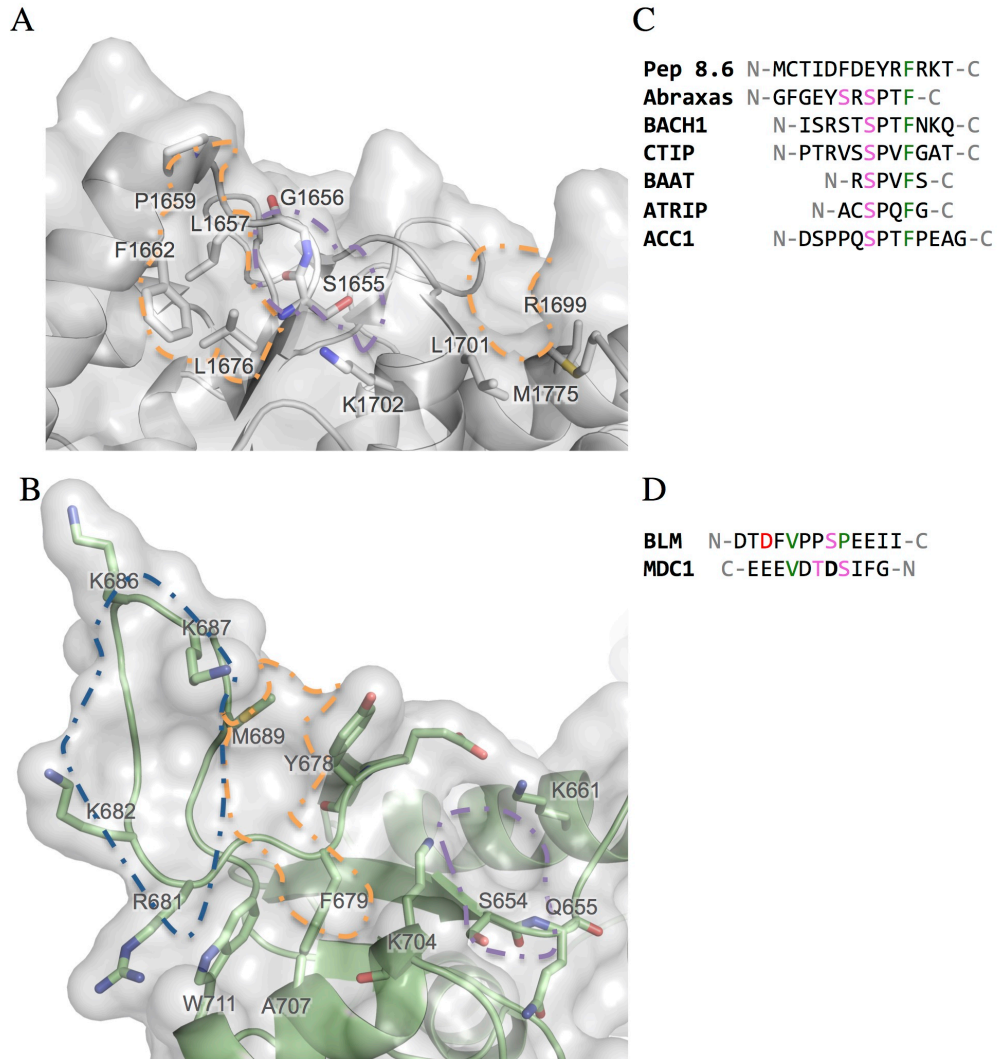


**Figure 5-2. Structure features of TopBP1 BRCT4/5 and BRCA1 BRCTs interactions with their partner proteins.**

Detail structure features of protein interaction surface on (A) BRCA1 BRCTs (PDB ID: 1JNX) and (B) TopBP1 BRCT4/5 (PDB ID: 3UEN) are presented here. All the important residues involved in protein-protein interactions are highlighted in stick view. Major areas with different features on the proteins are circled by dash-line. The purple indicates phosphate-binding pocket, orange indicates hydrophobic pockets, and blue area indicates positively charged platform. Sequence alignment of peptide partners of (C) BRCA1 BRCTs and (D) TopBP1 BRCT4/5. All the important phosphorylated residues are shown in pink, hydrophobic residues are shown in green, and acidic residues are shown in red.

domains have the well-constructed phosphate-binding pockets capable of phosphopeptide binding. BRCT1/2 of Rad4<sup>TopBP1</sup> is a good example of such tandem BRCT repeats (Qu et al., 2013). The central beta sheets from Rad4<sup>TopBP1</sup> BRCT1/2 are almost perpendicular to each other, making the two phosphate-binding pockets isolated onto two almost perpendicular dimensions (Figure 5-1C). Both BRCTs of Rad4<sup>TopBP1</sup> are found to interact with the N-terminal loop region of Crb2<sup>53BP1</sup> with multiple phosphorylated threonine sites. The BRCT1/2 of the N-terminal triple BRCTs from TopBP1 also exhibit domain architectures that are similar to Rad4<sup>TopBP1</sup> BRCT1/2 (Huo et al., 2010). However, only TopBP1 BRCT1 is found to be involved in the interaction with Rad9 of the 9-1-1 complex. The phosphate-binding pocket of BRCT2 is likely involved with a yet unknown protein partner of TopBP1 BRCT0/1/2.

### 5.3 Novel aspects of BRCT mediated protein interactions

In spite of their differences, BRCA1 BRCTs and TopBP1 BRCT4/5 also share some intriguing features. Firstly, they both have a type I phosphate binding pocket that can interact with either pSer or pThr. This type of phosphate-binding pocket interacts with phosphate using two side chains (S1655/S654, K1702/K704 in BRCA1/TopBP1, respectively) and one main chain NH (G1656/Q655 in BRCA1/TopBP1) (Figure 5-3A,B). This is different from the type II phosphate-binding pocket that only interacts with pThr, as we observed in Rad4<sup>TopBP1</sup> BRCT2. In addition to the side chain of Thr110 and Lys151 and the main chain NH of Asn111, the side chain guanidinium of Arg117 from Rad4<sup>TopBP1</sup> BRCT2 also engages the phosphate head group of threonine from Crb2<sup>53BP1</sup> (Figure 5-3C).

Secondly, the interactions between their phosphate binding pockets and the phosphate of their partner protein can both be partially replaced by polar residues. Overlay of BRCA1/nonphosphopeptide complex with BRCA1/BACH1 phosphopeptide complex structure shows that the nonphosphopeptide inhibitor of BRCA1 uses glutamate to maintain

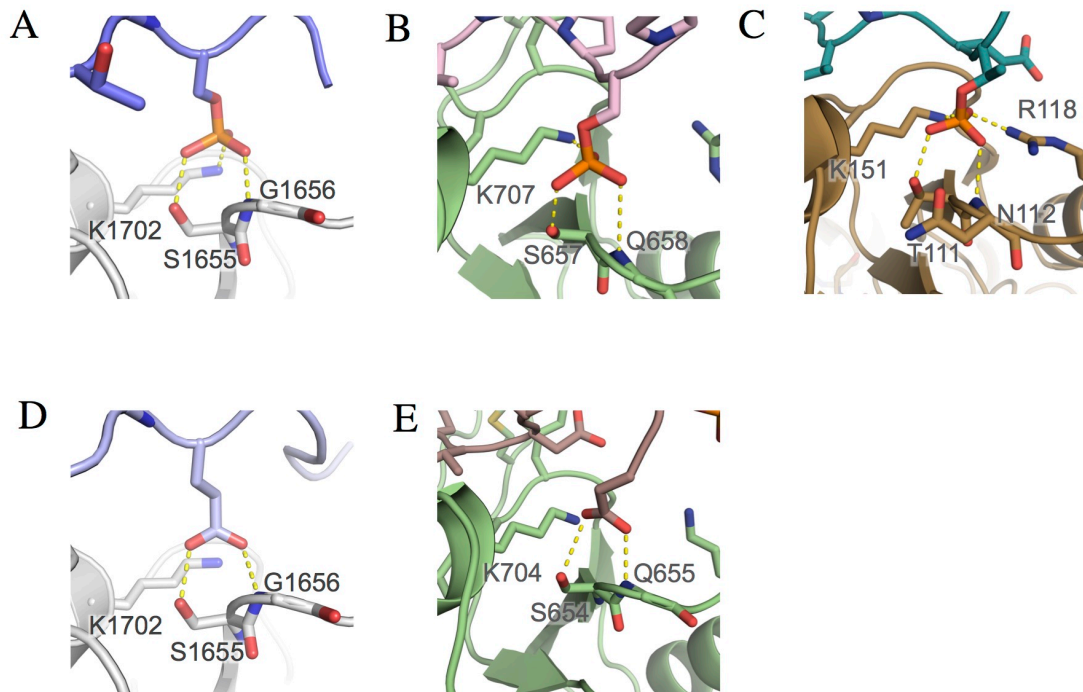


**Figure 5-3. Phosphorylation-dependent and independent interactions of tandem BRCTs.**

Phosphorylation-dependent interaction of (A) BRCA1 BRCTs in complex (PDB ID:1T15). (B) TopBP1 BRCT4/5 in complex with pSer 304 BLM peptide (PDB ID:5U6K). (C) Rad4 BRCT2 in complex with pThr Crb2 peptide (PDB ID: 4BU0) are presented here with the focus on the phosphate binding pockets of each structure. All hydrogen bonds are indicated by yellow dashed lines. Similarly, phosphorylation-independent interaction of (D) BRCA1 BRCTs in complex with nonphosphorylated peptide inhibitor (PDB ID: 4OFB). (E) TopBP1 BRCT4/5 in complex with MDC1 SDT repeat peptide (PDB ID:3UEO) are presented with alignment against existing protein complex structures in panel (A) and (B) accordingly.

two out of three hydrogen bonds found in interaction with pSer of phosphopeptide BACH1 (Figure 5-3A, D). Besides, structural comparison of TopBP1 BRCT5 interaction with BLM and MDC1 suggests that asparatate can also form two hydrogen bonds with phosphate binding pockets to mimic the role of phosphate (Figure 5-3B, E)

Thirdly, when interacting with phosphopeptide in a phosphorylation-dependent manner, both proteins utilize a hydrophobic pocket formed by residues downstream of the phosphate-binding pocket on the tandem BRCTs. In the case of BRCA1 BRCTs, this hydrophobic pocket targets residues from the +3 position of the phosphopeptide, and preferentially recognizes Phe. Therefore, it is no surprise that the core pS-X-X-F motif is largely preserved in phosphopeptide partners of BRCA1, including BACH1, CtIP and Abraxas (Liu and Ladas, 2013; Varma et al., 2005; Wu et al., 2016) (Figure 5-2A, C). This hydrophobic pocket plays a crucial role in phosphorylation independent protein recognition of BRCA1 BRCTs as well. My study of the nonphosphopeptide inhibitor of BRCA1 BRCTs has already proved that an E-X-X-F motif can partially mimic the pS-X-X-F motif of phosphopeptides. Meanwhile, hydrophobic interactions between residues upstream of pSer and the second hydrophobic groove on N terminal BRCA1 BRCT likely compensate for the loss of one hydrogen bond in phosphate binding pocket and further secure the nonphosphopeptide. DNA-PKcs was suggested to interact with BRCA1 BRCTs in a phosphorylation-independent manner via its 1500-2182 region (Davis et al., 2014). We have identified four fragments that contain an E-X-X-F motif from this region (discussed in Chapter 2, see Figure 2-10). Recently, the X-ray crystal structure of DNA PKcs was solved at 4.3 Å (Sibanda et al., 2017). While three of the fragments we found turn out to be from a packed structural region of DNA PKcs, the fragment of residue 1767-1782 appears to be from an unstructured loop region that is now present in the crystal structure. This suggests these residues are likely from a solvent-exposed region of DNA PKcs, making them a good target for PPI with BRCA1 BRCTs. It will be interesting to further examine this region to

see whether DNA PKcs obeys similar model of interaction observed for the nonphosphopeptide inhibitor.

Interestingly, the role of the hydrophobic pocket on TopBP1 BRCT5 varies on a case-by-case basis. Despite their opposite peptide orientations, both MDC1 and BLM place a Val in the hydrophobic pocket (Figure 5-2B, D). However, the hydrophobic interaction is only essential for the highly phosphorylation-dependent interaction between BLM and TopBP1 BRCT5. The positively charged loop only plays a supportive role in the phosphorylation-dependent interaction of TopBP1 BRCT4/5. Although the MDC1 SDT repeat peptide also contains a D-X-X-V motif that can mimic the V-X-X-pS motif of BLM, my mutagenesis studies have shown that a Val to Asp mutation on MDC1 can easily compensate the loss of hydrophobic interaction within the hydrophobic pocket with new electrostatic interactions with the neighboring positively charged loop. In fact, the interaction between double phosphorylated MDC1 SDT repeat peptide and TopBP1 BRCT4/5 appears to have less phosphorylation dependency but more electrostatic dependency. While neither pSer nor pThr from the MDC1 peptide fits well in the phosphate binding pockets, the overall negative charge of this peptide makes it highly attractive to the positively charged loop on TopBP1 BRCT5.

Therefore, I propose that both BRCA1 BRCTs and TopBP1 BRCT4/5 interact with various protein partners using two different models: one is highly phosphorylation-dependent, the other is likely not. I hypothesize that the dual model of interacting mechanisms exhibited by these two sets of tandem repeats may assist the regulation of their interaction with multiple protein partners under different cell cycles to activate different signal cascades. Since many BRCT family proteins act as important scaffold proteins that involve in many PPIs, it will be interesting to look into other proteins with tandem BRCT repeats.

#### **5.4 Therapeutic potential in BRCT family proteins**

Dominated by proteins involved in cell cycle regulation, DNA damage response, and repair, BRCT family proteins are ideal targets for the development of DNA damaging cancer therapy. For instance, mutations in BRCA1 are found in about 50% of hereditary breast cancer patients (Miki et al., 1994). In particular, truncations or mutations, such as M1755R/K, in BRCA1 BRCT domains disable the BRCT mediated PPI of BRCA1, and sensitize the cancer cell to DNA damaging cancer therapy (Kennedy et al., 2003; Paul and Paul, 2014). However, over 95% of sporadic breast and ovarian cancer patients carry WT BRCA1 (Johnson et al., 2013). Therefore, cell-permeable PPI inhibitors that target the BRCA1 BRCT are potential anticancer agents. TopBP1 also seems to be a good target for cancer therapy, as it contains multiple sets of functional BRCTs that are involved in regulation of multiple oncogenic pathways. For example, calcein has been suggested recently in selective targeting of TopBP1 BRCT7/8 to block TopBP1 oligomerization and inhibit p53 binding (Chowdhury et al., 2014). This subsequently reactivates E2F1-dependent apoptosis, and blocks mutp53 gain-of-function in cancer cells.

However, unlike enzymes or receptors with highly compact and well-defined active sites or pockets, targeting of BRCT remains challenging. The BRCT domains have an extensive protein-protein interface with rather shallow phosphate-binding pockets, and additional specificity from neighboring hydrophobic pocket or charged surfaces. Since the middle of 20th century, small molecule (< 500Da) inhibitors have been the mainstream pharmaceutical compounds. Benefiting from their small sizes, they often have advantages in solubility and cell-permeability (Craik et al., 2013). In particular, the development of small molecule cancer drugs has blossomed in the last 20 years (Coussens et al., 2017). Unfortunately, their limited sizes also restrained the numbers of functional groups they have, so they often fail to provide sufficient free energy for interaction with a large protein-protein interface, such as the one on BRCT domain. Previous attempts to identify small molecule inhibitors for BRCA1 BRCTs using either structural based computational

docking method or experimental high-throughput small molecule screening method both failed to reveal any useful compounds (Campbell, 2012). Instead, peptide mimetic based inhibitors caught the eyes of many researchers, because peptides have larger surface areas and can be easily screened by array technologies (Katz et al., 2011).

Being the best defined pocket on BRCT domains, the phosphate-binding pocket of BRCT has been the primary target of inhibitor design. However, an ideal phosphopeptide inhibitor requires delicate chemical engineering to guard the phosphate group of the key amino acid during cellular penetration process before it reaches the targets. Previous collaboration between my lab and Dr. Amarnath Natarajan's group (University of Nebraska Medical Center) has come up with a phosphopeptide inhibitor of BRCA1 BRCT, but successful cellular uptake of this inhibitor requires conjugation to other cell-penetrating peptides (Pessetto et al., 2012, 2016; Yuan et al., 2011). On the other hand, my study in collaboration with Dr. Matthew C. T. Hartman's group (Massey Cancer Center, Virginia Commonwealth University) has revealed the first unphosphorylated peptide inhibitor of BRCA1 BRCT (White et al., 2015). The study of nonphosphopeptide interaction with BRCA1 BRCT provides new structural insights that were overlooked in previous structure studies. This suggests that incorporation of unnatural amino acids into the mRNA-displayed peptide library helps the discovery of new peptide target of BRCA1 BRCTs. We believe this so-called PURE system used by Dr. Hartman's group, could be beneficial for the development of peptide mimetic inhibitors of other BRCT domains, and screening of the three sets of BRCTs from TopBP1, including BRCT4/5, is currently carried out by Dr. Hartman's lab. Since my study of TopBP1 BRCT4/5 has suggested that it may also be involved in PPI via a less phosphorylation-dependent mechanism (Leung et al., 2013), development of nonphosphopeptide inhibitors that target TopBP1 BRCT4/5 seems promising.

Interestingly, Dr. Shao Q. Yao's group (Department of Chemistry, National University of Singapore) recently developed a peptide-hybrid small-molecule microarray

(SSM) system that converted peptide-based PPI inhibitors of BRCT domains to cell-permeable small-molecule-like compounds using a fragment-based combinational approach (Figure 5-4). Using this method, they have identified two cell-permeable inhibitors of BRCT domains: compound 15/15a that target BRCA1 BRCTs, and (+/+) gossypol that targets PARP1 BRCTs (Figure 5-5) (Na et al., 2014; Na et al., 2015). Unfortunately, I failed to validate their BRCA1 BRCTs inhibitor function by FP *in vitro*, and attempts to crystallize this inhibitor in complex with BRCA1 BRCTs also yielded no result. It is unclear why I observed no activity with the compound as the chemical property of this compound had been validated by mass spectrometry (MS) after we received the sample. It is possible that the organic solvent, 100% DMSO, used in their inhibitor sample has somehow interfered the compound activity. Further investigation on the specificity of compound 15 and gossypol in targeting BRCT domains is needed to evaluate the efficacy of this SSM based method.

In summary, we believe the development of peptide mimetic inhibitors of BRCT family proteins is very beneficial for oncology drug discovery. With recent technical advances in synthetic chemistry and molecular biology, methods that provide more efficient peptide productions and larger diversity in chemical modifications all promotes the development of peptide-like drugs (Alexandru-Crivac et al., 2017; Hamzeh-Mivehroud et al., 2013; Wang and Liu, 2011). For example, the PURE system developed by Dr. Hartman's lab is not only efficient in generating a large peptide library that incorporates various chemical modifications on peptides, but also allows direct *in vitro* selection of inhibitors against targets, such as BRCT domains. Although the delivery of peptides to cellular targets has its challenges, further modifications on peptides to form cyclized peptide or peptide conjugates often resolve these issues (Ahrens et al., 2012; Craik et al., 2013). Besides, peptide mimetic inhibitors can also play a significant role in scientific research. Like we observed with the SSM system developed by Dr. Yao's lab, the development of peptide mimetic inhibitors often lead to the discovery of new small

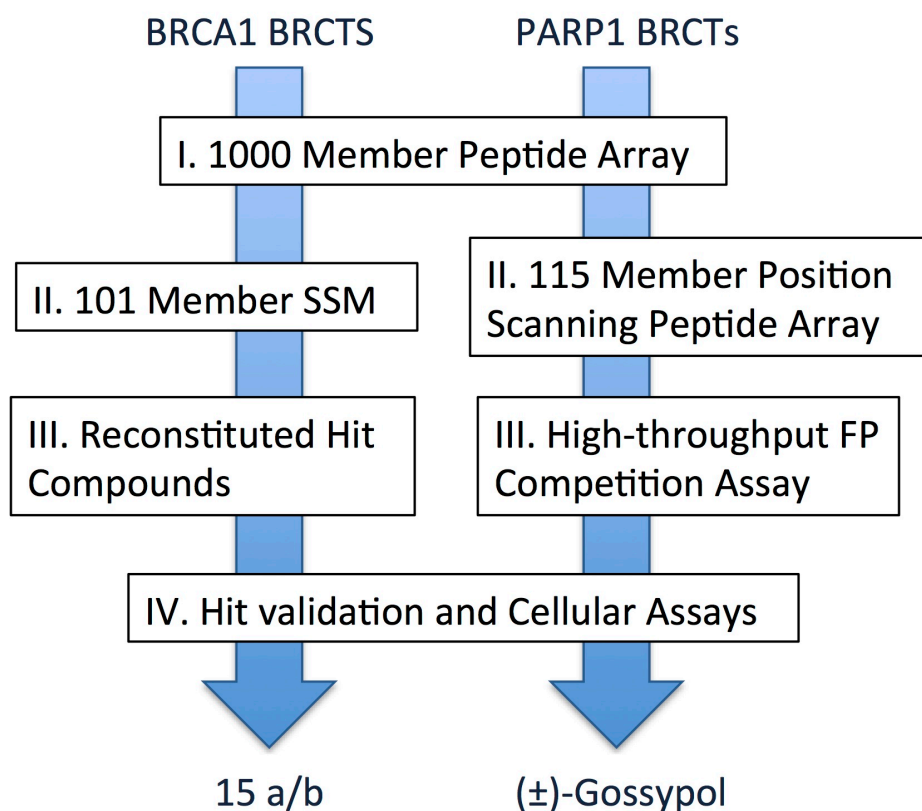


**Figure 5-4. Workflow of the microarray assisted discovery of cell-permeable small-molecule-like PPI inhibitors of BRCT family proteins.**

Starting from a 1000-member universal phosphopeptide microarray screened against Cy5-labeled BRCT family proteins. It first determined the most preferred (BRCT)<sub>2</sub>-binding motif of the phosphopeptide (Step I). From this point, they can carry out a peptide microarray screening against Cy5-labeled PARP1 BRCT. In these phosphopeptides, residues from the preferred motif are individually substituted with each of the 20 natural amino acids (Step II). The best phosphopeptide partner of PARP1 BRCT was attached with an N-terminal fluorescein dye and used as the probe for High-throughput screening of a small molecule compound library (Step III). Or they can employ the fragment-based combinatorial approach and synthesize a peptide-hybrid small-molecule library of BRCA1 BRCT. All these compounds have a biotin tag for subsequent SMM immobilization (Step II). Then the hit compounds were reconstituted without the biotin tag (Step III). In both studies, final hits were further validated by *in vitro* quantitative binding assays (FP, thermal shifts, ITC) and *in situ* cell-based assays (Step IV).

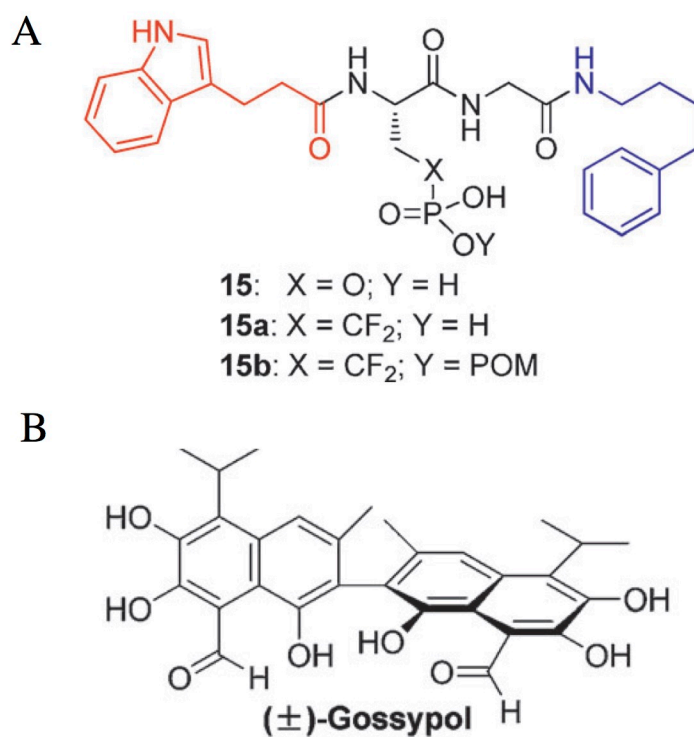


**Figure 5-5. Small molecule inhibitors of BRCT family proteins.**

Structures of small molecule inhibitor compounds of (A) BRCA1 BRCTs and (B) PARP1 BRCTs. The structure shown in (B) only represent the (-)-Gossypol.

molecule compounds. Therefore, research that deciphers the molecular details of PPI of BRCT family proteins is critical for the further therapeutic development of genomic instability diseases, especially cancers, in humans.

## 5.5 Reference

1. Ahrens, V.M., Bellmann-Sickert, K., and Beck-Sickinger, A.G. (2012). Peptides and peptide conjugates: therapeutics on the upward path. *Future Med Chem* 4, 1567-1586.
2. Alexandru-Crivac, C.N., Umeobika, C., Leikoski, N., Jokela, J., Rickaby, K.A., Grilo, A.M., Sjo, P., Plowright, A.T., Idress, M., Siebs, E., *et al.* (2017). Cyclic peptide production using a macrocyclase with enhanced substrate promiscuity and relaxed recognition determinants. *Chem Commun (Camb)* 53, 10656-10659.
3. Campbell, S. J. Insights into the recruitment of BRCA1 to double strand DNA breaks. (2012) University of Alberta, Retrieved from ProQuest Dissertations and Theses. (Accession Order No. AAT. NR89610)
4. Chowdhury, P., Lin, G.E., Liu, K., Song, Y., Lin, F.T., and Lin, W.C. (2014). Targeting TopBP1 at a convergent point of multiple oncogenic pathways for cancer therapy. *Nat Commun* 5, 5476.
5. Coussens, N.P., Braisted, J.C., Peryea, T., Sittampalam, G.S., Simeonov, A., and Hall, M.D. (2017). Small-Molecule Screens: A Gateway to Cancer Therapeutic Agents with Case Studies of Food and Drug Administration-Approved Drugs. *Pharmacol Rev* 69, 479-496.
6. Craik, D.J., Fairlie, D.P., Liras, S., and Price, D. (2013). The future of peptide-based drugs. *Chem Biol Drug Des* 81, 136-147.
7. Davis, A.J., Chi, L., So, S., Lee, K.J., Mori, E., Fattah, K., Yang, J., and Chen, D.J. (2014). BRCA1 modulates the autophosphorylation status of DNA-PKcs in S phase of the cell cycle. *Nucleic Acids Res* 42, 11487-11501.
8. Hamzeh-Mivehroud, M., Alizadeh, A.A., Morris, M.B., Church, W.B., and Dastmalchi, S. (2013). Phage display as a technology delivering on the promise of peptide drug discovery. *Drug Discov Today* 18, 1144-1157.
9. Huo, Y.G., Bai, L., Xu, M., and Jiang, T. (2010). Crystal structure of the N-terminal region of human Topoisomerase IIbeta binding protein 1. *Biochem Biophys Res Commun* 401, 401-405.
10. Johnson, N., Johnson, S.F., Yao, W., Li, Y.C., Choi, Y.E., Bernhardt, A.J., Wang, Y., Capelletti, M., Sarosiek, K.A., Moreau, L.A., *et al.* (2013). Stabilization of mutant

BRCA1 protein confers PARP inhibitor and platinum resistance. *Proc Natl Acad Sci U S A* *110*, 17041-17046.

11. Katz, C., Levy-Beladev, L., Rotem-Bamberger, S., Rito, T., Rudiger, S.G., and Friedler, A. (2011). Studying protein-protein interactions using peptide arrays. *Chem Soc Rev* *40*, 2131-2145.
12. Kennedy, R.D., Quinn, J.E., Mullan, P.B., and Harkin, D.P. (2003). The biology of breast carcinoma. *Cancer* *98*, 1327-1328; author 1328-1329.
13. Leung, C.C., Gong, Z., Chen, J., and Glover, J.N. (2011). Molecular basis of BACH1/FANCI recognition by TopBP1 in DNA replication checkpoint control. *J Biol Chem* *286*, 4292-4301.
14. Leung, C.C., Sun, L., Gong, Z., Burkat, M., Edwards, R., Assmus, M., Chen, J., and Glover, J.N. (2013). Structural insights into recognition of MDC1 by TopBP1 in DNA replication checkpoint control. *Structure* *21*, 1450-1459.
15. Liu, X., and Ladias, J.A. (2013). Structural basis for the BRCA1 BRCT interaction with the proteins ATRIP and BAAT1. *Biochemistry* *52*, 7618-7627.
16. Miki, Y., Swensen, J., Shattuck-Eidens, D., Futreal, P.A., Harshman, K., Tavtigian, S., Liu, Q., Cochran, C., Bennett, L.M., Ding, W., *et al.* (1994). A strong candidate for the breast and ovarian cancer susceptibility gene BRCA1. *Science* *266*, 66-71.
17. Na, Z., Pan, S., Uttamchandani, M., and Yao, S.Q. (2014). Discovery of cell-permeable inhibitors that target the BRCT domain of BRCA1 protein by using a small-molecule microarray. *Angew Chem Int Ed Engl* *53*, 8421-8426.
18. Na, Z., Peng, B., Ng, S., Pan, S., Lee, J.S., Shen, H.M., and Yao, S.Q. (2015). A small-molecule protein-protein interaction inhibitor of PARP1 that targets its BRCT domain. *Angew Chem Int Ed Engl* *54*, 2515-2519.
19. Paul, A., and Paul, S. (2014). The breast cancer susceptibility genes (BRCA) in breast and ovarian cancers. *Front Biosci (Landmark Ed)* *19*, 605-618.
20. Passetto, Z.Y., Yan, Y., Bessho, T., and Natarajan, A. (2012). Inhibition of BRCT(BRCA1)-phosphoprotein interaction enhances the cytotoxic effect of olaparib in breast cancer cells: a proof of concept study for synthetic lethal therapeutic option. *Breast Cancer Res Treat* *134*, 511-517.

21. Pessetto, Z.Y., Yan, Y., Bessho, T., and Natarajan, A. (2016). Erratum to: Inhibition of BRCT(BRCA1)-phosphoprotein interaction enhances the cytotoxic effect of olaparib in breast cancer cells: a proof of concept study for synthetic lethal therapeutic option. *Breast Cancer Res Treat* 155, 613.
22. Qu, M., Rappas, M., Wardlaw, C.P., Garcia, V., Ren, J.Y., Day, M., Carr, A.M., Oliver, A.W., Du, L.L., and Pearl, L.H. (2013). Phosphorylation-dependent assembly and coordination of the DNA damage checkpoint apparatus by Rad4(TopBP1). *Mol Cell* 51, 723-736.
23. Sibanda, B.L., Chirgadze, D.Y., Ascher, D.B., and Blundell, T.L. (2017). DNA-PKcs structure suggests an allosteric mechanism modulating DNA double-strand break repair. *Science* 355, 520-524.
24. Stucki, M., Clapperton, J.A., Mohammad, D., Yaffe, M.B., Smerdon, S.J., and Jackson, S.P. (2005). MDC1 directly binds phosphorylated histone H2AX to regulate cellular responses to DNA double-strand breaks. *Cell* 123, 1213-1226.
25. Varma, A.K., Brown, R.S., Birrane, G., and Ladias, J.A. (2005). Structural basis for cell cycle checkpoint control by the BRCA1-CtIP complex. *Biochemistry* 44, 10941-10946.
26. Wang, H., and Liu, R. (2011). Advantages of mRNA display selections over other selection techniques for investigation of protein-protein interactions. *Expert Rev Proteomics* 8, 335-346.
27. White, E.R., Sun, L., Ma, Z., Beckta, J.M., Danzig, B.A., Hacker, D.E., Huie, M., Williams, D.C., Edwards, R.A., Valerie, K., *et al.* (2015). Peptide library approach to uncover phosphomimetic inhibitors of the BRCA1 C-terminal domain. *ACS Chem Biol* 10, 1198-1208.
28. Williams, R.S., Lee, M.S., Hau, D.D., and Glover, J.N. (2004). Structural basis of phosphopeptide recognition by the BRCT domain of BRCA1. *Nat Struct Mol Biol* 11, 519-525.
29. Wu, Q., Jubb, H., and Blundell, T.L. (2015). Phosphopeptide interactions with BRCA1 BRCT domains: More than just a motif. *Prog Biophys Mol Biol* 117, 143-148.
30. Wu, Q., Paul, A., Su, D., Mehmood, S., Foo, T.K., Ochi, T., Bunting, E.L., Xia, B., Robinson, C.V., Wang, B., *et al.* (2016). Structure of BRCA1-BRCT/Abraxas

Complex Reveals Phosphorylation-Dependent BRCT Dimerization at DNA Damage Sites. *Mol Cell* 61, 434-448.

31. Yuan, Z., Kumar, E.A., Campbell, S.J., Palermo, N.Y., Kizhake, S., Mark Glover, J.N., and Natarajan, A. (2011). Exploiting the P-1 pocket of BRCT domains toward a structure guided inhibitor design. *ACS Med Chem Lett* 2, 764-767.

## Bibliography List

1. Abraham, R.T. (2001). Cell cycle checkpoint signaling through the ATM and ATR kinases. *Genes Dev* 15, 2177-2196.
2. Acevedo, J., Yan, S., and Michael, W.M. (2016). Direct Binding to Replication Protein A (RPA)-coated Single-stranded DNA Allows Recruitment of the ATR Activator TopBP1 to Sites of DNA Damage. *J Biol Chem* 291, 13124-13131.
3. Adams, P.D., Afonine, P.V., Bunkoczi, G., Chen, V.B., Davis, I.W., Echols, N., Headd, J.J., Hung, L.W., Kapral, G.J., Grosse-Kunstleve, R.W., *et al.* (2010). PHENIX: a comprehensive Python-based system for macromolecular structure solution. *Acta Crystallogr D Biol Crystallogr* 66, 213-221.
4. Ahrens, V.M., Bellmann-Sickert, K., and Beck-Sickinger, A.G. (2012). Peptides and peptide conjugates: therapeutics on the upward path. *Future Med Chem* 4, 1567-1586.
5. Aguilera, A., and Gomez-Gonzalez, B. (2008). Genome instability: a mechanistic view of its causes and consequences. *Nat Rev Genet* 9, 204-217.
6. Alexandru-Crivac, C.N., Umeobika, C., Leikoski, N., Jokela, J., Rickaby, K.A., Grilo, A.M., Sjo, P., Plowright, A.T., Idress, M., Siebs, E., *et al.* (2017). Cyclic peptide production using a macrocyclase with enhanced substrate promiscuity and relaxed recognition determinants. *Chem Commun (Camb)* 53, 10656-10659.
7. Anantha, R.W., Simhadri, S., Foo, T.K., Miao, S., Liu, J., Shen, Z., Ganesan, S., and Xia, B. (2017). Functional and mutational landscapes of BRCA1 for homology-directed repair and therapy resistance. *Elife* 6.
8. Anisimov, V.M., Ziemys, A., Kizhake, S., Yuan, Z., Natarajan, A., and Cavasotto, C.N. (2011). Computational and experimental studies of the interaction between phospho-peptides and the C-terminal domain of BRCA1. *J Comput Aided Mol Des* 25, 1071-1084.
9. Arora, H., Chacon, A.H., Choudhary, S., McLeod, M.P., Meshkov, L., Nouri, K., and Izakovic, J. (2014). Bloom syndrome. *Int J Dermatol* 53, 798-802.
10. Avery, O.T., Macleod, C.M., and McCarty, M. (1944). Studies on the Chemical Nature of the Substance Inducing Transformation of Pneumococcal Types : Induction of Transformation by a Desoxyribonucleic Acid Fraction Isolated from Pneumococcus Type Iii. *J Exp Med* 79, 137-158.

11. Bakkenist, C.J., and Kastan, M.B. (2003). DNA damage activates ATM through intermolecular autophosphorylation and dimer dissociation. *Nature* 421, 499-506.
12. Barreto, J.N., McCullough, K.B., Ice, L.L., and Smith, J.A. (2014). Antineoplastic agents and the associated myelosuppressive effects: a review. *J Pharm Pract* 27, 440-446.
13. Bartek, J., and Lukas, J. (2003). Chk1 and Chk2 kinases in checkpoint control and cancer. *Cancer Cell* 3, 421-429.
14. Bartkova, J., Tommiska, J., Oplustilova, L., Aaltonen, K., Tamminen, A., Heikkinen, T., Mistrik, M., Aittomaki, K., Blomqvist, C., Heikkila, P., *et al.* (2008). Aberrations of the MRE11-RAD50-NBS1 DNA damage sensor complex in human breast cancer: MRE11 as a candidate familial cancer-predisposing gene. *Mol Oncol* 2, 296-316.
15. Baskar, R., Lee, K.A., Yeo, R., and Yeoh, K.W. (2012). Cancer and radiation therapy: current advances and future directions. *Int J Med Sci* 9, 193-199.
16. Birrane, G., Varma, A.K., Soni, A., and Ladias, J.A. (2007). Crystal structure of the BARD1 BRCT domains. *Biochemistry* 46, 7706-7712.
17. Bizard, A.H., and Hickson, I.D. (2014). The dissolution of double Holliday junctions. *Cold Spring Harb Perspect Biol* 6, a016477.
18. Blackford, A.N., and Jackson, S.P. (2017). ATM, ATR, and DNA-PK: The Trinity at the Heart of the DNA Damage Response. *Mol Cell* 66, 801-817.
19. Bork, P., Hofmann, K., Bucher, P., Neuwald, A.F., Altschul, S.F., and Koonin, E.V. (1997). A superfamily of conserved domains in DNA damage-responsive cell cycle checkpoint proteins. *Faseb J* 11, 68-76.
20. Braman, J., Papworth, C., and Greener, A. (1996). Site-directed mutagenesis using double-stranded plasmid DNA templates. *Methods Mol Biol* 57, 31-44.
21. Bryant, H.E., Schultz, N., Thomas, H.D., Parker, K.M., Flower, D., Lopez, E., Kyle, S., Meuth, M., Curtin, N.J., and Helleday, T. (2005). Specific killing of BRCA2-deficient tumours with inhibitors of poly(ADP-ribose) polymerase. *Nature* 434, 913-917.
22. Byun, T.S., Pacek, M., Yee, M.C., Walter, J.C., and Cimprich, K.A. (2005). Functional uncoupling of MCM helicase and DNA polymerase activities activates the ATR-dependent checkpoint. *Genes Dev* 19, 1040-1052.

23. Campbell, S. J. Insights into the recruitment of BRCA1 to double strand DNA breaks. (2012) University of Alberta, Retrieved from ProQuest Dissertations and Theses. (Accession Order No. AAT. NR89610)
24. Campbell, S.J., Edwards, R.A., and Glover, J.N. (2010). Comparison of the structures and peptide binding specificities of the BRCT domains of MDC1 and BRCA1. *Structure* 18, 167-176.
25. Cancer Genome Atlas, N. (2012). Comprehensive molecular characterization of human colon and rectal cancer. *Nature* 487, 330-337.
26. Cantor, S.B., Bell, D.W., Ganesan, S., Kass, E.M., Drapkin, R., Grossman, S., Wahrer, D.C., Sgroi, D.C., Lane, W.S., Haber, D.A., *et al.* (2001). BACH1, a novel helicase-like protein, interacts directly with BRCA1 and contributes to its DNA repair function. *Cell* 105, 149-160.
27. Castel, A.L., Cleary, J.D., and Pearson, C.E. (2010). Repeat instability as the basis for human diseases and as a potential target for therapy. *Nat Rev Mol Cell Bio* 11, 165-170.
28. Castilla, L.H., Couch, F.J., Erdos, M.R., Hoskins, K.F., Calzone, K., Garber, J.E., Boyd, J., Lubin, M.B., Deshano, M.L., Brody, L.C., *et al.* (1994). Mutations in the BRCA1 gene in families with early-onset breast and ovarian cancer. *Nat Genet* 8, 387-391.
29. Cescutti, R., Negrini, S., Kohzaki, M., and Halazonetis, T.D. (2010). TopBP1 functions with 53BP1 in the G1 DNA damage checkpoint. *EMBO J* 29, 3723-3732.
30. Chaganti, R.S., Schonberg, S., and German, J. (1974). A manyfold increase in sister chromatid exchanges in Bloom's syndrome lymphocytes. *Proc Natl Acad Sci U S A* 71, 4508-4512.
31. Chapman, J.R., and Jackson, S.P. (2008). Phospho-dependent interactions between NBS1 and MDC1 mediate chromatin retention of the MRN complex at sites of DNA damage. *EMBO Rep* 9, 795-801.
32. Chehab, N.H., Malikzay, A., Appel, M., and Halazonetis, T.D. (2000). Chk2/hCds1 functions as a DNA damage checkpoint in G(1) by stabilizing p53. *Genes Dev* 14, 278-288.
33. Chen, L., Gilkes, D.M., Pan, Y., Lane, W.S., and Chen, J. (2005). ATM and Chk2-dependent phosphorylation of MDMX contribute to p53 activation after DNA damage. *EMBO J* 24, 3411-3422.

34. Chen, V.B., Arendall, W.B., 3rd, Headd, J.J., Keedy, D.A., Immormino, R.M., Kapral, G.J., Murray, L.W., Richardson, J.S., and Richardson, D.C. (2010). MolProbity: all-atom structure validation for macromolecular crystallography. *Acta Crystallogr D Biol Crystallogr* *66*, 12-21.
35. Chen, Y.H., Matsumoto, Y., Shibutani, S., and Bogenhagen, D.F. (1991). Acetylaminofluorene and aminofluorene adducts inhibit in vitro transcription of a *Xenopus* 5S RNA gene only when located on the coding strand. *Proc Natl Acad Sci U S A* *88*, 9583-9587.
36. Choi, J.H., Kim, S.Y., Kim, S.K., Kemp, M.G., and Sancar, A. (2015). An Integrated Approach for Analysis of the DNA Damage Response in Mammalian Cells: NUCLEOTIDE EXCISION REPAIR, DNA DAMAGE CHECKPOINT, AND APOPTOSIS. *J Biol Chem* *290*, 28812-28821.
37. Choi, J.H., Lindsey-Boltz, L.A., and Sancar, A. (2009). Cooperative activation of the ATR checkpoint kinase by TopBP1 and damaged DNA. *Nucleic Acids Res* *37*, 1501-1509.
38. Choi, S.H., and Yoo, H.Y. (2016). Mdc1 modulates the interaction between TopBP1 and the MRN complex during DNA damage checkpoint responses. *Biochem Biophys Res Commun* *479*, 5-11.
39. Chowdhury, P., Lin, G.E., Liu, K., Song, Y., Lin, F.T., and Lin, W.C. (2014). Targeting TopBP1 at a convergent point of multiple oncogenic pathways for cancer therapy. *Nat Commun* *5*, 5476.
40. Chun, S.G., Shaeffer, D.S., and Bryant-Greenwood, P.K. (2011). The Werner's Syndrome RecQ helicase/exonuclease at the nexus of cancer and aging. *Hawaii Med J* *70*, 52-55.
41. Ciccia, A., McDonald, N., and West, S.C. (2008). Structural and functional relationships of the XPF/MUS81 family of proteins. *Annu Rev Biochem* *77*, 259-287.
42. Clapperton, J.A., Manke, I.A., Lowery, D.M., Ho, T., Haire, L.F., Yaffe, M.B., and Smerdon, S.J. (2004). Structure and mechanism of BRCA1 BRCT domain recognition of phosphorylated BACH1 with implications for cancer. *Nat Struct Mol Biol* *11*, 512-518.
43. Cleary, S.P., Cotterchio, M., Jenkins, M.A., Kim, H., Bristow, R., Green, R., Haile, R., Hopper, J.L., LeMarchand, L., Lindor, N., *et al.* (2009). Germline MutY human

homologue mutations and colorectal cancer: a multisite case-control study. *Gastroenterology* *136*, 1251-1260.

44. Comen, E.A., and Robson, M. (2010). Poly(ADP-ribose) polymerase inhibitors in triple-negative breast cancer. *Cancer J* *16*, 48-52.
45. Coster, G., and Goldberg, M. (2010). The cellular response to DNA damage: a focus on MDC1 and its interacting proteins. *Nucleus* *1*, 166-178.
46. Coussens, N.P., Braisted, J.C., Peryea, T., Sittampalam, G.S., Simeonov, A., and Hall, M.D. (2017). Small-Molecule Screens: A Gateway to Cancer Therapeutic Agents with Case Studies of Food and Drug Administration-Approved Drugs. *Pharmacol Rev* *69*, 479-496.
47. Craik, D.J., Fairlie, D.P., Liras, S., and Price, D. (2013). The future of peptide-based drugs. *Chem Biol Drug Des* *81*, 136-147.
48. Crick, F.H., Brenner, S., Watstobi.Rj, and Barnett, L. (1961). General Nature of Genetic Code for Proteins. *Nature* *192*, 1227-&.
49. Croteau, D.L., Popuri, V., Opresko, P.L., and Bohr, V.A. (2014). Human RecQ helicases in DNA repair, recombination, and replication. *Annu Rev Biochem* *83*, 519-552.
50. Cussiol, J.R., Jablonowski, C.M., Yimit, A., Brown, G.W., and Smolka, M.B. (2015). Dampening DNA damage checkpoint signalling via coordinated BRCT domain interactions. *EMBO J* *34*, 1704-1717.
51. Dahm, R. (2008). Discovering DNA: Friedrich Miescher and the early years of nucleic acid research. *Hum Genet* *122*, 565-581.
52. Davis, A.J., Chi, L., So, S., Lee, K.J., Mori, E., Fattah, K., Yang, J., and Chen, D.J. (2014). BRCA1 modulates the autophosphorylation status of DNA-PKcs in S phase of the cell cycle. *Nucleic Acids Res* *42*, 11487-11501.
53. De Bont, R., and van Larebeke, N. (2004). Endogenous DNA damage in humans: a review of quantitative data. *Mutagenesis* *19*, 169-185.
54. De Lorenzo, S.B., Patel, A.G., Hurley, R.M., and Kaufmann, S.H. (2013). The Elephant and the Blind Men: Making Sense of PARP Inhibitors in Homologous Recombination Deficient Tumor Cells. *Front Oncol* *3*, 228.

55. de Renty, C., and Ellis, N.A. (2017). Bloom's syndrome: Why not premature aging?: A comparison of the BLM and WRN helicases. *Ageing Res Rev* *33*, 36-51.
56. Delacroix, S., Wagner, J.M., Kobayashi, M., Yamamoto, K., and Karnitz, L.M. (2007). The Rad9-Hus1-Rad1 (9-1-1) clamp activates checkpoint signaling via TopBP1. *Genes Dev* *21*, 1472-1477.
57. Delaney, G., Jacob, S., Featherstone, C., and Barton, M. (2005). The role of radiotherapy in cancer treatment: estimating optimal utilization from a review of evidence-based clinical guidelines. *Cancer* *104*, 1129-1137.
58. Densham, R.M., Garvin, A.J., Stone, H.R., Strachan, J., Baldock, R.A., Daza-Martin, M., Fletcher, A., Blair-Reid, S., Beesley, J., Johal, B., *et al.* (2016). Human BRCA1-BARD1 ubiquitin ligase activity counteracts chromatin barriers to DNA resection. *Nat Struct Mol Biol* *23*, 647-655.
59. Drozdetskiy, A., Cole, C., Procter, J., and Barton, G.J. (2015). JPred4: a protein secondary structure prediction server. *Nucleic Acids Res* *43*, W389-394.
60. Emsley, P., and Cowtan, K. (2004). Coot: model-building tools for molecular graphics. *Acta Crystallogr D Biol Crystallogr* *60*, 2126-2132.
61. Esashi, F., Christ, N., Gannon, J., Liu, Y., Hunt, T., Jasin, M., and West, S.C. (2005). CDK-dependent phosphorylation of BRCA2 as a regulatory mechanism for recombinational repair. *Nature* *434*, 598-604.
62. Falck, J., Coates, J., and Jackson, S.P. (2005). Conserved modes of recruitment of ATM, ATR and DNA-PKcs to sites of DNA damage. *Nature* *434*, 605-611.
63. Farmer, H., McCabe, N., Lord, C.J., Tutt, A.N., Johnson, D.A., Richardson, T.B., Santarosa, M., Dillon, K.J., Hickson, I., Knights, C., *et al.* (2005). Targeting the DNA repair defect in BRCA mutant cells as a therapeutic strategy. *Nature* *434*, 917-921.
64. Fekairi, S., Scaglione, S., Chahwan, C., Taylor, E.R., Tissier, A., Coulon, S., Dong, M.Q., Ruse, C., Yates, J.R., 3rd, Russell, P., *et al.* (2009). Human SLX4 is a Holliday junction resolvase subunit that binds multiple DNA repair/recombination endonucleases. *Cell* *138*, 78-89.
65. Feng, H., Parker, J.M., Lu, J., and Cao, W. (2004). Effects of deletion and site-directed mutations on ligation steps of NAD<sup>+</sup>-dependent DNA ligase: a biochemical analysis of BRCA1 C-terminal domain. *Biochemistry* *43*, 12648-12659.

66. Feng, L., and Chen, J. (2012). The E3 ligase RNF8 regulates KU80 removal and NHEJ repair. *Nat Struct Mol Biol* 19, 201-206.
67. Fernandez-Capetillo, O., Lee, A., Nussenzweig, M., and Nussenzweig, A. (2004). H2AX: the histone guardian of the genome. *DNA Repair (Amst)* 3, 959-967.
68. Fong, P.C., Boss, D.S., Yap, T.A., Tutt, A., Wu, P., Mergui-Roelvink, M., Mortimer, P., Swaisland, H., Lau, A., O'Connor, M.J., *et al.* (2009). Inhibition of poly(ADP-ribose) polymerase in tumors from BRCA mutation carriers. *N Engl J Med* 361, 123-134.
69. Forma, E., Krzeslak, A., Bernaciak, M., Romanowicz-Makowska, H., and Brys, M. (2012). Expression of TopBP1 in hereditary breast cancer. *Mol Biol Rep* 39, 7795-7804.
70. Fourquet, A., Stoppa-Lyonnet, D., Kirova, Y.M., Sigal-Zafrani, B., Asselain, B., Institut Curie Breast Cancer Study, G., and Institut Curie Breast Ovary Cancer Risk Study, G. (2009). Familial breast cancer: clinical response to induction chemotherapy or radiotherapy related to BRCA1/2 mutations status. *Am J Clin Oncol* 32, 127-131.
71. Frangioni, J.V., and Neel, B.G. (1993). Solubilization and purification of enzymatically active glutathione S-transferase (pGEX) fusion proteins. *Anal Biochem* 210, 179-187.
72. Futreal, P.A., Liu, Q., Shattuck-Eidens, D., Cochran, C., Harshman, K., Tavtigian, S., Bennett, L.M., Haugen-Strano, A., Swensen, J., Miki, Y., *et al.* (1994). BRCA1 mutations in primary breast and ovarian carcinomas. *Science* 266, 120-122.
73. Galkin, V.E., Esashi, F., Yu, X., Yang, S., West, S.C., and Egelman, E.H. (2005). BRCA2 BRC motifs bind RAD51-DNA filaments. *Proc Natl Acad Sci U S A* 102, 8537-8542.
74. Garber, K. (2002). Synthetic lethality: killing cancer with cancer. *J Natl Cancer Inst* 94, 1666-1668.
75. Garcia, V., Furuya, K., and Carr, A.M. (2005). Identification and functional analysis of TopBP1 and its homologs. *DNA Repair* 4, 1227-1239.
76. Garrett, M.D., and Collins, I. (2011). Anticancer therapy with checkpoint inhibitors: what, where and when? *Trends Pharmacol Sci* 32, 308-316.
77. German, J. (1993). Bloom-Syndrome - a Mendelian Prototype of Somatic Mutational Disease. *Medicine* 72, 393-406.
78. German, J., Archibald, R., and Bloom, D. (1965). Chromosomal Breakage in a Rare and Probably Genetically Determined Syndrome of Man. *Science* 148, 506-507.

79. Glover, J.N., Williams, R.S., and Lee, M.S. (2004). Interactions between BRCT repeats and phosphoproteins: tangled up in two. *Trends Biochem Sci* 29, 579-585.
80. Gong, Z., Kim, J.E., Leung, C.C., Glover, J.N., and Chen, J. (2010). BACH1/FANCI acts with TopBP1 and participates early in DNA replication checkpoint control. *Mol Cell* 37, 438-446.
81. Goodarzi, A.A., Yu, Y., Riballo, E., Douglas, P., Walker, S.A., Ye, R., Harer, C., Marchetti, C., Morrice, N., Jeggo, P.A., *et al.* (2006). DNA-PK autophosphorylation facilitates Artemis endonuclease activity. *EMBO J* 25, 3880-3889.
82. Greer, D.A., Besley, B.D., Kennedy, K.B., and Davey, S. (2003). hRad9 rapidly binds DNA containing double-strand breaks and is required for damage-dependent topoisomerase II beta binding protein 1 focus formation. *Cancer Res* 63, 4829-4835.
83. Gu, J., Lu, H., Tsai, A.G., Schwarz, K., and Lieber, M.R. (2007). Single-stranded DNA ligation and XLF-stimulated incompatible DNA end ligation by the XRCC4-DNA ligase IV complex: influence of terminal DNA sequence. *Nucleic Acids Res* 35, 5755-5762.
84. Hamzeh-Mivehroud, M., Alizadeh, A.A., Morris, M.B., Church, W.B., and Dastmalchi, S. (2013). Phage display as a technology delivering on the promise of peptide drug discovery. *Drug Discov Today* 18, 1144-1157.
85. Helleday, T., Eshtad, S., and Nik-Zainal, S. (2014). Mechanisms underlying mutational signatures in human cancers. *Nat Rev Genet* 15, 585-598.
86. Hoeijmakers, J.H. (2009). DNA damage, aging, and cancer. *N Engl J Med* 361, 1475-1485.
87. Huen, M.S., Grant, R., Manke, I., Minn, K., Yu, X., Yaffe, M.B., and Chen, J. (2007). RNF8 transduces the DNA-damage signal via histone ubiquitylation and checkpoint protein assembly. *Cell* 131, 901-914.
88. Huen, M.S., Sy, S.M., and Chen, J. (2010). BRCA1 and its toolbox for the maintenance of genome integrity. *Nat Rev Mol Cell Biol* 11, 138-148.
89. Huo, Y.G., Bai, L., Xu, M., and Jiang, T. (2010). Crystal structure of the N-terminal region of human Topoisomerase IIbeta binding protein 1. *Biochem Biophys Res Commun* 401, 401-405.

90. Jaffe, N. (2014). Historical perspective on the introduction and use of chemotherapy for the treatment of osteosarcoma. *Adv Exp Med Biol* 804, 1-30.
91. Jeong, S.Y., Kumagai, A., Lee, J., and Dunphy, W.G. (2003). Phosphorylated claspin interacts with a phosphate-binding site in the kinase domain of Chk1 during ATR-mediated activation. *J Biol Chem* 278, 46782-46788.
92. Johnson, N., Johnson, S.F., Yao, W., Li, Y.C., Choi, Y.E., Bernhardt, A.J., Wang, Y., Capelletti, M., Sarosiek, K.A., Moreau, L.A., *et al.* (2013). Stabilization of mutant BRCA1 protein confers PARP inhibitor and platinum resistance. *Proc Natl Acad Sci U S A* 110, 17041-17046.
93. Joseph, P.R., Yuan, Z., Kumar, E.A., Lokesh, G.L., Kizhake, S., Rajarathnam, K., and Natarajan, A. (2010). Structural characterization of BRCT-tetrapeptide binding interactions. *Biochem Biophys Res Commun* 393, 207-210.
94. Karow, J.K., Chakraverty, R.K., and Hickson, I.D. (1997). The Bloom's syndrome gene product is a 3'-5' DNA helicase. *J Biol Chem* 272, 30611-30614.
95. Kasai, H., Hayami, H., Yamaizumi, Z., Saito, H., and Nishimura, S. (1984). Detection and identification of mutagens and carcinogens as their adducts with guanosine derivatives. *Nucleic Acids Res* 12, 2127-2136.
96. Katz, C., Levy-Beladev, L., Rotem-Bamberger, S., Rito, T., Rudiger, S.G., and Friedler, A. (2011). Studying protein-protein interactions using peptide arrays. *Chem Soc Rev* 40, 2131-2145.
97. Kemp, M.G., Akan, Z., Yilmaz, S., Grillo, M., Smith-Roe, S.L., Kang, T.H., Cordeiro-Stone, M., Kaufmann, W.K., Abraham, R.T., Sancar, A., *et al.* (2010). Tipin-replication protein A interaction mediates Chk1 phosphorylation by ATR in response to genotoxic stress. *J Biol Chem* 285, 16562-16571.
98. Kennedy, R.D., Quinn, J.E., Mullan, P.B., and Harkin, D.P. (2003). The biology of breast carcinoma. *Cancer* 98, 1327-1328; author 1328-1329.
99. Kilkenny, M.L., De Piccoli, G., Perera, R.L., Labib, K., and Pellegrini, L. (2012). A conserved motif in the C-terminal tail of DNA polymerase alpha tethers primase to the eukaryotic replisome. *J Biol Chem* 287, 23740-23747.
100. Kilkenny, M.L., Dore, A.S., Roe, S.M., Nestoras, K., Ho, J.C., Watts, F.Z., and Pearl, L.H. (2008). Structural and functional analysis of the Crb2-BRCT2 domain reveals

distinct roles in checkpoint signaling and DNA damage repair. *Genes Dev* 22, 2034-2047.

101. Kim, G., Ison, G., McKee, A.E., Zhang, H., Tang, S., Gwise, T., Sridhara, R., Lee, E., Tzou, A., Philip, R., *et al.* (2015). FDA Approval Summary: Olaparib Monotherapy in Patients with Deleterious Germline BRCA-Mutated Advanced Ovarian Cancer Treated with Three or More Lines of Chemotherapy. *Clin Cancer Res* 21, 4257-4261.
102. King, M.C., Marks, J.H., Mandell, J.B., and New York Breast Cancer Study, G. (2003). Breast and ovarian cancer risks due to inherited mutations in BRCA1 and BRCA2. *Science* 302, 643-646.
103. Kobayashi, M., Figaroa, F., Meeuwenoord, N., Jansen, L.E., and Siegal, G. (2006). Characterization of the DNA binding and structural properties of the BRCT region of human replication factor C p140 subunit. *J Biol Chem* 281, 4308-4317.
104. Kolas, N.K., Chapman, J.R., Nakada, S., Ylanko, J., Chahwan, R., Sweeney, F.D., Panier, S., Mendez, M., Wildenhain, J., Thomson, T.M., *et al.* (2007). Orchestration of the DNA-damage response by the RNF8 ubiquitin ligase. *Science* 318, 1637-1640.
105. Kolodner, R.D. (2016). A personal historical view of DNA mismatch repair with an emphasis on eukaryotic DNA mismatch repair. *DNA Repair (Amst)* 38, 3-13.
106. Koonin, E.V., Altschul, S.F., and Bork, P. (1996). BRCA1 protein products ... Functional motifs. *Nat Genet* 13, 266-268.
107. Koska, J., Spassov, V.Z., Maynard, A.J., Yan, L., Austin, N., Flook, P.K., and Venkatachalam, C.M. (2008). Fully automated molecular mechanics based induced fit protein-ligand docking method. *J Chem Inf Model* 48, 1965-1973.
108. Krejci, L., Altmannova, V., Spirek, M., and Zhao, X. (2012). Homologous recombination and its regulation. *Nucleic Acids Res* 40, 5795-5818.
109. Kulkarni, A., and Wilson, D.M., 3rd (2008). The involvement of DNA-damage and -repair defects in neurological dysfunction. *Am J Hum Genet* 82, 539-566.
110. Kumagai, A., and Dunphy, W.G. (2003). Repeated phosphopeptide motifs in Claspin mediate the regulated binding of Chk1. *Nat Cell Biol* 5, 161-165.
111. Kumagai, A., Kim, S.M., and Dunphy, W.G. (2004). Claspin and the activated form of ATR-ATRIP collaborate in the activation of Chk1. *J Biol Chem* 279, 49599-49608.

112. Kunkel, T.A. (1985). Rapid and efficient site-specific mutagenesis without phenotypic selection. *Proc Natl Acad Sci U S A* 82, 488-492.
113. Lambert, W.C., and Lambert, M.W. (2015). Development of effective skin cancer treatment and prevention in xeroderma pigmentosum. *Photochem Photobiol* 91, 475-483.
114. Lavin, M.F. (2008). Ataxia-telangiectasia: from a rare disorder to a paradigm for cell signalling and cancer. *Nat Rev Mol Cell Biol* 9, 759-769.
115. Lavin, M.F., and Kozlov, S. (2007). ATM activation and DNA damage response. *Cell Cycle* 6, 931-942.
116. Le Guen, T., Ragu, S., Guirouilh-Barbat, J., and Lopez, B.S. (2015). Role of the double-strand break repair pathway in the maintenance of genomic stability. *Mol Cell Oncol* 2, e968020.
117. Lee, M.S., Edwards, R.A., Thede, G.L., and Glover, J.N. (2005). Structure of the BRCT repeat domain of MDC1 and its specificity for the free COOH-terminal end of the gamma-H2AX histone tail. *J Biol Chem* 280, 32053-32056.
118. Lee, M.S., Green, R., Marsillac, S.M., Coquelle, N., Williams, R.S., Yeung, T., Foo, D., Hau, D.D., Hui, B., Monteiro, A.N., *et al.* (2010). Comprehensive analysis of missense variations in the BRCT domain of BRCA1 by structural and functional assays. *Cancer Res* 70, 4880-4890.
119. Leung, C. C. (2011). Molecular basis of TopBP1 BRCT domain interactions in the DNA damage response. University of Alberta, Retrieved from ProQuest Dissertations and Theses. (Accession Order No. AAT. NR89258)
120. Leung, C.C., and Glover, J.N. (2011). BRCT domains: easy as one, two, three. *Cell Cycle* 10, 2461-2470.
121. Leung, C.C., Gong, Z., Chen, J., and Glover, J.N. (2011). Molecular basis of BACH1/FANCI recognition by TopBP1 in DNA replication checkpoint control. *J Biol Chem* 286, 4292-4301.
122. Leung, C.C., Kellogg, E., Kuhnert, A., Hanel, F., Baker, D., and Glover, J.N. (2010). Insights from the crystal structure of the sixth BRCT domain of topoisomerase IIbeta binding protein 1. *Protein Sci* 19, 162-167.

123. Leung, C.C., Sun, L., Gong, Z., Burkat, M., Edwards, R., Assmus, M., Chen, J., and Glover, J.N. (2013). Structural insights into recognition of MDC1 by TopBP1 in DNA replication checkpoint control. *Structure* 21, 1450-1459.
124. Levene, P.A. (1917). The structure of yeast nucleic acid. *Journal of Biological Chemistry* 31, 591-598.
125. Levene, P.A. (1918). The structure of yeast nucleic acid II. Uridinephosphoric acid. *Journal of Biological Chemistry* 33, 229-U221.
126. Levene, P.A. (1920). The structure of yeast nucleic acid. V. Ammonia hydrolysis. *Journal of Biological Chemistry* 41, 19-23.
127. Levene, P.A., and La Forge, F.B. (1912). The yeast nucleic acid. V. The structure of pyrimidin-nucleoside. *Ber Dtsch Chem Ges* 45, 608-620.
128. Li, Y., Luo, K., Yin, Y., Wu, C., Deng, M., Li, L., Chen, Y., Nowsheen, S., Lou, Z., and Yuan, J. (2017). USP13 regulates the RAP80-BRCA1 complex dependent DNA damage response. *Nat Commun* 8, 15752.
129. Lieber, M.R. (2010). The mechanism of double-strand DNA break repair by the nonhomologous DNA end-joining pathway. *Annu Rev Biochem* 79, 181-211.
130. Lindahl, T. (1974). N-Glycosidase from Escherichia-Coli That Releases Free Uracil from DNA Containing Deaminated Cytosine Residues. *P Natl Acad Sci USA* 71, 3649-3653.
131. Lindahl, T. (1993). Instability and decay of the primary structure of DNA. *Nature* 362, 709-715.
132. Lindahl, T., and Andersson, A. (1972). Rate of chain breakage at apurinic sites in double-stranded deoxyribonucleic acid. *Biochemistry* 11, 3618-3623.
133. Liu, K., Lin, F.T., Ruppert, J.M., and Lin, W.C. (2003). Regulation of E2F1 by BRCT domain-containing protein TopBP1. *Mol Cell Biol* 23, 3287-3304.
134. Liu, K., Paik, J.C., Wang, B., Lin, F.T., and Lin, W.C. (2006). Regulation of TopBP1 oligomerization by Akt/PKB for cell survival. *EMBO J* 25, 4795-4807.
135. Liu, S., Shiotani, B., Lahiri, M., Marechal, A., Tse, A., Leung, C.C., Glover, J.N., Yang, X.H., and Zou, L. (2011). ATR autophosphorylation as a molecular switch for checkpoint activation. *Mol Cell* 43, 192-202.

136. Liu, X., and Ladas, J.A. (2013). Structural basis for the BRCA1 BRCT interaction with the proteins ATRIP and BAAT1. *Biochemistry* 52, 7618-7627.
137. Lokesh, G.L., Muralidhara, B.K., Negi, S.S., and Natarajan, A. (2007). Thermodynamics of phosphopeptide tethering to BRCT: the structural minima for inhibitor design. *J Am Chem Soc* 129, 10658-10659.
138. Lokesh, G.L., Rachamalla, A., Kumar, G.D., and Natarajan, A. (2006). High-throughput fluorescence polarization assay to identify small molecule inhibitors of BRCT domains of breast cancer gene 1. *Anal Biochem* 352, 135-141.
139. Lord, C.J., and Ashworth, A. (2017). PARP inhibitors: Synthetic lethality in the clinic. *Science* 355, 1152-1158.
140. Lu, A.L., Li, X., Gu, Y., Wright, P.M., and Chang, D.Y. (2001). Repair of oxidative DNA damage: mechanisms and functions. *Cell Biochem Biophys* 35, 141-170.
141. Sun, L., Huang, Y., Edwards, R. A., Yang, S., Blackford, A. N., Niedzwiedz, W. and Glover, J. N. M. (2017). Structural Insight into BLM Recognition by TopBP1. *Structure* 25, 1582-1588
142. Lv, Y., Huo, Y., Yu, X., Liu, R., Zhang, S., Zheng, X., and Zhang, X. (2016). TopBP1 contributes to the chemoresistance in non-small cell lung cancer through upregulation of p53. *Drug Des Devel Ther* 10, 3053-3064.
143. Lv, Y., Liu, R., Xie, S., Zheng, X., Mao, J., Cai, Y., and Chen, W. (2017). Calcein-acetoxymethyl ester enhances the antitumor effects of doxorubicin in nonsmall cell lung cancer by regulating the TopBP1/p53RR pathway. *Anticancer Drugs*.
144. Ma, Y., Lu, H., Tippin, B., Goodman, M.F., Shimazaki, N., Koiwai, O., Hsieh, C.L., Schwarz, K., and Lieber, M.R. (2004). A biochemically defined system for mammalian nonhomologous DNA end joining. *Mol Cell* 16, 701-713.
145. Ma, Y., Pannicke, U., Schwarz, K., and Lieber, M.R. (2002). Hairpin opening and overhang processing by an Artemis/DNA-dependent protein kinase complex in nonhomologous end joining and V(D)J recombination. *Cell* 108, 781-794.
146. Ma, Z., and Hartman, M.C. (2012). In vitro selection of unnatural cyclic peptide libraries via mRNA display. *Methods Mol Biol* 805, 367-390.
147. Maciejczyk, M., Mikoluc, B., Pietrucha, B., Heropolitanska-Pliszka, E., Pac, M., Motkowski, R., and Car, H. (2017). Oxidative stress, mitochondrial abnormalities and

antioxidant defense in Ataxia-telangiectasia, Bloom syndrome and Nijmegen breakage syndrome. *Redox Biol* *11*, 375-383.

148. Mailand, N., Bekker-Jensen, S., Faustrup, H., Melander, F., Bartek, J., Lukas, C., and Lukas, J. (2007). RNF8 ubiquitylates histones at DNA double-strand breaks and promotes assembly of repair proteins. *Cell* *131*, 887-900.
149. Manke, I.A., Lowery, D.M., Nguyen, A., and Yaffe, M.B. (2003). BRCT repeats as phosphopeptide-binding modules involved in protein targeting. *Science* *302*, 636-639.
150. McCoy, A.J. (2007). Solving structures of protein complexes by molecular replacement with Phaser. *Acta Crystallogr D Biol Crystallogr* *63*, 32-41.
151. McCoy, A.J., Grosse-Kunstleve, R.W., Adams, P.D., Winn, M.D., Storoni, L.C., and Read, R.J. (2007). Phaser crystallographic software. *J Appl Crystallogr* *40*, 658-674.
152. Melander, F., Bekker-Jensen, S., Falck, J., Bartek, J., Mailand, N., and Lukas, J. (2008). Phosphorylation of SDT repeats in the MDC1 N terminus triggers retention of NBS1 at the DNA damage-modified chromatin. *J Cell Biol* *181*, 213-226.
153. Mermershtain, I., and Glover, J.N. (2013). Structural mechanisms underlying signaling in the cellular response to DNA double strand breaks. *Mutat Res* *750*, 15-22.
154. Miki, Y., Swensen, J., Shattuck-Eidens, D., Futreal, P.A., Harshman, K., Tavtigian, S., Liu, Q., Cochran, C., Bennett, L.M., Ding, W., *et al.* (1994). A strong candidate for the breast and ovarian cancer susceptibility gene BRCA1. *Science* *266*, 66-71.
155. Ming, X., Feng, Y., Yang, C., Wang, W., Wang, P., and Deng, J. (2016). Radiation-induced heart disease in lung cancer radiotherapy: A dosimetric update. *Medicine (Baltimore)* *95*, e5051.
156. Monnat, R.J., Jr. (2010). Human RECQ helicases: roles in DNA metabolism, mutagenesis and cancer biology. *Semin Cancer Biol* *20*, 329-339.
157. Morra, F., Merolla, F., Napolitano, V., Ilardi, G., Miro, C., Paladino, S., Staibano, S., Cerrato, A., and Celetti, A. (2017). The combined effect of USP7 inhibitors and PARP inhibitors in hormone-sensitive and castration-resistant prostate cancer cells. *Oncotarget* *8*, 31815-31829.
158. Moudry, P., Watanabe, K., Wolanin, K.M., Bartkova, J., Wassing, I.E., Watanabe, S., Strauss, R., Troelsgaard Pedersen, R., Oestergaard, V.H., Lisby, M., *et al.* (2016).

TOPBP1 regulates RAD51 phosphorylation and chromatin loading and determines PARP inhibitor sensitivity. *J Cell Biol* 212, 281-288.

159. Murai, J. (2017). Targeting DNA repair and replication stress in the treatment of ovarian cancer. *Int J Clin Oncol*.
160. Na, Z., Pan, S., Uttamchandani, M., and Yao, S.Q. (2014). Discovery of cell-permeable inhibitors that target the BRCT domain of BRCA1 protein by using a small-molecule microarray. *Angew Chem Int Ed Engl* 53, 8421-8426.
161. Na, Z., Peng, B., Ng, S., Pan, S., Lee, J.S., Shen, H.M., and Yao, S.Q. (2015). A small-molecule protein-protein interaction inhibitor of PARP1 that targets its BRCT domain. *Angew Chem Int Ed Engl* 54, 2515-2519.
162. Nagaraju, G., and Scully, R. (2007). Minding the gap: the underground functions of BRCA1 and BRCA2 at stalled replication forks. *DNA Repair (Amst)* 6, 1018-1031.
163. Narod, S.A. (2010). Compliance with tamoxifen in women with breast cancer and a BRCA1 or BRCA2 mutation. *J Clin Oncol* 28, e698-699; author reply e700.
164. Nelson, M., and McClelland, M. (1992). *Methods Enzymol* 216, 24.
165. Nowsheen, S., and Yang, E.S. (2012). The intersection between DNA damage response and cell death pathways. *Exp Oncol* 34, 243-254.
166. O'Connor, M.J. (2015). Targeting the DNA Damage Response in Cancer. *Mol Cell* 60, 547-560.
167. Oliver, A.W., Paul, A., Boxall, K.J., Barrie, S.E., Aherne, G.W., Garrett, M.D., Mittnacht, S., and Pearl, L.H. (2006). Trans-activation of the DNA-damage signalling protein kinase Chk2 by T-loop exchange. *EMBO J* 25, 3179-3190.
168. Otwinowski, Z., and Minor, W. (1997). Processing of X-ray diffraction data collected in oscillation mode. *Methods Enzymol* 276, 307-326.
169. Paul, A., and Paul, S. (2014). The breast cancer susceptibility genes (BRCA) in breast and ovarian cancers. *Front Biosci (Landmark Ed)* 19, 605-618.
170. Peasland, A., Wang, L.Z., Rowling, E., Kyle, S., Chen, T., Hopkins, A., Cliby, W.A., Sarkaria, J., Beale, G., Edmondson, R.J., *et al.* (2011). Identification and evaluation of a potent novel ATR inhibitor, NU6027, in breast and ovarian cancer cell lines. *Br J Cancer* 105, 372-381.

171. Pessetto, Z.Y., Yan, Y., Bessho, T., and Natarajan, A. (2012). Inhibition of BRCT(BRCA1)-phosphoprotein interaction enhances the cytotoxic effect of olaparib in breast cancer cells: a proof of concept study for synthetic lethal therapeutic option. *Breast Cancer Res Treat* 134, 511-517.
172. Pessetto, Z.Y., Yan, Y., Bessho, T., and Natarajan, A. (2016). Erratum to: Inhibition of BRCT(BRCA1)-phosphoprotein interaction enhances the cytotoxic effect of olaparib in breast cancer cells: a proof of concept study for synthetic lethal therapeutic option. *Breast Cancer Res Treat* 155, 613.
173. Petrucelli, N., Daly, M.B., and Pal, T. (1993). BRCA1- and BRCA2-Associated Hereditary Breast and Ovarian Cancer. In *GeneReviews(R)*, R.A. Pagon, M.P. Adam, H.H. Ardinger, S.E. Wallace, A. Amemiya, L.J.H. Bean, T.D. Bird, N. Ledbetter, H.C. Mefford, R.J.H. Smith, and K. Stephens, eds. (Seattle (WA)).
174. Phillips, D.H., and Venitt, S. (2012). DNA and protein adducts in human tissues resulting from exposure to tobacco smoke. *Int J Cancer* 131, 2733-2753.
175. Pleschke, J.M., Kleczkowska, H.E., Strohm, M., and Althaus, F.R. (2000). Poly(ADP-ribose) binds to specific domains in DNA damage checkpoint proteins. *J Biol Chem* 275, 40974-40980.
176. Plummer, R., Jones, C., Middleton, M., Wilson, R., Evans, J., Olsen, A., Curtin, N., Boddy, A., McHugh, P., Newell, D., *et al.* (2008). Phase I study of the poly(ADP-ribose) polymerase inhibitor, AG014699, in combination with temozolomide in patients with advanced solid tumors. *Clin Cancer Res* 14, 7917-7923.
177. Prevo, R., Fokas, E., Reaper, P.M., Charlton, P.A., Pollard, J.R., McKenna, W.G., Muschel, R.J., and Brunner, T.B. (2012). The novel ATR inhibitor VE-821 increases sensitivity of pancreatic cancer cells to radiation and chemotherapy. *Cancer Biol Ther* 13, 1072-1081.
178. Purnell, M.R., and Whish, W.J. (1980). Novel inhibitors of poly(ADP-ribose) synthetase. *Biochem J* 185, 775-777.
179. Puyo, S., Montaudon, D., and Pourquier, P. (2014). From old alkylating agents to new minor groove binders. *Crit Rev Oncol Hematol* 89, 43-61.
180. Qu, M., Rappas, M., Wardlaw, C.P., Garcia, V., Ren, J.Y., Day, M., Carr, A.M., Oliver, A.W., Du, L.L., and Pearl, L.H. (2013). Phosphorylation-dependent assembly and coordination of the DNA damage checkpoint apparatus by Rad4(TopBP1). *Mol Cell* 51, 723-736.

181. Qu, M., Yang, B., Tao, L., Yates, J.R., 3rd, Russell, P., Dong, M.Q., and Du, L.L. (2012). Phosphorylation-dependent interactions between Crb2 and Chk1 are essential for DNA damage checkpoint. *PLoS Genet* 8, e1002817.
182. Rappas, M., Oliver, A.W., and Pearl, L.H. (2011). Structure and function of the Rad9-binding region of the DNA-damage checkpoint adaptor TopBP1. *Nucleic Acids Res* 39, 313-324.
183. Rasmussen, R.E., and Painter, R.B. (1964). Evidence for Repair of Ultra-Violet Damaged Deoxyribonucleic Acid in Cultured Mammalian Cells. *Nature* 203, 1360-&.
184. Rodriguez, M., Yu, X., Chen, J., and Songyang, Z. (2003). Phosphopeptide binding specificities of BRCA1 COOH-terminal (BRCT) domains. *J Biol Chem* 278, 52914-52918.
185. Rodriguez, M.C., and Songyang, Z. (2008). BRCT domains: phosphopeptide binding and signaling modules. *Front Biosci* 13, 5905-5915.
186. Rothblum-Oviatt, C., Wright, J., Lefton-Greif, M.A., McGrath-Morrow, S.A., Crawford, T.O., and Lederman, H.M. (2016). Ataxia telangiectasia: a review. *Orphanet J Rare Dis* 11, 159.
187. Samadder, P., Aithal, R., Belan, O., and Krejci, L. (2016). Cancer TARGETases: DSB repair as a pharmacological target. *Pharmacol Ther* 161, 111-131.
188. Scharer, O.D. (2013). Nucleotide excision repair in eukaryotes. *Cold Spring Harb Perspect Biol* 5, a012609.
189. Shibutani, S., Takeshita, M., and Grollman, A.P. (1991). Insertion of specific bases during DNA synthesis past the oxidation-damaged base 8-oxodG. *Nature* 349, 431-434.
190. Shin, H., Jo, S.J., Kim, D.H., Kwon, O., and Myung, S.K. (2015). Efficacy of interventions for prevention of chemotherapy-induced alopecia: a systematic review and meta-analysis. *Int J Cancer* 136, E442-454.
191. Sibanda, B.L., Chirgadze, D.Y., Ascher, D.B., and Blundell, T.L. (2017). DNA-PKcs structure suggests an allosteric mechanism modulating DNA double-strand break repair. *Science* 355, 520-524.
192. Simons, A.M., Horwitz, A.A., Starita, L.M., Griffin, K., Williams, R.S., Glover, J.N., and Parvin, J.D. (2006). BRCA1 DNA-binding activity is stimulated by BARD1. *Cancer Res* 66, 2012-2018.

193. Sjøttem, E., Rekdal, C., Svineng, G., Johnsen, S.S., Klenow, H., Uglehus, R.D., and Johansen, T. (2007). The ePHD protein SPBP interacts with TopBP1 and together they co-operate to stimulate Ets1-mediated transcription. *Nucleic Acids Res* *35*, 6648-6662.
194. Smith, J., Tho, L.M., Xu, N., and Gillespie, D.A. (2010). The ATM-Chk2 and ATR-Chk1 pathways in DNA damage signaling and cancer. *Adv Cancer Res* *108*, 73-112.
195. Spycher, C., Miller, E.S., Townsend, K., Pavic, L., Morrice, N.A., Janscak, P., Stewart, G.S., and Stucki, M. (2008). Constitutive phosphorylation of MDC1 physically links the MRE11-RAD50-NBS1 complex to damaged chromatin. *J Cell Biol* *181*, 227-240.
196. Stucki, M., Clapperton, J.A., Mohammad, D., Yaffe, M.B., Smerdon, S.J., and Jackson, S.P. (2005). MDC1 directly binds phosphorylated histone H2AX to regulate cellular responses to DNA double-strand breaks. *Cell* *123*, 1213-1226.
197. Sugimoto, M., Esaki, N., Tanaka, H., and Soda, K. (1989). A simple and efficient method for the oligonucleotide-directed mutagenesis using plasmid DNA template and phosphorothioate-modified nucleotide. *Anal Biochem* *179*, 309-311.
198. Swenberg, J.A., Lu, K., Moeller, B.C., Gao, L., Upton, P.B., Nakamura, J., and Starr, T.B. (2011). Endogenous versus exogenous DNA adducts: their role in carcinogenesis, epidemiology, and risk assessment. *Toxicol Sci* *120 Suppl 1*, S130-145.
199. Sy, S.M., Huen, M.S., and Chen, J. (2009). PALB2 is an integral component of the BRCA complex required for homologous recombination repair. *Proc Natl Acad Sci U S A* *106*, 7155-7160.
200. Taylor, C.W., and Kirby, A.M. (2015). Cardiac Side-effects From Breast Cancer Radiotherapy. *Clin Oncol (R Coll Radiol)* *27*, 621-629.
201. Taylor, J.W., Ott, J., and Eckstein, F. (1985). The rapid generation of oligonucleotide-directed mutations at high frequency using phosphorothioate-modified DNA. *Nucleic Acids Res* *13*, 8765-8785.
202. Terwilliger, T.C., Grosse-Kunstleve, R.W., Afonine, P.V., Moriarty, N.W., Adams, P.D., Read, R.J., Zwart, P.H., and Hung, L.W. (2008). Iterative-build OMIT maps: map improvement by iterative model building and refinement without model bias. *Acta Crystallogr D Biol Crystallogr* *64*, 515-524.
203. Tomkinson, A.E., and Sallmyr, A. (2013). Structure and function of the DNA ligases encoded by the mammalian LIG3 gene. *Gene* *531*, 150-157.

204. Touchefeu, Y., Montassier, E., Nieman, K., Gastinne, T., Potel, G., Bruley des Varannes, S., Le Vacon, F., and de La Cochetiere, M.F. (2014). Systematic review: the role of the gut microbiota in chemotherapy- or radiation-induced gastrointestinal mucositis - current evidence and potential clinical applications. *Aliment Pharmacol Ther* 40, 409-421.
205. Truninger, K., Menigatti, M., Luz, J., Russell, A., Haider, R., Gebbers, J.O., Bannwart, F., Yurtsever, H., Neuweiler, J., Riehle, H.M., *et al.* (2005). Immunohistochemical analysis reveals high frequency of PMS2 defects in colorectal cancer. *Gastroenterology* 128, 1160-1171.
206. Vandeyar, M.A., Weiner, M.P., Hutton, C.J., and Batt, C.A. (1988). A simple and rapid method for the selection of oligodeoxynucleotide-directed mutants. *Gene* 65, 129-133.
207. Varma, A.K., Brown, R.S., Birrane, G., and Ladas, J.A. (2005). Structural basis for cell cycle checkpoint control by the BRCA1-CtIP complex. *Biochemistry* 44, 10941-10946.
208. Vinckier, N.K., Chworos, A., and Parsons, S.M. (2011). Improved isolation of proteins tagged with glutathione S-transferase. *Protein Expr Purif* 75, 161-164.
209. Wallace, S.S. (2014). Base excision repair: a critical player in many games. *DNA Repair (Amst)* 19, 14-26.
210. Wang, H., and Liu, R. (2011). Advantages of mRNA display selections over other selection techniques for investigation of protein-protein interactions. *Expert Rev Proteomics* 8, 335-346.
211. Wang, J., Chen, J., and Gong, Z. (2013). TopBP1 controls BLM protein level to maintain genome stability. *Mol Cell* 52, 667-678.
212. Wang, J., Gong, Z., and Chen, J. (2011). MDC1 collaborates with TopBP1 in DNA replication checkpoint control. *J Cell Biol* 193, 267-273.
213. Wang, Y.G., Nnakwe, C., Lane, W.S., Modesti, M., and Frank, K.M. (2004). Phosphorylation and regulation of DNA ligase IV stability by DNA-dependent protein kinase. *J Biol Chem* 279, 37282-37290.
214. Wardlaw, C.P., Carr, A.M., and Oliver, A.W. (2014). TopBP1: A BRCT-scaffold protein functioning in multiple cellular pathways. *DNA Repair* 22, 165-174.
215. Warren, G.W., and Cummings, K.M. (2013). Tobacco and lung cancer: risks, trends, and outcomes in patients with cancer. *Am Soc Clin Oncol Educ Book*, 359-364.

216. Watson, J.D., and Crick, F.H.C. (1953). The Structure of DNA. *Cold Spring Harb Sym* 18, 123-131.
217. Weissman, L., de Souza-Pinto, N.C., Stevnsner, T., and Bohr, V.A. (2007). DNA repair, mitochondria, and neurodegeneration. *Neuroscience* 145, 1318-1329.
218. West, S.C. (2003). Molecular views of recombination proteins and their control. *Nat Rev Mol Cell Biol* 4, 435-445.
219. White, E.R., Sun, L., Ma, Z., Beckta, J.M., Danzig, B.A., Hacker, D.E., Huie, M., Williams, D.C., Edwards, R.A., Valerie, K., *et al.* (2015). Peptide library approach to uncover phosphomimetic inhibitors of the BRCA1 C-terminal domain. *ACS Chem Biol* 10, 1198-1208.
220. Williams, R.J. (1957). The Chemical Basis of Heredity - Mcelroy,Wd, Glass,B. *Eugen Quart* 4, 171-171.
221. Williams, R.S., Dodson, G.E., Limbo, O., Yamada, Y., Williams, J.S., Guenther, G., Classen, S., Glover, J.N., Iwasaki, H., Russell, P., *et al.* (2009). Nbs1 flexibly tethers Ctp1 and Mre11-Rad50 to coordinate DNA double-strand break processing and repair. *Cell* 139, 87-99.
222. Williams, R.S., Green, R., and Glover, J.N. (2001). Crystal structure of the BRCT repeat region from the breast cancer-associated protein BRCA1. *Nat Struct Biol* 8, 838-842.
223. Williams, R.S., Lee, M.S., Hau, D.D., and Glover, J.N. (2004). Structural basis of phosphopeptide recognition by the BRCT domain of BRCA1. *Nat Struct Mol Biol* 11, 519-525.
224. Williams, R.S., Williams, J.S., and Tainer, J.A. (2007). Mre11-Rad50-Nbs1 is a keystone complex connecting DNA repair machinery, double-strand break signaling, and the chromatin template. *Biochem Cell Biol* 85, 509-520.
225. Wold, M.S. (1997). Replication protein A: a heterotrimeric, single-stranded DNA-binding protein required for eukaryotic DNA metabolism. *Annu Rev Biochem* 66, 61-92.
226. Wollmann, Y., Schmidt, U., Wieland, G.D., Zipfel, P.F., Saluz, H.P., and Hanel, F. (2007). The DNA topoisomerase IIbeta binding protein 1 (TopBP1) interacts with poly (ADP-ribose) polymerase (PARP-1). *J Cell Biochem* 102, 171-182.

227. Woods, N.T., Mesquita, R.D., Sweet, M., Carvalho, M.A., Li, X., Liu, Y., Nguyen, H., Thomas, C.E., Iversen, E.S., Jr., Marsillac, S., *et al.* (2012). Charting the landscape of tandem BRCT domain-mediated protein interactions. *Sci Signal* 5, rs6.
228. Wu, L., Luo, K., Lou, Z., and Chen, J. (2008). MDC1 regulates intra-S-phase checkpoint by targeting NBS1 to DNA double-strand breaks. *Proc Natl Acad Sci U S A* 105, 11200-11205.
229. Wu, L.C., Wang, Z.W., Tsan, J.T., Spillman, M.A., Phung, A., Xu, X.L., Yang, M.C., Hwang, L.Y., Bowcock, A.M., and Baer, R. (1996). Identification of a RING protein that can interact in vivo with the BRCA1 gene product. *Nat Genet* 14, 430-440.
230. Wu, Q., Jubb, H., and Blundell, T.L. (2015). Phosphopeptide interactions with BRCA1 BRCT domains: More than just a motif. *Prog Biophys Mol Biol* 117, 143-148.
231. Wu, Q., Paul, A., Su, D., Mehmood, S., Foo, T.K., Ochi, T., Bunting, E.L., Xia, B., Robinson, C.V., Wang, B., *et al.* (2016). Structure of BRCA1-BRCT/Abraxas Complex Reveals Phosphorylation-Dependent BRCT Dimerization at DNA Damage Sites. *Mol Cell* 61, 434-448.
232. Xu, K., Chen, Z., Cui, Y., Qin, C., He, Y., and Song, X. (2015). Combined olaparib and oxaliplatin inhibits tumor proliferation and induces G2/M arrest and gamma-H2AX foci formation in colorectal cancer. *Onco Targets Ther* 8, 3047-3054.
233. Yamane, K., Katayama, E., and Tsuruo, T. (2000). The BRCT regions of tumor suppressor BRCA1 and of XRCC1 show DNA end binding activity with a multimerizing feature. *Biochem Biophys Res Commun* 279, 678-684.
234. Yamane, K., and Tsuruo, T. (1999). Conserved BRCT regions of TopBP1 and of the tumor suppressor BRCA1 bind strand breaks and termini of DNA. *Oncogene* 18, 5194-5203.
235. Yamane, K., Wu, X., and Chen, J. (2002). A DNA damage-regulated BRCT-containing protein, TopBP1, is required for cell survival. *Mol. Cell. Biol.* 22, 555-566.
236. Yarosh, D.B., Rice, M., Day, R.S., 3rd, Foote, R.S., and Mitra, S. (1984). O6-Methylguanine-DNA methyltransferase in human cells. *Mutat Res* 131, 27-36.
237. Yu, Y., Mahaney, B.L., Yano, K., Ye, R., Fang, S., Douglas, P., Chen, D.J., and Lees-Miller, S.P. (2008). DNA-PK and ATM phosphorylation sites in XLF/Cernunnos are not required for repair of DNA double strand breaks. *DNA Repair (Amst)* 7, 1680-1692.

238. Yu, Y., Wang, W., Ding, Q., Ye, R., Chen, D., Merkle, D., Schriemer, D., Meek, K., and Lees-Miller, S.P. (2003). DNA-PK phosphorylation sites in XRCC4 are not required for survival after radiation or for V(D)J recombination. *DNA Repair (Amst)* 2, 1239-1252.
239. Yuan, Z., Kumar, E.A., Campbell, S.J., Palermo, N.Y., Kizhake, S., Mark Glover, J.N., and Natarajan, A. (2011). Exploiting the P-1 pocket of BRCT domains toward a structure guided inhibitor design. *ACS Med Chem Lett* 2, 764-767.
240. Yun, M.H., and Hiom, K. (2009). CtIP-BRCA1 modulates the choice of DNA double-strand-break repair pathway throughout the cell cycle. *Nature* 459, 460-463.
241. Zhang, X., Morera, S., Bates, P.A., Whitehead, P.C., Coffey, A.I., Hainbucher, K., Nash, R.A., Sternberg, M.J., Lindahl, T., and Freemont, P.S. (1998). Structure of an XRCC1 BRCT domain: a new protein-protein interaction module. *EMBO J* 17, 6404-6411.
242. Zhao, W., Steinfeld, J.B., Liang, F., Chen, X., Maranon, D.G., Jian Ma, C., Kwon, Y., Rao, T., Wang, W., Sheng, C., *et al.* (2017). BRCA1-BARD1 promotes RAD51-mediated homologous DNA pairing. *Nature* 550, 360-365.

## **Appendix A**

### **Interaction between TopBP1 and Brd4 regulates DNA damage- induced replication stress response**

**A version of this chapter has been submitted in:**

Lam, F.C., Huang, Q., Sun, L., Lim, D.C., Maffa, A.D., Balkanska-Sinclair, E., Filippakopoulos, P., Glover, J.N.M, Yaffe, M.B., and Floyd, S.R. A BRD4-TopBP1 Interaction Maintains Chromatin Stability and Regulates the DNA Damage Replication Stress Response. *Cell*

## A.1 Introduction

Brd4 is a member of the bromodomain and extra-terminal domain (BET) family proteins. It has three major domains: the bromodomain and extra-terminal (ET) domain, which are highly conserved within the BET family; and a C-terminal domain, which varies between different BET proteins (Taniguchi, 2016). Brd4 plays important roles in controlling cell proliferation by regulating the expression of transcription factors (Dey et al., 2000). Like other BET family proteins, Brd4 can recognize acetylated lysine residues on histones through its bromodomain and controls the movement of RNA polymerase II (RNA Pol II) on chromatin (Dey et al., 2003). In addition, Brd4 can also enhance recruitment of positive transcription elongation factor b (P-TEFb) through its CT domain (Itzen et al., 2014; Jang et al., 2005; Yang et al., 2005). However, the function of the ET domain remains unclear. It has been suggested to involve in the interaction with several transcriptional co-activators (Rahman et al., 2011) and retroviral integration proteins (Crowe et al., 2016).

We have previously shown that MDC1 can recruit TopBP1 to a DSB site through direct protein-protein interaction (PPI), and further amplifying the ATR activation in cells (Chapter 2). However, it remains unclear how cells regulate the TopBP1 and MDC1 recruitment to DNA damage sites. Recently, evidence supporting the roles of Brd4 in regulating DDR started to surface. Brd4 was found to recruit condensin II chromatin remodeling complex to acetylated histones using its bromodomain. This then allows Brd4 to alter chromatin structures to modulate ionizing radiation (IR) induced DDR signaling cascade (Floyd et al., 2013). Through an unbiased proteomic screen, our collaborator Dr. Yaffe's lab (Koch Institute for Integrative Cancer Research, Massachusetts Institute of Technology), revealed a novel interaction between Brd4, MDC1, and TopBP1. They have also proved that inhibition of Brd4 bromodomain interaction with acetyl-lysine of histones can induce replication stress and DNA damage in cells. Interested in how TopBP1 interacts with Brd4, we carried out a series of pull-down assays *in vitro*. Our result reveals that the ET domain of Brd4 can interact with the BRCT6 of TopBP1 to stabilize the TopBP1-MDC1

chromatin scaffold. Disruption of the Brd4 interaction with TopBP1 may induce endogenous replication stress and DNA damage. However, the interactions between TopBP1 BRCT6 and Brd4 ET domain is not strong enough to form a stable complex *in vitro*, which limited further structural investigation on this interaction alone.

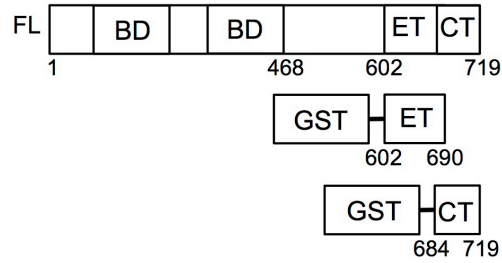
## **A.2 Results**

### **A.2.1 Brd4 interacts with TopBP1 BRCT6 through its ET domain**

To identify the functional domains involved in TopBP1 interaction with Brd4, we first designed various truncation constructs of both proteins and expressed them individually with a glutathione S-transferase (GST) tag in *E. coli* (Figure A-1). The interactions between different domains on both proteins were then examined by dual GST pull-down assays. We first isolated the GST tagged ET or CT domain of Brd4 from crude cell lysate using GST-affinity beads, then we apply purified proteins of functional TopBP1 BRCTs to the Brd4 bound beads (Figure A-2A). We were only able to observe clear co-existence of TopBP1 BRCT6 and GST-Brd4 ET on the beads (Figure A-3A, B). Our control experiment with GST alone on the beads shows no presence of TopBP1 BRCT6, indicating GST cannot interact with TopBP1 BRCT6 (Figure A-3C). To further validate our results, we carried out a reverse pull-down assay by applying purified GST-TopBP1 BRCT6 to beads, and then crude purified Brd4-ET protein (Figure A-2B). As expected, we found most Brd4 ET proteins from load were co-localized with TopBP1 BRCT6 on the bead (Figure A-4).

However, there was one issue with visualizing our pull-down result by coomassie blue staining on SDS-PAGE gels. Due to the similarity in protein size, the band position of GST-ET overlapped with TopBP1 BRCT0/1/2 (Figure A-3A), and the band position GST-CT overlapped with TopBP1 BRCT0/1/2 and TopBP1 7/8 (Figure A-3B). It seems

### Brd4



### TopBP1

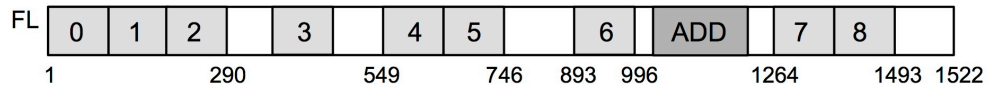


### Figure A-1. Construct overview of TopBP1 and Brd4 proteins.

Two GST tagged constructs of Brd4 used in our study are presented here. All functional domains of TopBP1 are also highlighted here. GST tagged constructs of BRCT0/1/2, BRCT4/5, BRCT6, BRCT7/8 domains were made based on the fragments indicated here.



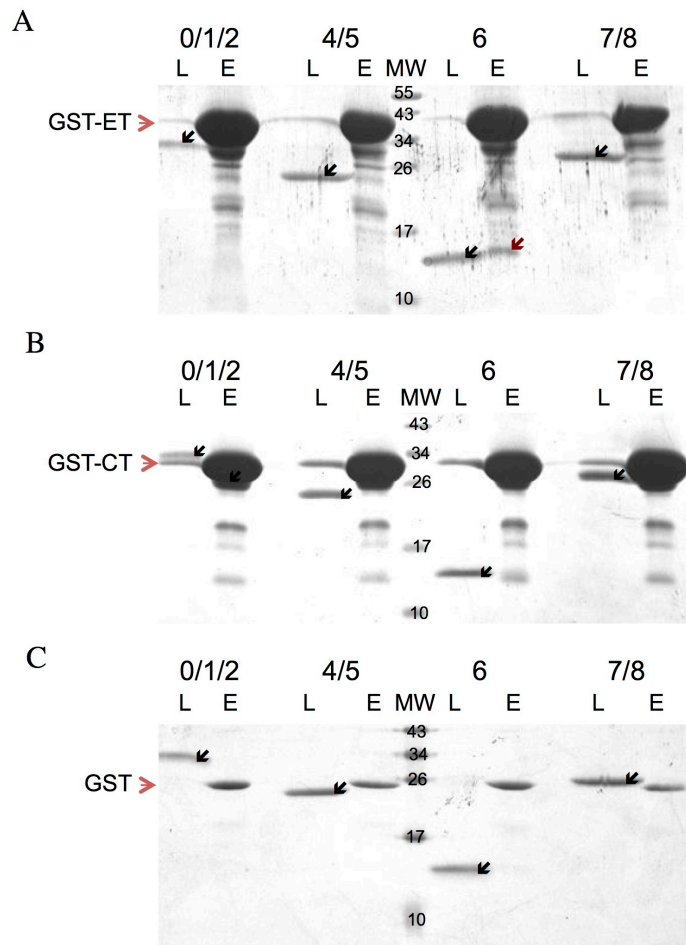


**Figure A-3. Cross-matched interaction study of various Brd4 domains with TopBP1 BRCTs.**

The interactions between purified TopBP1 BRCT0/1/2, BRCT4/5, BRCT6, and BRCT7/8 domains and GST tagged (A) CT domain, (B) ET domain, or (C) GST tag alone examined by GST pull-down assay. L indicates loaded purified TopBP1 BRCTs controls. E represents elution from GST pull-down. MW: molecular weight standard. Black arrows indicate bands of different BRCTs, and brown arrows indicate potential positive interactions.

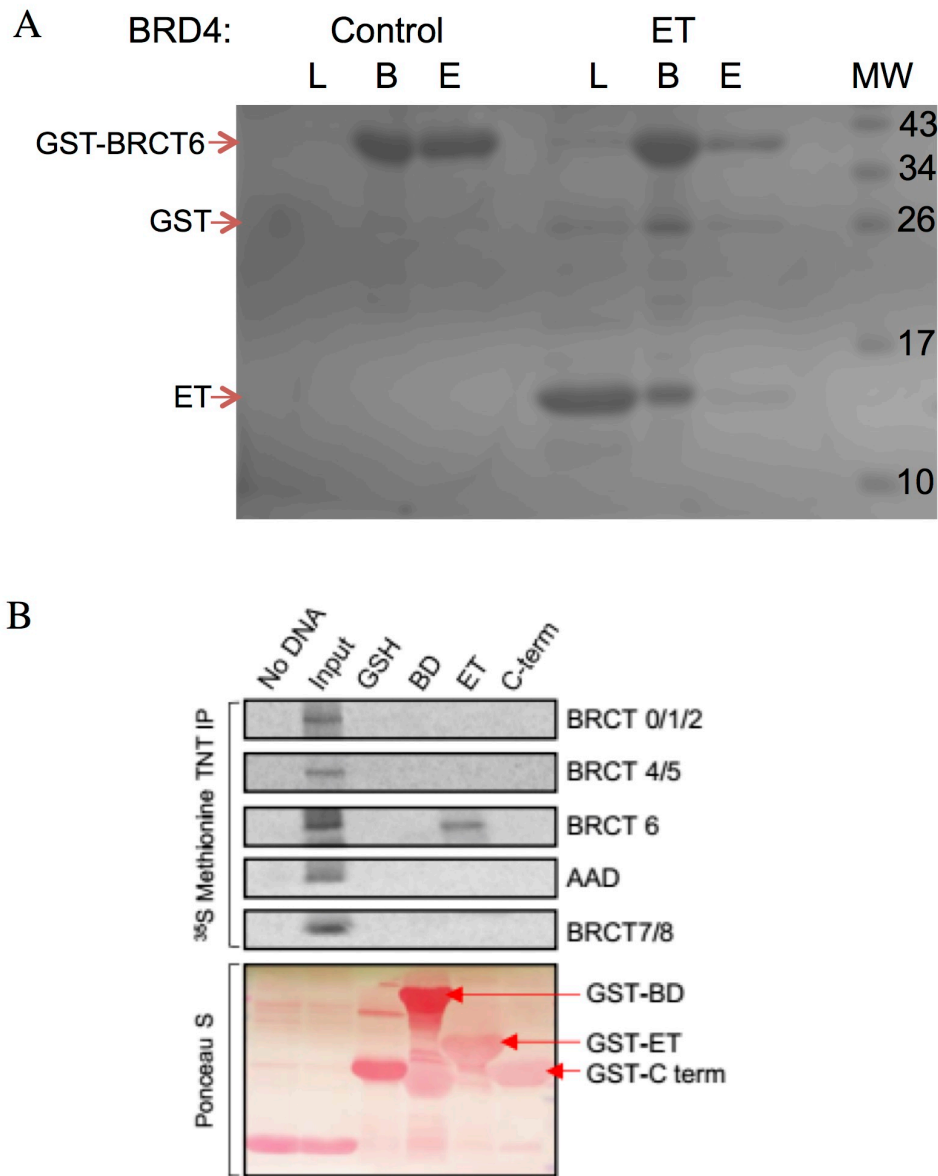


**Figure A-4. Validation of Brd4 ET domain interaction with TopBP1 BRCT6.**

(A) Reverse GST pull-down assay of Brd4 ET domain with GST tagged TopBP1 BRCT6. L represents loaded purified Brd4 ET proteins, and only protein buffer used for Brd4 ET is loaded for the control. B represents protein samples bound on the glutathione beads, and E represents protein sample eluted from beads. MW: molecular weight standard. (B)  $S^{35}$  methionine pull-down assay of TopBP1 functional domains with different GST tagged Brd4 domains. The IP result (top panel) only shows the  $S^{35}$  labeled TopBP1 protein variants, while the purity of GST tagged Brd4 protein variants are visualized by ponceau S staining (bottom panel). Data in Panel B is from Dr. Yaffe's group.

impossible to judge with certainty whether these proteins co-localize on beads. Therefore, I designed a similar S<sup>35</sup>-Methionine label based pull-down assay, which our collaborator (Dr. Lam from Dr. Yaffe's lab in MIT, USA) carried out (Figure A-2C). In agreement with our observation, they were only able to find the interaction between Brd4 ET domain and TopBP1 BRCT6 as well (Figure A-4B). Together, our results suggest that the interaction between TopBP1 and Brd4 occurs specifically between the TopBP1 BRCT6 and the Brd4 ET domain.

### **A.2.2 Disruptions of TopBP1/Brd4 interaction induces replication stress and DNA damage**

Interested in the function of TopBP1/Brd4 interaction in cells, our collaborator first examined the localization of WT TopBP1, Brd4 and truncated TopBP1-BRCT6 $\Delta$ , Brd4-ETA $\Delta$  in HCT116 cells (Figure A-5). They found a discrete reticular and punctate staining pattern in the nuclei of resting cells expressing full length BRD4 and TopBP1. In contrast, expression of either BRD4-ETA $\Delta$  or TopBP1-BRCT6 $\Delta$  resulted in a uniformly diffuse pattern of staining. This implies the disruption of Brd4-TopBP1 interaction may alter the chromatin scaffold formation in cells. Interestingly, immunoprecipitation (IP) results show full length TopBP1 (F-TopBP1) interact with both MDC1 and Brd4. Since MDC1 is known to interact with TopBP1 and histone  $\gamma$ H2AX of chromatin, disruption of TopBP1-MDC1 interaction may also effect chromatin scaffold formation. However, F-TopBP1 BRCT6 $\Delta$  still interacts with MDC1, not Brd4, indicating deletion of BRCT6 solely abolishes TopBP1-Brd4 interaction.

To examine whether the Brd4-TopBP1 interaction was required for TopBP1 localization to HU (Hydroxyurea)-induced damage foci on chromatin, HCT116 cells were co-transfected with BRD4 and either WT TopBP1 or TopBP1-BRCT6 $\Delta$  in a 1:1 ratio. The recruitment to damage foci was assessed with or without an eight hours treatment of 2mM

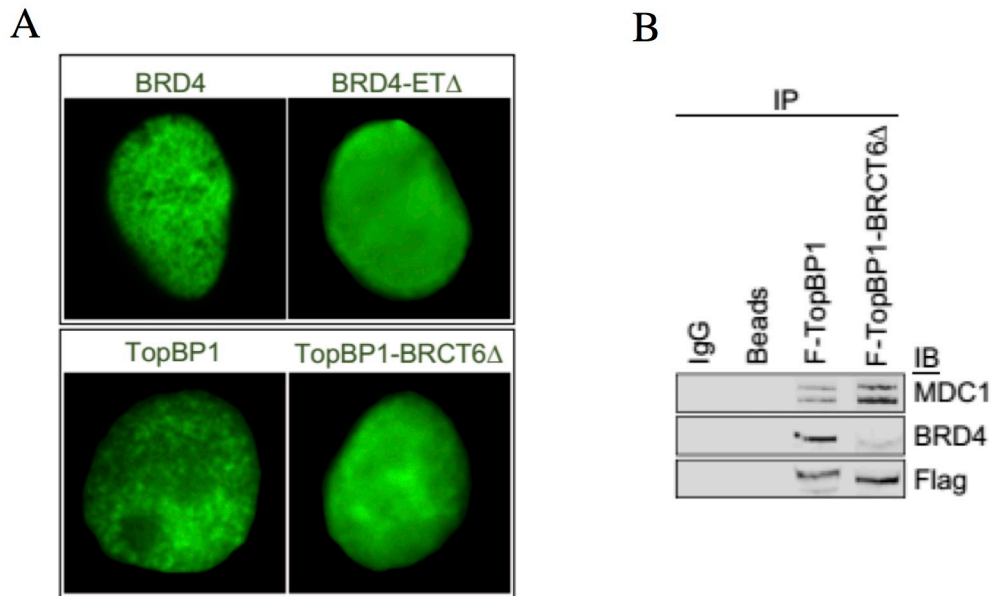


**Figure A-5. Disruption of Brd4-TopBP1 interaction alters the chromatin scaffold formation.**

(A) Representative images that demonstrate discrete reticular and punctate staining pattern in the nuclei of resting cells transfected with full length BRD4 or TopBP1. In contrast, cells expressing Brd4 lacking the ET domain (Brd4-ET $\Delta$ ) or TopBP1 lacking the BRCT6 domain (TopBP1-BRCT6 $\Delta$ ) demonstrate uniformly diffuse nuclear staining. The green color indicates staining for the Brd4 protein in cells. (B) Western blot of co-IP of MDC1 and Brd4 using flag-tagged TopBP1 (F-TopBP1) with loss of interaction with Brd4 using TopBP1 lacking BRCT6 (F-TopBP1-BRCT6 $\Delta$ ). Data in this figure is from Dr. Yaffe's group.

HU. It has been shown previously by our collaborator that inhibition of Brd4 bromodomain activity by the small molecular inhibitor JQ1 can also induce DNA damage. (Unpublished data) Interested in the role of Brd4-TopBP1 interaction under Brd4 inhibition, treatment with 1 mM JQ1 in addition to 2 mM HU was also included. They observed apparent co-localization of BRD4 with full length TopBP1 (Figure A-6A, top panels, and 6C) but not with TopBP1-BRCT6 $\Delta$  (Figure A-6B, top panels, and 6C) in cells at their basal state (DMSO treated). The basal  $\gamma$ H2AX foci, caused by endogenous DNA damage in cells, co-localized with both BRD4 and TopBP1 (Figure A-6A, top panels, and 6C). Upon HU treatment, the number of these triple-staining foci was greatly enhanced (Figure A-6A middle panels and 6C, D). Disruption of bromodomain interactions with JQ1 (Figure A-6A bottom panels and 6C) and expression of TopBP1-BRCT6 $\Delta$  (Figure A-6B) both resulted in the loss of discrete  $\gamma$ H2AX, BRD4, and TopBP1-BRCT6 $\Delta$  foci in HU-treated cells. They observed pan-nuclear  $\gamma$ H2AX staining and reduced BRD4-TopBP1-BRCT6 $\Delta$  co-localization (Figure A-6B middle panels and 6C) that was minimally altered by JQ1 treatment (Figure A-6B lower panels and 6C) in cells expressed TopBP1-BRCT6 $\Delta$ . Together, their results demonstrate that BRD4 co-localizes with TopBP1 to both endogenous and HU-induced sites of DNA damage. The loss of the functional interaction between BRD4 and TopBP1 can disrupt the chromatin scaffold formation, causing chromatin instability, and inducing replication stress, and DNA damage.

### **A.2.3 Protein complex of TopBP1 BRCT6/Brd4 ET domain is unstable *in vitro***

Given the functional importance of Brd4 interaction with TopBP1, we would like to gain more structural insight on this interaction. However, to further examine this interaction structurally using X-ray crystallography, it is crucial to obtain a stable complex of TopBP1/Brd4 first. Interested in whether TopBP1 BRCT6 can form a stable complex with the Brd4 ET domain in solution, we analyzed the freshly made TopBP1 BRCT6/ Brd4

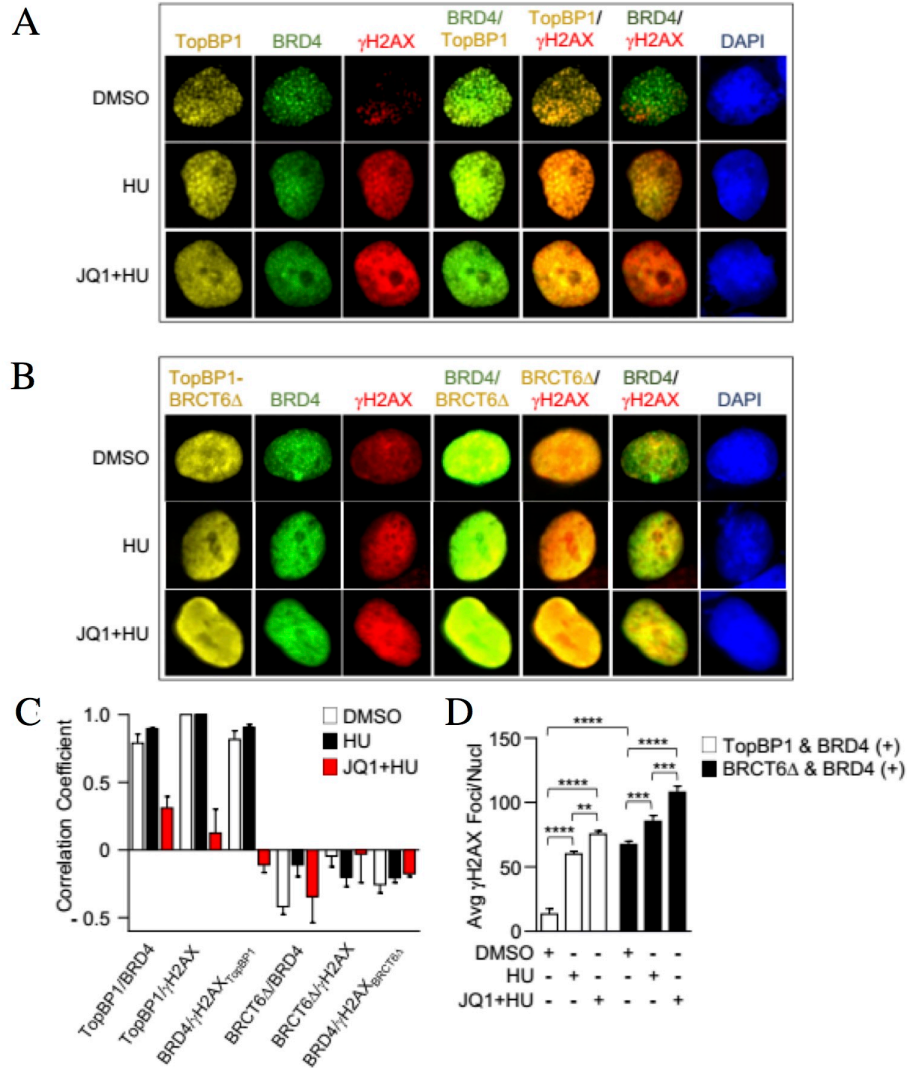


**Figure A-6. Disruption of the Brd4-TopBP1 interaction prevents recruitment of TopBP1 to replication stress-induced DNA damage foci.**

(A) Cells show colocalization of transfected full-length TopBP1 and full-length Brd4 to endogenous damage foci in basal state cells (DMSO; upper panel). Treatment with HU increases colocalization of TopBP1 and Brd4 to replication stress-induced  $\gamma$ H2AX foci (middle panel). Co-treatment of cells with JQ1 and HU results in loss of discrete  $\gamma$ H2AX, BRD4, and TopBP1 foci (JQ1+HU; lower panel). (B) Cells transfected with full-length Brd4 and TopBP1-BRCT6 $\Delta$  show loss of colocalization of TopBP1-BRCT6 $\Delta$  with Brd4 and also demonstrate pan-nuclear  $\gamma$ H2AX staining under basal conditions (DMSO; upper panel). Full-length Brd4 and TopBP1-BRCT6 $\Delta$  fail to colocalize to HU-induced damage foci and demonstrate a diffuse nuclear staining pattern. (C) Co-localization analysis of full-length TopBP1/ BRD4/ $\gamma$ H2AX foci compared to TopBP1-BRCT6 $\Delta$ / Brd4/ $\gamma$  H2AX foci. (D) IF quantification of  $\gamma$ H2AX in cells co-expressing full-length TopBP1 and Brd4 and in cells co-expressing full-length Brd4 and TopBP1-BRCT6 $\Delta$ . Cells are treated with 1 mM JQ1 and/or 2 mM HU for 8 hrs. Data in this figure is from Dr. Yaffe's group.

ET mixture using size exclusion chromatography. In control runs with single protein species, we observed TopBP1 BRCT6 elution peaked at 12.6 ml while Brd4 ET peaked around 13.3 ml (Figure A-7), indicating TopBP1 BRCT6 has larger molecular weight (MW) than Brd4 ET. This is further validated by gel electrophoresis, as we found BRCT6 runs higher than ET on the SDS-PAGE gel. Both results agree with the fact that Brd4 ET has a smaller estimated MW (10.5 kDa) than TopBP1 BRCT6 (11.9 kDa). Surprisingly, we only observed a single elution peak at 13.3 ml with a slightly wider left shoulder for the TopBP1 BRCT6/Brd4 ET mixture. Since the protein complex of TopBP1/Brd4 has a bigger MW and should elute faster than both controls, our result indicates that the complex of Brd4 ET/TopBP1 BRCT6 is not stable on its own in solution.

Chemical crosslinking has been commonly used in PPI studies, and for complex stabilization in structure studies (Tran et al., 2016) (Tang and Bruce, 2009). BS<sup>3</sup> cross-linking is a powerful method that can induce protein oligomerization as well as stabilize protein-protein interactions (Kilkenny et al., 2012; Lay et al., 2012). Therefore, we attempted to obtain a stable Brd4/TopBP1 heterodimer using BS<sup>3</sup> cross-linking. Control experiments of Brd4 ET and TopBP1 BRCT6 protein alone indicated that both proteins exist mostly as monomers in solution (Figure A-8A). Upon BS<sup>3</sup> treatment, both proteins slowly shift to a dimer form in concentrations higher than 50  $\mu$ M, then possibly a tetramer form at 500  $\mu$ M. This BS<sup>3</sup> induced oligomerization in solution appears to be more evident in TopBP1 BRCT6. We then applied the BS<sup>3</sup> treatment on the Brd4/TopBP1 complex sample. Unfortunately, we observed a triple shift at 50  $\mu$ M, indicating the BRD4/TopBP1 heterodimer coexists with the homodimer of BRD4 or TopBP1 in solution (Figure A-8B). This suggested that the interaction between TopBP1 BRCT6 and Brd4 ET domains is too weak, and BS3 crosslinking is not suitable for stabilizing TopBP1 BRCT6/Brd4 ET complex because it also triggers self-oligomerization of both protein domains.

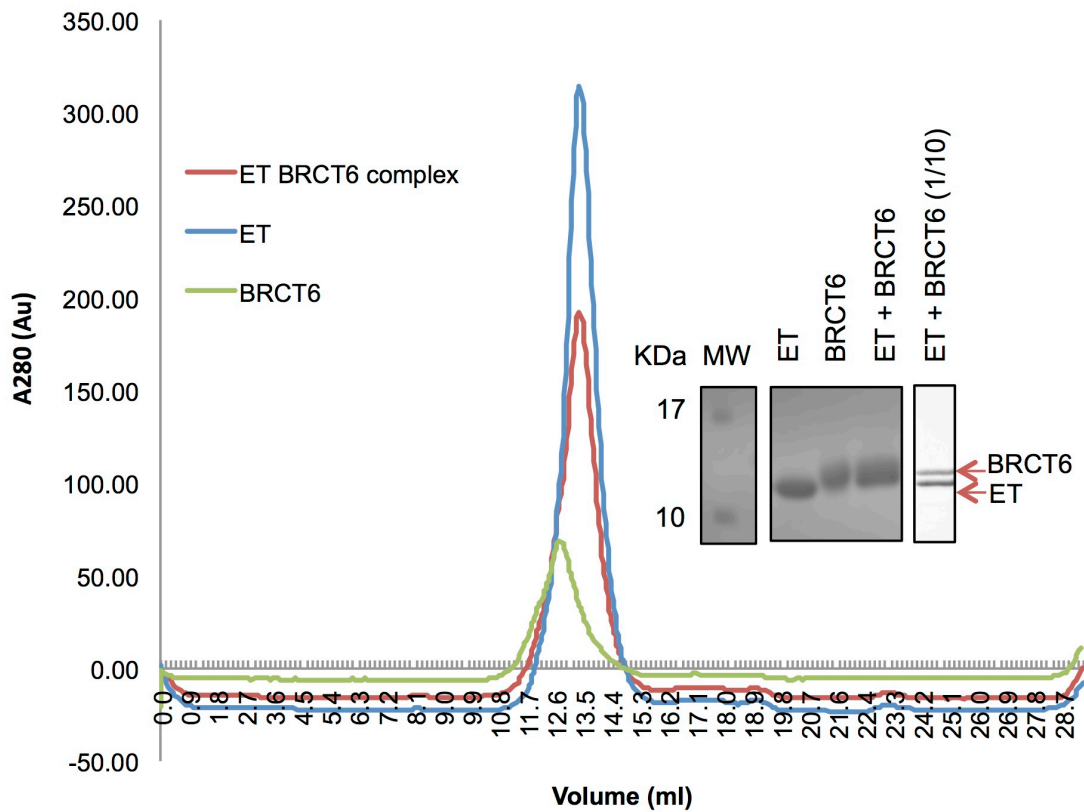


**Figure A-7. Analyze of Brd4 ET/ TopBP1 BRCT6 complex stability in solution by gel filtration chromatography.**

An equivalent amount of purified TopBP1 BRCT6, Brd4 ET, or Brd4 ET/TopBP1 BRCT6 complex samples were analyzed by size exclusion chromatography (Superdex 75 10/300). The composition of samples collected from elution peaks are visualized by gel electrophoresis. Due to overload of sample, limited resolution of the Brd4 ET/TopBP1 BRCT6 mixture sample was found on the first gel. This same sample was reload after 1/10 dilution on another SDS-PAGE gel to achieve better resolution.

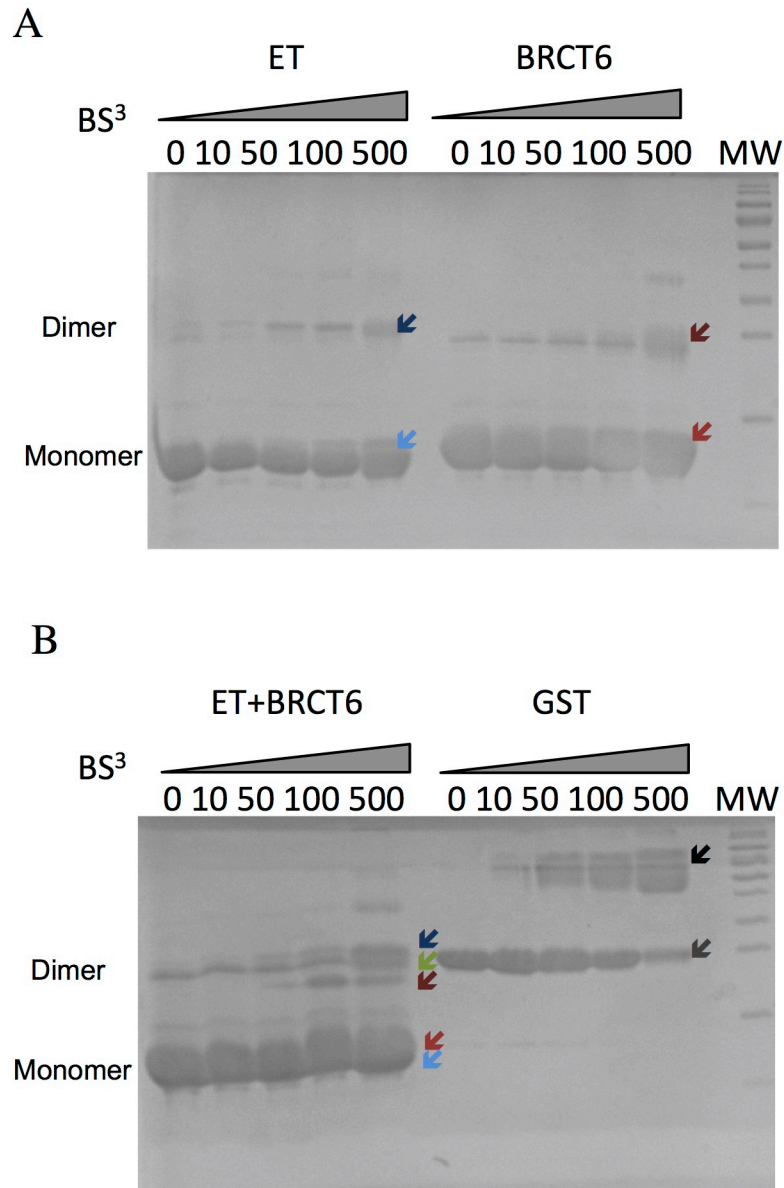


**Figure A-8. BS<sup>3</sup> cross-linking treatment for stabilizing Brd4 ET/ TopBP1 BRCT6 complex.**

(A) BS<sup>3</sup> treatment results of Brd4 ET or TopBP1 BRCT6 alone. (B) BS<sup>3</sup> treatment results of Brd4 ET/ TopBP1 BRCT6 mixture, with GST protein as a positive control.

### **A.3 Discussion**

It was shown previously by our collaborator that Brd4 co-localized with both TopBP1 and MDC1 on chromatin. They also proved that inhibition of Brd4 by JQ1 could block the interaction of Brd4 bromodomain with acetylated lysine of histone and disrupt recruitment of TopBP1/MDC1 scaffold on chromatin. Our study has revealed that the Brd4 ET domain interacts exclusively with the BRCT6 domain of TopBP1. While the direct interaction between Brd4 and MDC1 has yet to be proved, we have already shown that TopBP1 can interact with the SDT repeats of MDC1 through its BRCT5 (Chapter 2). Therefore, we speculate that Brd4 may recruit MDC1 indirectly through TopBP1 to form the large protein scaffold on chromatin as well.

To our surprise, our results suggest that TopBP1 BRCT6 by itself cannot form a stable complex with Brd4 ET. Although a TopBP1 BRCT6 has been implicated in interaction with several DDR proteins, including the phosphorylated E2F1 and PARP1, the precise mechanisms of these interactions remain mysteries (Liu et al., 2003; Wollmann et al., 2007). A recent structural and biochemical study of TopBP1 BRCT6 from our lab indicated that BRCT6 does not contain a functional phosphate-binding pocket to interact with phosphopeptide, and its PAR-binding motif is likely an artifact (Leung et al., 2010). Therefore, further investigation would be needed to understand the detailed mechanism of TopBP1 BRCT6 interaction with Brd4 ET domain. While the interaction between MDC1 and TopBP1 BRCT5 has been suggested in helping to recruit TopBP1 to DNA damage site (Chapter 2), results from this study indicate that Brd4 can also assist in the recruitment of TopBP1. Thus, the instability of TopBP1 BRCT6/Brd4 ET implies either it only exists as a transient complex in cells, or it is part of a bigger complex that is stabilized through other interactions.

Human papillomavirus (HPV) 16 is the most common HPV that can cause many cancers in humans, including cervical and head and neck cancer (zur Hausen, 2009).

Targeting regulation of viral DNA replication could have therapeutic benefits in treating these cancers. Recently, evidence supporting the role of TopBP1 and Brd4 in the initiation of viral DNA replication surfaced (Gauson et al., 2015). While both Brd4 and TopBP1 were found to co-localize with HPV16 E1/E2-containing nuclear foci in cells, only the interaction between HPV16 E2 and Brd4 C-terminus was defined structurally (Abbate et al., 2006). Although it was shown previously both *in vivo* and *in vitro* that HSV16 E2 could interact with the C-terminal fragment of TopBP1 (BRCT6-8) (Boner et al., 2002), the detailed mechanism of this interaction remains unclear. Since we have shown here that BRD4 can interact with the BRCT6 of TopBP1 through its ET domain, it is reasonable to hypothesize that this interaction may help to bridge the interaction between TopBP1 and HSV16 E2 or vice versa.

#### **A.4 Material and Methods**

##### ***Cloning, expression, and purification***

Human TopBP1 BRCT0/1/2 (1-290), BRCT4/5 (549-746), BRCT6 (893-996), BRCT7/8 (1264-1493) were all cloned into pGEX-6P-1 (GE Healthcare). All these GST fusion proteins were expressed in *Escherichia coli* (*E. coli*) BL21-Gold cells and purified using GST affinity chromatography with glutathione sepharose 4B beads (GE Healthcare) and eluted with elution buffer (20 mM Tris-HCl pH 7.5, 150 mM NaCl, 20 mM reduced glutathione and 0.1%  $\beta$ ME).

##### **TopBP1 BRCT0/1/2 (1-290)**

Cell pellet was lysed in Lysis buffer (50 mM Tris-Base, pH 8.0, 150 mM NaCl, 5 mM MgCl<sub>2</sub>, 5% Glycerol, 1 mM EDTA) by sonication. Solubilized GST-TopBP1 BRCT0/1/2 was then purified using GST affinity chromatography with glutathione sepharose 4B beads (GE Healthcare) and eluted with elution buffer (25 mM Tris-Base pH 8.0, 150 mM NaCl, 30mM reduced glutathione, 1 mM EDTA). GST-TopBP1 BRCT0/1/2 was cleaved by PreScission

protease at 4 °C overnight, then BRCT0/1/2 was purified by cation exchange chromatography using SP Sepharose Fast Flow column (GE Healthcare) (buffer A: 50 mM Tris-Base pH 8.0, 1 mM EDTA; buffer B: 50 mM Tris-Base pH 8.0, 1M NaCl, 1 mM EDTA). Further purification was done by gel filtration chromatography using Superdex 75 16/60 column (GE Healthcare) in storage buffer (50 mM Tris-Base, pH 8.0, 150 mM NaCl, 5 mM MgCl<sub>2</sub>, 1 mM EDTA)

#### BRCT4/5 (549-746)

GST-fusion protein of TopBP1 BRCT4/5 was cleaved with PreScission protease overnight at 4 °C. BRCT4/5 was purified by anion exchange chromatography using the Q Sepharose Fast Flow column (GE Healthcare) (buffer A: 50 mM HEPES pH 7.0, 0.1% βME; buffer B: 50 mM HEPES pH 7.0, 1 M NaCl, 0.1% βME). Residual GST was removed by incubation with glutathione sepharose 4B beads (GE Healthcare) prior to a final purification step on a Superdex 75 26/60 column in storage buffer (10 mM Tris-HCl pH 7.5, 150 mM NaCl, 1 mM DTT)

#### BRCT6 (893-996)

GST-fusion protein of TopBP1 BRCT6 was cleaved by PreScission protease at 4 °C overnight, and then BRCT6 was purified by gel filtration chromatography using Superdex 75 16/60 column (GE Healthcare) in storage buffer (10mM Tris-HCl pH 8.0, 150 mM NaCl, 1 mM DTT)

#### BRCT7/8 (1264-1493)

GST-fusion protein of TopBP1 BRCT7/8 was cleaved by PreScission protease at 4 °C overnight, and then BRCT7/8 was purified by cation exchange chromatography using SP Sepharose Fast Flow column (GE Healthcare) (buffer A: 50 mM HEPES pH 6.6, 0.1% βME; buffer B: 50 mM HEPES pH 6.6, 1M NaCl, 0.1% βME). Further purification was done by gel filtration chromatography using Superdex 75 16/60 column (GE Healthcare) in storage buffer (10 mM Tris-HCl pH 7.5, 400 mM NaCl, 1 mM TCEP)

Human Brd4 CT (684-719) and ET (602-690) were cloned into pGEX6P1 and expressed in *E.coli* BL21-Gold cells. Cells were grown in LB broth with 50 µg/mL kanamycin and 50 µg/mL Ampicillin at 28 °C until cell density reached 0.6. The cells were then induced with 0.5 mM Isopropyl β-D-1-thiogalactopyranoside (IPTG) for overnight growth at 20 °C. Cells were pelleted then sonicated in Lysis Buffer (50 mM Tris-HCl pH 8.0, 150 mM NaCl, 0.1% EDTA and 0.1% βME), the crude cell lysates were obtained after 30 mins of 17000rpm centrifugation. GST-Brd4 ET can be purified using GST affinity chromatography with glutathione sepharose 4B beads (GE Healthcare). After cleaving the GST tag with PreScission protease at 4 °C overnight, Brd4 ET can be further purified on Superdex75 16/60 column with storage buffer (150 mM Tris-HCl pH 8.0, 150 mM NaCl, 1 mM DDT).

#### ***Glutathione S-transferase (GST) pull-down assay***

In the first set of pull-down assay, GST affinity beads were first incubated with crude lysate of *E.coli* cell expressing different bait proteins (GST-Brd4 ET, GST-Brd4 CT or GST) at 4 °C for 1 hr. After removing other proteins through intensive washes (Washing buffer: 150 mM Tris-HCl pH 8.0, 150 mM NaCl, 1 mM DDT), 2 mg of purified prey proteins (TopBP1 BRCT0/1/2, BRCT4/5, BRCT6 and BRCT7/8) were applied to the beads for 1hr at 4 °C to interact with bait proteins. The beads were rewashed to remove unbound prey proteins, and the remaining GST tagged proteins complex on beads were eluted (Elution buffer: 150 mM Tris-HCl, pH 8.0, 150 mM NaCl, 30 mM reduced glutathione, 1 mM DDT) and analyzed by gel electrophoresis on an SDS-PAGE gel. In the second set of reverse pull-down assay, purified TopBP1 BRCT6 was used as bait protein, and purified Brd4 ET was used as prey protein. The procedure is the same as described above for the first pull-down assay.

#### ***S<sup>35</sup>-Methionine pull-down assay***

We have provided the purified proteins as well as expression constructs of different TopBP1 domains to our collaborator. This experiment was carried out by Dr. Lam from Dr. Yaffe's group.

### ***Size exclusion chromatography***

Superdex 75 16/60 column was pre-calibrated with sample buffer (10 mM Tris-HCl pH 7.5, 150 mM NaCl, 1 mM DTT). 200  $\mu$ L of 1mg/mL purified protein sample of TopBP1 BRCT6 or BRD4 ET domain was first analyzed individually on the column as controls. Then 200  $\mu$ L of 1mg/ml mixture sample was prepared at 1:1 ratio of TopBP1 BRCT6: BRD4 ET domain and incubated for 1hr at 4 °C. The mixture sample was analyzed on the same column, and samples from peak elution fractions of all three runs were analyzed by gel electrophoresis on an SDS-PAGE gel.

### ***BS<sup>3</sup> cross-linking***

Purified protein samples (TopBP1 BRCT6, BRD4 ET, GST, or TopBP1 BRCT6/ BRD4 mixture) were diluted in PBS buffer (20 mM Sodium Phosphate, 0.15 M NaCl, 20 mM HEPES, pH 7.5) to a final concentration of 1 $\mu$ g/ $\mu$ L. A mixture of TopBP1 BRCT6/BRD4 ET was made by incubated both proteins at 1:1 molar ratio in PBS buffer for 30mins on ice. In five aliquots that contain 10  $\mu$ g of protein each, BS<sup>3</sup> (Bis[sulfosuccinimidyl] suberate) was added to final concentration of 0, 10  $\mu$ M, 50  $\mu$ M, 100  $\mu$ M, 500  $\mu$ M After 30 minutes incubation at room temperature, 1 $\mu$ L of 1M Tris-HCl (pH 7.5) was used to quench the reaction for 5 minutes. Protein samples were then analyzed by gel electrophoresis on an SDS-PAGE gel.

## A.5 Reference

1. Abbate, E.A., Voitenleitner, C., and Botchan, M.R. (2006). Structure of the papillomavirus DNA-tethering complex E2:Brd4 and a peptide that ablates HPV chromosomal association. *Mol Cell* *24*, 877-889.
2. Boner, W., Taylor, E.R., Tsirimonaki, E., Yamane, K., Campo, M.S., and Morgan, I.M. (2002). A functional interaction between the human papillomavirus 16 transcription/replication factor E2 and the DNA damage response protein TopBP1. *Journal of Biological Chemistry* *277*, 22297-22303.
3. Crowe, B.L., Larue, R.C., Yuan, C., Hess, S., Kvaratskhelia, M., and Foster, M.P. (2016). Structure of the Brd4 ET domain bound to a C-terminal motif from gamma-retroviral integrases reveals a conserved mechanism of interaction. *Proc Natl Acad Sci U S A* *113*, 2086-2091.
4. Dey, A., Chitsaz, F., Abbasi, A., Misteli, T., and Ozato, K. (2003). The double bromodomain protein Brd4 binds to acetylated chromatin during interphase and mitosis. *Proc Natl Acad Sci U S A* *100*, 8758-8763.
5. Dey, A., Ellenberg, J., Farina, A., Coleman, A.E., Maruyama, T., Sciortino, S., Lippincott-Schwartz, J., and Ozato, K. (2000). A bromodomain protein, MCAP, associates with mitotic chromosomes and affects G(2)-to-M transition. *Mol Cell Biol* *20*, 6537-6549.
6. Floyd, S.R., Pacold, M.E., Huang, Q., Clarke, S.M., Lam, F.C., Cannell, I.G., Bryson, B.D., Rameseder, J., Lee, M.J., Blake, E.J., *et al.* (2013). The bromodomain protein Brd4 insulates chromatin from DNA damage signalling. *Nature* *498*, 246-250.
7. Gauson, E.J., Donaldson, M.M., Dornan, E.S., Wang, X., Bristol, M., Bodily, J.M., and Morgan, I.M. (2015). Evidence supporting a role for TopBP1 and Brd4 in the initiation but not continuation of human papillomavirus 16 E1/E2-mediated DNA replication. *J Virol* *89*, 4980-4991.
8. Itzen, F., Greifenberg, A.K., Bosken, C.A., and Geyer, M. (2014). Brd4 activates P-TEFb for RNA polymerase II CTD phosphorylation. *Nucleic Acids Res* *42*, 7577-7590.
9. Jang, M.K., Mochizuki, K., Zhou, M., Jeong, H.S., Brady, J.N., and Ozato, K. (2005). The bromodomain protein Brd4 is a positive regulatory component of P-TEFb and stimulates RNA polymerase II-dependent transcription. *Mol Cell* *19*, 523-534.

10. Kilkenny, M.L., De Piccoli, G., Perera, R.L., Labib, K., and Pellegrini, L. (2012). A conserved motif in the C-terminal tail of DNA polymerase alpha tethers primase to the eukaryotic replisome. *J Biol Chem* 287, 23740-23747.
11. Lay, F.T., Mills, G.D., Poon, I.K., Cowieson, N.P., Kirby, N., Baxter, A.A., van der Weerden, N.L., Dogovski, C., Perugini, M.A., Anderson, M.A., *et al.* (2012). Dimerization of plant defensin NaD1 enhances its antifungal activity. *J Biol Chem* 287, 19961-19972.
12. Leung, C.C., Kellogg, E., Kuhnert, A., Hanel, F., Baker, D., and Glover, J.N. (2010). Insights from the crystal structure of the sixth BRCT domain of topoisomerase IIbeta binding protein 1. *Protein Sci* 19, 162-167.
13. Liu, K., Lin, F.T., Ruppert, J.M., and Lin, W.C. (2003). Regulation of E2F1 by BRCT domain-containing protein TopBP1. *Mol Cell Biol* 23, 3287-3304.
14. Rahman, S., Sowa, M.E., Ottinger, M., Smith, J.A., Shi, Y., Harper, J.W., and Howley, P.M. (2011). The Brd4 extraterminal domain confers transcription activation independent of pTEFb by recruiting multiple proteins, including NSD3. *Mol Cell Biol* 31, 2641-2652.
15. Tang, X., and Bruce, J.E. (2009). Chemical cross-linking for protein-protein interaction studies. *Methods Mol Biol* 492, 283-293.
16. Taniguchi, Y. (2016). The Bromodomain and Extra-Terminal Domain (BET) Family: Functional Anatomy of BET Paralogous Proteins. *Int J Mol Sci* 17.
17. Tran, B.Q., Goodlett, D.R., and Goo, Y.A. (2016). Advances in protein complex analysis by chemical cross-linking coupled with mass spectrometry (CXMS) and bioinformatics. *Biochim Biophys Acta* 1864, 123-129.
18. Wollmann, Y., Schmidt, U., Wieland, G.D., Zipfel, P.F., Saluz, H.P., and Hanel, F. (2007). The DNA topoisomerase IIbeta binding protein 1 (TopBP1) interacts with poly (ADP-ribose) polymerase (PARP-1). *J Cell Biochem* 102, 171-182.
19. Yang, Z., Yik, J.H., Chen, R., He, N., Jang, M.K., Ozato, K., and Zhou, Q. (2005). Recruitment of P-TEFb for stimulation of transcriptional elongation by the bromodomain protein Brd4. *Mol Cell* 19, 535-545.

20. zur Hausen, H. (2009). Papillomaviruses in the causation of human cancers - a brief historical account. *Virology* 384, 260-265.

## **Appendix B**

**Structure analogs of TopBP1 BRCT4/5 in *Saccharomyces cerevisiae***

## B.1 Introduction

The maintenance of genome stability is essential for cell survival, and if compromised, may ultimately lead to the development of various genetic diseases in humans including cancer. Topoisomerase binding protein 1 (TopBP1) is an important scaffold protein involved heavily in DNA damage response (DDR) including initiation of DNA replication, ATR-dependent checkpoint signaling, and transcriptional regulation. Its abundant BRCA1 C-terminal (BRCT) domains in particular, are essential for mediating interactions with different DDR proteins.

In yeast systems, there are two well-known homologs of TopBP1 that also play important roles in checkpoint activation and DNA replication initiation: the Rad4<sup>TopBP1</sup> in *S. pombe*, and the Dpb11<sup>TopBP1</sup> in *Saccharomyces cerevisiae* (*S. cerevisiae*) (Wardlaw et al., 2014). Both Rad4<sup>TopBP1</sup> and Dpb11<sup>TopBP1</sup> have two sets of tandem BRCT repeats that function collaboratively while interacting with phosphorylated protein partners (Figure B-1A). In *S. pombe*, Rad4<sup>TopBP1</sup> uses its C-terminal BRCT3/4 repeats to interact with phosphorylated Rad9. And this interaction is believed to promote the Crb2<sup>53BP1</sup> recruitment via the N-terminal BRCT1/2 repeats of Rad4<sup>TopBP1</sup> (Taricani and Wang, 2006). Three CDK phosphorylation sites on Crb2<sup>53BP1</sup> are phosphorylated sequentially in order to interact with the BRCT1/2 of Rad4<sup>TopBP1</sup>. While phosphorylation of Crb2<sup>53BP1</sup> at Thr215 and Thr235 initiates the interaction with Rad4<sup>TopBP1</sup> BRCT1/2 repeats, the recruitment of Cdc2/Cdc13<sup>CDK/CyclinB</sup> along with Rad4<sup>TopBP1</sup> induces further phosphorylation of Crb2<sup>53BP1</sup> at Thr187. Since Crb2<sup>53BP1</sup> self-dimerized via its C-terminal tandem BRCTs (Kilkenny et al., 2008), the interaction between Rad4<sup>TopBP1</sup> BRCT1/2 repeats and Thr187 residues from the homo-dimer of Crb2<sup>53BP1</sup> results in the formation of a larger tetrameric complex (Qu et al., 2013). This complex is found to promote Crb2<sup>53BP1</sup> phosphorylation by Rad3<sup>ATR</sup> and downstream recruitment/activation of checkpoint kinase Chk1 (Qu et al., 2012).

In *S. cerevisiae*, a similar pathway for checkpoint activation exists. Upon Mec1<sup>ATR</sup>

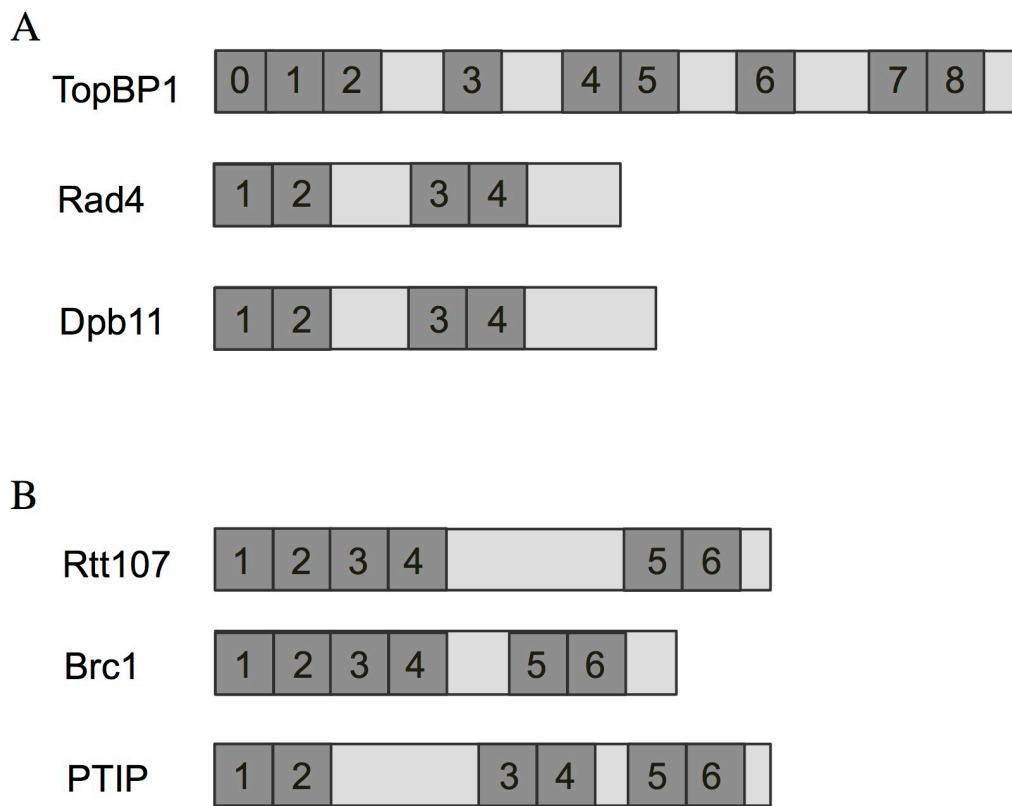


**Figure B-1. The protein homologs of BRCT family proteins.**

(A) Human TopBP1 and its homologs Rad4 from *S. pombe* and Dpb11 from *S. cerevisiae*.  
 (B) Rtt107 from *S. cerevisiae* and its homologs Brc1 from *S. Pombe* and PTIP from humans. The length of each light grey bar reflects the known protein sequences length of each protein. The BRCT domains are indicated by similar size grey box and numbered sequentially.

dependent phosphorylation at T602, the Ddc1 of Ddc1-Mec3-Rad17 (9-1-1) complex recruits Dpb11<sup>TopBP1</sup> through interacting with its BRCT3/4 repeats. Meanwhile, the N-terminal BRCT1/2 repeats of Dpb11<sup>TopBP1</sup> interacts with CDK phosphorylated *scRad9*<sup>53BP1</sup>. Together, both interactions promote the recruitment and activation of downstream checkpoint kinase Rad53 (Pfander and Diffley, 2011). It is worth noting that Dpb11<sup>TopBP1</sup> has an ADD-like domain on its C-terminus that can interact with Mec1-Cdc2. This interaction can activate Mec1<sup>ATR</sup> kinase activity and phosphorylate Ddc1. However, whether this interaction is essential for DNA damage-induced checkpoint activation remains debatable (Germann et al., 2011; Pfander and Diffley, 2011). Therefore, it is not a surprise that this ADD-like domain was recently shown to be absent in the Rad4<sup>TopBP1</sup> protein (Yue et al., 2014).

Benefiting from the existing structures of Rad4<sup>TopBP1</sup> BRCT domains, it is easier to examine the evolutionary trend of TopBP1 BRCT domains between *S. pombe* and higher eukaryotes. Using structural comparison between human TopBP1 BRCT4/5 and Rad4<sup>TopBP1</sup> BRCT1/2, we have successfully identified the potential pSer target of TopBP1 BRCT4/5 on 53BP1 (Chapter 3). Therefore, we believed that solving the structure of Dpb11<sup>TopBP1</sup> BRCT domains can further our understanding of TopBP1 BRCT domains as well. Using protein sequences alignment of Rad4<sup>TopBP1</sup> and Dpb11<sup>TopBP1</sup> in combination with secondary structure prediction of Dpb11<sup>TopBP1</sup>, we have defined the regions of BRCT1/2 and BRCT3/4 domains on Dpb11<sup>TopBP1</sup>. We then engineered the GST-tagged Dpb11<sup>TopBP1</sup> BRCTs constructs for bacterial-based expression in *E. coli* cells, and designed the purification protocol for obtaining untagged Dpb11<sup>TopBP1</sup> BRCT proteins for further study.

Interestingly, the regulator of Ty1 transposition protein 107 (Rtt107) is also an important scaffold protein in *S. cerevisiae*. It recruits many proteins via its six BRCT domains during DDR, including DNA replication initiation and checkpoint activation (Figure B-1B). The BRCT3/4 and BRCT5/6 of Rtt107 work collaboratively in the recruitment of endonuclease Slx4 to DNA lesion (Leung et al., 2016). While the BRCT5/6 of Rtt107 interacts with  $\gamma$ H2A at DNA damage site, the BRCT3/4 recruits Slx4 with the help from

BRCT1/2. The Slx4/Rtt107 complex then induces Slx4 phosphorylation by Mec1<sup>ATR</sup>, which allows Slx4 to interact with BRCT1/2 of Dbp11<sup>TopBP1</sup> (Ohouo et al., 2010). This blocks the Dbp11<sup>TopBP1</sup> BRCT1/2 interaction with scRad9<sup>53BP1</sup> and down regulates Rad53 phosphorylation and checkpoint activation (Ohouo et al., 2013). Moreover, as part of the large N-terminal BRCT domains (BRCT1/2/3/4) of Rtt107, BRCT3/4 also play important roles in multiple PPIs that support replication progression with partner SUMO and ubiquitin ligases (Hang et al., 2015). This N terminal BRCTs of Rtt107 can either interact with Smc5/6 to form a SUMO ligase complex together with Nse2 or interact with Cullin Rtt101 to form a ubiquitin ligase complex together with Mms22/1.

Previously, a homolog search of Rtt107 has identified Brc1 in *S. pombe* and PTIP in humans as potential homologs of Rtt107 (Figure B-1B). Similarly to Rtt107, both Brc1 and PTIP have C-terminal BRCT repeats that can interact with phosphorylated H2A (Williams et al., 2010; Yan et al., 2011). However, crystal structures of apo Rtt107 BRCT5/6 and Rtt107 BRCT5/6 in complex with H2A have revealed an interface that is quite distinct from Brc1 BRCT5/6 (Li et al., 2012). In addition, it has been noted that aside from high sequence similarity, there are very low functional and structural similarities between Rtt107 and PTIP. (Gohler et al., 2008) This implies that Brc1 and PTIP may not be very good homologs of Rtt107. Using sequence alignment assisted by secondary structure prediction, we have shown that Rtt107 BRCT3/4 is likely the structural analog of human TopBP1 BRCT4/5. We have designed a few constructs of Rtt107 BRCT3/4 (with either GST tagged or His tag) based on our structural predictions and attempted to express these proteins in *E. coli*. Our preliminary results indicated we could successfully express GST-Rtt107 BRCT3/4 constructs in *E. coli* *BL21 Gold* cells and purify them using a GST affinity column, but the yield of these proteins after purification seems to be limited by their solubility. On the other hand, we only observed expression of His-Rtt107<sup>265-466</sup> in *E. coli* *BL21 DES* cells. Likely due to protein instability in the current buffer, we failed to purify this protein using size exclusion chromatography.

Further experimenting with different buffer composition is needed. However, exploring the option of other fusion tags, especially MBP tag, may provide a good solution.

## **B.2 Results**

### **B.2.1 Engineering of bacteria based expression constructs of Dpb11 BRCTs**

We first carried out pairwise protein sequences alignment of full-length Rad4 and Dpb11 (Figure B-2). The overall sequence conservation between these two proteins is fairly low (22.4% identity / 35% similarity). However, the localized sequence conservation between several BRCT domains from these proteins seems higher. The BRCT1 of Dpb11<sup>1-87</sup> aligned quite well with regions from both BRCT1 (36% identity / 55% similarity) and BRCT2 (33% identity / 65% similarity) of Rad4 (Figure B-3A). Both threonine and lysine residues from the phosphate-binding pockets of BRCT1/BRCT2 of Rad4 are conserved in Dpb11 BRCT1. In addition, the Arg40 of Dpb11 BRCT1 aligned with the Arg 137 of Rad4 BRCT2, which may further interact with the phosphate head group from pThr/pSer of the phosphopeptide. Moreover, the Leu38, Phe58 and His62 from Dpb11 BRCT1 may also form a hydrophobic pocket like observed in Rad4 BRCT1 and BRCT2 (Figure B-3B). However, the BRCT2 of Dpb11 has lower sequence similarity with known Rad4 BRCT2, making it harder to define its region. Using conserved domain (CD) search result from NCBI database (Marchler-Bauer et al., 2017), we found a BRCT domain between residues 111-206. Therefore, we believed this is likely the BRCT2 of Dpb11 (Figure B-3C).

Meanwhile, residues 331-489 from Dpb11 aligned with residues 297-440 from Rad4 BRCT3/4 (Figure B-4A). The Ile343 and Pro386 of Dpb11 BRCT3 aligned with the hydrophobic residues (Try311 and Pro355) from BRCT3 of Rad4, suggesting the phosphate-binding pocket is also absent in the BRCT3 of Dpb11 (Figure B-4B). Using the CD search identified a BRCT domain between residues 326-405 of Dpb11, which we

```

Dpb11  1  ---MKPFQGITFCPTAINNEILAKKISKKIIKLGIFSKDLTRQVNVLVVGSTTNTNKFKFV  59
Rad4    1  MGSSKPLKGFVICCTSIDLK-QRTEISTKATKLGAAAYRSDFTKDVTHLIAGD-FDTPKYKFA  60

Dpb11  60  AKHRFDIIFIDIQAIDDIYQLWLSGEN----ILPDSNTATMTGSTYEMLKILYRRFSFKYLH  117
Rad4   61  AKSRPDIKIMSSEWIPVLYESWVQGEDLDDGLLVDKH-----FLPTLFK-----  104

Dpb11 118  NFNIFIGRITDTNITSIDSLVRSIKKLGCCSSYNYQNFVIKDTSSHNDQDQGNQGISIFVT  179
Rad4  105  -----CRVCLTNIGQPE---RS-----RIENYVLKHGGTFPCPD----LTRDVTHLIA  144

Dpb11 180  DTLLGARVNAAIEQNIPIVHFKWILDCQKRSALLPYDPYLLLPNIKDLPYDSIGSNSCDCWD  241
Rad4  145  GTSSGRKYEYALKWKINVVCVEWLWQSIQRNAVL--EPQYFQ---LDMPAEKIGLGAYVRD  201

Dpb11 242  KINTTFPTNIDAQSSLQRQSSSTLTPSLPKTSSLLNKFKPKGEK-----IWDK----AMSL  294
Rad4  202  PNTTEAKSYSENQKISKNKEKSGQSLAALAEADLEPVIMKRGGKRDRSILWEELNNGKFEF  263

Dpb11 295  QQHSKTNFVSLGQ-----SPLSINNKKEDLS-DNSTLIFKNCAFIIHHIFPGNHRHSILT  349
Rad4  264  SSRSEENSVLDDFTPETVQPLEENELDTELNIENEAKLFKNLTFYLYE-FPNTKVSRLHKC  324

Dpb11 350  VVQNGGKIETSYLSGIYDHSYIIPSNKALDSFNDLPEIIDDNDGIVTEFFIERCLYQKLL  411
Rad4  325  LSDNGGQI-SEFLSSTID--FVVIPIHYFPVD---ELPIF---SFPTVNEWWIERCLYKIF  377

Dpb11 412  ----HPIDLWSPFLSTIEFQVSSSSKLLHHEFSSSPFLN---VTITGFSGVELLHLTKVLN  466
Rad4  378  GIDEHAL---AKPFFRP-----SLVPYFNGLSIHLTGFKGEELSHLKKALT  420

Dpb11 467  LLKPMGINVVEYLNKSTDILLINLAALPSIPKT-----HP-----LW----SNEF  508
Rad4  421  IL---GAVVHEFLGVQRSILLVNTNE-PFSMKTRFKIQHATEWNVRVVGVAWLWNIQSGKF  478

Dpb11 509  SDLFTQFCINNNNDPGDNNR-KDF--QNNSI-----LRNSMKRKIEYIKKFHSIPVV  557
Rad4  479  IDQVSPWAI-----DKKENQEIKKFTNQNMVFPTSDRDRQLQNSLAQQ----PIGHSTPHN  531

Dpb11 558  TPAFIFKLLSAASGENNEIFLN-----NIKWCIIICPR-----GHKDD--FKCKIKKPY  604
Rad4  532  SPS---LLSVKKRQNNHIRSNTLIQLNSNSKDSTIFRRSVTVPGDKIDTVWKS SVTKPET  589

Dpb11 505  -TSSISSEKKYQNDPKIDKTILLKRNNSSLS----EHSMDTKNELLQKIRETDSGRKKRSV  661
Rad4  590  PTSPQEHVSYIDPDAQREKHKLYAQLTSNVDAIPPANDLQNGENGLL---LITESHKLR  648

Dpb11 662  SSSIMDVSSERQMPDTRIKLES LPKNFV PKQIKRTTSWGTIMSENVPT EQPTAISNPEEIP  713
Rad4      -----

Dpb11 714  RTEEVSHQVTYGSIQDKKRTASLEKPMRRQTRNQTKELDS  754
Rad4      -----

```

**Figure B-2. Pairwise protein sequence alignment of Dpb11 and Rad4.**

Full length Dpb11 and Rad4 protein sequences are aligned using EMBOSS Needle. All the spaces found in this alignment are indicated by “-”, residues from the phosphate binding pocket are colored pink, residues from the hydrophobic pocket are colored green.

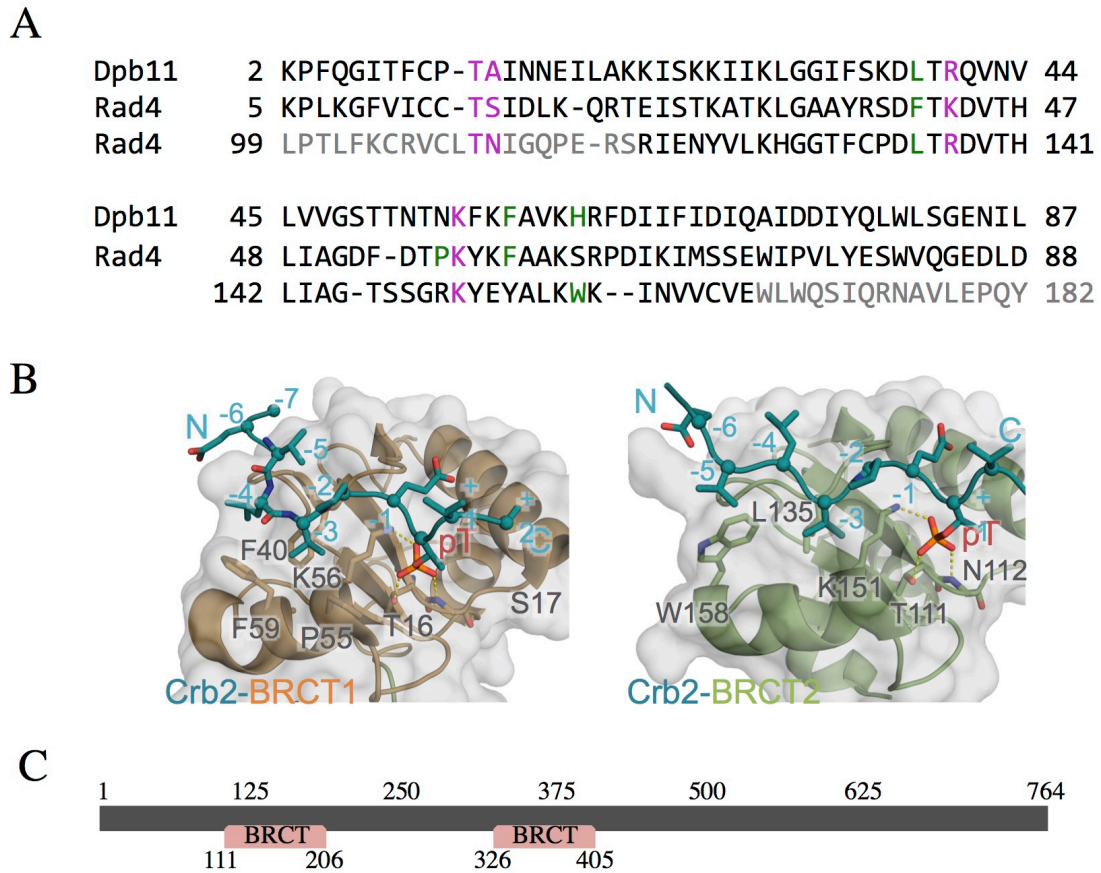


**Figure B-3. Comparison of Dpb11 BRCT1/2 and Rad4 BRCT1/2.**

(A) Protein sequence alignment of Dpb11 with Rad 4 BRCT1 and BRCT2 performed in PROMAL3D. All spaces in this alignment are indicated by “-”, residues from phosphate binding pocket are colored pink, residues from hydrophobic pocket are colored green. Since Rad4 BRCT2 only partially aligned with Dpb11, residues that did not align well were shown in grey. (B) Structural overview of Rad BRCT1 and BRCT2 interaction with Crb2 (PDB ID: 4BU0). (C) CD search result of BRCT domains on Dpb11 from NCBI database.

A

```

Dpb11 331 DNSTLIFKNCAFIIHHIFPGNHR SILTKIVVQNGGKIETSYLSGIYDHSYIIPS NKALD 380
Rad4   297 ENEAKLFKNLTFYLYE-FPNTKVSRLHKCLSDNGGQI-SEFLSSTID--FVWIPHYFPVD 352

Dpb11 381 SFNDLPEIIDDNDGIVTEFFIERCLTTQKLL----HPIDLWSPFLSTIEFQVSSSSKLL 436
Rad4   353 ---ELPIF---SFPTVNEWWIERCLYYKKIFGIDEHAL---AKPFFRP----- 391

Dpb11 437 HHEFSSSPFLN---VTITGFSGVELLHLTKVLNLLKPMGINYVEYLNKSTDILLIN 489
Rad4   392 ----SLVPYFNGLSIHLTGFKGEE LSHLKKALTIL---GAVVHEFLGVQRSILLVN 440

```

B

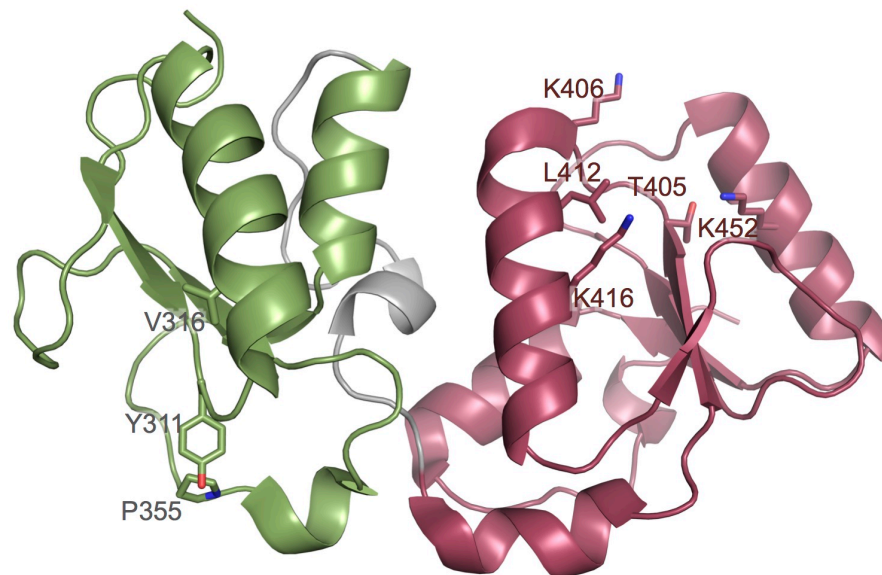


**Figure B-4. Comparison of Dpb11 BRCT3/4 and Rad4 BRCT3/4.**

(A) Protein sequence alignment of Dpb11 with Rad 4 BRCT1 and BRCT2 done by PROMAL3D. All spaces in this alignment are indicated by “-”, residues from the phosphate binding pocket are colored pink, residues from the hydrophobic pocket are colored green. Since Rad4 BRCT2 only partially aligns with Dpb11, residues that didn’t align well were shown in grey. (B) Structural overview of Rad4 BRCT3/4 (PDB ID: 4BMD) with BRCT3 colored in green, BRCT4 colored in red, and linker colored in silver. All residues from the proposed phosphate binding pocket are highlighted by stick representation.

proposed as the BRCT3 (Figure B-3C). Although a few residues from the protein interface of Rad4 BRCT4 (Thr 405 and Leu 412) are conserved in Dpb11 BRCT4 (Thr 451 and Leu 458), the region of BRCT4 on Dpb11 remains unclear.

To better estimate these BRCT domains of Dpb11<sup>TopBP1</sup>, we carried out secondary structure prediction of Dpb11 (Figure B-5). We observed a long unstructured loop region from residue 211-318. Since the BRCT3 of Dpb11 starts around residue 210, we proposed that residues 1-210 represent the Dpb11 BRCT1/2. Then we managed to identify four beta sheets of BRCT4 that are often conserved in BRCT domains. We found the 4<sup>th</sup> beta sheet was conjugated with an alpha helix, and followed by a very long unstructured loop region. Therefore, we proposed the BRCT4 ends right after the alpha helix, and residue 319-510 represent Dpb11 BRCT3/4.

We then estimated the basic protein properties of Dpb11 BRCT1/2 and BRCT3/4 using ProtParam (Table B-1) (Gasteiger et al., 2005). The Dpb11 BRCT3/4 has an instability index value of 40.56, indicating this protein is unstable. To resolve this issue and simplify the protein purification process, we incorporated GST tag on both proteins and re-examined their properties. The GST tag appears to stabilize the Dpb11 BRCT3/4. Therefore, both constructs of Dpb11 were cloned into the pGEX6P1 vector (Table B-2). The expression and purification protocols of Dpb11 BRCT1/2 and BRCT3/4 were then designed based on the typical GST tagged protein production and purification guide (Figure B-6)(Frangioni and Neel, 1993).

### **B.2.2 Rtt107 BRCT3/4 is the structural analog of TopBP1 BRCT4/5**

Based on the result from CD search, the BRCT3/4 of Rtt107 exists between residues 264-448 (Figure B-7D). We then carried out protein sequence alignment of Rtt107 with Rad4 using PROMALS3D (Pei et al., 2008). We found the region of residues 287-469 aligns well with the sequence around the Rad4 BRCT1/2 (7-178), suggesting Rtt107 BRCT3/4 may be a



**Figure B-5. Predicted secondary structure of Dpb11.**

The predicted secondary structure of Dpb11 presented here was generated by Jpred. Predicted structured regions from Dpb11 BRCT1/2 are colored in dark blue, from DpB11 BRCT3/4 are colored in blue, and the rest of regions with secondary structure are colored in pale blue. Residues from the proposed phosphate binding pocket are colored pink, residues from hydrophobic pocket are colored green.

**Table B-1. List of primers used for Dpb11 BRCTs constructs<sup>1</sup>**

Protein	Tag		MW <sup>3</sup> (KDa)	pI <sup>4</sup>	Instability Index		Extinction Coefficient <sup>5</sup>	
	Type	C-site <sup>2</sup>			Value	Class	(M <sup>-1</sup> cm <sup>-1</sup> )	Abs 0.1 %
BRCT1/2 (1-210)	N/A	N/A	23.9	9.20	28.82	Stable	20065/19940	0.839/0.834
BRCT1/2 (1-210)	GST	3C	52.3	7.59	33.81	Stable	63175/ 62800	1.207/1.200
BRCT3/4 (319-510)	N/A	N/A	21.9	5.78	40.56	Unstable	23045/22920	1.053/1.047
BRCT3/4 (319-510)	GST	3C	50.2	5.82	39.24	Stable	66155/65780	1.318/1.311

<sup>1</sup> All data from this take are estimated based on protein sequence of each construct using ProtParam

<sup>2</sup> Cleavage site

<sup>3</sup> Molecular weight

<sup>4</sup> Isoelectric point

<sup>5</sup> Two extinction coefficients are estimated, the first one assuming all Cys residue from cystines, the second one assuming all Cys residues are reduced

**Table B-2. List of primers used for Dpb11 BRCs constructs**

Proteins	Forward primer		Reverse primer		Vector
	Sequence <sup>1</sup>	R site <sup>2</sup>	Sequence <sup>1</sup>	R site <sup>2</sup>	
Full (1-727)	ACTATGAAGCCCTTCAAGGA	N/A	TTCCTCAGTTCTTGGGATCTC	N/A	N/A
BRCT1/2 (1-210)	CGCGGGAATCCATGAAGCCCC TTTCAAGGAATAACA	Eco RI	<u>CGCCGGCGTCAGCTTCTTTT</u> TGGCAATGC	Not I	pGEX6P1
BRCT3/4 (329-510)	CGCGGAAGGATCCAGTGATAA TAGTACTTTG	Bam HI	AGGGGGAAC <u>GCCGGCGT</u> CAAA GATCGCTAAATTC	Not I	pGEX6P1

<sup>1</sup> The regions from restriction digestion site are highlighted by underline in sequences.

<sup>2</sup> Restriction enzyme site selected on vector

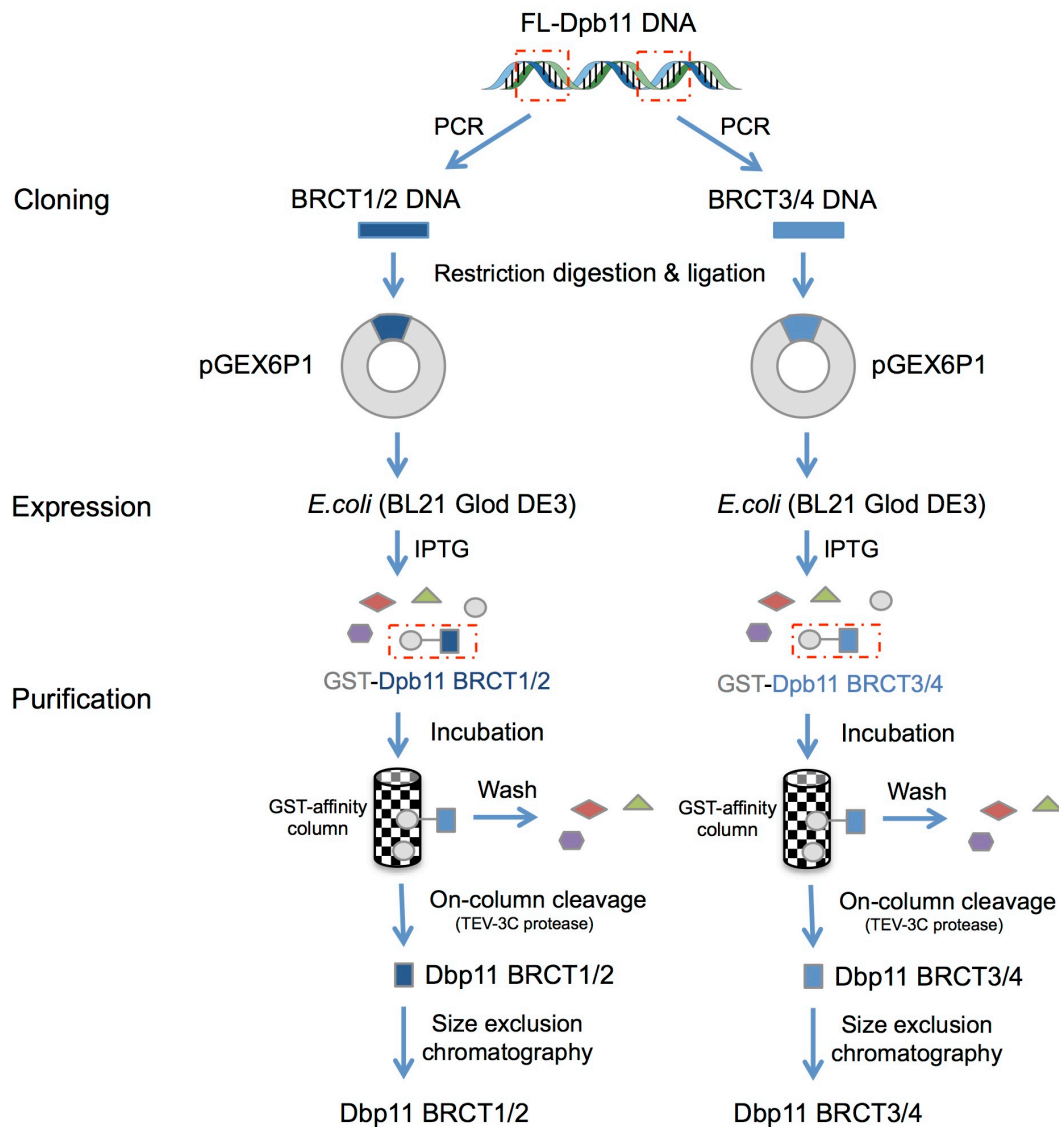


**Figure B-6. Flowchart of protein expression and purification process designed for Dpb11 BRCTs.**

Both Dpb11 BRCT1/2 and Dpb11 BRCT3/4 DNA are PCR amplified from FL-Dpb11 DNA (8-2191), then digested and inserted into the pGEX6P1 vector. These constructs are both expressed in *E. coli Gold* cells and purified by GST affinity column, then size exclusion column.

structural analog of Rad4 BRCT1/2 (Figure B-7A). The Lys 43 and Lys 56 from phosphate binding pocket of Rad4 BRCT1 are aligned with hydrophobic residues, Pro 315 and Ile 329, from Rtt107 BRCT3. This indicated there is no phosphate-binding pocket in the BRCT3 domain. However, the Thr 385, Arg 392 and Lys 425 aligned well with the Thr 111, Arg 137 and Lys 151 from the phosphate-binding pocket of Rad4 BRCT2. Since Rad4 BRCT1/2 is a homolog of TopBP1 BRCT4/5, interested in the similarity between Rtt107 and TopBP1, we carried out protein sequence alignment between these two proteins. We found residues 338-453 of Rtt107 aligns well with the region from TopBP1 BRCT5 (604-713). As expected, residues from the hydrophobic pocket (Phe 682, Ala 710, and Trp 714) of TopBP1 BRCT5 are mainly conserved in Rtt107 BRCT4, while residues from the phosphate-binding pocket (Ser 657, Lys 661, and Lys 707) of TopBP1 BRCT5 have similar polarity comparing to Rtt107 BRCT4 (Figure B-7B). Together, these indicate the Rtt107 BRCT3/4 may be a structural analog of TopBP1 BRCT4/5.

### **B.2.3 Constructs design of Rtt107 BRCT3/4 for bacteria based expression**

The sequence conservation between Rtt107 BRCT3/4 and Rad4 BRCT1/2 starts at residue 287, which is in the middle of an alpha helix based on secondary structure prediction of Rtt107 (Figure B-7C). Therefore, the region represents Rtt107 BRCT3/4 may begin from this alpha-helical structure. However, there is a predicted beta sheet that exists right before this alpha helix. Based on the CD search result, this beta sheet is also part of the BRCT3/4 domain. Therefore, we designed two protein constructs for BRCT3/4, which we referred to as Rtt107 (282-466) and Rtt107 (265-466). Although estimated protein properties of both protein constructs seem ideal, we cloned both constructs into a pGEX6P1 vector in order to make GST fusion proteins that can simplify the protein purification process (Table B-3).

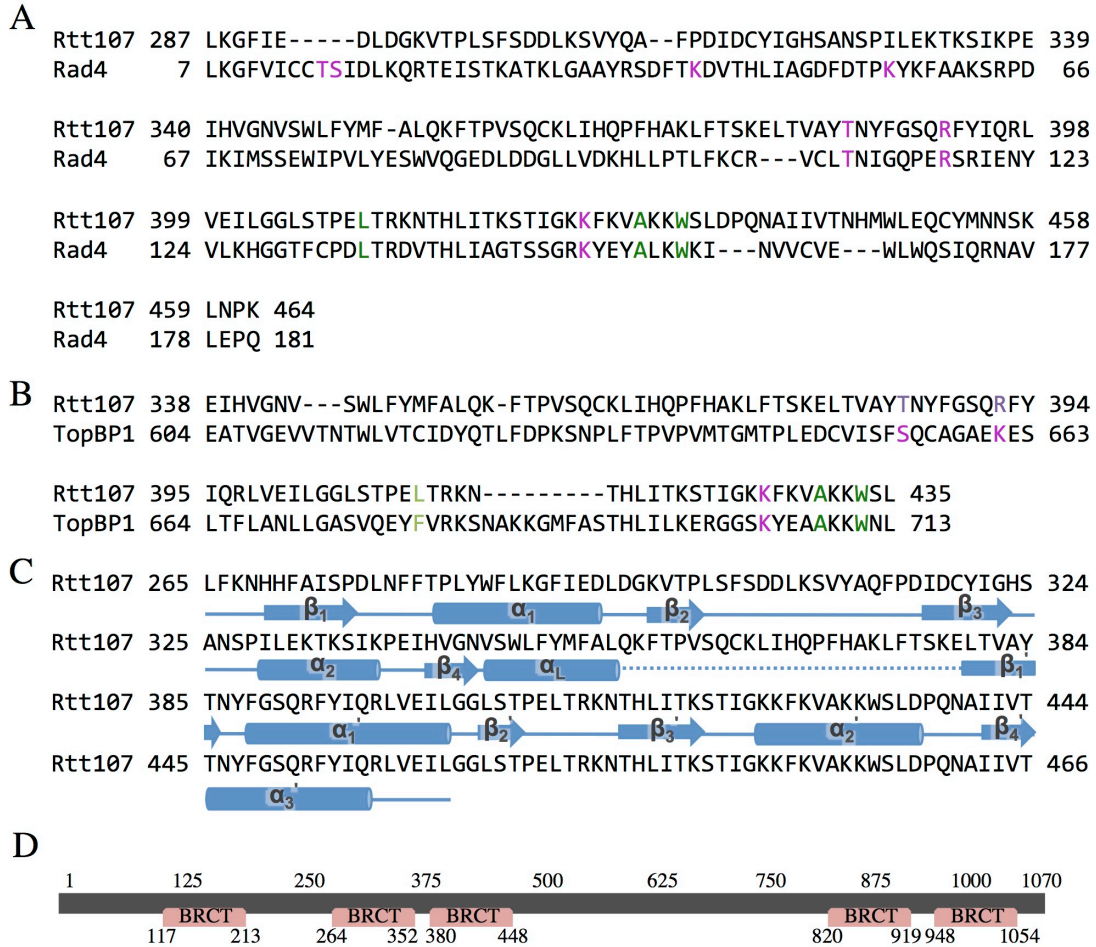


**Figure B-7. Comparison of Rtt107 BRCT and Rad4 BRCT1/2.**

Protein sequence alignments of Rtt107 with (A) Rad 4 BRCT1/2 and (B) TopBP1 BRCT4/5. All residues from phosphate binding pocket are colored pink, residues from hydrophobic pocket are colored green. (C) Secondary structure prediction of BRCT3/4 domains on Rtt107. (D) CD search result of BRCT domains on Rtt107 from NCBI database.

**Table B-3. List of primers used for Rtt107 BRCs constructs**

Proteins	Forward primer		Reverse primer		Vector
	Sequence <sup>1</sup>	R site <sup>2</sup>	Sequence <sup>1</sup>	R site <sup>2</sup>	
BRCT3/4 (282-466)	CGCGGCGGATCCCCTTTGTAT TGGTTTTTGAA	Bam HI	CGATATTGCGGCCGCTCAAA ATCTACTGTCTTTGGGT	Not I	pGEX6P1
BRCT3/4 (265-466)	CGCGGCGGATCCTTATTCAAA AATCACC ACTT	Bam HI	CGATATTGCGGCCGCTCAAA ATCTACTGTCTTTGGGT	Not I	pGEX6P1
BRCT3/4 (282-466)	CGCGGCGGATCCGCCTTTGTA TTGGTTTTTGAA	Bam HI	CGATATTGCGGCCGCTCAAA ATCTACTGTCTTTGGGT	Not I	pET47b
BRCT3/4 (265-466)	CGCGGCGGATCCGTTATTCAA AAATCACC ACTT	Bam HI	CGATATTGCGGCCGCTCAAA ATCTACTGTCTTTGGGT	Not I	pET47b

<sup>1</sup>The regions from restriction digestion site are highlighted by underline in sequences.

<sup>2</sup>Restriction enzyme site selected on vector

**Table B-4. Basic protein parameters of Rtt107 BRCT3/4 constructs<sup>1</sup>**

Protein	Tag		MW <sup>3</sup> (KDa)	pI <sup>4</sup>	Instability Index		Extinction Coefficient <sup>5</sup>	
	Type	C-site <sup>2</sup>			Value	Class	(M <sup>-1</sup> cm <sup>-1</sup> )	Abs 0.1%
BRCT3/4 (265-466)	N/A	N/A	23.4	9.24	28.91	Stable	34045/33920	1.453/1.448
BRCT3/4 (265-466)	GST	3C	52.5	7.63	33.59	Stable	78645/78670	1.468/1.461
BRCT3/4 (265-466)	His	3C	23.4	9.14	33.22	Stable	34045/33920	1.244/1.239
BRCT3/4 (282-466)	N/A	N/A	21.5	9.25	33.07	Stable	34045/33920	1.452/1.447
BRCT3/4 (282-466)	GST	3C	50.6	7.61	35.55	Stable	77155/76780	1.523/1.516
BRCT3/4 (282-466)	His	3C	25.6	9.13	30.19	Stable	34045/33920	1.342/1.337

<sup>1</sup> All data from this take are estimated based on protein sequence of each construct using ProtParam

<sup>2</sup> Cleavage site

<sup>3</sup> Molecular weight

<sup>4</sup> Isoelectric point

<sup>5</sup> Two extinction coefficients are estimated, the first one assuming all Cys residue from cystines, the second one assuming all Cys residues are reduced

#### **B.2.4 Purification of GST-Rtt107 BRCT3/4 produced by *E. coli* cells**

We first compared the protein expression levels of two constructs of GST tagged Rtt107 BRCT3/4 in *E. coli BL21 Gold* cells using an induction test. Comparison of samples from cells pre- and post-induction showed clearly induced protein expression after treatment with IPTG. A band between 43 kDa to 55 kDa is found in all lanes with post-induction samples, and the intensity of these bands is higher in cells treated with 0.5 mM IPTG than cells treated with 0.2 mM IPTG (Figure B-8A). Since GST-Rtt107<sup>265-466</sup> has an estimated MW of 52.5 kDa and GST-Rtt107<sup>282-466</sup> has an estimated MW of 50.6 kDa (Table B-4), we believed these bands represent the GST-Rtt107 BRCT3/4 proteins. To further support our prediction, the identities of these bands were validated by in-gel protein ID via mass spectrometry (Data not shown). Meanwhile, a band around 26 kDa is also observed in cells transformed with GST-Rtt107 constructs. Since GST has an estimated MW of ~26 kDa, and our positive control of *E. coli BL21 Gold* cells transformed with GST-TopBP1 BRCT4/5 construct also express this bands post-induction, we believed this band likely represents GST. Aside from GST-Rtt107 BRCT3/4, several other bands were also induced by IPTG treatment. Most of these bands are also observed in our positive control, suggesting they are from common leaking expression of proteins from this cell line itself. Overall, cells transformed with GST-Rtt107 (282-466) construct and induced by 0.5 mM IPTG have the highest expression level of GST-Rtt107 BRCT3/4 protein among all condition tested.

We solubilized the GST-Rtt107<sup>265-466</sup> protein from harvested cell pellets, and further purified it using a GST affinity column. The presence of band corresponding to GST-Rtt107<sup>265-466</sup> was unclear in lysis supernatant (IL) and we saw almost similar protein composition in the sample of flow-through (FT) after GST column, indicating most of the proteins solubilized in lysis buffer did not bind the GST column (Figure B-8B). Instead, a strong band at the position corresponding to GST-Rtt107<sup>265-466</sup> was observed in lysis pellet, indicating a significant amount of GST-Rtt107<sup>265-466</sup> proteins were insoluble. However, when comparing the GST affinity beads before and after incubation, we found bands corresponding

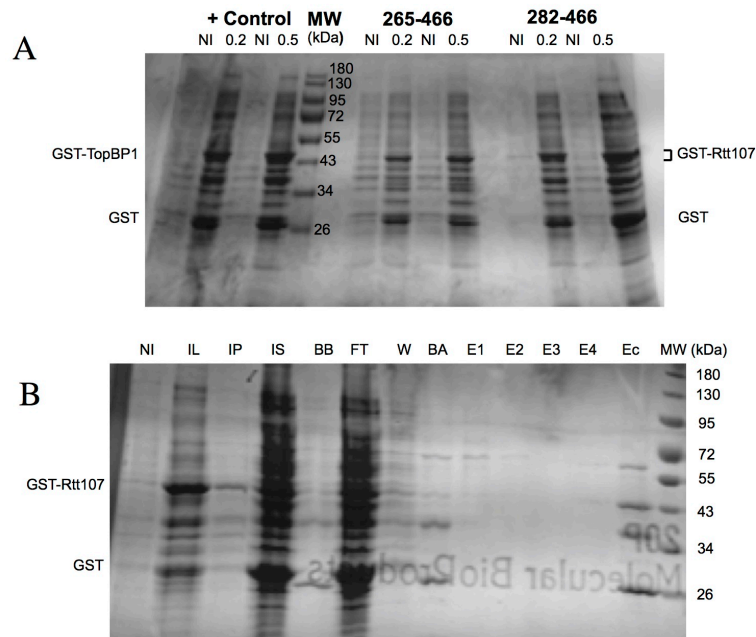


**Figure B-8. Preliminary protein expression and purification results of GST-Rtt107 BRCT3/4.**

(A) Induction test of two constructs of GST tagged Rtt107 BRCT3/4 proteins (265-466 or 282-466) expressed in *E. coli BL21 Gold* cells. NI: Non-induced cell lysate obtained before induction. 0.2 and 0.5: Cell lysate induced with 0.2 mM or 0.5 mM IPTG. Positive control of well-characterized GST-TopBP1 BRCT4/5 construct expressed in the same vector with the same cell line is also included. Both protein bands that highlighted as GST-Rtt107 BRCT3/4 proteins are validated by mass spectrometry. (B) Purification of cell lysate with GST tagged Rtt107 BRCT3/4 protein (282-466) by GST Affinity column. Samples from each step of the purification are shown here. NI: Non-induced cell lysate obtained before induction, IL: Induced cell lysate, IP: Induced cell pellet. IS: Induced cell supernatant. BB: Beads of GST affinity column before sample loading, FT: Flow-through sample from GST affinity column, W: Sample from last wash of beads, BA: GST affinity beads after sample loading, MW: Molecular weight standard. E1-E4 indicates elution fractions from the column and Ec indicates concentrated sample of all fractions. The position that equivalent to GST-Rtt107 is highlighted.

to GST and GST-Rtt107<sup>265-466</sup> were both presented on beads after incubation (BA) along with many other bands. Only a band around 26 kDa was found on beads before incubation (BB), suggesting the beads might contain some leftover GST but nothing else. However, the sample from last wash (W) still contains a mixture of many proteins. Therefore, the other bands in BA are likely unbound proteins that left on the beads due to insufficient washing. Although the band that represents GST-Rtt107<sup>265-466</sup> was almost invisible in elution fractions (E1 to E4), we were able to see this protein after concentrating all these fractions together to a 1 ml sample (Ec). However, the protein yield was already too low at this point, so we did not proceed further with the purification. Instead, we attempted to improve the solubility of GST-Rtt107<sup>265-466</sup> by introducing variations in the pH value (6.6, 6.8, and 7.0) and the salt concentration of lysis buffer (150mM NaCl and 300mM NaCl). Unfortunately, none of them improved the solubility of GST-Rtt107<sup>265-466</sup>.

### **B.2.5 Purification of His-Rtt107 BRCT3/4 produced by *E. coli* cells**

We re-cloned the Rtt107<sup>282-466</sup> and Rtt107<sup>265-466</sup> with N-terminal His tag (Table B-3) and examined the expression of these proteins by an induction test. The His-Rtt107<sup>282-466</sup> has an estimated MW of 23.4 kDa, while His-Rtt107<sup>265-466</sup> has an estimated MW of 25.4 kDa (Table B-4). The His-Rtt107<sup>265-466</sup> protein seems to express well as indicated by a strong band below 26 kDa post-induction (in the first lane), which is absent pre-induction (in the second lane). On the contrary, no strong band around 26 kDa was found in the last lane, so it was unclear whether the Rtt107<sup>282-466</sup> expressed post induction. However, three unknown bands between 34 kDa and 43 kDa were enhanced significantly post induction, indicating the application of IPTG did promote protein expression in cells (Figure B- 9A). To further analyze the proteins expressed in both cells, we purified sample from both cells using a Nickel (II) affinity column. In agreement with the induction test result, we observed the presence of bands below 26 kDa in elution fractions (E1 and E2), which further supported

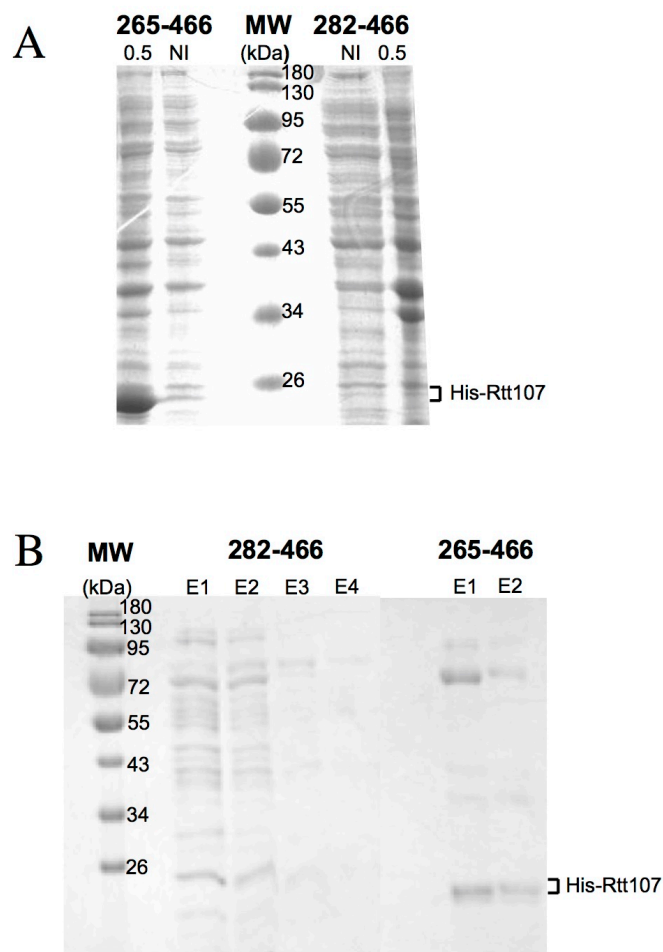


**Figure B-9. Preliminary protein expression and purification results of His-Rtt107 BRCT3/4.**

(A) Induction test of two constructs of His tagged Rtt107 BRCT3/4 proteins (265-466 or 282-466) expressed in *E. coli BL21 DE3* cells. NI: Non-induced cell lysate obtained before induction, 0.2 and 0.5: Cell lysate induced with 0.2 mM or 0.5 mM IPTG. (B) Purification of cell lysate with His tagged Rtt107 BRCT3/4 proteins (265-466 or 282-466) by Nickel (II) Affinity column. E indicates elution fractions. The positions that are equivalent to His-Rtt107 are pointed out on the right side of the gels.

supported they are His-Rtt107<sup>265-466</sup>. Interestingly, we also observed bands around 26 kDa in elution sample from the cell expressing His-Rtt107 (265-466) construct, indicating there may be some weak expressions of His-Rtt107<sup>282-466</sup>. However, the abundance of other proteins that elute together with His-Rtt107<sup>282-466</sup> makes it difficult to purify this protein further (Figure B-9B). Therefore, we only attempted to further purify the His-Rtt107<sup>265-466</sup> using size exclusion chromatography on a Superdex 75 16/60 column (data not shown), but we failed to observe a measurable quantity of His-Rtt107<sup>282-466</sup> protein in elution fractions.

### B.3 Discussion

Dpb11 and Rad4 are both known homologs of TopBP1. Based on protein sequences alignments in conjunction with secondary structure prediction, we propose res. 319-510 represent the BRCT3/4 and res.1-210 represent the BRCT1/2 of Dpb11. We believe that the BRCT1/2 of Dpb11 only has an N-terminal phosphate-binding pocket, consist of Thr 12, Arg 40 and Lys 55, on BRCT1. Meanwhile, the Leu 38, Phe 58 and His 62 from BRCT1 may form a hydrophobic pocket that provides additional specificity to its binding partners. Similar to BRCT3 of Rad4, the BRCT3 of Dpb11 has no phosphate-binding pocket. The BRCT4 of Dpb11 likely host a phosphate-binding pocket, but residues from this pocket remain unknown. In contradiction to our prediction, a recent publication proposed that the BRCT1 and the BRCT2 of Dpb11 both have phosphate-binding pockets (Cussioli et al., 2015). They predicted K55 from BRCT1 and R168 from BRCT2 are essential residues of these phosphate-binding pockets (Figure B-10A). However, their *in vitro* immune-precipitation result only showed that K55A and K55A/R168A mutations of BRCT1/2 interrupt Dpb11 interaction with Slx4. The R168A mutant seems to interact with Slx4 normally like the WT, indicating their proposed phosphate-binding pocket on BRCT2 is not real (Figure B-10B). In addition, they proposed K544 is from the phosphate-binding pocket of Dpb11 BRCT4, but they failed to provide any evidence as well. Once we successfully purified our protein

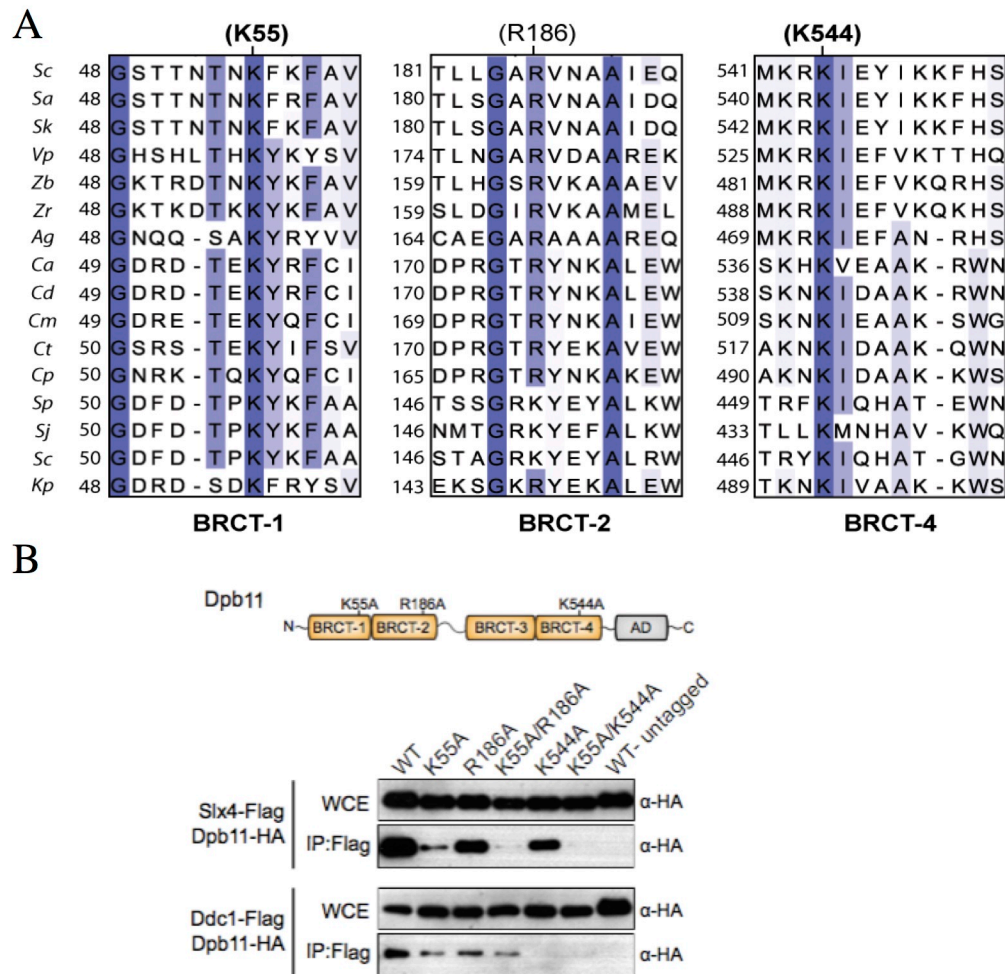


**Figure B-10. Dpb11 BRCT domains involved in the interaction with Slx4.**

(A) Multiple sequence alignment of Dpb11 BRCT domains 1, 2 and 4 from different fungal species. Each box represents the core region from Dpb11 BRCT domains 1, 2 and 4 with the respective conserved positively charged amino acid residue that was mutated in parentheses. Conserved amino acid residues are highlighted in blue. Species abbreviations and protein entry numbers are: *Sc* (*Saccharomyces cerevisiae*); *Sa* (*Saccharomyces arboricola*); *Sk* (*Saccharomyces kudriavzevii*); *Vp* (*Vanderwaltozyma polyspora*); *Zb* (*Zygosaccharomyces bailii*); *Zr* (*Zygosaccharomyces rouxii*); *Ag* (*Ashbya gossypii*); *Ca* (*Candida albicans*); *Cd* (*Candida dubliniensis*); *Cm* (*Candida maltose*); *Ct* (*Candida tropicalis*); *Cp* (*Candida parapsilosis*); *Sp* (*Schizosaccharomyces pombe*); *Sj* (*Schizosaccharomyces japonicus*); *Sc* (*Schizosaccharomyces cryophilus*); *Kp* (*Komagataella pastoris*). (B) Dpb11 containing the mutations indicated in the schematic illustration in top panel was expressed from a plasmid in yeast cells containing Flag-tagged Slx4 or Ddc1 for CoIP (Co-immunoprecipitation) experiments. AD: activation domain.

Figure adapted from (Cussioli et al., 2015).

construct of Dpb11 BRCT1/2, it will be interesting to generate the K55A and R168A mutants, and examine their function in comparison with the WT in our future study. Since K544 is not included in our current construct of Dpb11 BRCT3/4, it may be useful to generate a longer construct of Dpb11 BRCT3/4 for our future study.

We have also shown that Rtt107 BRCT3/4 is likely the structural analog of human TopBP1 BRCT4/5. We proposed Rtt107 BRCT3/4 poses a C-terminal phosphate-binding pocket, consists of Thr 385, Arg 392 and Lys 426. Similar to TopBP1 BRCT5 and Rad4 BRCT1, the BRCT4 domain of Rtt107 also has a small hydrophobic pocket, consist of Leu 410, Ala 430 and Trp 433. In consistence with our finding, a recent study from Dr. Michael Kobor's lab (University of British Columbia) reveals the BRCT3/4 domain plays a supportive in Rtt107 recruitment to DNA lesions, and K426M mutation in BRCT4 disrupt this function (Leung et al., 2016). To further examine the function of Rtt107 BRCT3/4 *in vitro*, we attempted to express and purify this protein. Unfortunately, preliminary testing results of our current expression and purification systems give a very low yield of targeting proteins. The GST-Rtt107<sup>282-466</sup> expressed very well in *E. coli BL21 Gold* cells. However, it has very low solubility in buffers examined so far. Since this protein has a theoretical pI value of 7.63 (Table B-4), perhaps only a buffer with pH < 6 may improve its solubility. The His-Rtt107<sup>265-466</sup> expressed better than His-Rtt107<sup>282-466</sup> in *E. coli BL21 DE3* cells. However, we failed to purify the His-Rtt107<sup>265-466</sup> using size exclusion chromatography after we obtained the elution samples containing His-Rtt107<sup>265-466</sup> protein from Nickel (II) affinity column. Therefore, we hypothesize that protein stability may be lower in the size exclusion buffer. Further experimenting with different buffer conditions will be done to test this scenario. Meanwhile, redesigning of the current expression construct with different protein tags is also a viable option. His-thioredoxin (TRX) and maltose binding protein (MBP) are two common types of tags that can be fused with targeting protein to improve the solubility of the protein. Based on protein parameters estimated by ProtParam, TRX-Rtt107 BRCT3/4

proteins have pI values around 7.7 (Table B-5), which are similar to the pI of GST-Rtt107 BRCT3/4 proteins (Table B-4), so they are unlikely to have good solubility under neutral pH as well. However, MBP-Rtt107 BRCT3/4 proteins have pI values around 6.2, so buffer with pH value between 7.5 and 8.0 provide good solubility for the proteins. In addition, MBP tag provides more specificity compare to His tag, because untagged proteins with internal histidines sometime bind to Nickel (II) affinity column as well. Therefore, expression and purification of MBP-Rtt107 BRCT3/4 seem promising.

## **B.4 Material and Methods**

### ***Designing of protein constructs***

Sequences of all proteins analyzed in this chapter are obtained from NCBI protein database. Pairwise full-length sequence alignment between Rad4 and Dpb11 is carried out by EMBOSS needle (Li et al., 2015; McWilliam et al., 2013; Rice et al., 2000). Structure-guided sequence alignments between Dpb11 BRCTs, Rtt107 BRCTs and Rad 4 BRCT1/2 (PDB ID: 4BU0), Rad4 BRCT3/4 (PDB ID: 4BMD), and TopBP1 BRCT4/5(PDB ID: 4UEN) are done by PROMAL3D (Pei et al., 2008). Secondary structure prediction of Dpb11 and Rtt107 are done by JPred4 (Drozdetskiy et al., 2015).

### ***Cloning of protein constructs***

#### **Dpb11**

We PCR amplified a long fragment of Dpb11 gene, which we referred to as Full construct (1-727), using the whole genomic DNA sample of *Saccharomyces cerevisiae* S288C stain (A kindly donation from Dr. Michael Schultz (Department of Biochemistry, University of Alberta) as the template first (Table B-1). All Dpb11 BRCT fragments were then PCR amplified using our Full construct as the template, and cloned into pGEX-6P-1 vectors (GE healthcare) encoding an N-terminal GST tag. Primers with Eco RI and Not I restriction sites

**Table B-5. Basic protein parameters of potential Rtt107 BRCT3/4 constructs<sup>1</sup>**

Protein	Tag		MW <sup>3</sup> (KDa)	pI <sup>4</sup>	Instability Index		Extinction Coefficient <sup>5</sup>	
	Type	C-site <sup>2</sup>			Value	Class	(M <sup>-1</sup> cm <sup>-1</sup> )	Abs 0.1%
BRCT3/4 (265-466)	MBP	3C	64.7	6.21	25.07	Stable	100395/100270	1.553/1.551
BRCT3/4 (265-466)	TRX	3C	37.1	7.71	33.22	Stable	48150/47900	1.300/1.293
BRCT3/4 (282-466)	MBP	3C	66.6	6.31	23.87	Stable	100395/100270	1.508/1.506
BRCT3/4 (282-466)	TRX	3C	35.1	7.69	24.9	Stable	48150/47900	1.370/1.363

<sup>1</sup> All data from this table are estimated based on protein sequence of each construct using ProtParam

<sup>2</sup> Cleavage site

<sup>3</sup> Molecular weight

<sup>4</sup> Isoelectric point

<sup>5</sup> Two extinction coefficients are estimated, the first one assuming all Cys residue from cystines, the second one assuming all Cys residues are reduced

were used for Dpb11 BRCT1/2 (1-210), and primers with Bam HI and Not I restriction sites were used for Dpb11 BRCT3/4 (329-510).

### Rtt107

Full-length Rtt107 DNA was generously provided by Dr. Kobor. We used two sets of primers with Bam HI and Not I restriction sites to clone two constructs of Rtt107 BRCT3/4 (288-466, 265-466) into pGEX-6P-1 vectors (Table B-2). The other two sets of primers with Bam HI and Not I restriction sites were used to clone the same constructs of Rtt107 BRCT3/4 (288-466, 265-466) into pET47b (-) vectors encoding an N-terminal His tag.

### ***Protein expression and induction test***

GST tagged Dpb11 BRCT1/2 or BRCT3/4 and GST tagged Rtt107 BRCT3/4 were both transformed into *E. coli* cell line BL21 Gold DE3. His tagged Rtt1077 BRCT3/4 constructs were transformed into *E. coli* cell line BL21 DE3. Cells expressing GST-Rtt07 BRCT3/4 were grown in Luria-Bertani (LB) broth media containing 50 µg/mL Kanamycin and 50 µg/mL Ampicillin at 28 °C. Cells expressing His-Rtt07 BRCT3/4 were grown with media containing only 50 µg/mL of Kanamycin at 28 °C. All cells were grown until they reach optimal cell density ( $OD_{600} > 0.600$ ), induced with 0.2 mM or 0.5 mM IPTG, then grown further at 20 °C for 16 hours. The changes of protein expressions in samples pre- and post-induction were analyzed by protein gel electrophoresis on SDS PAGE gels.

### ***Protein purification of Rtt107 BRCT3/4***

Cell pellets were re-suspended in lysis buffer (50 mM HEPES pH, 150 mM NaCl, 1 mM EDTA, 0.1% BME) with freshly added Halt protease inhibitors cocktail (Thermo Fisher), then lysed with 0.025 g/L egg white lysozyme (Sigma Aldrich) for 30 minutes at 4 °C. Cell lysate can be obtained after 5 times of 10 seconds subsequent sonication, followed by 30 minutes of centrifugation at 17000 rpm. Lysis supernatant was incubated with a GST affinity column containing glutathione sepharose 4B beads (GE Healthcare) for 2hrs. After releasing the flow-through (FT) sample of unbound proteins from the column, the beads were washed

extensively with 20 column volumes (CV) of washing buffer (50 mM HEPES pH 7.0, 150 mM NaCl, 1 mM EDTA, 0.1% BME). Proteins bounded on column were eluted in elution buffer (50 mM HEPES pH 7.0, 150 mM NaCl, 250 mM reduced glutathione, 0.1% BME) at 1 CV per fraction. As for cell expressing His tagged Rtt107 proteins, lysis supernatant was incubated on a Nickel (II) affinity column for 2 hrs. After releasing the flow-through (FT) sample of unbound proteins from the column, the beads were washed extensively with 20 column volumes (CV) of washing buffer (50 mM HEPES pH 7.0, 150 mM NaCl, 10 mM Imidazole, 0.1% BME). Proteins bounded on column were eluted in elution buffer (50 mM HEPES pH 7.0, 150 mM NaCl, 50 mM Imidazole, 0.1% BME) at 1 CV per fraction. All protein purification processes were monitored via SDS-PAGE calibrated with pre-stained protein standards.

## B.5 Reference

1. Cussiol, J.R., Jablonowski, C.M., Yimit, A., Brown, G.W., and Smolka, M.B. (2015). Dampening DNA damage checkpoint signalling via coordinated BRCT domain interactions. *EMBO J* 34, 1704-1717.
2. Drozdetskiy, A., Cole, C., Procter, J., and Barton, G.J. (2015). JPred4: a protein secondary structure prediction server. *Nucleic Acids Res* 43, W389-394.
3. Frangioni, J.V., and Neel, B.G. (1993). Solubilization and purification of enzymatically active glutathione S-transferase (pGEX) fusion proteins. *Anal Biochem* 210, 179-187.
4. Gasteiger, E., Hoogland, C., Gattiker, A., Duvaud, S., Wilkins, M.R., Appel, R.D., Bairoch, A. (2005). Protein Identification and Analysis Tools on the ExPASy Server. *The Proteomics Protocols Handbook*, Humana Press, 571-607
5. Germann, S.M., Oestergaard, V.H., Haas, C., Salis, P., Motegi, A., and Lisby, M. (2011). Dpb11/TopBP1 plays distinct roles in DNA replication, checkpoint response and homologous recombination. *DNA Repair (Amst)* 10, 210-224.
6. Gohler, T., Munoz, I.M., Rouse, J., and Blow, J.J. (2008). PTIP/Swift is required for efficient PCNA ubiquitination in response to DNA damage. *DNA Repair (Amst)* 7, 775-787.
7. Hang, L.E., Peng, J., Tan, W., Szakal, B., Menolfi, D., Sheng, Z., Lobachev, K., Branzei, D., Feng, W., and Zhao, X. (2015). Rtt107 Is a Multi-functional Scaffold Supporting Replication Progression with Partner SUMO and Ubiquitin Ligases. *Mol Cell* 60, 268-279.
8. Kilkenny, M.L., Dore, A.S., Roe, S.M., Nestoras, K., Ho, J.C., Watts, F.Z., and Pearl, L.H. (2008). Structural and functional analysis of the Crb2-BRCT2 domain reveals distinct roles in checkpoint signaling and DNA damage repair. *Genes Dev* 22, 2034-2047.
9. Leung, G.P., Brown, J.A., Glover, J.N., and Kobor, M.S. (2016). Rtt107 BRCT domains act as a targeting module in the DNA damage response. *DNA Repair (Amst)* 37, 22-32.
10. Li, W., Cowley, A., Uludag, M., Gur, T., McWilliam, H., Squizzato, S., Park, Y.M., Buso, N., and Lopez, R. (2015). The EMBL-EBI bioinformatics web and programmatic tools framework. *Nucleic Acids Res* 43, W580-584.

11. Li, X., Liu, K., Li, F., Wang, J., Huang, H., Wu, J., and Shi, Y. (2012). Structure of C-terminal tandem BRCT repeats of Rtt107 protein reveals critical role in interaction with phosphorylated histone H2A during DNA damage repair. *J Biol Chem* 287, 9137-9146.
12. Marchler-Bauer, A., Bo, Y., Han, L., He, J., Lanczycki, C.J., Lu, S., Chitsaz, F., Derbyshire, M.K., Geer, R.C., Gonzales, N.R., *et al.* (2017). CDD/SPARCLE: functional classification of proteins via subfamily domain architectures. *Nucleic Acids Res* 45, D200-D203.
13. McWilliam, H., Li, W., Uludag, M., Squizzato, S., Park, Y.M., Buso, N., Cowley, A.P., and Lopez, R. (2013). Analysis Tool Web Services from the EMBL-EBI. *Nucleic Acids Res* 41, W597-600.
14. Ohouo, P.Y., Bastos de Oliveira, F.M., Almeida, B.S., and Smolka, M.B. (2010). DNA damage signaling recruits the Rtt107-Slx4 scaffolds via Dpb11 to mediate replication stress response. *Mol Cell* 39, 300-306.
15. Ohouo, P.Y., Bastos de Oliveira, F.M., Liu, Y., Ma, C.J., and Smolka, M.B. (2013). DNA-repair scaffolds dampen checkpoint signalling by counteracting the adaptor Rad9. *Nature* 493, 120-124.
16. Pei, J., Kim, B.H., and Grishin, N.V. (2008). PROMALS3D: a tool for multiple protein sequence and structure alignments. *Nucleic Acids Res* 36, 2295-2300.
17. Pfander, B., and Diffley, J.F. (2011). Dpb11 coordinates Mec1 kinase activation with cell cycle-regulated Rad9 recruitment. *EMBO J* 30, 4897-4907.
18. Qu, M., Rappas, M., Wardlaw, C.P., Garcia, V., Ren, J.Y., Day, M., Carr, A.M., Oliver, A.W., Du, L.L., and Pearl, L.H. (2013). Phosphorylation-dependent assembly and coordination of the DNA damage checkpoint apparatus by Rad4(TopBP1). *Mol Cell* 51, 723-736.
19. Qu, M., Yang, B., Tao, L., Yates, J.R., 3rd, Russell, P., Dong, M.Q., and Du, L.L. (2012). Phosphorylation-dependent interactions between Crb2 and Chk1 are essential for DNA damage checkpoint. *PLoS Genet* 8, e1002817.
20. Rice, P., Longden, I., and Bleasby, A. (2000). EMBOSS: the European Molecular Biology Open Software Suite. *Trends Genet* 16, 276-277.

21. Taricani, L., and Wang, T.S. (2006). Rad4TopBP1, a scaffold protein, plays separate roles in DNA damage and replication checkpoints and DNA replication. *Mol Biol Cell* 17, 3456-3468.
22. Wardlaw, C.P., Carr, A.M., and Oliver, A.W. (2014). TopBP1: A BRCT-scaffold protein functioning in multiple cellular pathways. *DNA Repair* 22, 165-174.
23. Williams, J.S., Williams, R.S., Dovey, C.L., Guenther, G., Tainer, J.A., and Russell, P. (2010). gammaH2A binds Brc1 to maintain genome integrity during S-phase. *EMBO J* 29, 1136-1148.
24. Yan, W., Shao, Z., Li, F., Niu, L., Shi, Y., Teng, M., and Li, X. (2011). Structural basis of gammaH2AX recognition by human PTIP BRCT5-BRCT6 domains in the DNA damage response pathway. *FEBS Lett* 585, 3874-3879.
25. Yue, M., Zeng, L., Singh, A., and Xu, Y. (2014). Rad4 mainly functions in Chk1-mediated DNA damage checkpoint pathway as a scaffold protein in the fission yeast *Schizosaccharomyces pombe*. *PLoS One* 9, e92936.